

012

MSC-02557

DEVELOPMENT OF A THERMAL PROTECTION
SYSTEM FOR THE WING OF A
SPACE SHUTTLE VEHICLE
NASA-MSC CONTRACT NAS9-11224
PHASE I FINAL REPORT

VMSC REPORT NO. T143-5R-00044



D. M. While
D. M. While
Prepared By



G. B. Whisenhunt
G. B. Whisenhunt
Approved By

Vought Missiles and Space Company
LTV Aerospace Corporation
P. O. Box 6267
Dallas, Texas 75222

ACKNOWLEDGEMENT

This report was prepared by the Vought Missiles and Space Company of LTV Aerospace Corporation for the National Aeronautics and Space Administration - Manned Spacecraft Center, under Contract No. NAS9-11224. The period of performance was 1 August 1970 through 19 February 1971.

Mr. J. E. Pavlosky of the Structures and Mechanics Division, NASA-MSC was technical monitor for the program.

The technical work was directed by D. M. While, Project Leader, while materials development was directed by D. C. Rogers; thermal analysis, analytical evaluation of coating systems and interpretation of results were conducted by J. E. Medford; design was performed by A. S. Sotherlund, with W. E. Agan providing the structural and thermoelastic analysis.

Mr. B. A. Forcht, VMSC, and Dr. E. Rudy, Oregon Graduate Center, acted as consultants on materials development. Dr. W. C. Schwemer and T. E. Mackie of the LTV Research Center provided assistance on the hafnium-tantalum coating system.

The Space Division, North American Rockwell supported the program by providing design conditions and assisting in establishment of design criteria.

ABSTRACT

AST-62821 R3

TITLE OF REPORT Development of a Thermal Protection System For The Wing of a Space Shuttle Vehicle - Phase I Final Report			
ORIGINATING AGENCY AND LOCATION Vought Missiles and Space Company LTV Aerospace Corporation Post Office Box 6267 Dallas, Texas 75222		CLASSIFICATION	
		REPORT	ABSTRACT
AUTHORS D. M. While		ISSUE DATE 22 Feb. '71	LIMITATIONS ON DISTRIBUTION (IF ANY) Distribution List Included
ORIGINATING AGENCY'S REPORT NO. T143-5R-00044	DOD REFERENCES		OTHER IDENTIFYING REPORT NOS. NASA-MSC Number MSC-02557
	CONTRACT NO. NASA MSC NAS9-11224	PROJECT NO. T-143	
INDEXING Conceptual designs and analyses are given for an oxidation inhibited RPP shuttle wing leading edge. Test results from candidate oxidation inhibited RPP systems are given.			
A. SUMMARY SENTENCE(S): Conceptual designs and analyses are given for an oxidation inhibited RPP shuttle wing leading edge. Test results from candidate oxidation inhibited RPP systems are given.			
B. KEY WORDS: Oxidation Inhibitors, Reinforced Pyrolyzed Plastic (RFP), Leading Edge Design, Plasma Testing, Catalytic Phenomenon, Diffusion Coatings, Non-Destructive Test			
WEAPON SYSTEMS NUMBERS, MODEL NUMBERS, ETC. N/A			
ABSTRACT Conceptual designs and supporting analyses are given for the wing leading edge of the NASA shuttle. A typical baseline leading edge geometry is specified. Boost and sub-sonic cruise flight produce maximum airloads, while re-entry produces design temperatures up to 4000°F radiation equilibrium as well as maximum thermal gradients. It is shown that the use of a solid laminate design in lieu of sandwich structure significantly reduces thermal gradients and stresses. Equally important, stagnation temperature is reduced 370°F through the mechanism of cross-radiation. Thermal stresses are shown to be the most significant design parameter for coated RFP having high elastic modulus but is much less important for bare and coated RFP with low elastic moduli. Fifteen coating systems with five material constituents incorporated into RPP were screened. Screening tests included flexure, still air furnace for low temperature stability, and plasma arc for high temperature oxidation resistance performance. Two diffusion coated systems, siliconized RPP and zirconium-boron-silicon coated RPP, were selected and developed further. These systems have shown good performance, primarily due to low-catalytic behavior. This phenomenon retards the recombination of dissociated atoms at the surface of the material, thus reducing that portion of the imposed heat load due to heat of recombination. It has been estimated that in a shuttle entry environment producing 4000°F radiation equilibrium surface temperature, the combined effects of low catalyticity of siliconized RPP and cross-radiation would limit the maximum			

surface temperature to about 3000°F. Plasma testing has indicated that VMSC's siliconized RPP has a surface temperature capability of approximately 3200°F while still maintaining multimission capability. This shows that siliconized RPP has the potential for meeting the shuttle requirements. The zirconium-boron-silicon coated RPP exhibits high temperature oxidation performance about half that of the siliconized system but flexure strength is insensitive to temperature cycling in an oxidizing environment to 2300°F.

The non-catalytic phenomenon is discussed and correlated with test data. A comparison between the test environment and the shuttle flight environment reveals close agreement and suggests that the results obtained in VMSC's plasma arc should indeed be attainable in flight. Further testing and analysis is recommended to confirm low catalytic efficiency of the coating systems and its effect upon entry temperatures.

An alternate coating system, which is fully catalytic in behavior, was also recommended for further development. This coating, comprised of hafnium and tantalum, oxidizes during re-entry to produce a tough adherent oxide layer when applied to bare RPP. Repeated exposure at temperatures above 4000°F have indicated good potential for the shuttle environment.

TABLE OF CONTENTS

<u>Section</u>	<u>Page No.</u>
1.0 Introduction	1
2.0 Summary	3
2.1 Design Synthesis	4
2.2 Materials Development and Evaluation	8
2.3 Conclusions and Recommendations	22
3.0 Design Synthesis	25
3.1 Design Criteria	25
3.2 Design Concepts and Evaluation Criteria	29
3.3 Thermal Analysis	47
3.3.1 Aerodynamic Heating	48
3.3.2 Radiation Equilibrium Temperatures	50
3.3.3 Thermal Properties	53
3.3.4 Thermal Response of Design Concepts	53
3.3.5 Reduction of Skin Temperature Gradients	67
3.3.6 Surface Recession of Bare RPP	73
3.3.7 Conclusions and Recommendations	75
3.4 Structural Analysis	76
3.4.1 Element Analysis	78
3.4.2 Initial Airloads Analysis	80
3.4.3 Final Airloads Analysis	86
3.4.4 Thermoelastic Analysis	88
3.4.5 Conclusions and Recommendations	95
3.5 Conclusions	96
4.0 Materials Development	99
4.1 Substrates	101
4.2 Oxidation Inhibitors	108
4.2.1 Candidate Oxidation Inhibitor Systems	109
4.2.2 Add-Mix Systems	112

TABLE OF CONTENTS (Cont'd.)

<u>Section</u>	<u>Page No.</u>	
4.2.3	Combined Systems	116
4.2.4	Initial Diffusion Systems	122
4.2.5	Modified and Final Diffusion Systems	126
4.2.6	Overlay Systems	135
4.3	Conclusions	140
5.0	Materials Test Evaluation	143
5.1	Candidate Inhibitor Systems	143
5.1.1	Flexure Screening Tests	143
5.1.2	Furnace Screening Tests	148
5.1.3	Plasma Arc Screening Tests	150
5.2	Modified Inhibitor Systems Test	168
5.2.1	VMSC Plasma Arc Tests	168
5.2.2	NASA-MSD Evaluation of Siliconized RPP	199
5.3	Surface Catalytic Effects	201
5.3.1	Review of Surface Catalytic Effects	202
5.3.2	Frozen Boundary Layer Regime	206
5.3.3	Correlation of Plasma Test Data with Theory of Catalytic Effects	208
5.3.4	Application of Catalysis Theory to Reentry Environment	209
5.3.5	Substantiating Data	211
5.3.6	Effects Upon Downstream Catalytic Material	211
5.4	Inhibited RPP Characterization Data	214
5.4.1	Flexure Tests	214
5.4.2	Coefficient of Thermal Expansion	224
5.4.3	Emittance	225
5.4.4	Conductivity	225
5.4.5	Interlaminar Shear Strength	225
5.5	Conclusions	225
6.0	Nondestructive Testing (NDT)	229
References		242
Distribution		246

LIST OF FIGURES

<u>Figure</u>		<u>Page No.</u>
2-1	Shuttle Leading Edge Concept No. 3	7
2-2	Average Flexural Strength, Diffusion and Add-Mix Systems, Screening Tests	11
2-3	Plasma Arc Test, Mass Loss, Screening Flux, $q_c = 160 \text{ BTU/Ft}^2\text{-Sec}$	11
2-4	Typical Load-Deflection Curves, Diffusion Coated Flexure Bars, Screening Tests	11
2-5	Plasma Arc Test, Mass Loss Data, Siliconized RPP	14
2-6	Plasma Arc Test, Mass Loss Data, Zr-B-Si Treated RPP	15
2-7	Predicted Mission Capability-Inhibited RPP	17
2-8	Correlation of Inhibited and Bare Plasma Specimen Temperatures	17
2-9	Siliconized RPP Flexure Strength Summary	19
2-10	Boron-Zirconium-Silicon Coated RPP Flexure Strength Summary	19
3-1	Boost Condition Loads	27
3-2	Interference Factor and Local Heat Ratio	28
3-3	Radiation Equilibrium Temperatures Time of Peak Re-entry Heating	28
3-4	Limit Entry Pressure	30
3-5	Cruise Condition Loads	30
3-6	RPP Leading Edge, Concept "A"	33
3-7	RPP Leading Edge, Concept "B"	33
3-8	RPP Leading Edge, Concept "C"	35
3-9	RPP Leading Edge, Concept "D"	35
3-10	RPP Leading Edge, Concept "E"	37
3-11	RPP Leading Edge, Concept "F"	37
3-12	RPP Leading Edge, Concept "G"	39
3-13	RPP Leading Edge, Concept "H"	39

LIST OF FIGURES (Cont'd.)

<u>Figure</u>		<u>Page No.</u>
3-14	Expansion Joint Concepts	41
3-15	Interim Leading Edge Concepts	43
3-16	Shuttle Leading Edge, Concept No. 1	44
3-17	Shuttle Leading Edge Concept No. 3	46
3-18	Boost Aerodynamic Heating	49
3-19	Re-Entry Aerodynamic Heating	49
3-20	Interference Factor and Local Heat Ratio	51
3-21	Radiation Equilibrium Temperatures Time of Peak Re-Entry Heating	51
3-22	Radiation Equilibrium Temperature Time History	52
3-23	Baseline Thermal Properties Oxidation Inhibited RPP Laminate	52
3-24	Thermal Conductivity of Foam Core, Overlay and Attachment Insulator	54
3-25	Specific Heat of Foam Core, Attachment Insulator and Overlay	54
3-26	Thermal Response of Solid Laminate Max. Interference Heating, Stagnation Line	56
3-27	Maximum Temperature Drop Across RPP Laminate	56
3-28	Maximum Temperature Drop Across RPP Foam Core Sandwich	58
3-29	Thermal Response of Foam Core Sandwich	58
3-30	Thermal Response, Honeycomb Sandwich	59
3-31	Maximum Temperature Drop Across Cover/ Sandwich Combination	59
3-32	Effect of Joint Coefficient Upon Temperature Gradients	62
3-33	Temperature Reduction on Back Side Foam Core Sandwich	62
3-34	Maximum Temperature of RPP With Overlay	63
3-35	Maximum Temperature Drop Across Rib	63

LIST OF FIGURES (Cont'd.)

<u>Figure</u>		<u>Page No.</u>
3-36	Thermal Response of Rib	65
3-37	Thermal Response of Rib	65
3-38	Attachment Thermal Response	68
3-39	Effect of Circumferential Heat Conduction Upon Temperature Gradients	68
3-40	Thermal Model, Leading Edge With Internal Cross-Radiation Maximum Interference Heating Case	70
3-41	Thermal Response of RPP Laminate With Internal Cross-Radiation	71
3-42	Effect of Internal Cross-Radiation Upon Peak Temperatures	71
3-43	Re-Entry Surface Recession of Bare RPP	74
3-44	Optimum Face Thickness	79
3-45	Weight Sensitivity	79
3-46	Stress Sensitivity	81
3-47	Optimum Weight Sensitivity	81
3-48	Panel Thickness Initial Material Assumptions	83
3-49	Leading Edge Weight Initial Material Assumptions	83
3-50	Ultimate Moment and Shear Sandwich Designs	84
3-51	Rib Geometry	84
3-52	Rib Moment	85
3-53	Panel Thickness-One Intercostal	85
3-54	Panel Thickness - Four Intercostals	87
3-55	Leading Edge Unit Weight	87
3-56	Ultimate Thermoelastic Stress	89
3-57	Ultimate Thermoelastic Stress	89
3-58	Thermoelastic Tensile Stress	91
3-59	Thermoelastic Compression Stress	91

LIST OF FIGURES (Cont'd.)

<u>Figure</u>		<u>Page No.</u>
3-60	Rib Thermal Stress	94
3-61	Thermal Expansion Relative to Cold Front Beam	94
4-1	Typical Load Deflection Curves Flexure Specimens	105
4-2	Typical Photomicrograph of Diffusion Coated Specimen (50X). Specimen from Experimental Run Number 8	123
4-3	Photograph of Selected Specimens Diffusion Coated During Preliminary Experiments After Still Air Oxidation Test at 2300 ^o F	123
4-4	Photograph of Sectioned Flexure Bars After Carbon Burnout at 1500 ^o F	125
5-1	Load - Deflection Curves Diffusion Coated Flexure Bars	145
5-2	Surface Appearance of Add-Mix Specimens After 2300 ^o F Still Air Oxidation Test	151
5-3	Surface Appearance of Diffusion Coated Specimens After 2300 ^o F Still Air Oxidation Test	151
5-4	Plasma Arc Simulation of Re-Entry Oxidation	156
5-5	Plasma Arc Test Surface Heat Balance Screening Tests	156
5-6	Plasma Arc Test, Surface Recession Data Relative to Specimen Surface Temperature	159
5-7	Plasma Arc Test, Surface Recession Data Relative to Bare RPP Surface Temperature	159
5-8	Add-Mix Specimens After Plasma Test	163
5-9	Diffusion Coated Specimens After First Series Plasma Test	163
5-10	Diffusion Coated Specimens After Second Series Plasma Test	164
5-11	Diffusion Coated Specimens Alternate Silicon Carbide Coatings After Plasma Test	164

LIST OF FIGURES (Cont'd.)

<u>Figure</u>		<u>Page No.</u>
5-12	Surface Temperature of Siliconized RPP	170
5-13	Surface Temperature of Zr-Br-Si Treated RPP	170
5-14	Correlation of Inhibited and Bare Plasma Specimen Temperatures	171
5-15	Plasma Arc Test, Mass Loss Data Siliconized RPP	173
5-16	Plasma Arc Test, Mass Loss Data Zr-B-Si Treated RPP	174
5-17	Mass Loss Rate Vs Re-Entry Time Siliconized RPP	177
5-18	Predicted Mission Capability - Inhibited RPP	177
5-19	Plasma Arc Test Mass Loss Data Reaction Rate Control Correlation	179
5-20	Selected Specimens 3/4" Dia. After Plasma Arc Exposure	181
5-21	Candidate Coating Systems Following Plasma Arc Exposure 3/4 In. Dia. Specimens	182
5-22	Siliconized Specimen After Exposure to NASA- MSC Plasma-Arc	183
5-23	Effect of Noncatalytic Surface Upon Stagnation Point Heat Transfer	205
5-24	State of Boundary Layer Flow Re-Entry and Plasma Arc Test	205
5-25	Heating Reduction Due to Low Catalytic Efficiency Surface	210
5-26	Heating Reduction Comparison	210
5-27	Heat Transfer to Catalytic and Noncatalytic Surfaces, Plasma Arc Test Data Vs Theory	212
5-28	Room Temperature Stress-Strain Curves Flexure	216
5-29	Coefficient of Thermal Expansion Warp Direction	219

LIST OF FIGURES (Cont'd.)

<u>Figure</u>		<u>Page No.</u>
5-30	Coefficient of Thermal Expansion Fill Direction	219
6-1	Comparison of Bare RPP X-Ray Photographs Before and After Immersion in Carbon Tetrachloride	230
6-2	Correlation of Ultrasonic C-Scan Recording and X-Ray of Bare RPP Impregnated with Carbon Tetrachloride, Showing Delaminations and Void Areas	231
6-3	Comparison of Infrared and Ultrasonic Inspection Techniques on Bare RPP	232
6-4	Photographs From X-Ray Negatives Using P/N 55 Film with Contact Printer	233
6-5	Photographs of Ultrasonic C-Scan Recordings From Bare and Coated RPP	234
6-6	Non-Destructive Testing of Panel 2-1 - Correlation of Defect Indications	237
6-7	Metallographic Examination of Panel 2-1 to Confirm Non-Destructive Test Indications	238
6-8	Metallographic Examination of Typical Defects Observed with Non-Destructive Testing by Radiographic and Ultrasonic Inspection Techniques	239
6-9	Evaluation of Silixonized Specimen M10-5 Tested by NASA-MSD at Heat Flux = 100 BTU/Ft ² -Sec For 40 Minutes - Surface Temperature = 3000°F	240
6-10	Metallographic Examination of M-10-6, NASA MSD Plasma Test Specimen - After Exposure To a Heat Flux of 126 BTU/Ft ² -Seconds and a Surface Temperature of 3220°F.	241

LIST OF TABLES

<u>Table</u>		<u>Page No.</u>
3-1	Design Concept Evaluation Factors	31
3-2	Estimated Fabrication Costs of Concept No. 1	45
3-3	Rib Analysis Summary	66
3-4	Cross Radiation Analysis Summary	72
3-5	Material Properties Assumed for Analysis	77
4-1	Summary of Flexure Strength Comparative Results - Substrate Evaluation	103
4-2	Add-Mix Composites Data, Cured Panel Composition Goals Volume Percent	113
4-3	Add-Mix System Process Data Weight Changes Due to Processing	113
4-4	Add-Mix Composites Data, Pyrolyzed Panel Composition, Volume Percent	115
4-5	Combined Composites Data, Cured Panel Composition Goals, Volume Percent	117
4-6	Combined System Process Data, Weight Changes Due to Processing	117
4-7	Combined Composites Data, Pyrolyzed Panel Composition, Volume Percent	118
4-8	Preliminary Diffusion Coating Experiments	119
4-9	Diffusion Coating for Characterization Specimens	121
4-10	Diffusion Coating Experiments, Siliconized System	127
4-11	Diffusion Coating Experiments, Zirconium-Boron-Silicon System	129
5-1	Add-Mix System Flexure Data	146
5-2	Diffused Coating System Flexure Data	147
5-3	Weight Change Experienced by Add-Mix Specimens as a Result of 2300°F Oxidation Test	149
5-4	Weight Change Experienced by Diffusion Coated Specimens as a Result of 2300°F Oxidation Test	150

LIST OF TABLES (Cont'd.)

<u>Table</u>		<u>Page No.</u>
5-5	Plasma Arc Test Performance Summary - Screening	161
5-6	Plasma Arc Test Summary - Initial Screening	162
5-7	Plasma Arc Test Summary	184
5-8	Plasma Arc Test Summary, NASA-MSA Tests	200
5-9	Typical Plasma Arc Test Results for RPP	202
5-10	Flexure Strength and Elastic Modulus, Siliconized RPP	217
5-11	Weight Change After Thermal Cycling in Air at 2300 ^o F	221
5-12	Coating Thicknesses on R. T. Flex Specimens at Point of Fracture	222
5-13	Flexure Strength and Elastic Modulus, Zirconium-Boron-Silicon Coated RPP	223
5-14	Conductivity of Siliconized RPP	226
6-1	Flexure Data After Immersion in NDT Fluids	235

1.0 INTRODUCTION

This report summarizes the technical work accomplished by the Vought Missiles and Space Company (VMSC) of LTV Aerospace Corporation, under Phase I of a two phase program, "Development of a Thermal Protection System for the Wing of a Space Shuttle Vehicle", NASA-MSC Contract No. NAS9-11224, reference (1). The thermal protection system, directed toward application to the leading edge structure of the NASA Orbiter wing and tail surfaces, must sustain multiple exposure to all environments through earth launch, orbital operation, entry and landing. The goal is to achieve a reliable leading edge design and material system with 100-mission life capability, while withstanding a maximum temperature level up to 4000°F.

The thermal protection system development in this program is restricted to the oxidation resistant carbon-carbon reinforced pyrolyzed plastic (RPP) composites. This class of materials has shown the potential for long term exposure in an oxidizing atmosphere at temperatures exceeding the limits of coated metals. In addition, the substrate materials, comprised of graphite cloth or filaments, offer low density with good strength at operational temperatures. In addition to the materials development task, the program effort includes consideration of all aspects of design, fabrication, and inspection relative to realistic flight hardware.

Phase I consisted of two major tasks: (1) Materials Development and Evaluation and (2) Design Synthesis. Materials Development Evaluation was primarily concerned with the selection of candidate inhibitor and substrate materials, the integration and fabrication of these into RPP composites, and the testing and subsequent modification of these composites to develop a system(s) potentially suitable for the Orbiter wing leading edge application.

The Design Synthesis task was devoted to the generation of practical design concepts, the analysis of these concepts to determine best approaches, and the establishment of materials property performance goals and material structural composite configurations.

Phase II will consist of development of physical and mechanical design property data for the two selected coating systems and verification of preliminary leading edge design concepts by laboratory testing.

Two diffusion coating systems, siliconized RPP and zirconium-boron-silicon coated RPP, have been selected for continued development in Phase II. In addition, a hafnium/tantalum coating, although not evaluated to the extent of the diffusion systems, has indicated outstanding high temperature performance in limited plasma arc testing, and is also recommended for further evaluation and development in Phase II.

Significant accomplishments achieved in the Phase I program include:

(1) Conception of a leading edge design that employs cross radiation from hot areas to cooler regions to reduce stagnation temperature by 370°F under maximum heating conditions. The design is calculated to weigh less than 2 lb/ft² using state-of-the-art fabrication techniques for the solid laminate substrate.

(2) Development of a siliconized diffusion coating system that is projected to provide high temperature oxidation resistance to meet a 100-mission life capability at 3500°F radiation equilibrium temperature and 10-mission life capability at 3710°F radiation equilibrium temperature. This performance is predicted even without the benefit of the temperature reduction from cross-radiation. True temperature at the surface of the coated RPP under these conditions is only 2940°F and 3130°F, respectively. The difference between radiation equilibrium temperature and true temperature is attributed to low catalytic performance of the siliconized system. The low catalytic phenomenon retards recombination of dissociated molecules in the entry environment, thus reducing the heat load imposed at the material surface.

(3) Development of a zirconium-boron-silicon diffusion coating system that indicates high temperature performance half that of the siliconized system, but, evidently due to the boron constituent, possesses strength insensitive to low temperature oxidation. This coating, too, by virtue of the silicon addition has low catalyticity.

(4) Demonstration that a hafnium/tantalum coating, which converts to an oxide upon re-entry, has the potential of protecting RPP under multi-mission exposure to temperatures in excess of 4000°F. In contrast to the selected diffusion systems, the hafnium/tantalum coating is fully catalytic, thus reaching radiation equilibrium surface temperatures.

(5) Analysis of the low catalytic phenomenon to verify that the effect of reduced operating temperature observed in plasma arc testing is attributable to low-catalyticity. Furthermore, this analysis concludes that these same results will indeed be experienced by the shuttle leading edge materials in flight, and that the plasma arc testing conducted by VMSC is a good simulation of the actual entry conditions producing the phenomenon.

It is concluded that the high temperature, multi-mission requirements of the shuttle can be met by one of the three candidate RPP coating systems with continued development and refinement.

2.0 SUMMARY

Development of the thermal protection system for the space shuttle wing was performed as two major tasks, each proving mutually beneficial to the other. Design Synthesis produced initial conceptual designs and analyses that established materials performance goals, geometry constraints, and the relative importance of specific physical and mechanical properties to guide materials development. Armed with these guidelines, Materials Development and Evaluation efforts sought to produce oxidation inhibited RPP systems, meeting the contract goals that would prove to be practical solutions to the shuttle leading edge problem from performance, fabrication and cost considerations. Results of materials tests on candidate materials systems were in turn incorporated into concept refinements, where impact on leading edge design or the necessity for materials improvement were assessed. The design work thus assisted in establishing feasibility of employing inhibited RPP in realistic shuttle wing leading edge segments.

This combination of design and materials development efforts has yielded a leading edge system concept which is predicted to achieve a life of over 20 missions under worst stagnation heating conditions before leading edge segment replacement is necessary. This mission life is computed for VMSC siliconized RPP under environmental conditions producing 4000°F radiation equilibrium temperature at 0.8 emittance. Alternately, a 100 mission life is predicted for 3850°F equivalent radiation equilibrium temperature entry conditions. This capability is based on a design that promotes cross-radiation to reduce stagnation temperature, and on the direct application of the results of plasma arc testing; however, non-catalytic theory indicates even better performance is possible. Leading edge unit weight to achieve this performance is calculated to be under 2 lb/ft² of surface area.

The zirconium-boron-silicon diffusion coated RPP is predicted to provide half the mission life of the siliconized RPP but this system may ultimately be the better of the two because of its insensitivity to low temperature thermal cycling on strength.

Testing indicates the application of hafnium/tantalum to RPP will increase the surface temperature capability to higher than 4000°F, but data is insufficient to enable mission life predictions to be made.

This section of the report enumerates significant findings of the Phase I program and summarizes materials data and predicted system capability. Substantiating detail will be found in the design discussion of Section 3.0, materials synthesis and fabrication trials in Section 4.0, and the materials test results summarized in Section 5.0. Non-destructive test activities are documented in Section 6.0.

2.1 DESIGN SYNTHESIS

Design synthesis included the conception of possible leading edge designs, and the evaluation of these by thermal and structural analysis to select best approaches consistent with material capability. Functional elements of the leading edge, such as airload panels, support ribs, expansion joints, and support points were analyzed parametrically to establish trends and enable selection of optimum designs.

Design criteria, design conditions, and philosophy, compatible with Phase B shuttle requirements, were documented to provide uniform and consistent design criteria for the leading edge. Support in this endeavor was given by North American Rockwell. It was found that boost condition airloads at a maximum dynamic pressure of 610 psf design the lower airload panels. Maneuver loads of 2.5 g, during subsonic cruise when the structure is cool, produce critical loads for support ribs and the upper surface airload panels. Maximum temperatures and worst thermal gradients occur during entry, when airloads are minimal.

Baseline geometry around which design and analysis were conducted was based on the straight wing orbitor as generally configured in the contract work statement. The selected airfoil section, representing the region of maximum interference heating has a 214 inch chord and NACA 0012-64 airfoil. The front beam of the wing box to which the leading edge attaches was assumed to be at 15% chord. Designs, analyses, and material performance should be scalable to the delta wing orbitor and other wing section geometry.

Eight initial designs were conceived to establish the spectrum of functional elements for analysis. Evaluation criteria were itemized to assure consideration in the selection process of all aspects of design, fabrication, inspection, and operations.

Thermal analyses were conducted on various solid laminate and sandwich designs to define expected temperatures and thermal gradients; benefits of cross-radiation heat transfer from hotter to cooler regions were assessed; details of the leading edge to wing support joint insulation requirements were established to maintain wing structure within allowable temperature limits; and bare RPP surface recession during entry was computed to provide a basis of comparison with the enhancement afforded by coatings.

Structural analyses were devoted to determining optimum proportions for solid and sandwich laminates; sizing of functional elements to meet airloads requirements; and evaluating the significance and methods of reduction of thermoelastic stresses.

These analyses, based on best material property data available, resulted in the following important conclusions on which the current leading edge design concept is based.

(1) Cross-radiation permits a 370°F reduction of stagnation temperature under worst interference heating conditions and reduces RPP coating temperature requirements accordingly. Alternately, for a given coating, the mission life or temperature margin are increased for greater reliability.

These gains are achieved with solid laminate designs but sandwich configurations inherently block cross radiation and provide little temperature reduction.

(2) Cross-radiation reduces in-plane thermal gradients around the leading edge by 58% during heatup and 75% at maximum temperature under worst heating conditions. Again, solid laminate designs offer these advantages, but little benefit is gained with sandwich laminates. Designing for cross-radiation thus provides increased thermal fatigue life and/or greater reliability.

(3) Shingles or overlay coatings offer insignificant insulative capacity and could only serve to reduce the quantity of oxygen reaching the coated RPP beneath. This, however, may be a desirable attribute, but must be traded off against weight and cost penalties.

(4) Sandwich designs produce thermal gradients in the thickness direction of 500°F and 1500°F respectively for honeycomb and foam cores. By contrast, solid laminates 0.20 inch thick under the same conditions experience only 87°F gradients, and even with cross radiation develop only 278°F gradient. The lower gradient results in lower thermoelastic stress and greater reliability.

(5) Leading edge support point insulation requirements at nominal heating conditions are not severe. An insulator size of 1.0 inch diameter is sufficient to protect titanium support fittings on the wing structure to a maximum of 680°F.

(6) Coated RPP having a high modulus of elasticity and/or high coefficient of thermal expansion produce high thermoelastic stress. Designs based on materials of this type tend to require close rib spacing to reduce rib stresses to tenable values, while sandwich designs develop extremely high compressive stresses and appear infeasible. On the other hand, materials with low elastic modulus and/or low expansion coefficient are designed by airloads rather than thermal stresses. This allows wide rib spacing because rib height and load carrying capacity are no longer constrained by thermal stress considerations. A thermal stress parameter $\frac{F}{E\alpha} > 600^\circ\text{F}^*$ is required to avoid severe thermal stress problems.

(7) Diffusion coated laminates can be treated as a sandwich material with coating depth optimized on the basis of maximizing moment carrying capability per unit weight. This assumes density and stiffness of the coating exceed the values of bare material, and that failure is initiated in the coating. Where

*
$$\frac{\text{Allowable Stress, } F}{\text{Elastic Modulus, } E \times \text{Expansion Coefficient, } \alpha} = \frac{F}{E\alpha}$$

property differences between the coated layer and bare core are small, weight efficiency is relatively insensitive to coating depth.

Laminates of the prime candidate coating systems developed by VMSC in Phase I produce a thermal stress parameter, $\frac{F}{EX}$, of approximately 3000°F

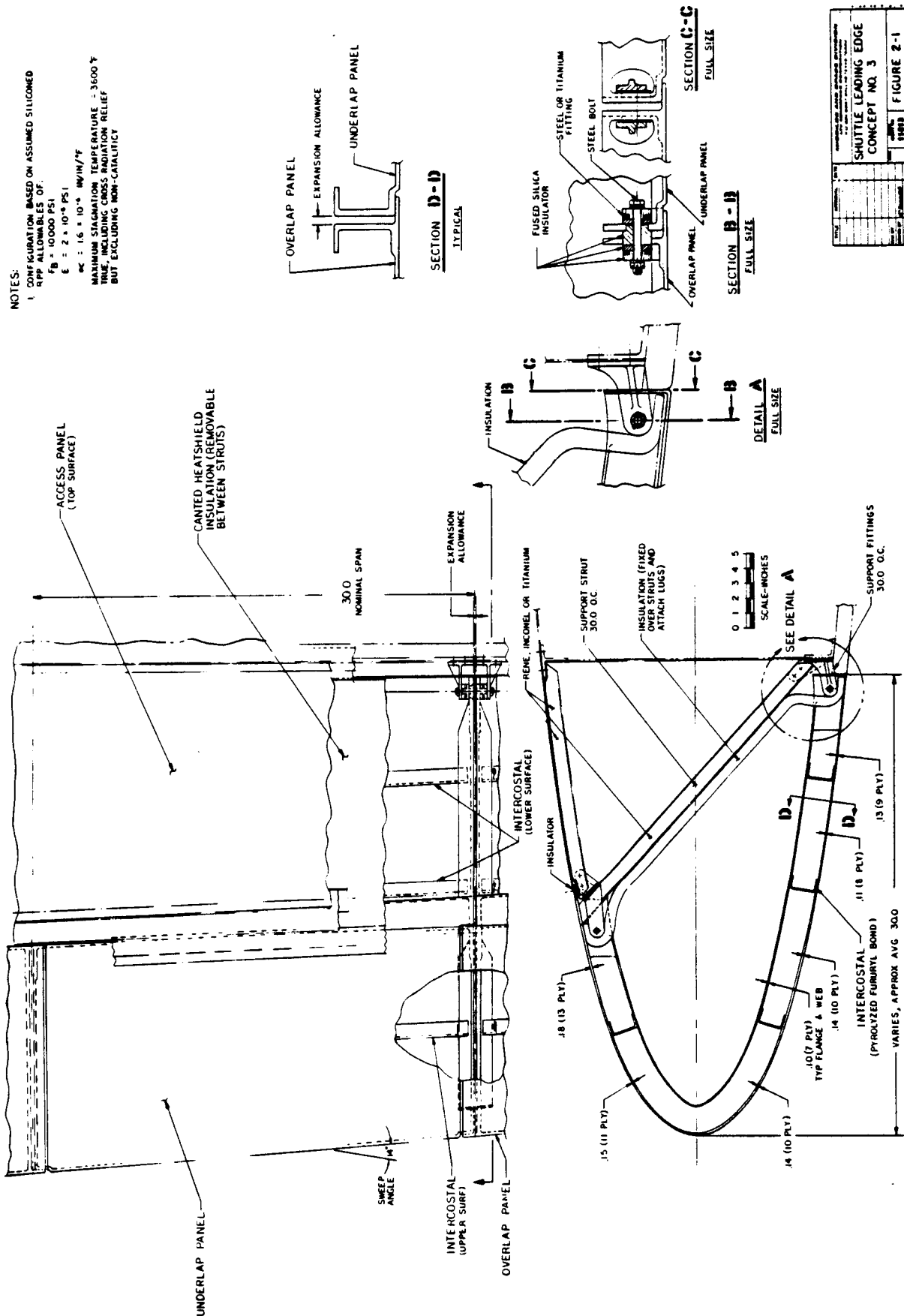
and exhibit properties that indicate coating values do not differ greatly from bare material. This indicates that thermoelastic stresses resulting from thermal gradients are not serious for these materials, and weight efficiency should be insensitive to coating depth.

However, where the coating is not defect free, and does not contribute significantly to laminate strength, a thin coating consistent with oxidation resistant requirements should yield the lightest structure with the highest strength. VMSC has established a goal of 0.015-0.020 inch for coating depth and assumes an erosion allowance of 0.010 inch. Less coating depth appears realistic on inside surfaces and those external areas not subject to maximum heating.

Concept No. 3, shown in Figure 2-1, illustrates the current design concept which has evolved from considerations of the above guidelines, design analyses, cost analysis, and materials performance. Design is based on material properties exhibiting bending strengths of 10,000 psi and elastic modulus of 2×10^6 psi, which are nominally consistent with VMSC coated RPP. It is a solid laminate design with thicknesses varying from 0.10 inch to 0.18 inch, except in the attachment area, where local thickening is assumed to increase bearing area. The segment span is 30 inches but greater spans appear feasible since VMSC coated RPP has a low coefficient of thermal expansion. This means that expansion joints may be more widely separated, but at a slight weight penalty. Ribs are formed integral with the airload panels to avoid joint problems where loads are transferred from the airload panels to the ribs. Intercostals break up the airload panels into smaller sizes to reduce weight and deflection. On the lower surface the intercostals are loaded by compression from the airload panels, thus minimizing joint peel problems. However, the upper intercostal is loaded by tension from the airload panels, thus presenting a joint application which requires investigation in Phase II. It is envisioned that peeling stresses can be alleviated by an intercostal formed from back-to-back channels or angle stiffeners. Neither location nor sizing of intercostals has been optimized. It is apparent that optimization could improve airload panel thickness variations and should result in a slight weight decrease. Current design weight is computed to be 1.8 lb/ft^2 including panels, ribs, intercostals, integral expansion joint seal strip, support fitting insulation and shear bolt. Neither the heatshield, heatshield insulation, nor wing support fittings are included in this estimate, since these are not a part of the current design scope.

Leading edge segments are alternately underlapping and overlapping. Thus a minimum of one and a maximum of three segments must be removed to replace a given segment. Attachment to the wing support structure is through

NOTES:
 1. CONFIGURATION BASED ON ASSUMED SILICOMER
 4PP ALLOWABLES OF:
 $E = 2 \times 10^{-6}$ PSI
 $\alpha = 1.6 \times 10^{-6}$ IN/IN/°F
 MAXIMUM STAGNATION TEMPERATURE = 3600 °F
 TRUE, INCLUDING CROSS RADIATION RELIEF
 BUT EXCLUDING NON-CATALYTIC



SHUTTLE LEADING EDGE CONCEPT NO. 3	
DATE	FIGURE 2-1
REV	
APP	
CHK	
DES	
DRW	
ENG	
MAN	
PROJ	
SCALE	
UNIT	
NO.	
REV	
DATE	
BY	
CHK	
APP	
DATE	

FIGURE 2-1 SHUTTLE LEADING EDGE CONCEPT NO. 3

insulated shear joints, two at the lower side and two at the upper surface per segment. Each panel is secured to the support structure at one panel edge, while the opposite edge is free to slide on the insulator to accommodate relative thermal expansion.

The trim line of the upper surface of the leading edge has been arbitrarily set at about 6 1/2% of the chord. This permits utilization of lower weight uncoated metal in those areas where it can be employed practically. In addition, the coated heatshield is envisioned as an aid to concentrating heat from the lower surface to the upper forward region of the leading edge to reduce circumferential thermal gradients and attendant thermal stresses.

VMSC believes that the design approach, as conveyed by Concept No. 3 represents a reasonable and practical concept for application to the shuttle leading edge. The concept offers light weight, ease of fabrication, ability to inspect all areas between flights, and is a low cost approach. The thickness of the airload panels provide a degree of oxidation protection against catastrophic failure in the event of coating burn-through during re-entry.

2.2 MATERIALS DEVELOPMENT AND EVALUATION

Materials development included both the evaluation of RPP substrates and oxidation inhibitors for RPP substrates. Substrates were assessed on the basis of fabricability and strength in the bare and siliconized coated condition. Coatings were rated according to fabricability, high and medium temperature oxidation resistance, and flexure strength.

Substrates - Seven substrates were examined as follows:

- (1) WCA graphite cloth
- (2) VCA carbon cloth
- (3) VYB carbon filaments, cross ply layup
- (4) Kreha KGF-200 carbon filaments, cross ply layup
- (5) Modmor II high modulus graphite filaments, cross ply layup
- (6) Hyfil high modulus graphite filaments, 0°, 45°, 90°, and 0°, 30°, 60°, 90° layup
- (7) Supertemp laminate

The WCA laminates performed satisfactorily through all steps of processing, including siliconizing, and remains the prime VMSC candidate for shuttle application. Complete processing, however, on all of the substrates was not accomplished in Phase I. Because some of the untested substrates have higher strength in the bare condition and for other technical considerations discussed below, it is recommended that evaluation be continued in Phase II to determine their performance with respect to WCA in the coated state. It is the strength properties in the coated and not bare condition that are meaningful for multi-mission shuttle application.

In Phase I comparative evaluations, VCA carbon cloth bare laminates were 31% stronger than WCA, but in the coated condition WCA was superior to the best VCA tested by 56%.

Two VYB panels were fabricated: The first exhibited very low strength due to a processing problem, while the second arrived at VMSC too late to complete processing through coating. Evaluation should continue in Phase II.

Like the VYB, a Kreha KGF-200 panel fabricated from Japanese fibers arrived too late for final coating evaluation and should be completed in Phase II even though after final pyrolysis, bare strength was about the same as WCA laminates.

Two Modmor II panels were evaluated. The first (molded at 80 psig) delaminated badly during densification and ~~strengthening~~ processing, which involves re-impregnation with furfuryl alcohol and re-pyrolysis. The second panel molded at higher pressure (175 psig) than the first, also delaminated during densification but only at the mid layer. This indicated considerable improvement. (Additional resin/molding pressure variations could be expected to correct this.) Subsequent siliconizing appeared to have no detrimental effect on the laminate and is very encouraging. The delamination prevented meaningful strength data from being obtained. From a technologies standpoint, further examination of the Modmor II is recommended in Phase II. A candidate application for this material is in local ~~strengthening~~ or stiffening of WCA laminates by effectively building a sandwich panel with WCA as the center plies.

Two Rolls Royce Hyfil panels were processed through densification but partially delaminated. Then, upon siliconizing, delamination was severe indicating gross mismatch problems.

Super-Temp laminates have a high density (1.6 g/cc) and a strength level about equivalent to the 20-22,000 psi that can be obtained with WCA. Initial attempts to coat this material with VMSC's siliconized coating produced poor penetration but continued examination of this material is recommended because of its advertised compatibility with silicon carbide coatings.

Oxidation Inhibitor Trials - Bare RPP was found to offer only a one or two mission leading edge segment life. It was, therefore, necessary for coating systems to improve on this significantly to make the pursuit of coating development worthwhile. Eight material elements formulated in a variety of compounds were studied to select best coating systems for RPP. Their incorporation with RPP to achieve oxidation inhibition took the following forms:

(1) Add-mix systems, wherein the metal powder constituents are mixed with the resin during initial panel layup, and subsequently reacted at

temperature to produce oxidation resistant compounds.

(2) Diffusion systems where the coating constituents are diffused into and reacted with the RPP. VMSC diffusion coatings employ pack cementation of slurried constituents.

(3) Combined systems that introduce one metal constituent into the RPP as in the add-mix approach, while the other constituent is diffused into the RPP and reacted with the carbon and first metal powder.

(4) Overlay systems that provide an oxide layer over the top of one of the above coating systems to enhance oxidation resistance performance.

The add-mix laminates proved to have both low strength and plasma arc test performance inferior to the diffusion systems. This is graphically illustrated by the data in Figures 2-2 and 2-3 obtained during initial screening of candidate coatings. Add-mix laminates are seen to produce less than half the strength level of their diffusion coated counterparts. Add-mix panels were not fabricated for the silicon or tantalum/silicon systems. Plasma arc performance of coated RPP is compared in Figure 2-3 against bare RPP at the flux level used for screening. The add-mix systems produce limited improvement over bare material but the benefits to be derived from diffusion systems are more evident.

Combined systems employing zirconium diboride, zirconium hydride, and titanium with a diffusion coating of silicon failed to survive the siliconizing processing. Cracking and delamination were severe so work on those systems was discontinued.

It was felt that further exploration of the add-mix and combined systems would produce significantly improved results. However, pursuit of those approaches was stopped due to schedule and funding limitations and because of the superior performance demonstrated by diffusion coatings. Accordingly, emphasis was placed on (1) modifying and improving the siliconized coating, which showed exceptionally good oxidation resistance in the plasma arc, and (2) a coating comprised of zirconium, boron and silicon constituents. The latter coating system received attention primarily because of the postulated performance that these constituents should produce. The boron addition was expected to provide oxidation resistance at moderate temperatures (below 2000°F), the silicon was included for the temperature range up to 3200°F, and the zirconium was expected to perform at higher temperatures. These elements are reacted during processing and appear as compounds such as carbides, oxides, and diborides.

One challenge associated with RPP and coated materials in general is brittle fracture behavior. Coated RPP was found to fail in a quasi-plastic manner exhibiting limited "yielding", although failure is actually taking place.

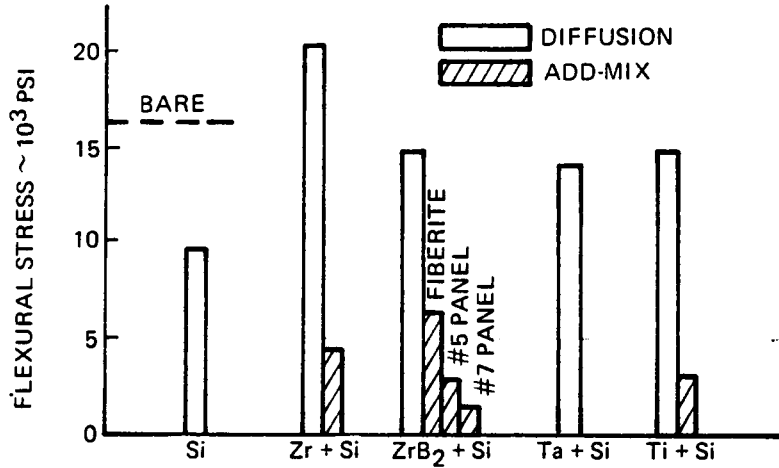


FIGURE 2-2 AVERAGE FLEXURAL STRENGTH DIFFUSION AND ADD-MIX SYSTEMS SCREENING TESTS

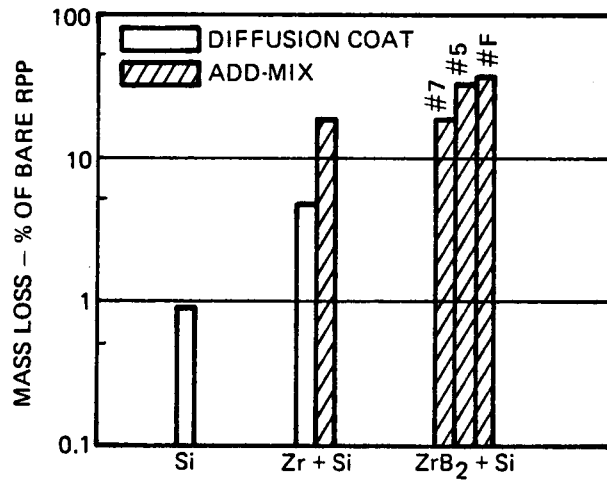


FIGURE 2-3 PLASMA ARC TEST MASS LOSS SCREENING FLUX, $\dot{q}_c = 160$ BTU/FT²-SEC

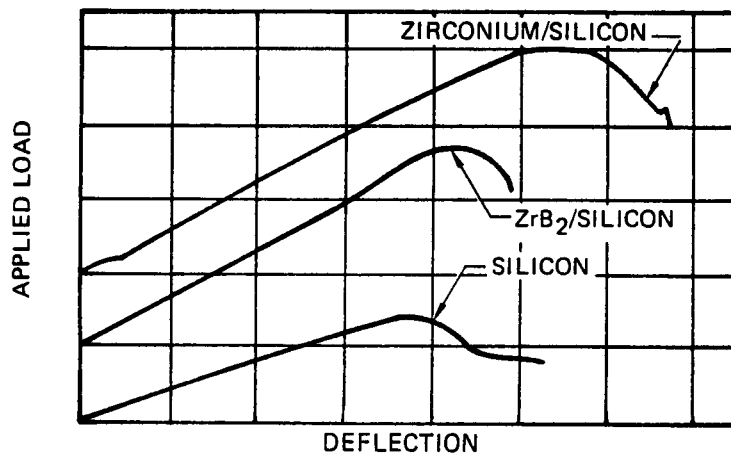


FIGURE 2-4 TYPICAL LOAD-DEFLECTION CURVES DIFFUSION COATED FLEXURE BARS SCREENING TESTS

This is illustrated in Figure 2-4 where flexural load-deflection curves of typical diffusion coating systems are shown. In redundant load path structure, such as the airload panels, this behavior permits some degree of load redistribution near the point of failure and could prevent catastrophic collapse of the structure. The exact degree of benefit available from this feature is a matter of specific application and analysis.

Modifications to the silicon system took two paths: (1) attempts to produce a greater proportion of alpha-phase silicon carbide to hopefully gain higher temperature oxidation protection than obtained with the predominantly beta-phase, and (2) attempts to improve coating fabricability by enhancing both part removal from the pack and specimen cleanup. Alpha phase silicon carbide was produced by both siliconizing at 4000°F, and siliconizing at 3400°F with subsequent heat treatment at 4000°F. Unfortunately, plasma arc testing showed inferior performance compared to the siliconized RPP processed at 3400°F, so that further pursuit of the alpha-phase was discontinued.

Fabrication improvement trials proved highly successful where recovery of testable specimens from the cementation pack was increased from a low of about 50% to the current 100% recovery. This was achieved without a loss in oxidation resistance and was accomplished primarily through substitution of silicon carbide pack material for alumina. Alumina, which is apparently necessary for maximum coating performance is retained as an ingredient in the slurry applied to the specimens.

Examinations of the zirconium-boron-silicon system were based on a two-stage diffusion coating. Either the boron or zirconium were applied first with the remaining ingredients applied in a second application. It was found that zirconium would not readily diffuse into RPP so this approach was abandoned. Boron on the other hand moved freely into the RPP.

The composition of the zirconium/silicon slurry second layer was varied over wide limits in an effort to discover a technique of introducing zirconium into the system. Compositions rich in zirconium failed to penetrate the RPP, such that very little zirconium was obtained. At the other end of the scale, where the slurry was rich in silicon, greater amounts of zirconium were discovered in the specimens. The best composition examined was a slurry comprised of 75 wt. % silicon and 25 wt. % zirconium. This system performed only half as well as the siliconized system in plasma testing and, although a zirconia rich surface layer develops during plasma exposure, the system remains in the low catalytic region. Characterization data was obtained on this system because of its good oxidation performance and strength characteristics.

Characterization of Diffusion Coated Oxidation Inhibitor Systems - The two candidate diffusion coating systems, siliconized RPP and zirconium-boron-silicon coated RPP, were characterized with respect to the following:

- (1) High temperature oxidation resistance in a plasma arc simulating entry conditions.
- (2) Flexure testing at -250°F , R. T., 1400°F , 2700°F , and 3100°F .
- (3) Flexure testing at R. T. after 10 load cycles at 55% of average room temperature failing stress.
- (4) Flexure testing at R. T. after exposure to one, five, and ten thermal cycles to 2300°F of approximately 20 minutes duration in an air furnace.
- (5) Coefficient of thermal expansion from -250°F to 3600°F .
- (6) Thermal conductivity parallel and perpendicular to the laminate from R. T. to 3000°F .
- (7) Emittance at 3000°F .

Significant results of this testing are discussed below. It was discovered that the siliconized system has a potential deficiency as a result of the 2300°F thermal cycling and should be improved. The zirconium-boron-silicon system on the other hand was insensitive to thermal cycling, evidently due to the boron ingredient. In fact the average failing stress remained essentially constant throughout the temperature range. It was postulated that a system incorporating only the boron and silicon would produce a coating exhibiting the best high and low temperature properties of both characterized coatings. However, attempts to achieve this goal were not concluded at program's end. Further investigation of this approach is recommended for Phase II.

Plasma arc test data for the siliconized and zirconium-boron-silicon (Zr-B-Si) systems are summarized in Figures 2-5 and 2-6. These curves are in the form normally used for presentation of plasma arc data, where the correlation parameter is mass loss divided by heat transfer coefficient. The data plotted is the result of exposure to the plasma arc test conditions in five minute increments. Numbers adjacent to the points indicate the particular exposure represented by the data point, whether it be the first, second, third or fourth.

The siliconized RPP data on Figure 2-5 shows two siliconized coatings. An earlier version represented by the upper data is the result of VMSC tests.

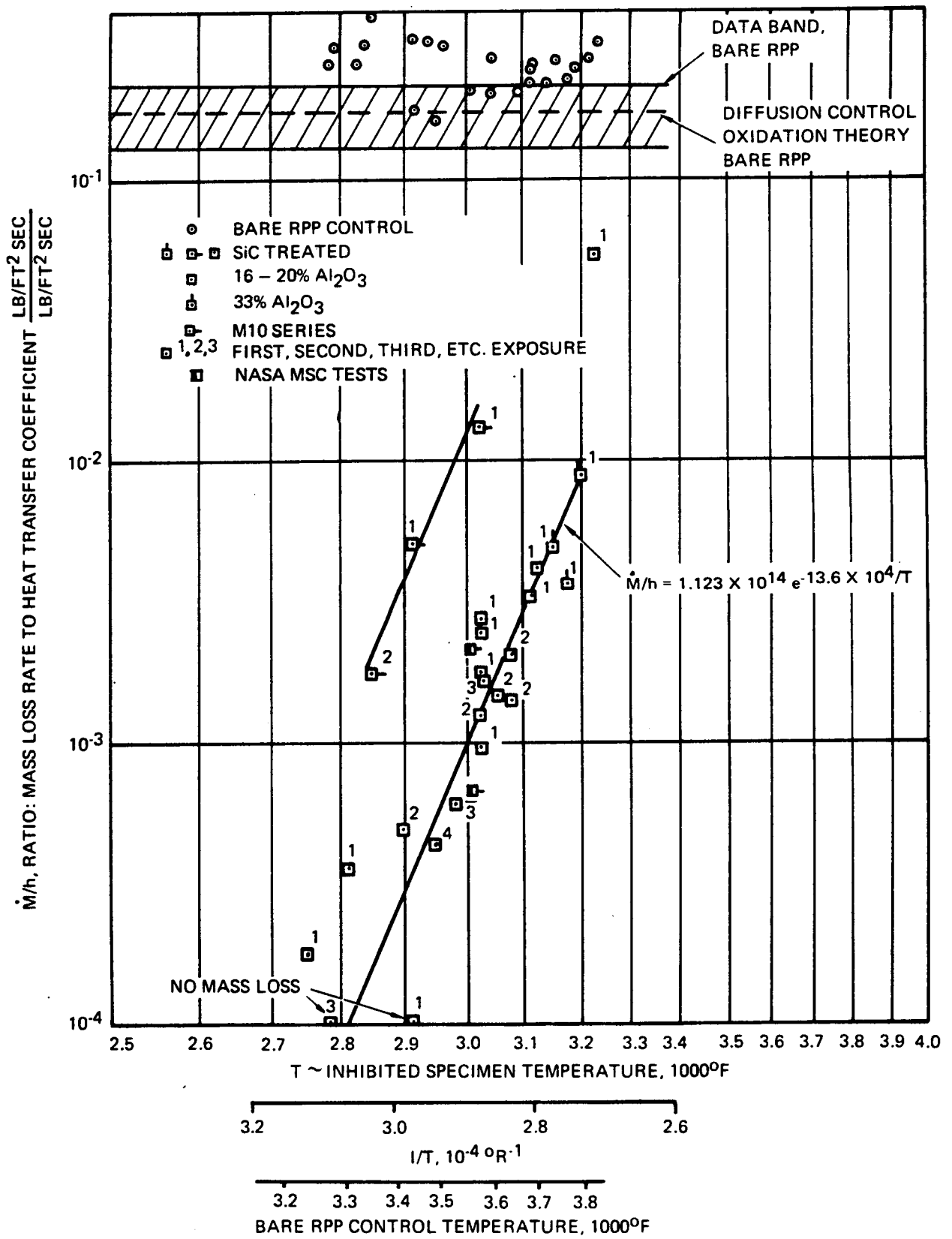


FIGURE 2-5 PLASMA ARC TEST, MASS LOSS DATA SILICONIZED RPP

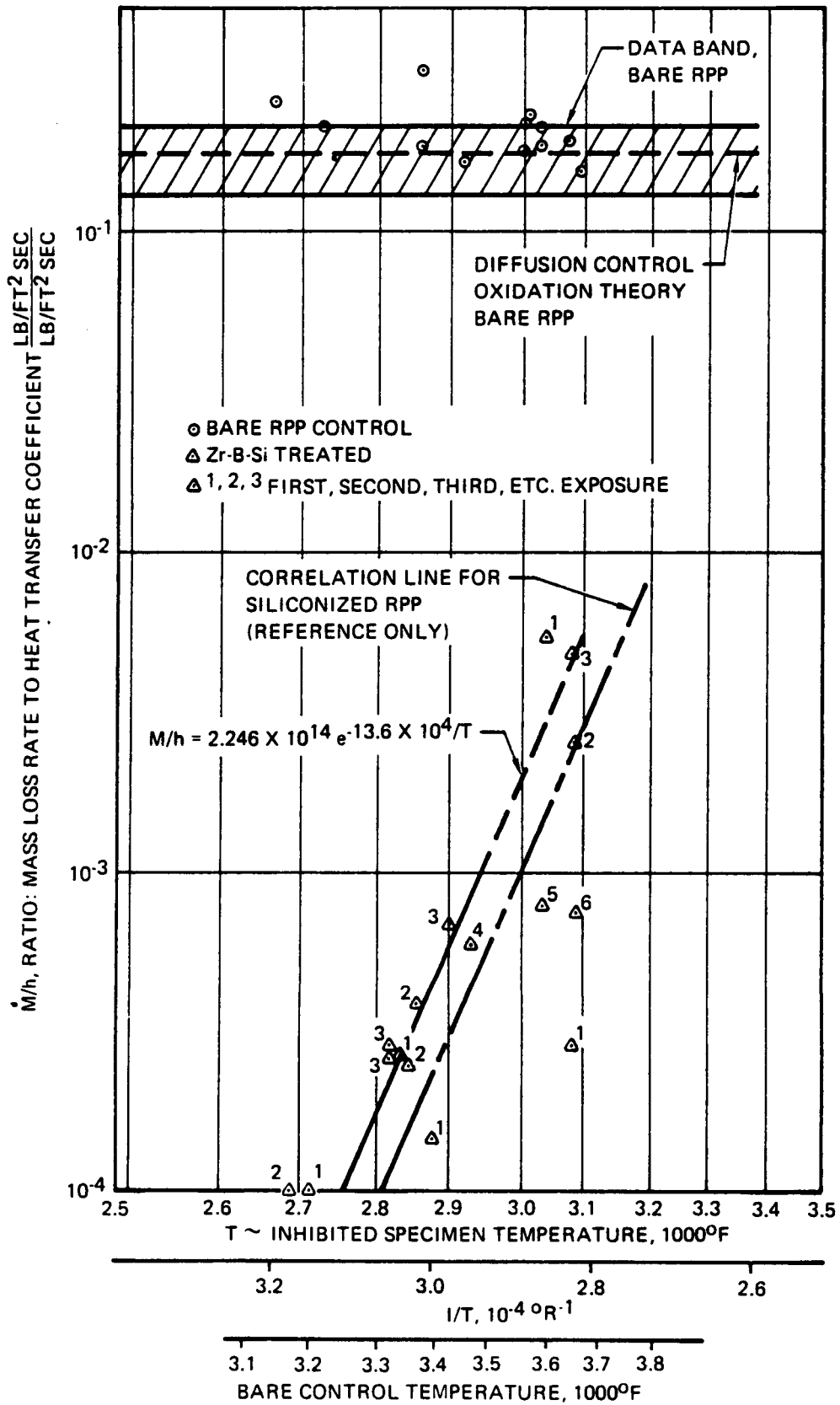


FIGURE 2-6 PLASMA ARC TEST, MASS LOSS DATA Zr-B-Si TREATED RPP

Under NASA-MSD tests of this same system little weight loss and no surface recession were recorded after 40 minutes exposure to a heat flux level of 100 Btu/ft² sec that produced 3000°F surface temperature in an equivalent 3550°F radiation equilibrium environment. Another sample burned through within about 100 seconds after exposure to 126 Btu/ft² sec. Surface temperature reached 3220°F, where coating degradation is expected. The vast improvement realized from the latest siliconized system with different processing is evident by the lower set of data.

The Zr-B-Si system in Figure 2-6 shows high temperature performance less dramatic than the siliconized system but still providing good mission life. This is illustrated in Figure 2-7 where predicted mission life for each coating is plotted against bare RPP surface temperature. Bare RPP temperature represents radiation equilibrium temperature as determined from VMSC plasma arc testing, where bare RPP is used for controls data.

The mission life prediction is established by integrating the mass loss rates of Figures 2-5 or 2-6 over the entry trajectory to determine single mission mass loss and surface recession (assuming all mass loss is the result of surface recession). Further, assuming that 0.010 inches recession at the stagnation point for 0.020 inch thick coatings constitutes leading edge segment life, the number of missions before segment replacement is required can be computed. It has been calculated that mass loss during one mission is equivalent to a square heating pulse of 105 sec duration at the maximum temperature under VSMC plasma arc test conditions. Thus, the 15 minute exposure in three separate cycles normally employed by VMSC in the plasma arc for testing coating systems, actually is equivalent to slightly over 8.5 missions.

Utilizing the calculated 370°F reduction from cross-radiation for Concept No. 3, it is seen that for entry conditions equivalent to 4000°F radiation equilibrium temperature, a mission life of 24 is predicted for siliconized RPP and 12 for Zr-B-Si coated RPP. This is subject to error since it is based on extrapolation of test specimens with three exposures (8.5 missions) each. Additional testing is required to better define leading edge segment life. However, current data is encouraging and generally shows that mass loss on second and third exposure is less than on first. Similarly, for a 100 mission life requirement and again assuming 370°F benefit from cross-radiation an allowable radiation equilibrium temperature of about 3870° is indicated for siliconized RPP and 3800° F for Zr-B-Si RPP. It is interesting to note that for the straight wing orbiter North American Rockwell computes a maximum stagnation temperature of only 3290°F for a nominal reentry. Thus, the apparent temperature margin is 510-580°F, depending on coating system, for a 100 mission life requirement for the shuttle leading edge and nominal interference heating predictions.

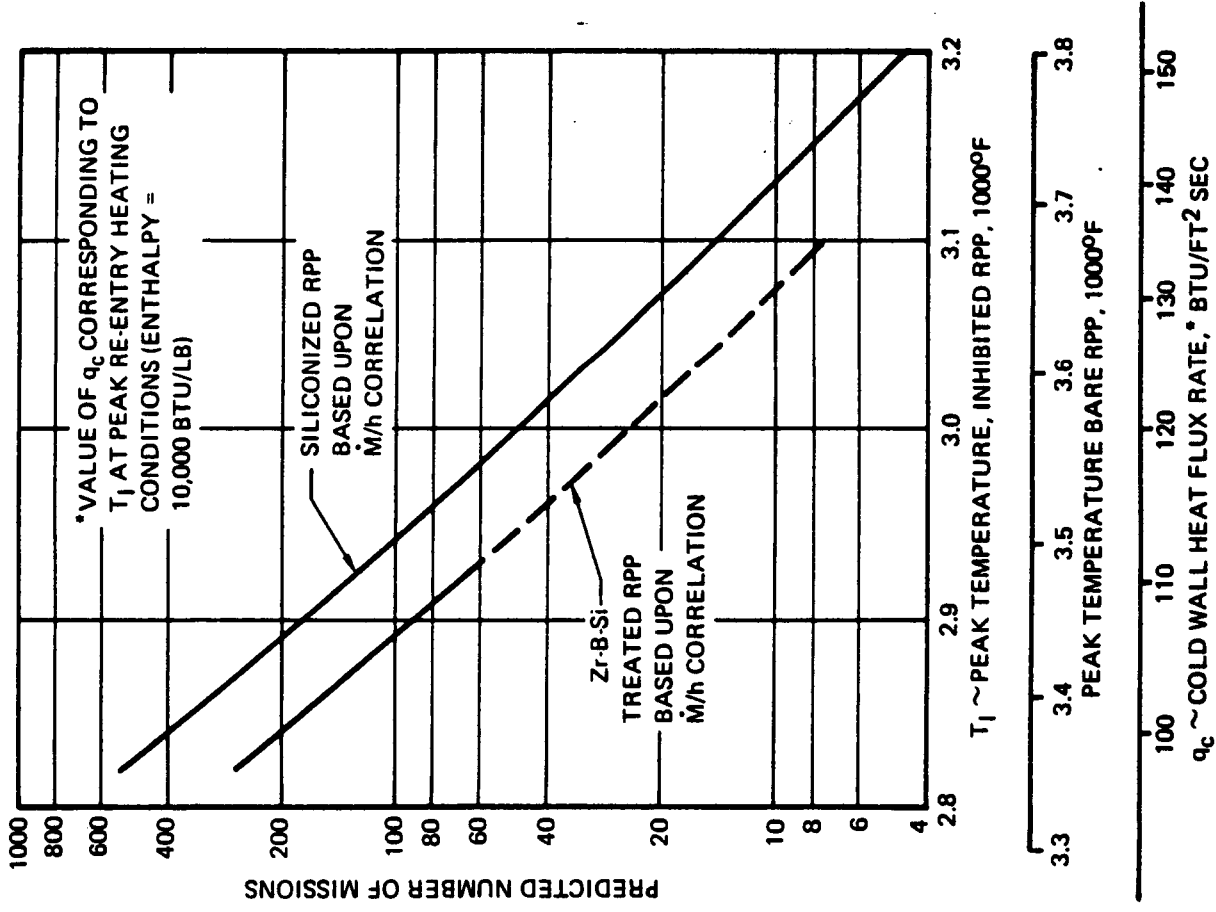


FIGURE 2-7 PREDICTED MISSION CAPABILITY - INHIBITED RPP

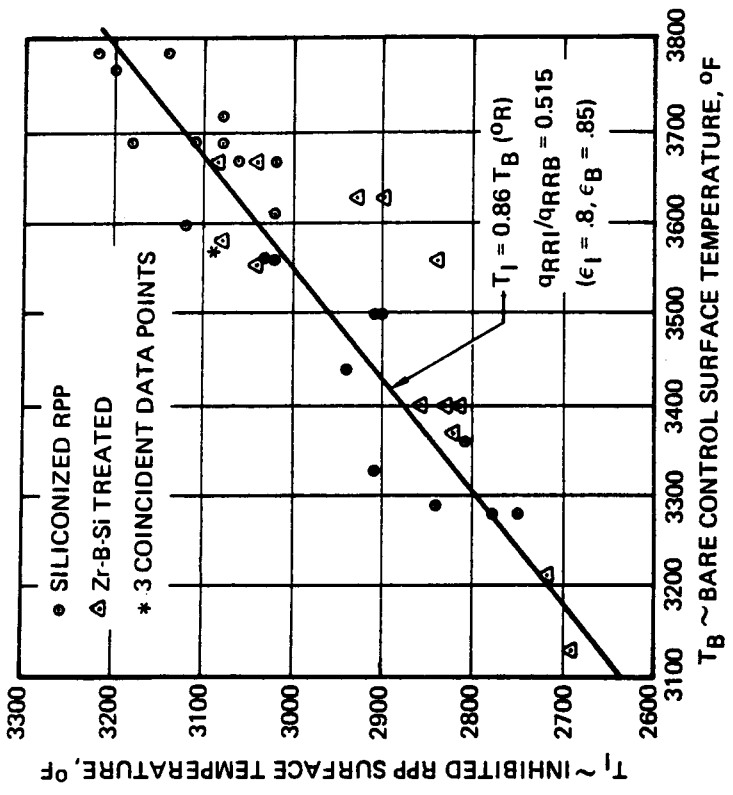


FIGURE 2-8 CORRELATION OF INHIBITED AND BARE PLASMA SPECIMEN TEMPERATURES

The major contribution to the exceptional high temperature oxidation resistant performance of these two coatings is low catalysis exhibited by both systems. This is believed due to the silicon content, although the exact nature of the involvement is not yet known. A low catalytic material is one that suppresses the recombination of disassociated atoms in the non-equilibrium and frozen flow regimes during entry. This suppression thus relieves the surface material from experiencing the heat of recombination and results in a lower heat flux being imposed on the leading edge material. The leading edge, therefore, operates at temperatures considerably below radiation equilibrium, and permits the VMSC diffusion coated systems, which have a surface temperature limitation of about 3200°F, to operate in entry environmental conditions producing significantly higher radiation equilibrium temperature. The correlation curve is shown in Figure 2-8 where the fully catalytic bare RPP temperature is taken as equivalent to radiation equilibrium. Under identical conditions, the coated material consistently operates 14% or several hundred degrees cooler than bare RPP.

Analysis of this phenomenon in the entry environment and correlation with theory indicates that low catalyticity and low surface temperatures will indeed be experienced on the shuttle during entry and that it is not a marginal condition for the pressures and leading edge geometry typical of the shuttle. This subject is so significant that a detailed presentation of the theory and analysis of the phenomenon is given in Section 5.3.

Downstream effects on catalytic materials located behind non-catalytic materials was examined briefly for entry conditions producing 3500°F stagnation radiation equilibrium temperature. Indications were that at the 15% chord location, a temperature increase of 300°F to a value of 2680°F would be reached by the catalytic material. Alternately, extending the non-catalytic material 12 inches farther aft would reduce the temperature of the catalytic material back to the original 2380°F limit. This would appear to be a tenable situation for shuttle design, but additional in-depth analyses of this effect should be conducted.

The results of flexure testing of the siliconized RPP and the Zr-B-Si coated RPP are summarized on Figures 2-9 and 2-10. The cross-hatched portion of the bars on the figures illustrate the range or scatter of data obtained. Both VMSC and Southern Research Institute (SRI) conducted the tests as indicated.

Focusing on the siliconized system it is encouraging that the strength at low and room temperature conditions average 12,400 psi. Ten-cycle fatigue strength at 55% of the average room temperature failing load shows a slight 10% decrease in strength when loaded to failure. The selected load level is based on establishing a limit allowable stress level by assuming 20% data scatter and 1.5 ultimate factor of safety. The strength loss is attributed

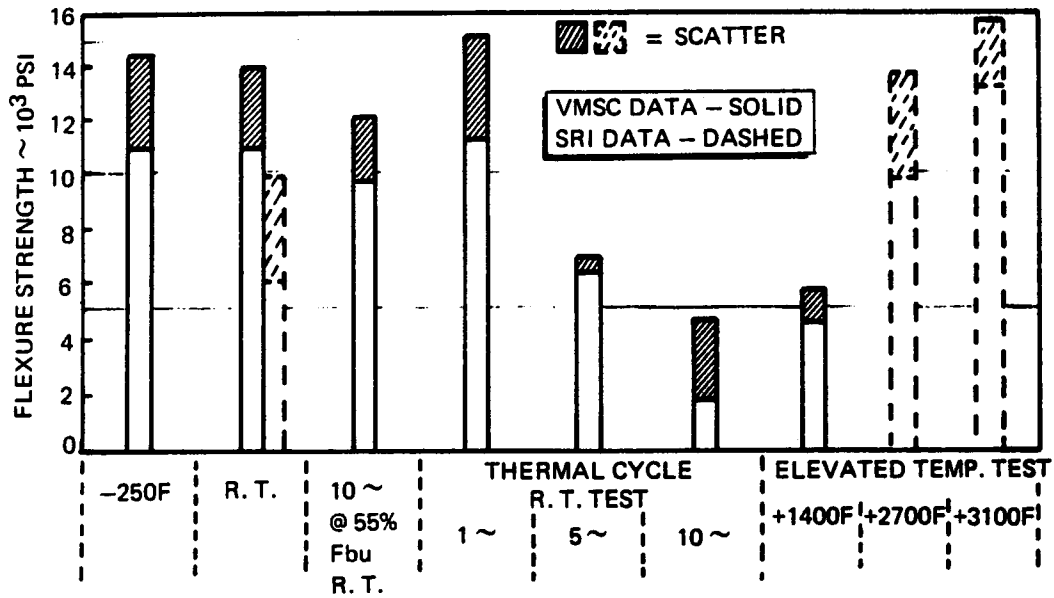


FIGURE 2-9 SILICONIZED RPP FLEXURE STRENGTH SUMMARY

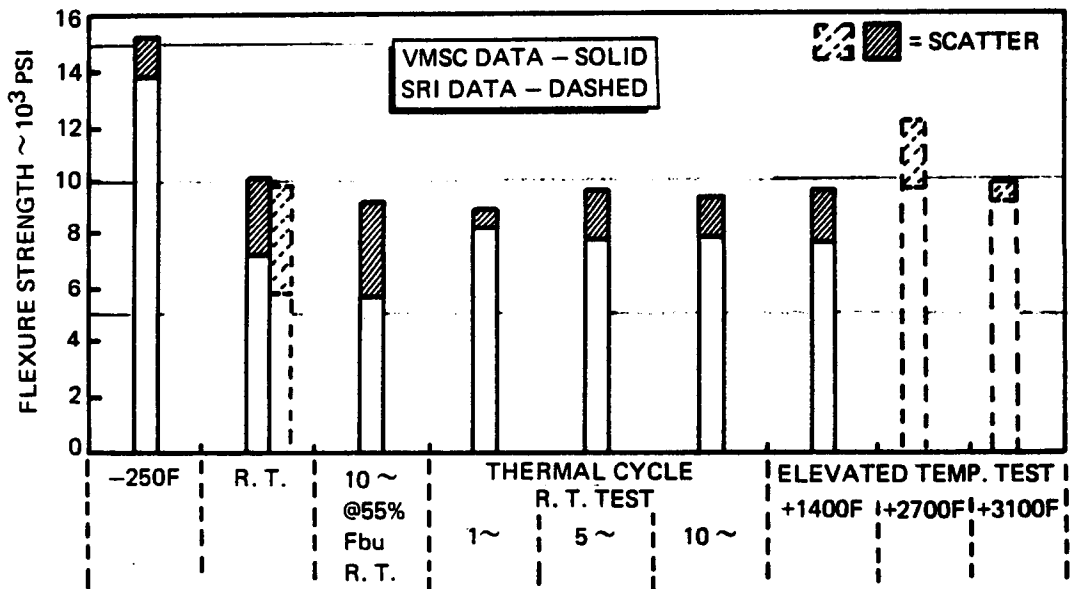


FIGURE 2-10 BORON-ZIRCONIUM-SILICON COATED RPP FLEXURE STRENGTH SUMMARY

in part to the possibility of coating crazing or cracks, which may reduce fatigue life and identifies an area for concentration in Phase II to improve fatigue strength. Thermal cycling data is disappointing. While the test, which was conducted in air at one atmosphere, is considered conservative relative to actual flight conditions, it points up a potential deficiency in the siliconized coating. It is believed that this can be corrected with the addition of boron; however, studies of this approach were not completed. It is recommended that this work continue in Phase II.

The elevated temperature strength of the siliconized system is roughly equal to the room temperature strength attained. However, at 1400 F the strength is less than half of the room temperature value. It is postulated that this is the result of large differential between expansion coefficients of the core and face material in this temperature region, which could induce high tensile stresses in the core. This would have the effect of reducing the amount of bending stress that could be carried by the core in combination with the induced tensile stress and result in a low calculated bending stress allowable.

By contrast the Zr-B-Si coating appears completely unaffected by thermal cycling and adds credence to the belief that the boron addition provides the low (under 2000°F) temperature protection. In addition, the Zr-B-Si system retains its strength at elevated temperature throughout the temperature range of testing. The coating on which this data was obtained was rough appearing partly because the initial boronizing treatment was not as uniform as on previous trials. It is felt that improved strength and particularly better fatigue strength will follow with more uniform coating. The high strength at -250°F may illustrate the potential for this coating system. It is difficult to conceive that temperature effects alone could produce the strength increase at low temperature for the materials involved, yet examination of other factors such as specimen location in the pack during coating, test equipment or technique, and moisture (ice) entrapment do not suggest an answer. The siliconized system was unaffected by cryogenic temperature. Additional examination of this effect is suggested because it may be possible to take advantage of this feature to increase room temperature strength.

In general both the VMSC and SRI flexure tests showed that the Zr-B-Si coated RPP failed in the quasi-plastic manner discussed previously while the siliconized RPP tended to experience a more brittle fracture. Room temperature tests of siliconized RPP produced load deflection curves that indicated increased stiffening at the higher load levels. At elevated temperature, however, the stress-strain curves for both coating systems showed a high initial modulus followed by a lower secondary modulus. This is believed due to the differential expansion between the coated faces of the laminate and the bare core, producing a preload compression stress in the face material. This apparently has the effect of stiffening the material at lower bending stress levels, but once the preload is relieved by tension the laminate stiffness is reduced and a lower elastic modulus results.

The strength and plasma arc test results of the two coating systems were very encouraging. They indicate that a marriage of the two coatings would produce a system with good strength, unaffected by thermal cycling or elevated temperature, and would have superior high temperature oxidation resistance.

Thermal expansion data obtained for both coating systems shows little difference from bare RPP. In the warp direction at 3500°F for example, bare RPP, Zr-B-Si coated RPP, and siliconized RPP have 1.6×10^{-6} in/in/°F, expansion coefficient. This value is lower than expected for coated material and minimizes thermal stresses produced from thermal gradients.

Emittance data obtained for the candidate coating systems at 3000°F shows values 0.82 and 0.84 for the Zr-B-Si and siliconized RPP, respectively, which is in the range used in evaluation of plasma arc data.

Conductivity of the siliconized RPP was found to be significantly lower below 2000°F than the values assumed for analysis, which would have the effect of increasing circumferential thermal gradients slightly. However, above 2000°F conductivity was higher than assumed. This would tend to lower stagnation temperature and make current predictions slightly conservative.

Hafnium/Tantalum Coating - An 80-weight percent hafnium, 20-weight percent tantalum coating system successfully protected bulk graphite from oxidation at temperatures up to 3300°F in tests conducted by the LTV Research Center several years ago. This same coating system offered the potential for providing 4000°F oxidation resistance to RPP material. Initial coating trials conducted on bare RPP were highly successful. The coating was applied by a melt technique and was found to thoroughly wet and flow onto and into as-pyrolyzed RPP. Under entry environmental exposure the coating converts from the metal to the metal oxide and provides the high temperature oxidation protection mechanism. In plasma arc testing a sample of this system was exposed to five cycles at 140 Btu/ft² sec heat flux level for a total of 25 minutes (equivalent to 14 missions) and then subjected to a heat flux of 100 Btu/ft² sec for another five minutes. Surface temperature reached a maximum of 4180°F. Total weight loss was minimal, being only 1% of the original weight, and upon cross-sectioning no indication of substrate attack was observed. The oxide coating remained strong and adherent to the substrate.

While the test experience with the hafnium-tantalum on bare RPP is very limited, the outstanding performance exhibited thus far in plasma arc tests suggests that emphasis be placed on this coating system in Phase II. A more thorough evaluation of the potential of the coating is required, since time did not permit this in Phase I.

Non-Destructive Test (NDT) - NDT was conducted in Phase I to (1) begin to establish a backlog of data on RPP and coating systems, (2) to support the materials development effort through identification of in-process defects, and (3) to determine best NDT techniques for specific defects. X-ray radiography, ultrasonic pulse-echo, infrared, low frequency sound and eddy current approaches were examined. X-ray and ultrasonic through transmission provided the best results, although infrared techniques correlated well with the other two.

It was found that the use of an x-ray attenuator, such as carbon tetrachloride absorbed into the RPP, provided considerable enhancement to the x-ray technique and readily permitted identification of porous or delaminated areas. Evaluation of the effect of carbon-tetrachloride on bare and coated RPP showed no evidence of degradation.

Ultrasonic c-scan has been used as a backup to x-ray radiography and in at least one instance, was able to correct a false indicator exposed by x-ray, when the "defect" was found to be carbon-tetrachloride which had flowed under adherent pack material.

NDT in Phase I has been more exploratory, but in Phase II additional data will be gathered to enable the eventual establishment of NDT standards.

In summary, VMSC believes that the designs and material systems produced in Phase I offer the potential for meeting shuttle leading edge requirements with continued refinement. Fabrication techniques, materials and designs are straightforward and should lead to the lowest cost approach, while yielding low weight.

2.3 CONCLUSIONS AND RECOMMENDATIONS

(1) Design, analysis, materials development, and element test evaluation show that oxidation inhibited carbon-carbon RPP systems are feasible and attractive for the Shuttle leading edge requirements.

(2) Solid laminate leading edge designs offer a stagnation temperature reduction of several hundred degrees fahrenheit through the mechanism of cross-radiation.

(3) The VMSC leading edge concept is computed to weight 1.8 lb/ft^2 of surface area and would not exceed 2.5 lb/ft^2 even if a 50% tolerance on allowable stress were assumed.

(4) VMSC's proposed siliconized and Zr-B-Si coated RPP systems repeatedly operate at temperatures 14% below those of bare RPP. This is attributed to low-catalytic behavior and is a major factor in the high temperature capability of the VMSC diffusion coating systems.

(5) Analysis of the low-catalytic phenomenon and correlation with test data indicate that the low-catalytic materials will indeed exhibit this property in the shuttle entry environment. VMSC plasma arc testing is a close representation of the critical entry environment conditions.

(6) Siliconized RPP and Zr-B-Si coated RPP developed by VMSC, coupled with the proposed leading edge concept, have the high temperature oxidation resistance to achieve multi-mission capability under shuttle entry environments producing 4000 F radiation equilibrium temperature.

(7) Diffusion coated WCA graphite cloth laminates develop sufficient strength even at this early stage of development to produce competitive leading edge unit weight.

(8) Flexure strength of Zr-B-Si coated RPP is insensitive to low temperature oxidation. By contrast siliconized RPP has shown sensitivity to the same test conditions and requires more thorough examination to ensure realistic testing and evaluation.

(9) The siliconized and Zr-B-Si coated RPP exhibit low elastic moduli and low expansion coefficients which minimize thermoelastic stress. Each offers relatively high emittance and high thermal conductivity which minimizes both peak temperature and thermal gradients.

(10) The hafnium-tantalum coating system on as-pyrolyzed RPP offers the best multi-mission catalytic coating system tested for temperatures up to 4000°F.

It is recommended that:

(1) The low-catalytic phenomenon, produced by the VMSC siliconized and Zr-B-Si system, be exploited for the shuttle application.

(2) The siliconized and Zr-B-Si coating systems be developed and refined in Phase II.

(3) The hafnium-tantalum coating be evaluated more thoroughly in Phase II in an effort to develop this catalytic system.

3.0 DESIGN SYNTHESIS

Design synthesis was devoted to the generation and evaluation of realistic leading edge design concepts as an aid to channeling materials development in meaningful directions. Conceptual design and thermal and structural parametric analyses determined such design aspects as preference for solid laminates over sandwich configurations; thickness limits for realistic structure; coating depths desired for structural efficiency; the relative importance of specific properties, such as emittance, conductivity, elastic modulus, and flexure, compression or tensile stress; sensitivity of variations in certain properties on design efficiency; and the shape, size and structural configuration of best leading edge concepts. These data guided the materials effort in establishing material property goals, property data to emphasize, specimen thickness to employ, processes amenable to full scale hardware, and process variables.

3.1 DESIGN CRITERIA

Design criteria were specified by reference (3) to provide consistent and realistic requirements for the design and evaluation of leading edge materials and concepts. Much of the design criteria data was obtained from North American Rockwell (NAR), who supported VMSC during the Phase I Program. Criteria covered design philosophy, design factors, and design loading conditions.

In view of schedule and budget constraints, the entire wing leading edge of both the high and low cross range vehicles could not be analyzed. A representative configuration was therefore established to enable development of designs and meaningful analyses. The straight wing orbiter, low L/D vehicle as generally configured in the contract document, reference (1), was selected as the baseline because more information was available and leading edge temperatures were higher than on the delta winged high L/D vehicle. Designs and analyses for the selected configuration should be scaleable to alternate vehicles and geometry.

Since the region of maximum interference heating occurs at a location about 25% outboard from the wing/fuselage intersection, the airfoil at this location was selected for design. The particular chord length chosen was based on a vehicle containing a 15 foot diameter by 60 feet long payload volume. The resulting baseline airfoil configuration is as follows:

PRECEDING PAGE BLANK NOT FILMED

Airfoil Section - NACA 0012-64

Chord Length - 214 Inches

Front Beam Location - 15% Chord

Sweepback Angle - 14°

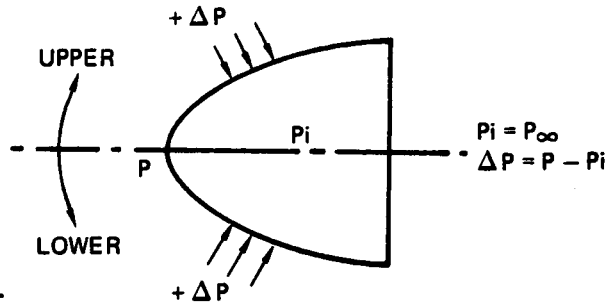
The use of design ultimate factors of safety of 1.4 for boost flight and 1.5 for all other flight conditions were in accord with Phase B Shuttle criteria. These factors were considered applicable to either airloads or thermoelastic stresses acting independently. A lower factor of safety on thermoelastic stresses was not felt justified in view of the lack of ductility of coated RPP systems. Combinations of thermal and airloads stresses were not evaluated because analysis shows, that at the time of maximum thermoelastic stress, airloads are very small and vice versa.

Each mission phase was identified and environmental conditions pertinent to that phase were specified, but only a few conditions actually design the leading edge. In the boost phase at maximum dynamic pressure the highest collapse pressures on the leading edge are experienced. This condition is given in figure 3-1 for two angles of attack. It has been assumed that the leading edge will vent to ambient, resulting in a stagnation point limit collapse pressure of 5.9 psi.

Entry conditions produce the highest temperatures and steepest thermal gradients around the leading edge. Heating rate distributions for design are provided in figure 3-2. These are generally in accordance with reference (4), which were obtained from NASA wind tunnel data, but the local distribution around the forward 2% of the chord was adjusted to conform to local leading edge radii. Contract requirements dictate that temperatures up to 4000°F (assumed at emittance of 0.8) be evaluated and therefore interference factors which would produce the corresponding interference heating level were established for design. The interference heating factor distribution on figure 3-2, forward of 15% chord, is an extrapolation of NASA wind tunnel data.

Conversion of the heating data on figure 3-2 to radiation equilibrium temperatures produces the distributions shown on figure 3-3. The effect of reduced emittance on temperature is indicated and the severity of the thermal gradient around the nose area of the leading edge is apparent. Also noted in figure 3-3 is the NAR maximum stagnation temperature prediction for the straight wing orbitor entering along a nominal trajectory.

HIGH q CONDITIONS
CHORD = 214 IN.



USE F. S. = 1.4 FOR BOOST

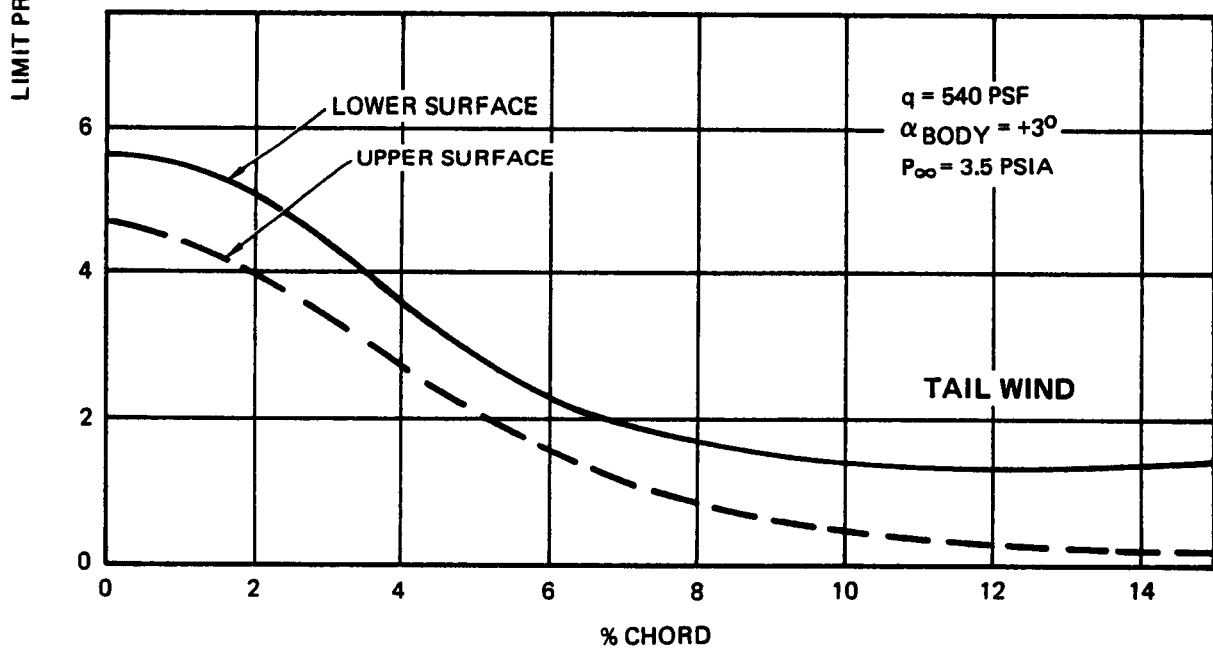
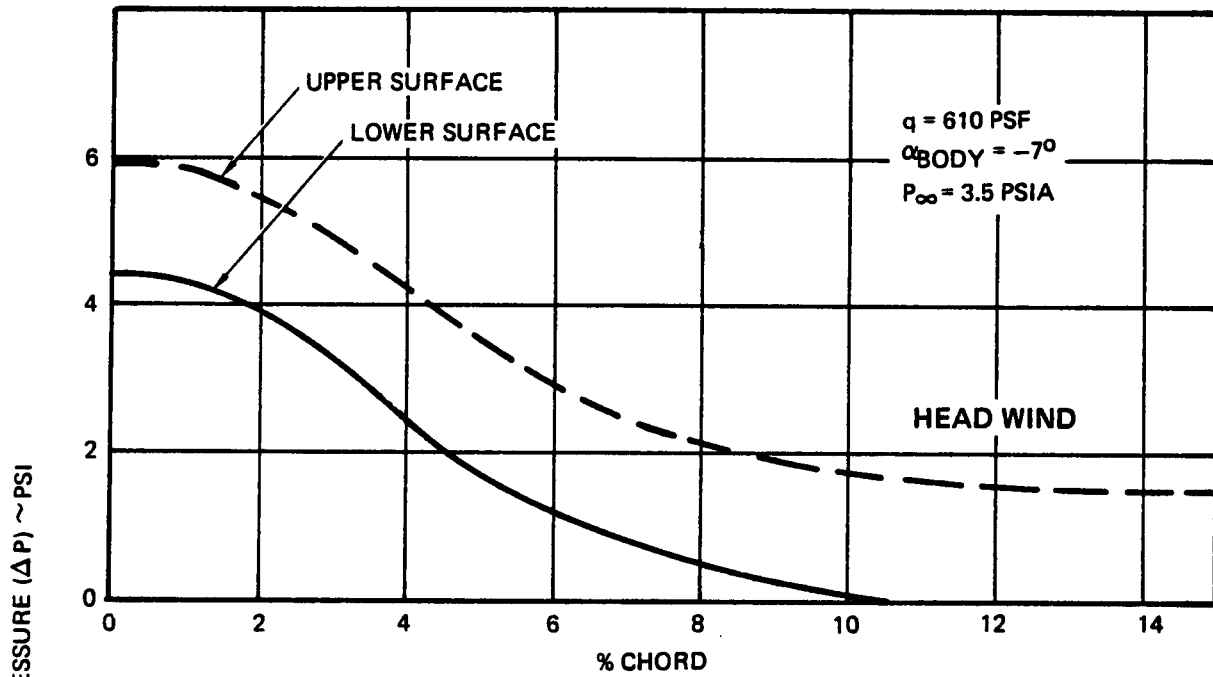


FIGURE 3-1 BOOST CONDITION LOADS

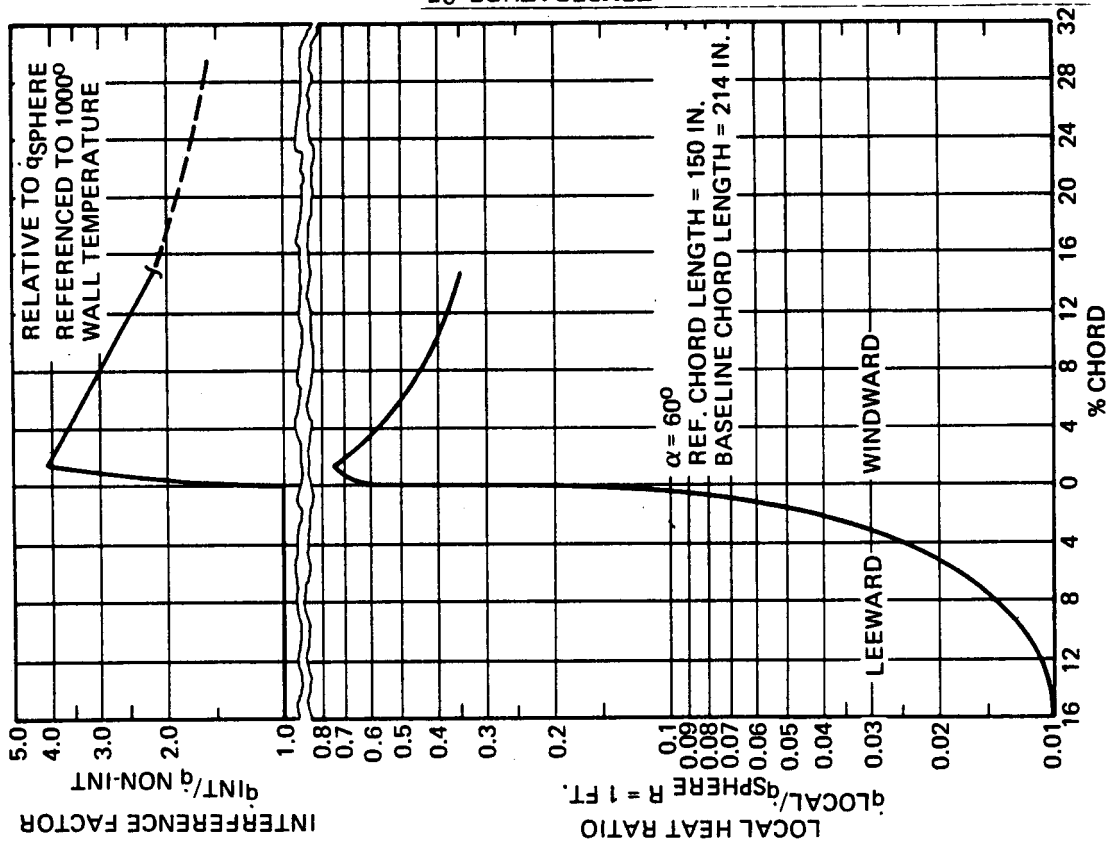


FIGURE 3-2 INTERFERENCE FACTOR AND LOCAL HEAT RATIO

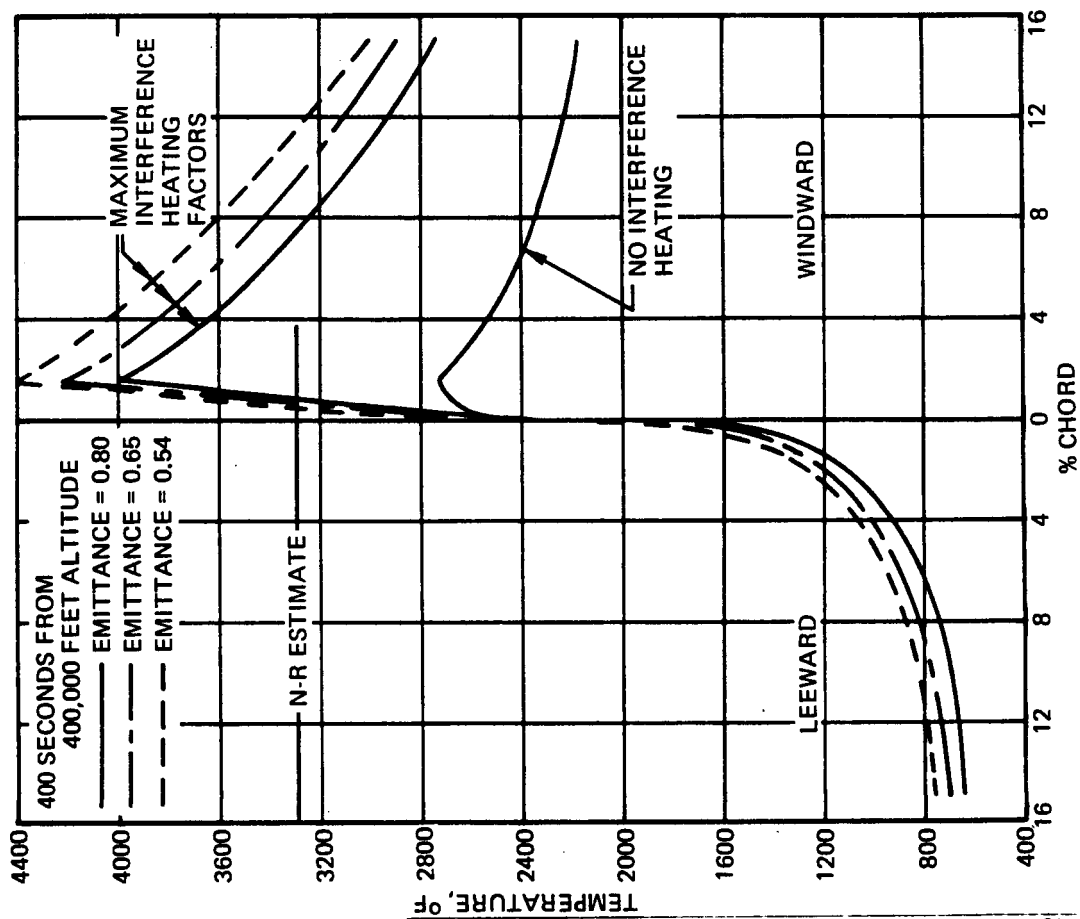


FIGURE 3-3 RADIATION EQUILIBRIUM TEMPERATURES TIME OF PEAK RE-ENTRY HEATING

Airloads experienced during high angle of attack entry, and subsonic cruise maneuvers are shown on figures 3-4 and 3-5, respectively. The high angle of attack pressure loads are greatest immediately prior to pushover when dynamic pressure is maximum. This produces only 0.3 psi pressure differential on the lower panel if internal pressure is assumed at ambient, and is therefore not a critical design condition.

Maximum cruise condition airloads, given on figure 3-5 are based on maneuver analysis of reference (7) and are for a limit load factor of 2.5 g. Assuming ambient internal conditions, peak pressure differential on the lower panel is only 0.80 psi limit, while a maximum of 5.0 psi limit is applied on the upper surface. This condition produces the most critical upper panel and rib design loads.

As Phase B shuttle design continues, revisions will be made to these loading conditions and VMSC is working with North American Rockwell to ensure adequate interchange and update of information. The current design conditions are believed, however, to represent realistic criteria on which to base conceptual design and parametric analysis.

3.2 DESIGN CONCEPTS AND EVALUATION CRITERIA

Initial conceptual design activity was performed concurrently with the analysis task to establish functional leading edge element configurations to be analyzed. These functional elements consisted of the airload panels, ribs, expansion joints and wing interface support joints. Parametric analyses were used to indicate trends, determine the soundness of concepts, dictate best design approaches and provide guidelines for materials development. Final analyses established leading edge concept sizing.

Eight initial conceptual designs were generated with varying degrees of emphasis on factors of weight, cost, thermal stress, or temperature of structural elements. Each of the concepts, pictured in figures 3-6 through 3-13 and discussed below, were created without the advantage of quantitative analyses to verify or discredit their validity. These analyses are now complete and are discussed in sections 3.3 and 3.4. The results were used in the design of concepts 1 and 3 detailed in figures 3-16 and 3-17.

Each of the eight concepts was rated against evaluation factors of cost, weight, sensitivity, inspection and maintenance, and aerodynamic considerations as listed in table 3-1. From this evaluation and supporting parametric analyses two designs evolved for further development, incorporating the best features of the original eight. These are shown in

ENTRY PHASE: $\alpha = 60^\circ$ $\alpha_{WING} = 64^\circ$
 STRAIGHT WING ORBITER

ALT. = 40,000 FT.
 MACH = 0.6
 $q = 43$ PSF

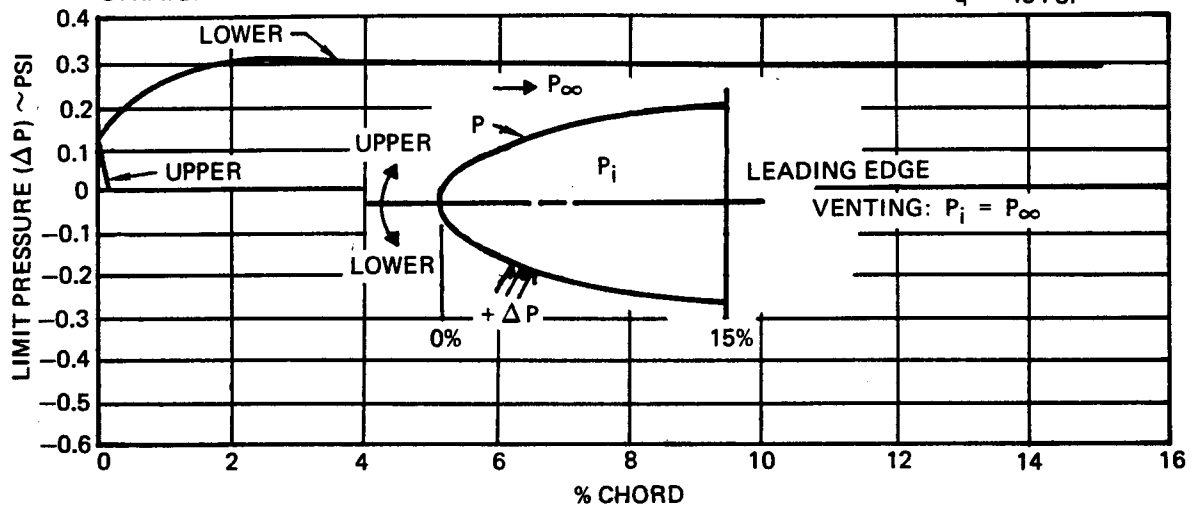


FIGURE 3-4 LIMIT ENTRY PRESSURE

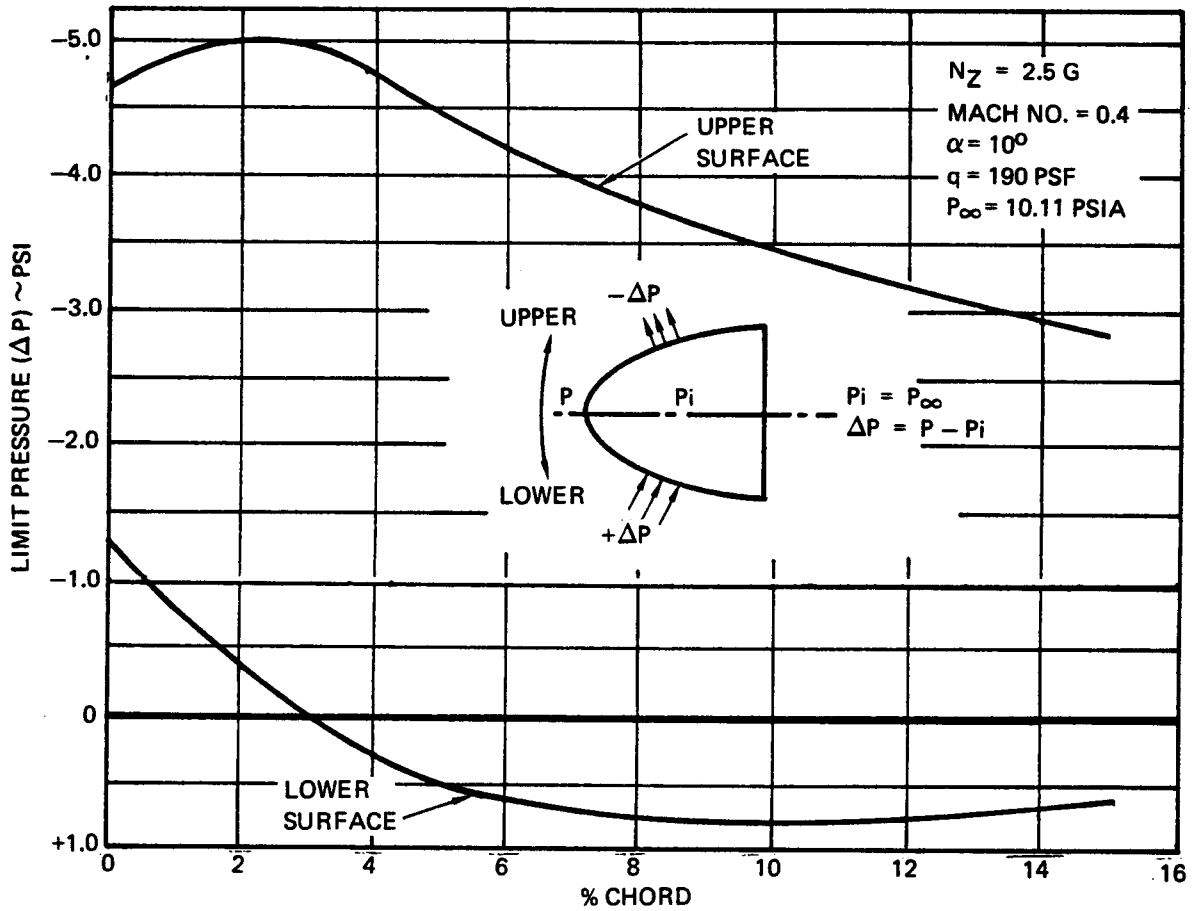


FIGURE 3-5 CRUISE CONDITION LOADS

TABLE 3-1 DESIGN CONCEPT EVALUATION FACTORS

<u>EVALUATION FACTORS</u>	<u>EVALUATION FACTORS</u>
<p><u>COST</u></p> <ul style="list-style-type: none"> MINIMUM TOOLING REQUIREMENTS MINIMUM NUMBER OF ELEMENTS MAXIMUM TOLERANCE ALLOWABLES MAXIMUM CAPABILITY TO FAB. MINIMUM DEVELOPMENT REQUIRED MINIMUM INSTALLATION COST MAXIMUM REPAIRABILITY MAXIMUM REPLACEABILITY MAXIMUM INTERCHANGEABILITY <p><u>WEIGHT</u></p> <ul style="list-style-type: none"> MAXIMUM LOAD PATH EFFICIENCY MAXIMUM EFFECTIVE USE OF MATERIALS MAXIMUM CONFIDENCE IN ANALYSIS MAXIMUM CONFIDENCE IN MATERIALS APPLICATION MAXIMUM THERMAL EFFICIENCY MAXIMUM EFFECTIVENESS OF RADIATION, CONDUCTION, HEAT SINK MINIMIZE THERMAL GRADIENTS IN STRUCTURE <p><u>INSPECTION AND MAINTENANCE</u></p> <ul style="list-style-type: none"> DURING FABRICATION INSPECTION BETWEEN MISSIONS INSPECTION <ul style="list-style-type: none"> ON SHUTTLE (MAX) OFF SHUTTLE (MIN) VISUAL (MAX) EQUIPMENT REQUIREMENTS (MIN) REPAIRABILITY <ul style="list-style-type: none"> ON THE SHUTTLE OFF THE SHUTTLE <p><u>AERODYNAMICS</u></p> <ul style="list-style-type: none"> AERODYNAMIC SMOOTHNESS <ul style="list-style-type: none"> MINIMIZE STEPS JOINT GAPS (EXPANSION) SEALING CHARACTERISTICS <ul style="list-style-type: none"> FLOW INTO CAVITY FLOW WINDWARD TO LEEWARD EFFECTS OF DEFLECTIONS EFFECTS OF EXPANSION 	<p><u>SENSITIVITY</u></p> <ul style="list-style-type: none"> THERMAL GRADIENTS/STRESSES <ul style="list-style-type: none"> FREEDOM FROM LOCAL HOT SPOTS <ul style="list-style-type: none"> IN-PLANE (MINIMIZE) THROUGH THE THICKNESS (MINIMIZE) AROUND THE NOSE (MINIMIZE) CONFIDENCE IN ANALYSIS (MAX) THERMAL EXPANSION <ul style="list-style-type: none"> INDUCTED LOADS (DEFLECTION INDUCTED) (MIN) FREEDOM FROM BINDING OR SEIZING (MIN) REPEATABILITY (MAXIMIZE) EFFICIENT USE OF MATERIAL PROPERTIES (MAX) NATURAL ENVIRONMENTS <ul style="list-style-type: none"> VACUUM-OUTGASSING, TRAPPED PRESSURE (MIN) RAIN & DUST - EROSION <ul style="list-style-type: none"> PHYSICAL PROPERTY DETERIORATION MECHANICAL PROPERTY DETERIORATION WEIGHT GAIN <ul style="list-style-type: none"> FREEZE DAMAGE MICROMETEOROID OR LOCAL DAMAGE LOADS - AIRLOADS, INERTIA <ul style="list-style-type: none"> REDUNDANCY OVERLOAD CAPABILITY GOOD LOAD PATHS GOOD USE OF MATERIAL PROPERTIES TOLERANCE TO LOCAL DAMAGE DEFLECTION INDUCTED STRAIN FREEDOM FROM BINDING AND SEIZING FATIGUE RESISTANCE LOADS - VIBRATION, ACOUSTIC NOISE <ul style="list-style-type: none"> POTENTIAL FATIGUE INTERFACE WEAR JOINT SLOP INDUCTED FAILURE MATERIAL COMPATIBILITY <ul style="list-style-type: none"> CHEMICAL (THROUGHOUT TEMPERATURE RANGE) THERMAL EXPANSION HANDLING AND SHIPPING <ul style="list-style-type: none"> RUGGEDNESS TOLERANCES <ul style="list-style-type: none"> FABRICATION INHERENT ASSEMBLY INHERENT INSTALLATION INHERENT (ON WING) ABILITY TO COMPENSATE FOR ON INSTALLATION REPRODUCIBILITY

figures 3-15 and 3-16 and discussed in detail in this section. Further evaluation using more recent material property data and preliminary cost analysis resulted in the current selected configuration shown in figure 3-17. The following discussion summarizes salient features and disadvantages of each concept conceived.

Concept A, Figure 3-6 - This design features a sandwich structure which could utilize RPP honeycomb, RPP foam, or other pyrolyzed core. Normally, the advantage of sandwich design is low weight if adequate core shear strength can be obtained at low density. Further, a sandwich design requires no separate ribs and should be relatively rugged. It was felt that a certain amount of insulative capacity might be afforded by the sandwich to diminish the temperature requirements on the insulation protecting the metal interface structure. However, analyses showed, that for the times and temperatures expected, only a small, 75°F, temperature relief would be experienced for a typical foam core design.

There are several disadvantages to this concept. Development costs, although not specifically analyzed, are anticipated to be high; surface temperature will reach radiation equilibrium because cross-radiation heat rejection is blocked; and temperature gradients will be severe, partly because of the inability to take advantage of cross-radiation.

VMSC's limited experience in fabricating oxidation inhibited honeycomb sandwich specimens has shown that the processing steps are greater and more intricate or difficult to control than for solid laminates. In addition, it is doubtful that reliable honeycomb or foam core material can meet the shear stress requirements of about 125 psi for less than 15 to 20 lb/ft³, and at this density solid laminate designs are weight competitive. Data obtained on 20 lb/ft³ RPP foam produced a nominal shear stress of 171 psi, indicating that an assumption of being able to employ appreciably lower density core cannot be justified.

Another important drawback of the sandwich concept is that thermal gradients through the thickness of foam core and honeycomb sandwich material are 1500°F and 500°F, respectively, while thermal gradients in the outer skin around the nose region are as high as 900°F/inch. Analysis shows that these gradients produce significantly higher thermoelastic stresses than solid laminate designs. Furthermore sandwich designs block the ability for effective cross radiation from the lower to the upper surface, thus placing a higher temperature requirement on the RPP oxidation inhibitor coating of as much as 370°F. This is discussed thoroughly in section 3.3.5.

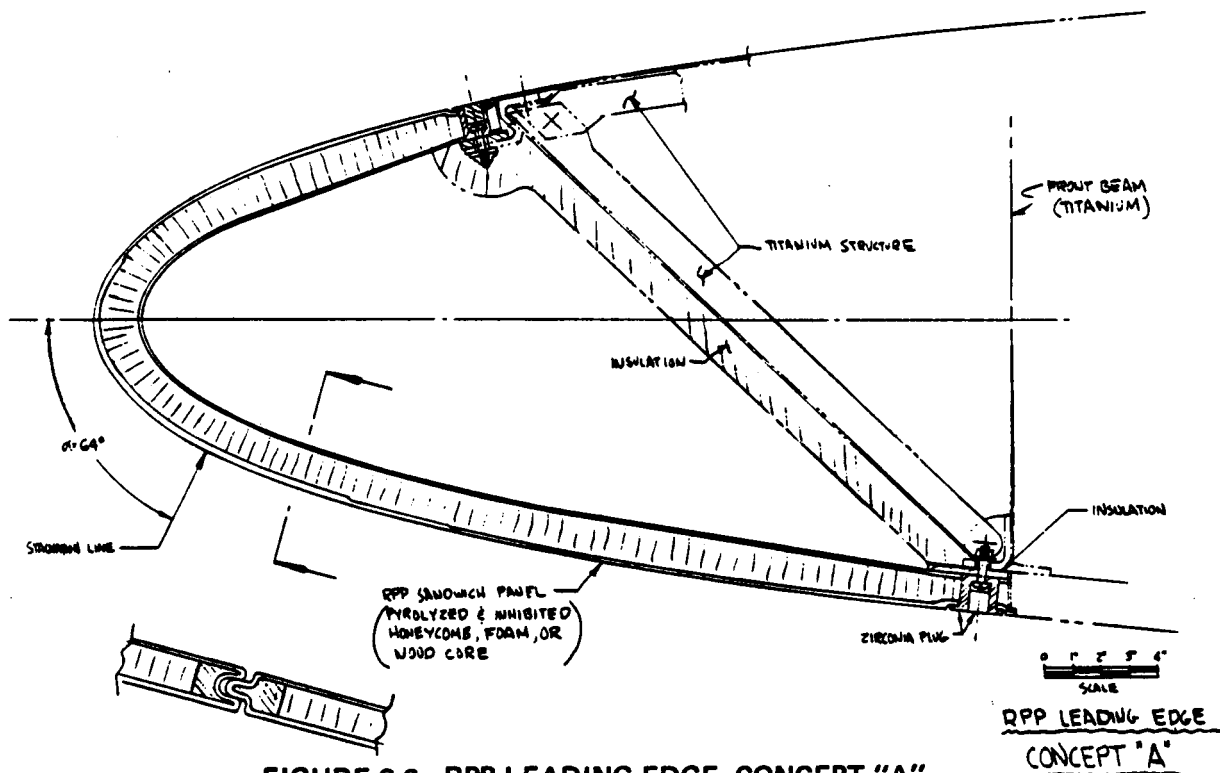


FIGURE 3-6 RPP LEADING EDGE, CONCEPT "A"

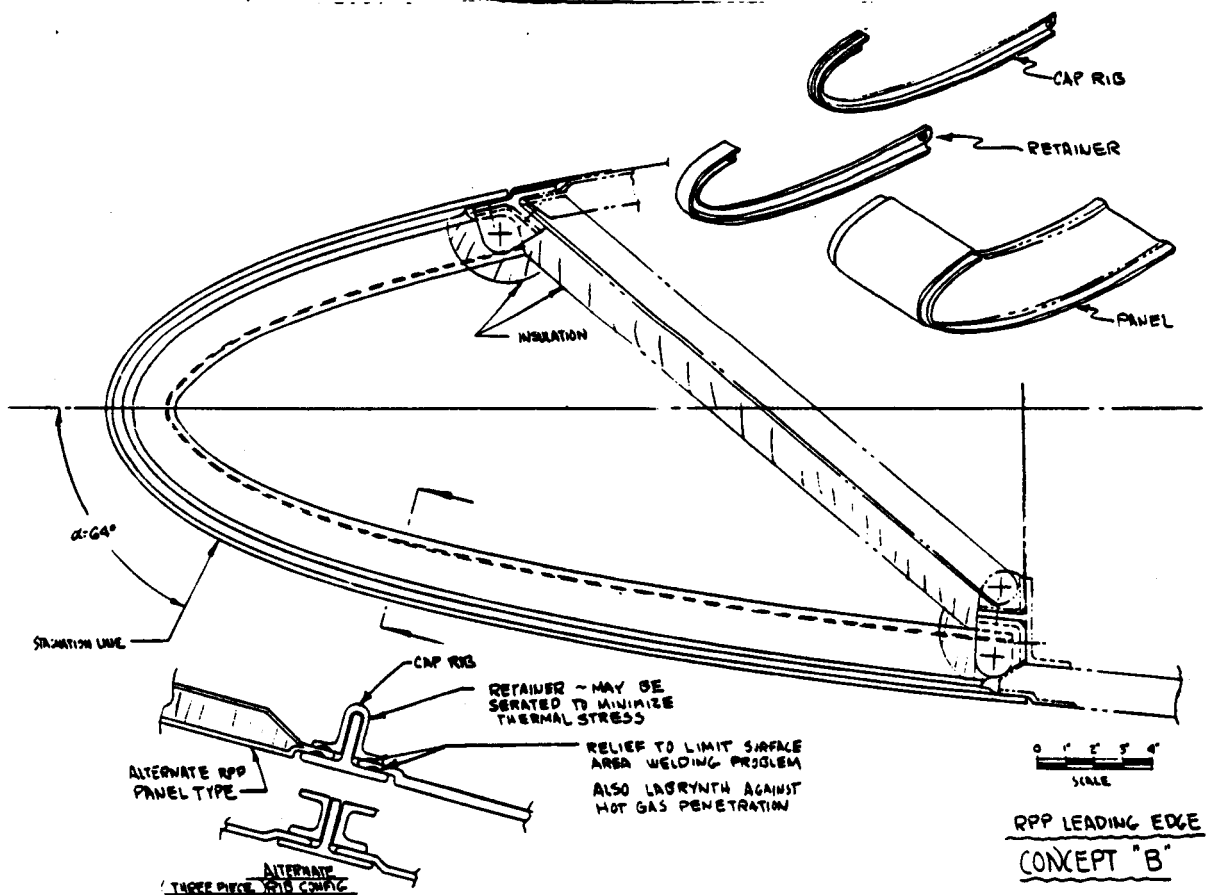


FIGURE 3-7 RPP LEADING EDGE, CONCEPT "B"

For these reasons sandwich designs are not considered as reliable nor as cost effective as their solid laminate counterparts.

Concept B, Figure 3-7 - The main feature of this concept is that the airload panels are rather simple to build and are trapped between the rib elements. The trapped panel provides a labyrinth to aid in sealing against hot gas flow into the leading edge cavity. While the sandwich panel is shown as an alternate, this is not considered desirable as noted in the discussion of Concept A. There are two possible approaches to the attachment of the retainer and cap: they may be attached only at the support structure in the lower temperature region as shown or they may be attached periodically around the entire leading edge. The latter approach would provide lighter weight, but would also require fasteners operating in a hotter zone. Zirconia pins should be feasible for that application. More detail analysis would be required before deciding on a final approach. The trapped panel feature of this concept was retained for one of the interim concept selections as shown in figure 3-15.

Concept B features shear type attachment of the support structure which eliminates fastener tension loads. Concept A, on the other hand, while still employing basically a shear attachment, experiences an undesirable tension load on the upper surface from cruise maneuver airloads. The shear bolt feature of Concept B is preferred and is used in the final designs.

Concept C, Figure 3-8 - Again both solid and sandwich panels are indicated but the sandwich design is felt undesirable as previously discussed. There are two features of this concept to be noted. One is the redundancy afforded by the two types of shear fastening at the support structure. However, this would add to tooling costs and make replacement of panels more difficult. The second feature is the use of overlay shingles which can be replaced along with the retainer cap without replacing the backup structure. Segmenting is shown as an approach to reducing thermal stresses from the severe gradients developed between the stagnation area and the geometric leading edge region. Analysis shows that little temperature reduction of the backup structure is obtained by shingling and there would, therefore, be little reduction in thermal gradients in the backup structure. The only advantage, therefore, is the replaceable feature for damaged or oxidized shingles.

While refurbishment costs may be relatively low, the higher weight and initial cost of this concept are unattractive in comparison with simple non-shingled designs. Although not seriously considered, local application of this concept in very high temperature regions could prove desirable if multi-mission coating performance cannot be achieved.

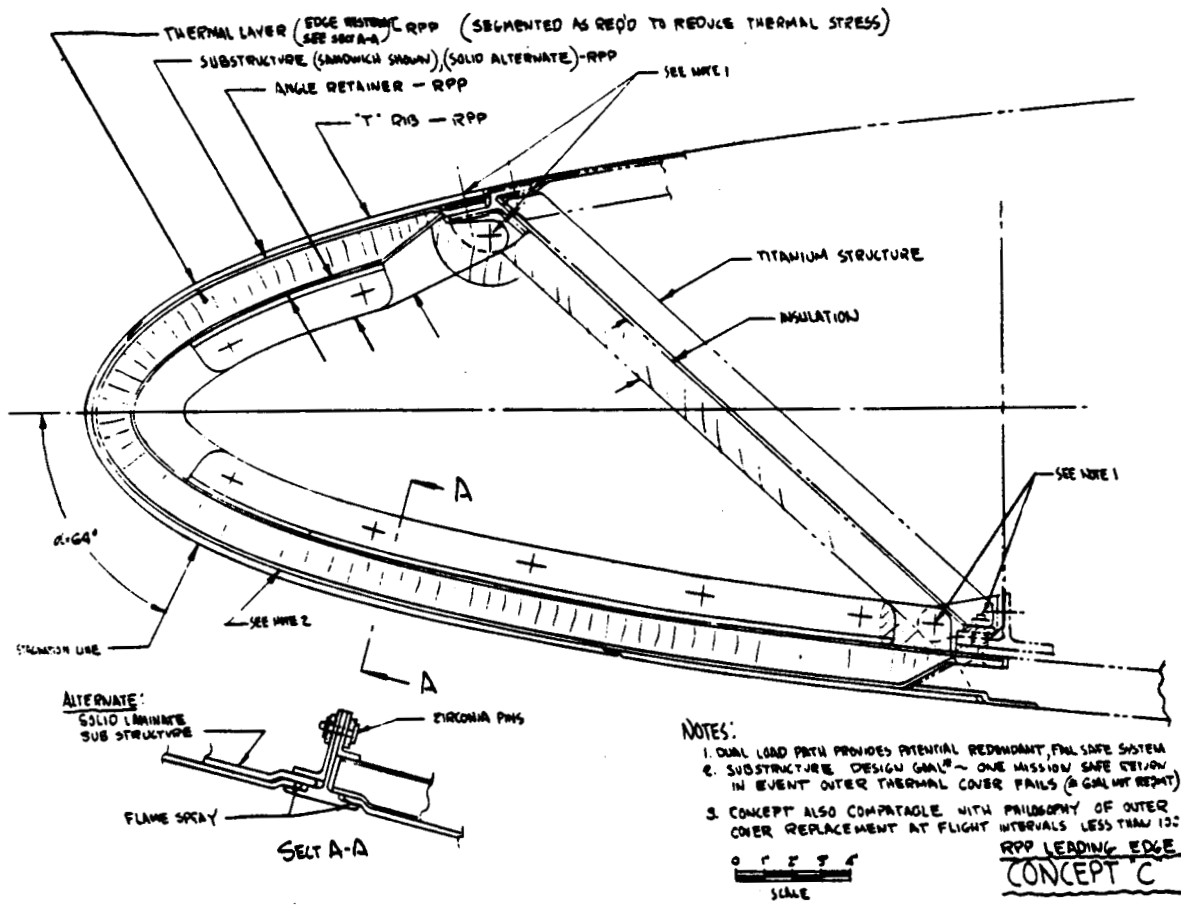


FIGURE 3-8 RPP LEADING EDGE, CONCEPT "C"

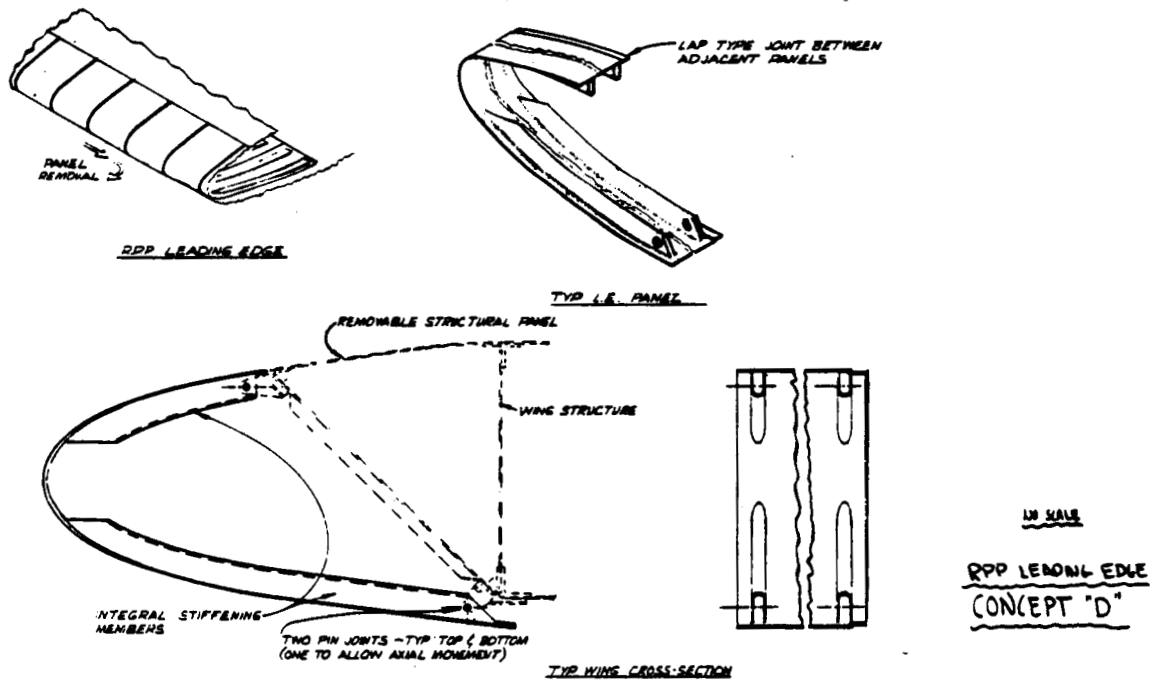


FIGURE 3-9 RPP LEADING EDGE, CONCEPT "D"

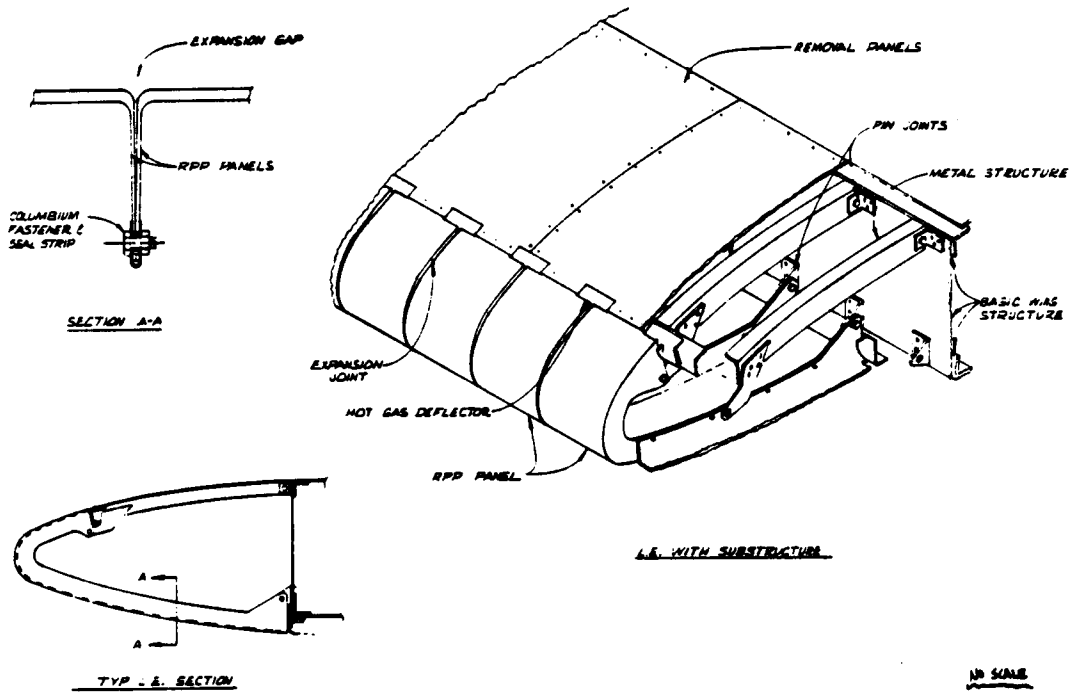
Concept D, Figure 3-9 - This is an integral rib and panel design. The closed rib is normally structurally efficient and therefore can be designed thin. However, for coated materials of large span, it is currently estimated that a thickness limit of 0.10 inches be established to avoid warping or expensive fabrication tooling and processes. The closed section therefore loses some of its advantage. If ribs are closely spaced, tooling and fabrication costs rise. In addition either weight must increase with reduced rib spacing or thickness must decrease to the point where there is no thermal protection margin afforded by the RPP if a coating failure occurs. Another disadvantage is that in order to minimize thermal gradients and stresses in the ribs at high skin temperature, it is desirable for the inner cap of the rib to absorb radiant energy from the skin. The closed rib is limited in the amount of hot skin from which it receives radiation. An open section on the other hand, such as a C or Z, is not so restricted.

The closed section may or may not offer coating problems. If the material is thin enough, diffusion coatings can penetrate from the outside. If not, application of the slurry coating to the inside would have to be solved. Inspection inside the closed ribs should be difficult.

Another idea illustrated by this concept is that of fixing or establishing the location of the inflection point (bending moment goes to zero) to optimize rib weight. This in effect places a pin joint in the rib and treats the rib geometry as a truss with curved members. The disadvantage of this is that it tends to localize rotation from rib deflection into the low stiffness region with attendant high bending stresses developed in the RPP skin. This appears unreliable. The concept can be made more feasible if the ribs are continuous but thinned down in the forward region. However, simple open rib geometry is preferred as discussed later and therefore this particular design was not recommended for further study.

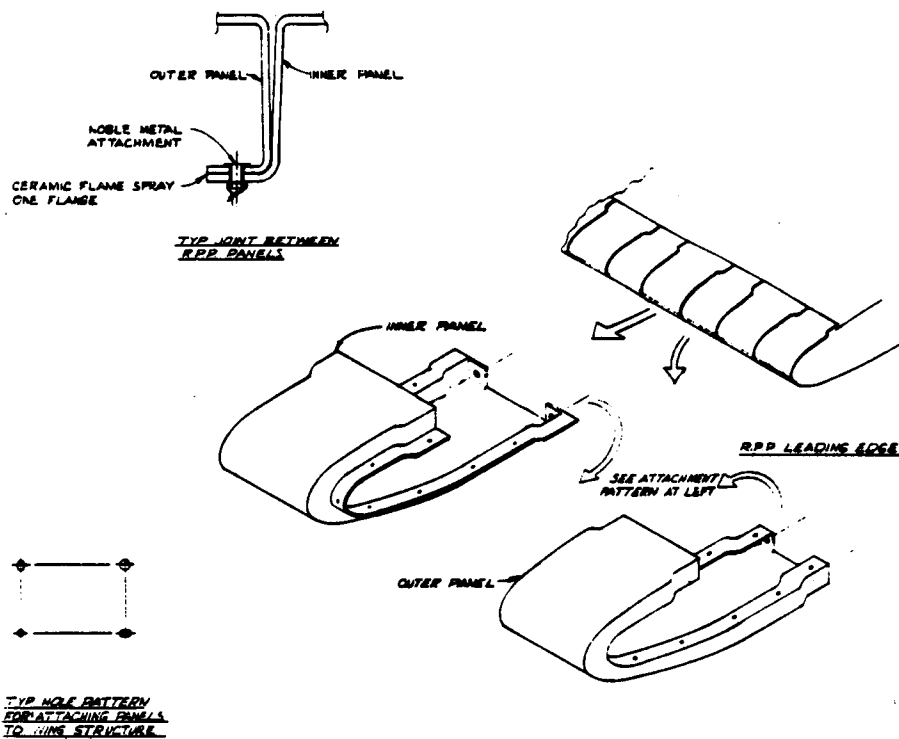
Concept E, Figure 3-10 - From an airload panel and rib standpoint, this concept is very simple. The rib will have high thermal gradients, however, and should therefore utilize a turned flange to absorb radiated heat from the skin to reduce thermal stresses as well as to increase bending efficiency.

The unique feature of this concept is the flexure type expansion joint. This design was conceived as an alternate to slip joints in the event that coating vitrification caused a welding of overlapping segments. If the stiffness of this joint can be kept low it might prove feasible, although for multiple cycling, and with the fatigue strength of coated RPP unknown, this joint is considered undesirable. Slot heating could be a factor in the consideration of this design if close control of segment tolerances is not maintained. Strain compatibility and unknown fatigue life preclude serious consideration of this design unless slip joints prove to be unacceptable.



NO SCALE
RPP LEADING EDGE
CONCEPT "E"

FIGURE 3-10 RPP LEADING EDGE, CONCEPT "E"



NO SCALE
RPP LEADING EDGE
CONCEPT "F"

FIGURE 3-11 RPP LEADING EDGE, CONCEPT "F"

Concept F, Figure 3-11 - This is similar to Concept E except that return flanges are used on the ribs and a tension type joint is shown at the support structure. Tension joints are undesirable compared to shear joints both from the fastener standpoint and from the local bending stresses introduced in the joint area of the leading edge segments. The simplicity of the integral rib and airload panel design is incorporated in the final selected concept.

Concept G, Figure 3-12 - In this concept the skin panel is a separate element from the rib as in Concept B, but restrained to the rib by fasteners in slotted holes. Panel to rib fore and aft restraint is provided at the forward most fastener, such that the hotter skin panel expands aft relative to the rib. This concept was envisioned as an approach to lowering rib thermal stresses by reducing heat transfer from the panel to the rib. Since this concept is similar to Concept B in operation, but does not provide an equal degree of support to the panel against possible vibration or flutter loads, and must rely on slip joint fastening, it was rated low and considered no further.

One other feature to note is the truss type rib with "blades" extending from the truss members to match outer contour. Because the leading edge resists airloads not unlike a bent truss (i. e., there is an inflection point near the nose) it was decided to examine a straight element truss. However, transitions and complications at joints makes this concept unattractive from a cost standpoint and it was dropped from further consideration.

Concept H, Figure 3-13 - This represents a different approach to the problem, but again, it breaks the leading edge up into a truss. The sandwich elements have the same problems as discussed in Concept A. One of the main disadvantages of this design is that, as the panel expands on the lower side relative to the upper panel, the nose of the leading edge will tend to move forward and rise. The posts, however, restrain the lower panel from free movement, and force the panel to bend locally at the post. This local bending can induce failures in an unforgiving non-metallic material. For this reason post stiffening has not been seriously considered. The basic post stiffening idea could be applicable to any of the other concepts if additional stiffening of the ribs were required for support of airloads, but very detailed analysis is required to prove feasibility of this kind of stiffening.

In all of the concepts presented the upper panel has been terminated short of the 15% chord point (front beam location), although extension aft is feasible. However, the designs shown permit the use of lighter metal construction in those temperature regions in which

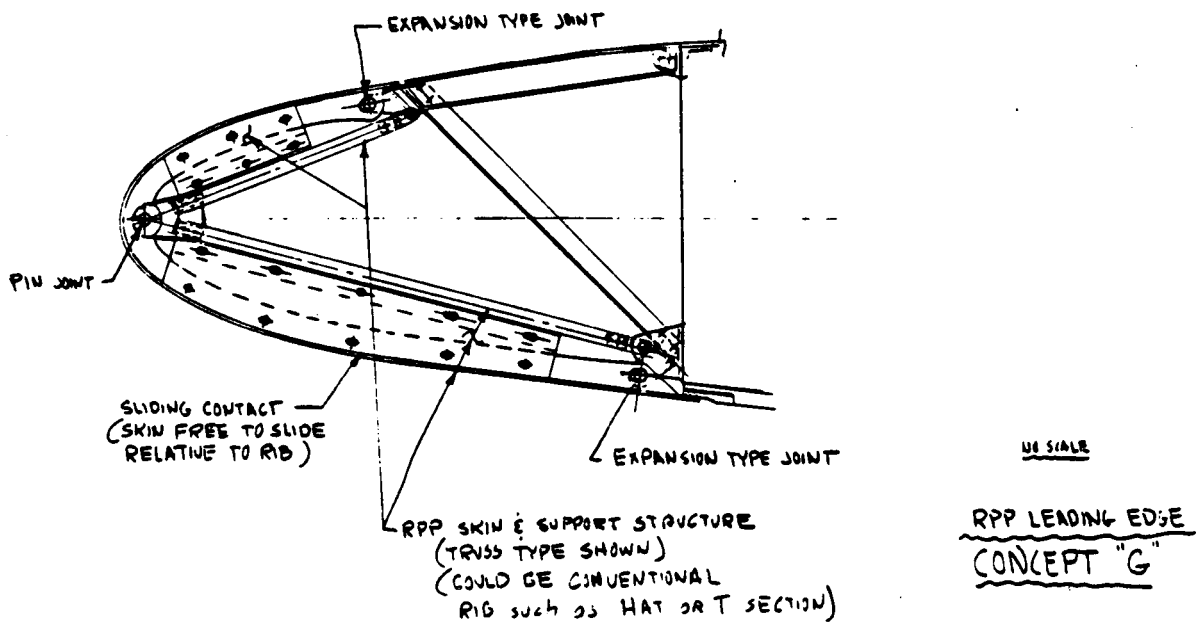
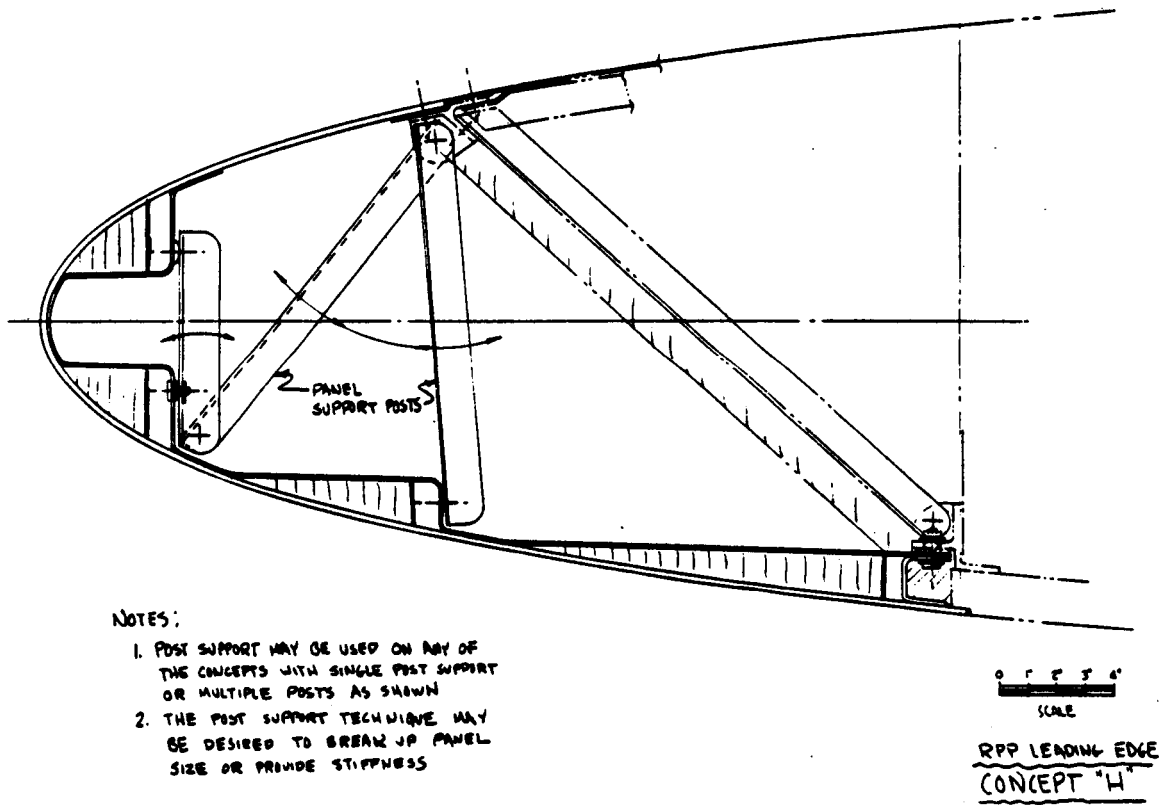


FIGURE 3-12 RPP LEADING EDGE, CONCEPT "G"



- NOTES:
1. POST SUPPORT MAY BE USED ON ANY OF THE CONCEPTS WITH SINGLE POST SUPPORT OR MULTIPLE POSTS AS SHOWN
 2. THE POST SUPPORT TECHNIQUE MAY BE DESIGNED TO BREAK UP PANEL SIZE OR PROVIDE STIFFNESS

FIGURE 3-13 RPP LEADING EDGE, CONCEPT "H"

Inconel, Rene, or possibly titanium are acceptable. It also allows focusing of radiant heat from the lower panel to the upper panel to decrease thermal gradients and stresses in the nose region. The metal structure combined with a removeable canted heatshield is envisioned as providing access to permit inspection of the RPP between flights. The heatshield should employ insulation currently under development by the shuttle contractors. Alternately, another material may be utilized like stabilized microquartz, which remains stable up to at least 3000^oF.

Several expansion joint designs were conceived during the study and are summarized in figure 3-14. These can be categorized as to types: trapped sliding, simple overlay sliding, and flexure. Concept 15a was previously discussed and shown as part of Concept B in figure 3-7. Concept 15B is a modification of 15a in which an integral rib and slip joint on one panel trap the adjacent panel. Figure 15c shows a non-structural seal strip sandwiched between integral panel ribs. This is probably lighter than 15a and 15b, but has the disadvantage of providing less sealing if the two adjacent panels experience differential motion to produce gapping under the "T". Allowable gapping and flow of high temperature air into the cavity must be determined before a decision can be made between the 15a and 15c type of joint.

A variation on figure 15c is shown by figure 15d in which the overlap seal is integral to one panel. This reduces the number of separate parts, although fabrication costs should be about the same. The simplicity of this joint lead to its' selection for Concept No. 3, the current baseline design.

The bending concepts of figure 15e and 15f were touched on previously in the discussion of rib concepts E and F. The acceptability or feasibility of this type joint is sensitive to material fatigue strength and stiffness, and to thermal gradients as flange length requirements become large. Analysis of these approaches has not been conducted because of the previously noted questionable areas. The overlap joints are much preferred unless a "welding" of the joint is possible through vitrification of the coating. Observations thus far have not indicated this to be a problem.

Each concept and its functional elements were rated by several members of the design team. A number of factors were considered in the evaluation and are summarized in table 3-1.

When all the advantages and disadvantages of the various leading edge and expansion point concepts were summed up, the following

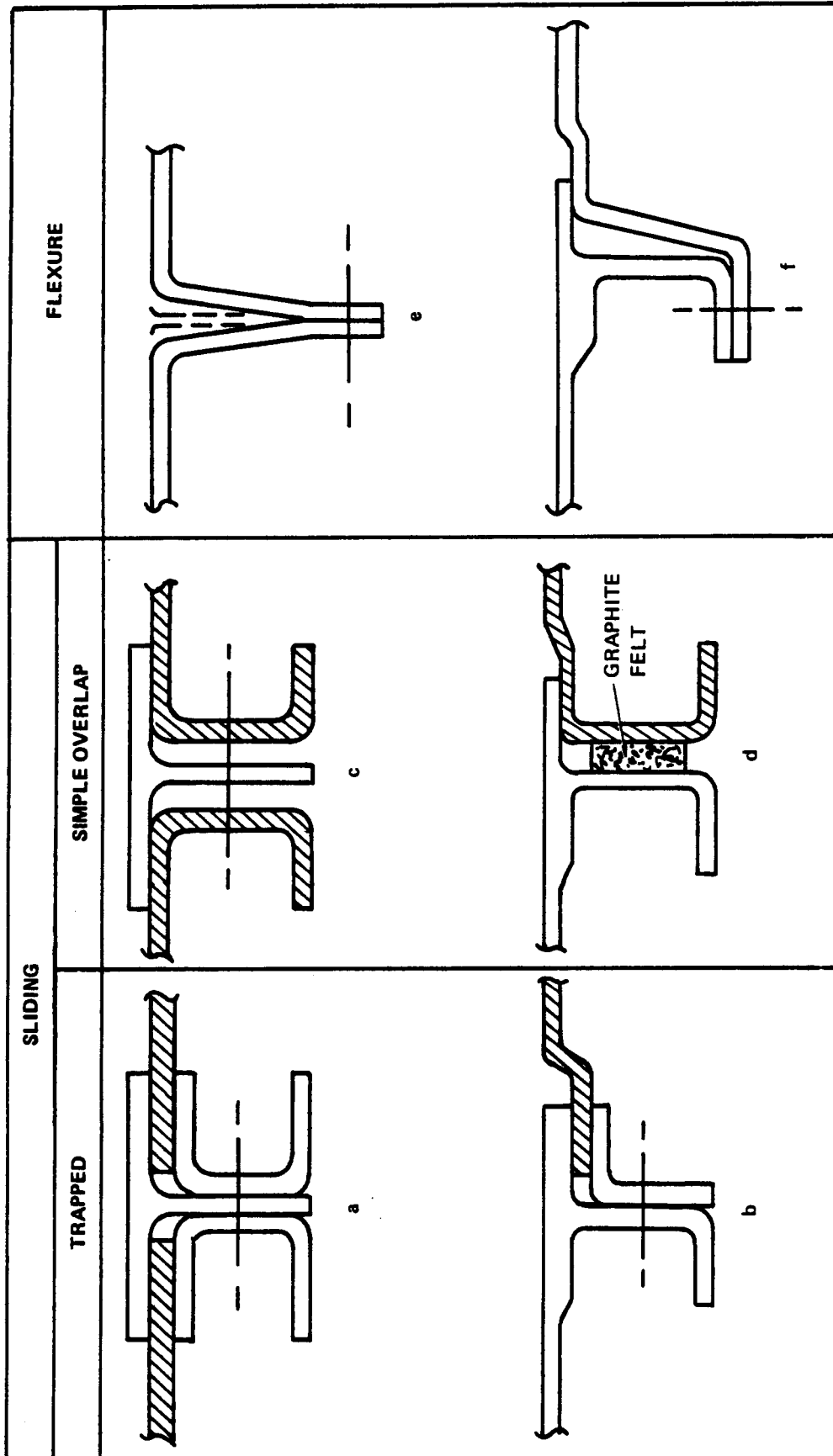


FIGURE 3-14 EXPANSION JOINT CONCEPTS

conclusions relative to desirable design features were drawn: use solid laminate to reduce both thermal stresses and maximum stagnation temperature; use open section ribs to minimize thermal gradients and thermoelastic stresses; use shear fastening at the support structure interface to utilize fasteners in their most favorable load carrying capacity; and use overlap slip type expansion joints. Interim Concepts 1 and No. 2 shown on figure 3-15 and 3-16 illustrate leading edge segments incorporating these features. These have now been superseded by Concept No. 3 (figure 3-17) which is now the prime system based on the compromises of weight and cost. Even though Concept No. 3 has emerged as the baseline design, an explanation of Concepts No. 1 and No. 2 is given to document design philosophy with high elastic modulus material.

Concept No. 1, detailed in figure 3-16 shows a segment span of 15 inches and rib and intercostal height limited to 1.0 inch because of anticipated thermal stress levels developed in the high elastic modulus material assumed for design. Lower and upper airload panels are 0.14 inches and 0.18 inches thick, respectively. A discussion of the reasoning for these dimensions is provided in the thermal and structural discussions of sections 3.3 and 3.4. The basis for the sizing is the material properties assumed in the analysis, the most important of which were the 15000 psi flexure strength and the 12×10^6 psi elastic modulus. Later test data on siliconized RPP showed that bending stress would be more nearly 10000 psi with an elastic modulus of 2.0×10^6 psi. Concept No. 3 is based on the lower allowables and can be compared with Concept No. 1 design approach.

Concept No. 1 features alternate overlapping and underlapping panels to permit ease of removal and replacement of individual segments. The integral overlap seal strip is shown since a more complex approach is not justified until proven necessary by analysis or test. Even with this simple seal design, additional sealing appears feasible using replaceable carbon felt inserted between panel ribs.

At the panel support points the hot RPP is insulated from the metal support fitting by ceramic bushings of alumina or zirconia. Radiation heat transfer from the panel to the metal structure is blocked by a non-load carrying insulation blanket. Analysis of this joint using fused silica insulators rather than zirconia shows that bushing diameter need only be 1.0 in. to limit the titanium support structure to 680°F.

Concept No. 2 differs from Concept No. 1 in that the trapped seal approach of figure 3-14a is used, which means that the airload panel and ribs are fabricated separately. Detail sizing and weight should be comparable to Concept No. 1.

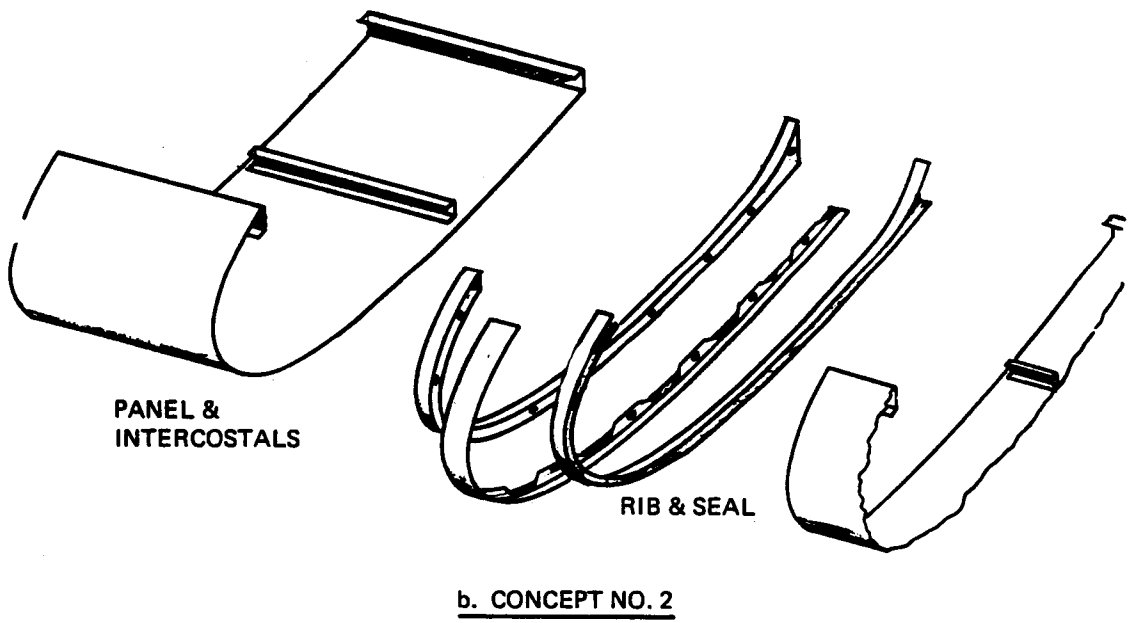
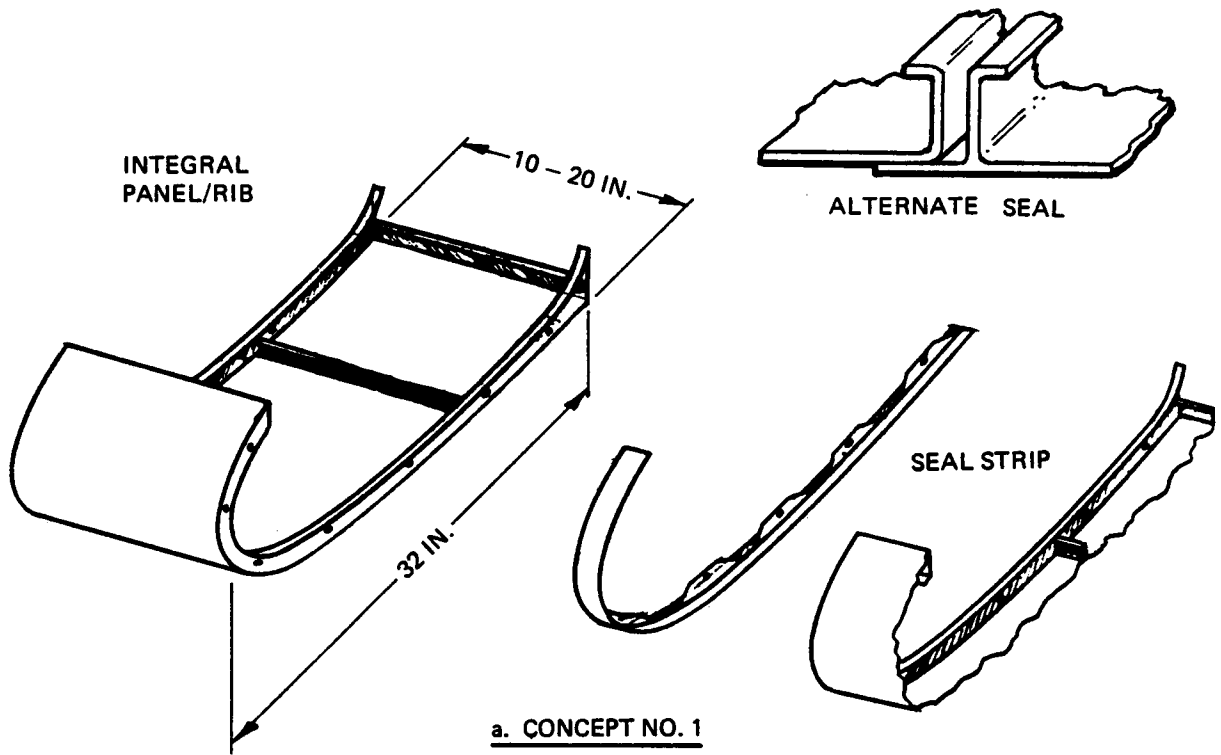
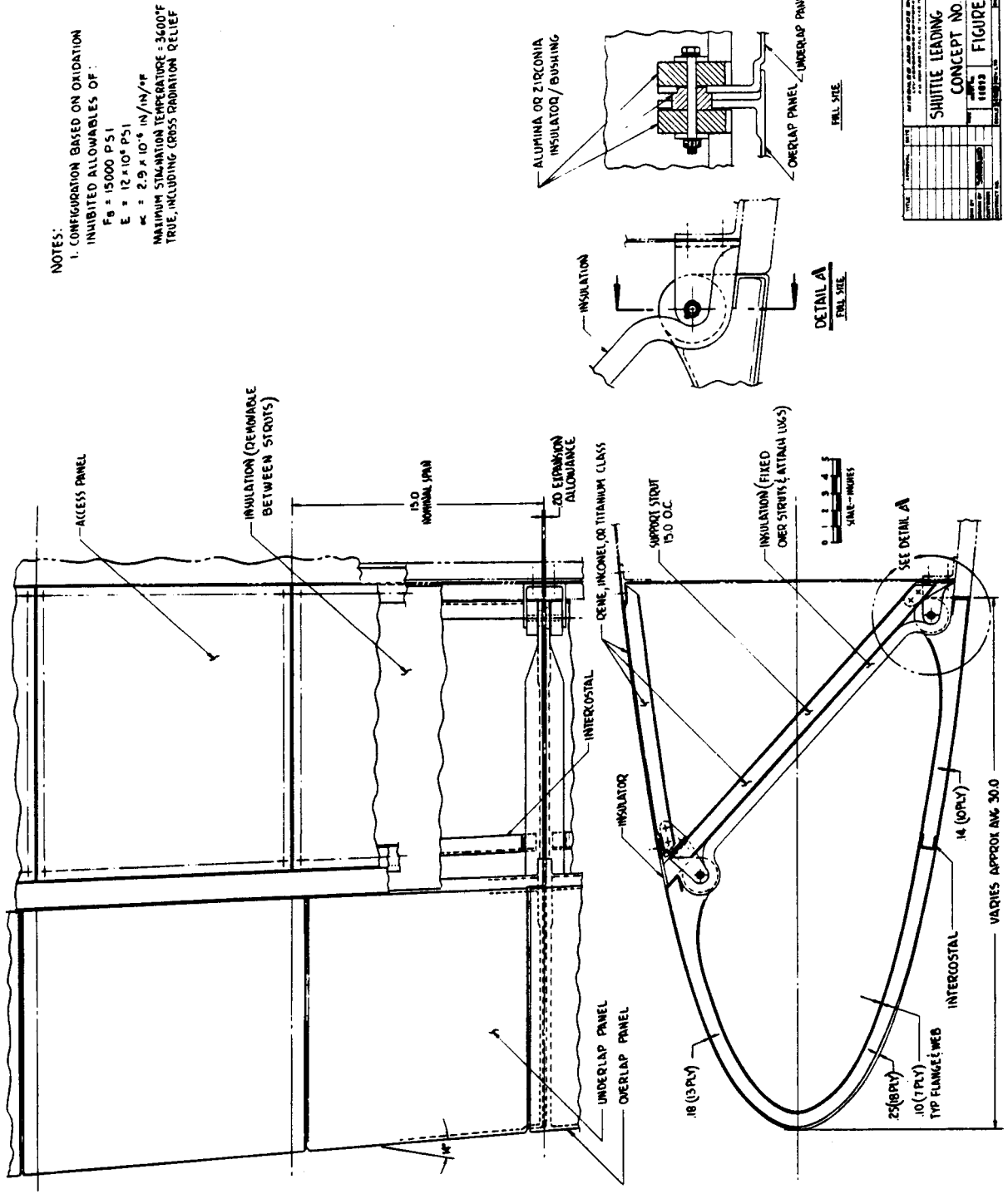


FIGURE 3-15 INTERIM LEADING EDGE CONCEPTS



NOTES:
 1. CONFIGURATION BASED ON OXIDATION INHIBITED ALLOWABLES OF:
 F₈ = 15000 PSI
 E = 12 x 10⁶ PSI
 K = 2.9 x 10⁻⁵ IN/IN/°F
 MAXIMUM STAGNATION TEMPERATURE = 3600°F
 TRUE, INCLUDING CROSS RADIATION RELIEF

DATE	REV	BY	CHKD	APP'D
SHUTTLE LEADING EDGE CONCEPT NO. 1				
1973				
FIGURE 17				

FIGURE 3-16 SHUTTLE LEADING EDGE, CONCEPT NO. 1

Production costs for leading edge assemblies, typical of Concept No. 1 with 15.0 inch segment size, were estimated in response to a request from North American Rockwell. For estimating purposes it was assumed that detail design and verification by test of typical leading edge assemblies would be successfully completed prior to Phase IV production orders; leading edge weight would be 2 lb./ft.²; surface area would be 264 ft.² per ship set; three ship sets would be delivered as part of the design, development, test and engineering phase; and that follow-on production would require delivery of an additional ten ship sets. Cost estimates generated and given in terms of dollars/ft.² are listed in table 3-2. Also shown are the equivalent dollars/lb.

Table 3-2

Estimated Fabrication Costs of Concept No. 1

	<u>DDT & E 3 Ship Sets</u>	<u>Production 10 Ship Sets</u>	<u>Total 13 Ship Sets</u>
Engineering	\$1310/ft. ²	\$ 120/ft. ²	\$ 400/ft. ²
Materials	580	240	320
Planning and Tooling	3260	170	890
Shop and Quality	<u>1630</u>	<u>1120</u>	<u>1240</u>
Total	\$6780/ft. ²	\$1650/ft. ²	\$2850/ft. ²
	\$3390/lb.	\$ 825/lb.	\$1425/lb.

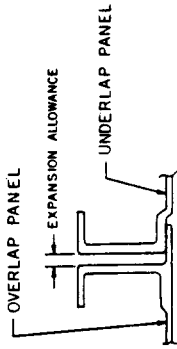
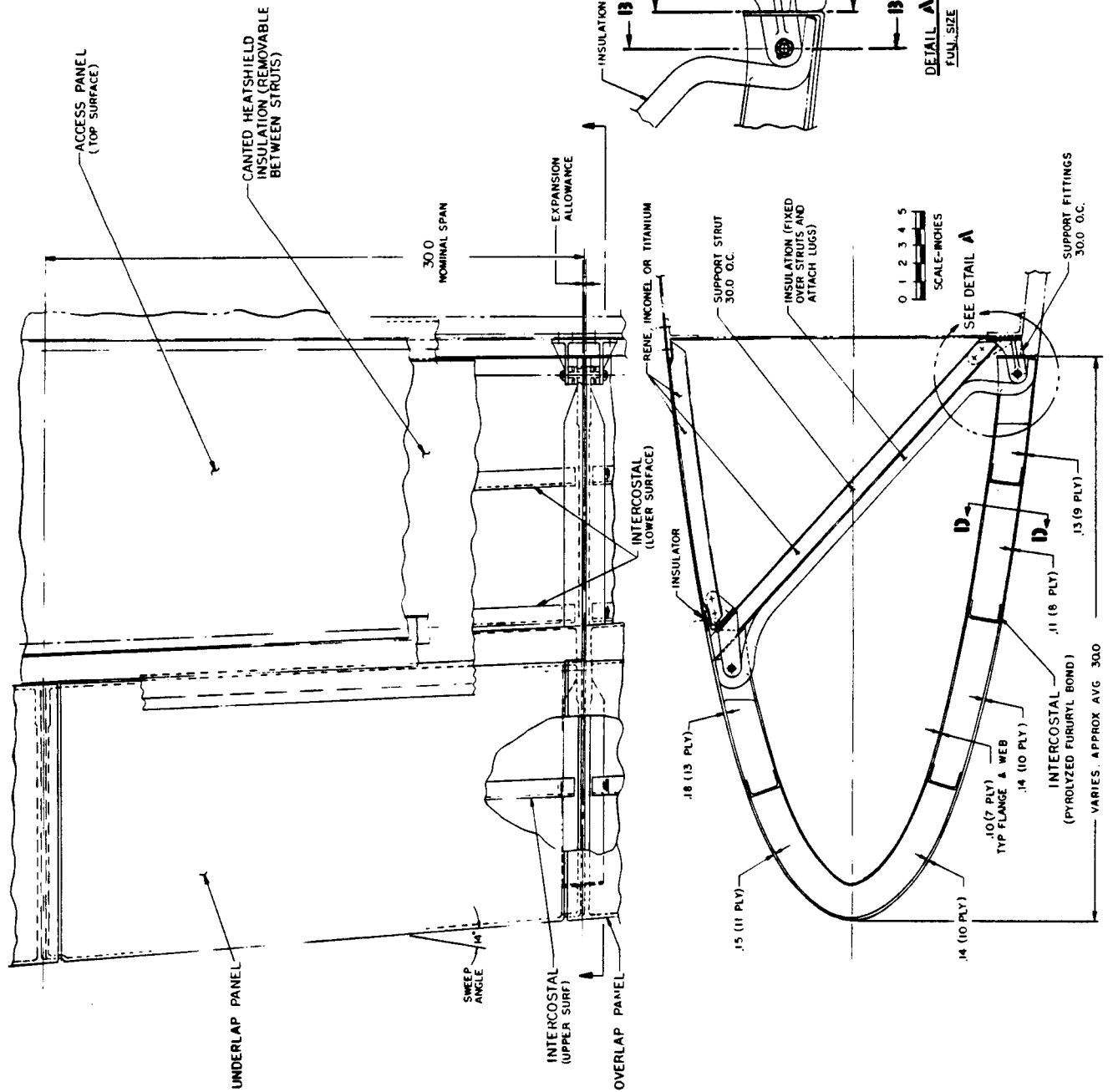
It is significant that tooling costs constitute nearly half of the total for the first three ship sets. This pointed out an area for concentration of effort to reduce costs. Accordingly, the current leading edge design, Concept No. 3, reflects an approach to decreasing tooling costs by doubling the span of each segment. This roughly reduces numbers of tools required by half. Intercoastals are added to meet strength, deflection and weight requirements but these lie along straight line elements and are much more readily fabricated than ribs. Through the use of the low modulus of elasticity material, increased span is made possible because thermo-elastic stresses cease to be a constraint on rib design. This permits deeper ribs with the greater load carrying capacity needed for larger spans.

Concept No. 3, shown in figure 3-17, retains the desirable features of Concept No. 1 but incorporates improvements and takes advantage of the cost reduction made possible by increased segment span. Three additional intercoastals are used to breakup the airload panels for

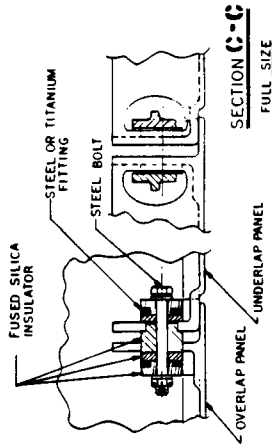


NOTES:

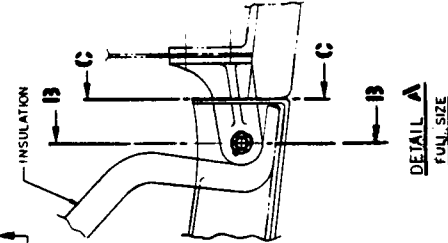
- 1. CONFIGURATION BASED ON ASSUMED SILICOMER RPP ALLOWABLES OF:
 $E = 10000 \text{ PSI}$
 $\nu = 2 \times 10^{-4} \text{ PSI}$
 $\alpha = 1.6 \times 10^{-4} \text{ IN/IN/}^\circ\text{F}$
- MAXIMUM STAGNATION TEMPERATURE = 3600 °F TRUE, INCLUDING CROSS RADIATION RELIEF BUT EXCLUDING NON-CATALYTICITY



SECTION D-D
TYPICAL



SECTION B-B
FULL SIZE



DETAIL A
FULL SIZE



APPROVED FOR RELEASE BY AEROSPACE TECHNOLOGY CENTER	
SHUTTLE LEADING EDGE	
CONCEPT NO. 3	
DATE	1988
BY	
FOR	
APP'D	
CHK'D	
DATE	

reduced weight. These are bonded to the airload panels with pyrolyzed furfuryl alcohol. Limited evaluation of this technique has indicated feasibility but the process must be examined in depth in Phase II. The location and geometry of the intercostals have not been optimized against overall weight and cross-radiation requirements. The leading edge attachment area to the wing support structure has been improved by more optimum distribution of hard insulation and a change from zirconia to fused silica. The leading edge has also been stiffened in this joint area to prevent cocking and binding as the RPP slides on the insulator to accommodate thermal expansion relative to the support structure. Thermal analysis has shown that locating the interface joints close to the skin, as shown, has little effect upon insulation requirements but should be more efficient structurally. Unit weight of this leading edge concept, including panel, rib, intercostals, seal strip, and support point insulator and bolt, is calculated to be under 2 lb. /ft. ².

3.3 THERMAL ANALYSIS

Parametric thermal analyses were performed on the Space Shuttle wing leading edge using estimated oxidation inhibited RPP material properties. The objectives of these analyses were to provide guidance to the materials development effort in tailoring composition and processing of RPP, and to support development of design concepts.

Aerodynamic heating rates were determined for boost and reentry environments. Since reentry heating is far more severe, the remainder of the analysis was devoted to that portion of flight. Radiation equilibrium temperature distribution around the leading edge was computed as a function of reentry time. Baseline thermal properties of inhibited RPP were selected based upon probable material constituents. Effects of property variations were assessed.

The thermal response of seven design concepts of functional elements was computed to obtain temperature time histories and temperature gradients. Means of reducing high circumferential temperature gradients were investigated, including conduction and internal cross radiation. Finally, surface recession of bare, uninhibited RPP was computed to provide a baseline for measuring performance of the inhibited material.

Results show that the most important thermal property of RPP, aside from oxidation resistance, is emittance, which should be 0.80 or higher. It is desirable that conductivity also be high, but this property is less significant.

Internal cross radiation was found to be very important in minimizing both peak temperature and circumferential temperature gradients with attendant reduction of thermal stresses. This factor favors solid laminate construction over a foam core or honeycomb sandwich. High temperature gradients were found to exist across foam core sandwich and structural rib concepts. Support point attachment insulation analysis for the nominal trajectory heating conditions show that 1.0 inch diameter insulator bushings will suffice for protecting titanium support fittings. Finally, surface recession of bare, unhibited RPP due to oxidation was found to be minimal on the leeward side or in areas of the wing with low heating rate, indicating reusability without oxidation protection in these areas.

3.3.1 Aerodynamic Heating

Aerodynamic heating rates during boost and reentry were computed using the trajectories from reference (3). In the continuum flow regime, below 300,000 feet altitude, the computer routine incorporates the real gas, stagnation point theory of Fay and Riddell, developed in reference (5). At higher altitudes, heating rates were based upon free molecular flow theory as discussed in reference (6).

Boost heat flux rates referenced to the stagnation point of a one foot radius sphere at 100°F are presented in figure 3-18. Similar data for reentry is given in figure 3-19, except that a reference temperature of 1000°F was chosen. Air stagnation enthalpy and stagnation pressure are also presented. Since maximum heating rates during reentry are several times higher than those during boost, the remainder of the thermal analysis was devoted to reentry.

Heating rates at local positions on the leading edge were normalized to the reference heating rates. They are presented in figure 3-20 as a function of percent chord distance from the geometrical leading edge. The lower curve presents the ratio ($q_{\text{local}}/q_{\text{sphere}}$) of local heat flux rate to the reference heat flux of figure 3-19. This curve is based primarily upon NASA-LRC wind tunnel data. However, in the local area forward of the stagnation line a theoretical distribution for cylindrical surfaces was employed.

Effects of fuselage flow interference increase local heating rates over the values given by the lower curve in figure 3-20. The magnitude and distribution of the interference effect in the leading edge region is presently uncertain, so an estimated distribution for the worst interference heating case was established as shown by the upper curve. This presents the ratio ($q_{\text{int}}/q_{\text{non-int}}$) of heat flux rate with interference effects to that

HEAT FLUX RATE REFERENCED TO 1 FT. RADIUS
SPHERE AT 100°F

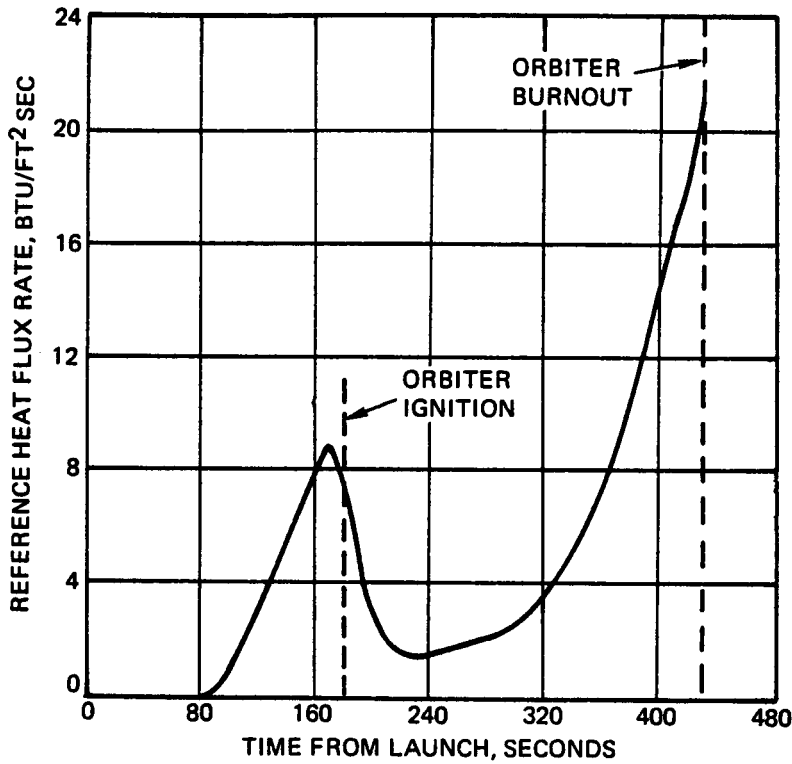


FIGURE 3-18 BOOST AERODYNAMIC HEATING

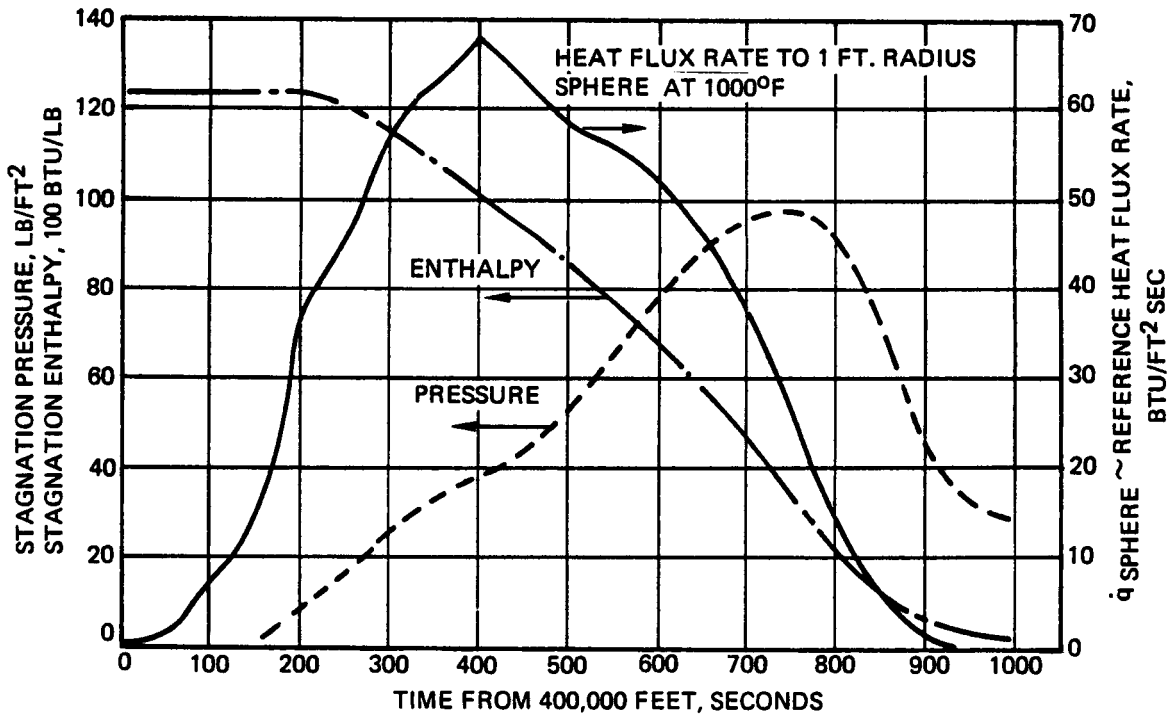


FIGURE 3-19 RE-ENTRY AERODYNAMIC HEATING

with no interference. The slope of the curve was based upon experimental data from reference (4), and the magnitude results in peak radiation equilibrium temperature of 4000°F for the baseline design configuration with a surface emittance of 0.80.

The lower curve in figure 3-20 is for a chord length of 150 inches. With a baseline chord length for this study of 214 inches a correction factor of $\sqrt{150/214}$ must be applied to obtain local heating rates. A hot wall correction is also necessary because the reference heat flux rate in figure 3-19 is for a 1000°F wall. The final expression for local heat flux rate to a wall at temperature T_W is as follows:

$$\dot{q}_{HOT} = \dot{q}_{SPHERE} \left[\frac{\dot{i}_R - \dot{i}_W}{\dot{i}_R - \dot{i}_C} \right] \sqrt{\frac{150}{214}} \left[\frac{\dot{q}_{INT}}{\dot{q}_{NON-INT}} \right] \left[\frac{\dot{q}_{LOCAL}}{\dot{q}_{SPHERE}} \right]$$

where,

$$\begin{aligned} \dot{i}_R &= \text{Air recovery enthalpy, BTU/LB} \\ \dot{i}_W &= \text{Air enthalpy at } T_W \text{ and local pressure} \\ \dot{i}_C &= \text{Air enthalpy at } 1000^\circ\text{F} \end{aligned}$$

Local pressures on the leading edge are given by the stagnation pressure in figure 3-19, together with pressure distributions from reference (7).

3.3.2 Radiation Equilibrium Temperatures

Because of the dominant contribution of surface re-radiation to disposal of the incident aerodynamic heating, radiation equilibrium temperatures provide an indication of reentry surface temperature of inhibited RPP. Radiation equilibrium temperatures assume that the incident heat is entirely removed by surface re-radiation to space. Hence, heat sink, conduction and internal cross-radiation effects are neglected. These effects are dependent upon specific design concepts and are considered in sections 3.3.4 and 3.3.5.

Temperatures were computed as a function of both leading edge location and reentry time as shown in figures 3-21 and 3-22 respectively. Figure 3-22 presents a temperature time plot for the stagnation line under maximum interference heating conditions, which results in a peak temperature of 4000°F at 400 seconds. It will be noted that the temperature-time curve is much flatter than the heat flux-time curve in figure 3-19 due to the fourth power relationship between re-radiated heat flux and temperature.

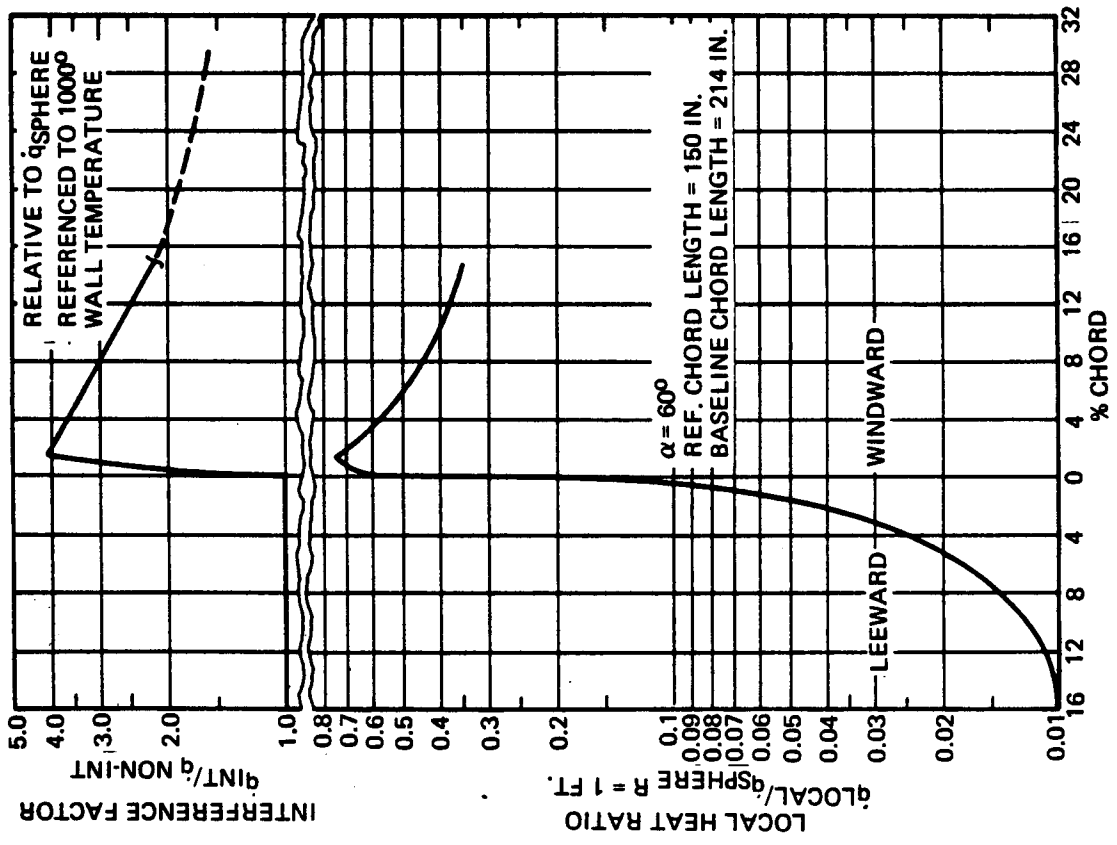


FIGURE 3-20 INTERFERENCE FACTOR AND LOCAL HEAT RATIO

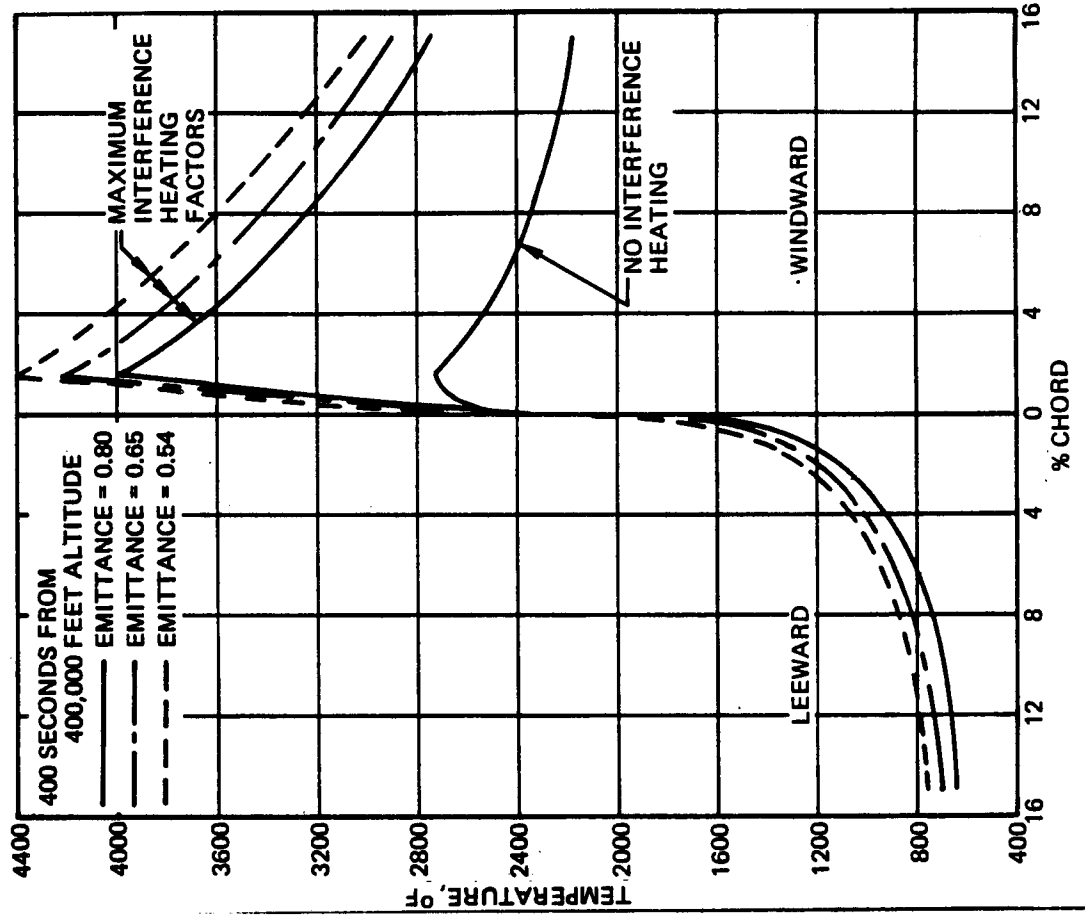


FIGURE 3-21 RADIATION EQUILIBRIUM TEMPERATURES TIME OF PEAK RE-ENTRY HEATING

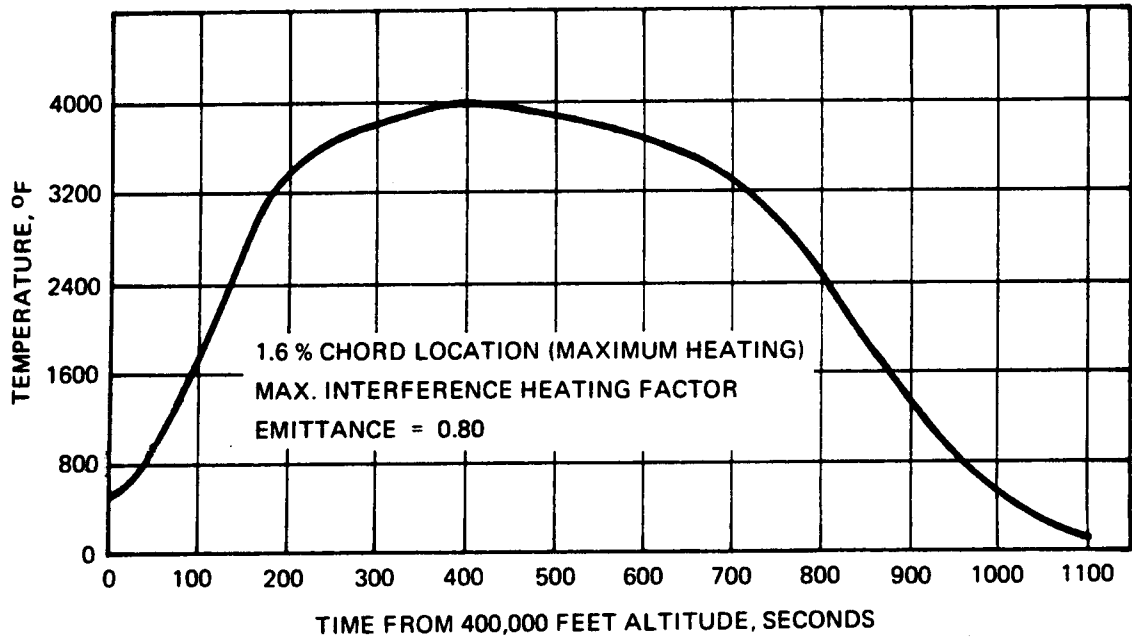


FIGURE 3-22 RADIATION EQUILIBRIUM TEMPERATURE TIME HISTORY

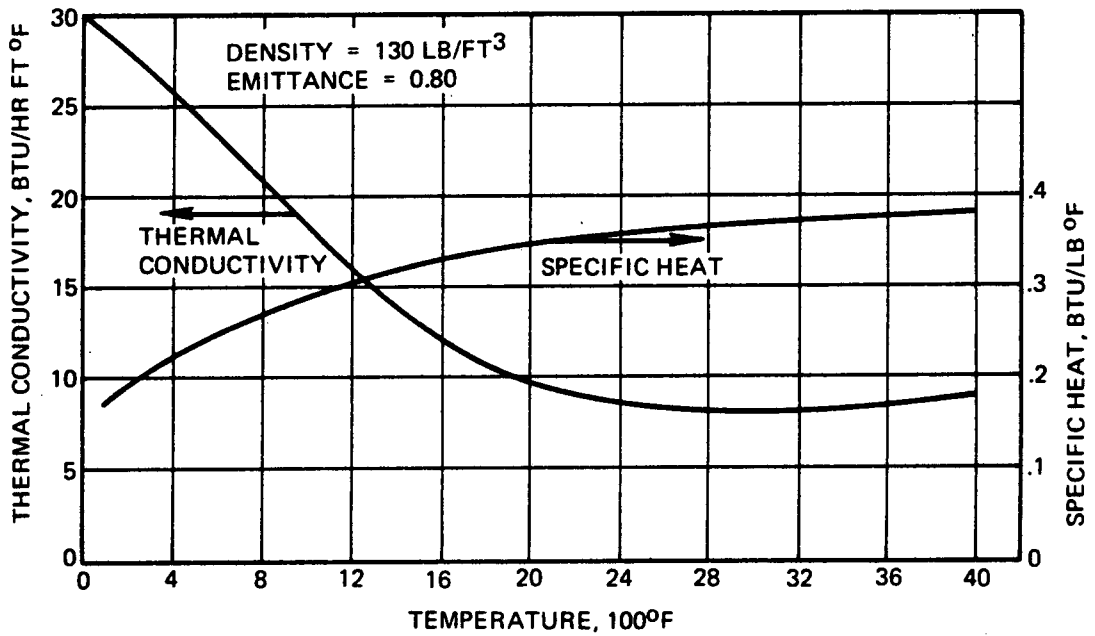


FIGURE 3-23 BASELINE THERMAL PROPERTIES OXIDATION INHIBITED RPP LAMINATE

Temperatures shown in figure 3-21 are a function of location on the leading edge, at the time of peak heating. Results are given for maximum interference heating and no interference heating, which yield peak temperatures of 4000 and 2720^oF respectively. The extreme circumferential temperature gradient near the leading edge is evident. Methods of reducing this gradient and resultant thermal stresses are covered in section 3.3.5.

In order to assess the influence of material emittance upon peak surface temperatures, a range of emittance values from 0.54 to the baseline value of 0.80 were considered. A resulting variation in peak surface temperature of 385^oF is illustrated in figure 3-21 establishing the importance of maintaining high emittance.

3.3.3 Thermal Properties

Baseline thermal properties selected for analysis of inhibited RPP laminates are shown in figure 3-23. These properties are based upon constituent property data and are most representative of a zirconium diboride add-mix system, but were expected to be reasonable representative of other systems as well, excluding the overlays. Thermal properties of zirconia overlay, shown in figures 3-24 and 3-25 are based upon data from reference (8). Properties of fused silica, used as an attachment insulator, and of silicon carbide foam, used in the foam core sandwich design concept are from references (8) - (10). A comparison between the properties used for analysis and those obtained on the selected material systems under development can be made by referring to section 5.4.

3.3.4 Thermal Response of Design Concepts

Transient thermal response analyses were performed to compute time history temperature distributions across seven leading edge design functional elements. The purpose of these analyses were to:

- (1) Support materials selection by determining maximum temperatures at various locations in the design elements.
- (2) Provide temperature gradients in the cross ply direction for use in thermal stress analyses.
- (3) Identify important material properties for guidance in materials development.
- (4) Assist in selection of preliminary design dimensions that will limit absolute temperatures and temperature gradients.

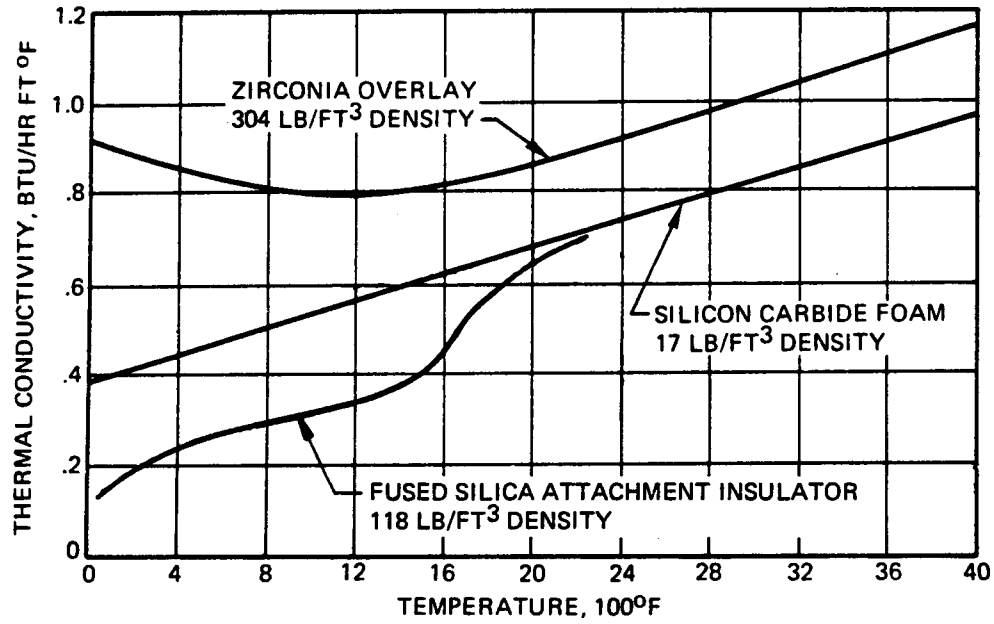


FIGURE 3-24 THERMAL CONDUCTIVITY OF FOAM CORE, OVERLAY AND ATTACHMENT INSULATOR

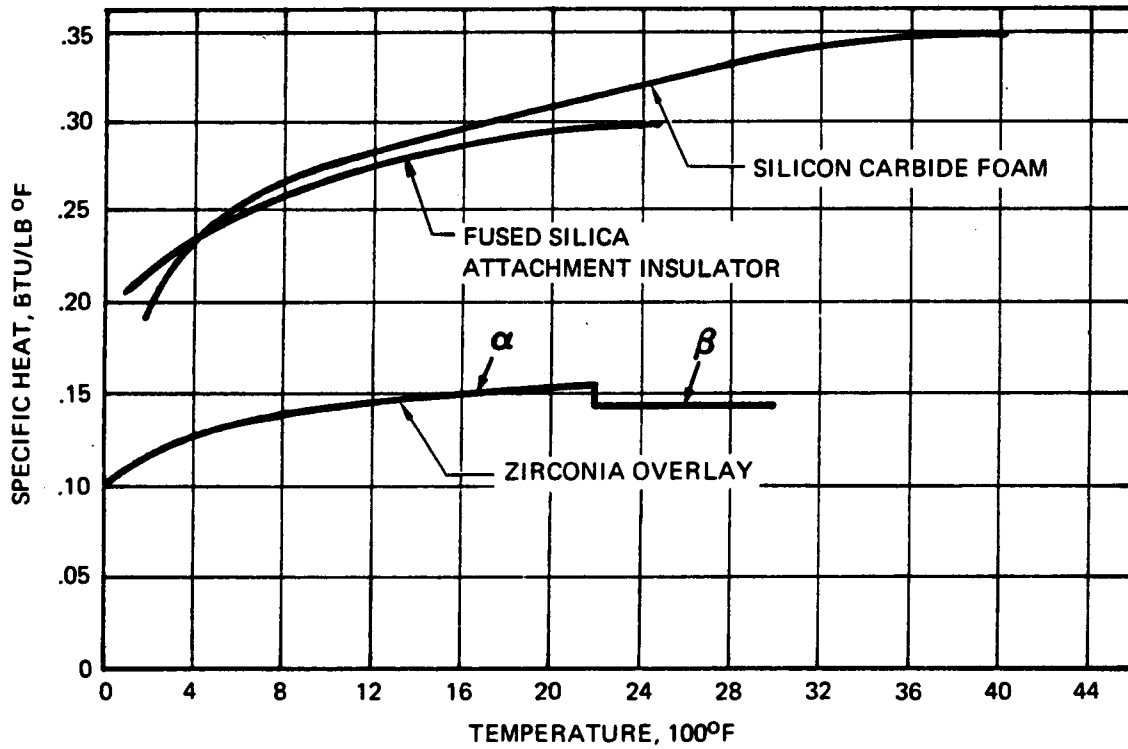


FIGURE 3-25 SPECIFIC HEAT OF FOAM CORE, ATTACHMENT INSULATOR AND OVERLAY

The following functional elements from section 3.2 were considered, all of which employ inhibited RPP.

- o Solid laminate skin
- o Foam core sandwich skin
- o Honeycomb sandwich skin
- o Solid laminate cover over foam core sandwich
- o Zirconia overlay on solid laminate skin
- o Structural rib
- o Attachment between leading edge segments and titanium wing support structure

Computer routines were employed for numerical calculations. In order to properly account for heat sink effects, a convective heating boundary condition was used at the heated surface, rather than imposing radiation equilibrium temperatures. Analyses were performed at three locations on the leading edge periphery and radiation equilibrium surface temperatures provided a basis for interpolating results to other locations.

Variation of thermal properties with temperature were taken into account in all analyses. Cross radiation between inside surfaces of design concepts and surrounding structure was not considered in the analyses of this section. The validity of this simplification for specific concepts is discussed in the following paragraphs. For the solid laminate skin, cross radiation effects are evaluated in section 3.3.5.

Solid Laminate Skin - One-dimensional transient analyses were performed to predict peak temperatures and maximum temperature differences across solid RPP laminates for a range of skin thicknesses. Resulting temperature-time response curves shown in figure 3-26 are for the outside and inside surfaces of a 0.15 inch thick laminate at the stagnation line with maximum interference heating. The transient response results are compared with radiation equilibrium temperatures, and it is seen that the differences are quite small except for times early and late in reentry, when the heating is low and changing rapidly. The reduction in peak temperature from the radiation equilibrium value was only 11°F. Analyses were performed for greater thicknesses with a maximum reduction of only 28°F for 0.50 inch thick laminate. This indicates that heat sink effects, which are a function of material specific heat, are ineffectual in reducing peak temperatures.

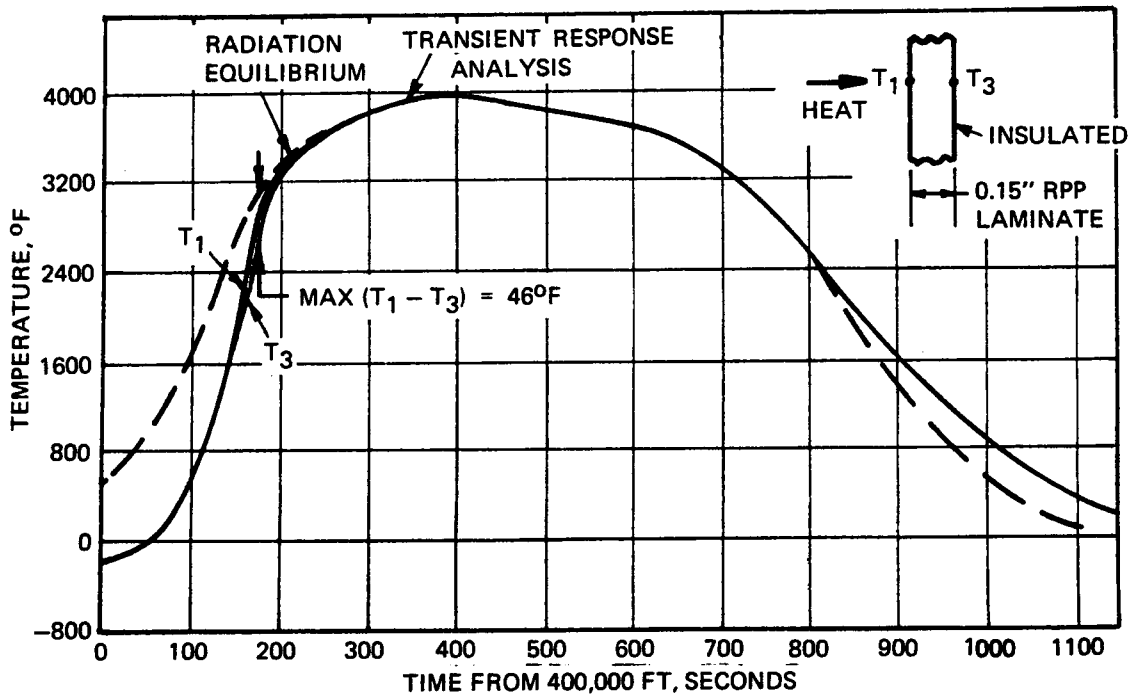


**FIGURE 3-26 THERMAL RESPONSE OF SOLID LAMINATE
MAX. INTERFERENCE HEATING, STAGNATION LINE**

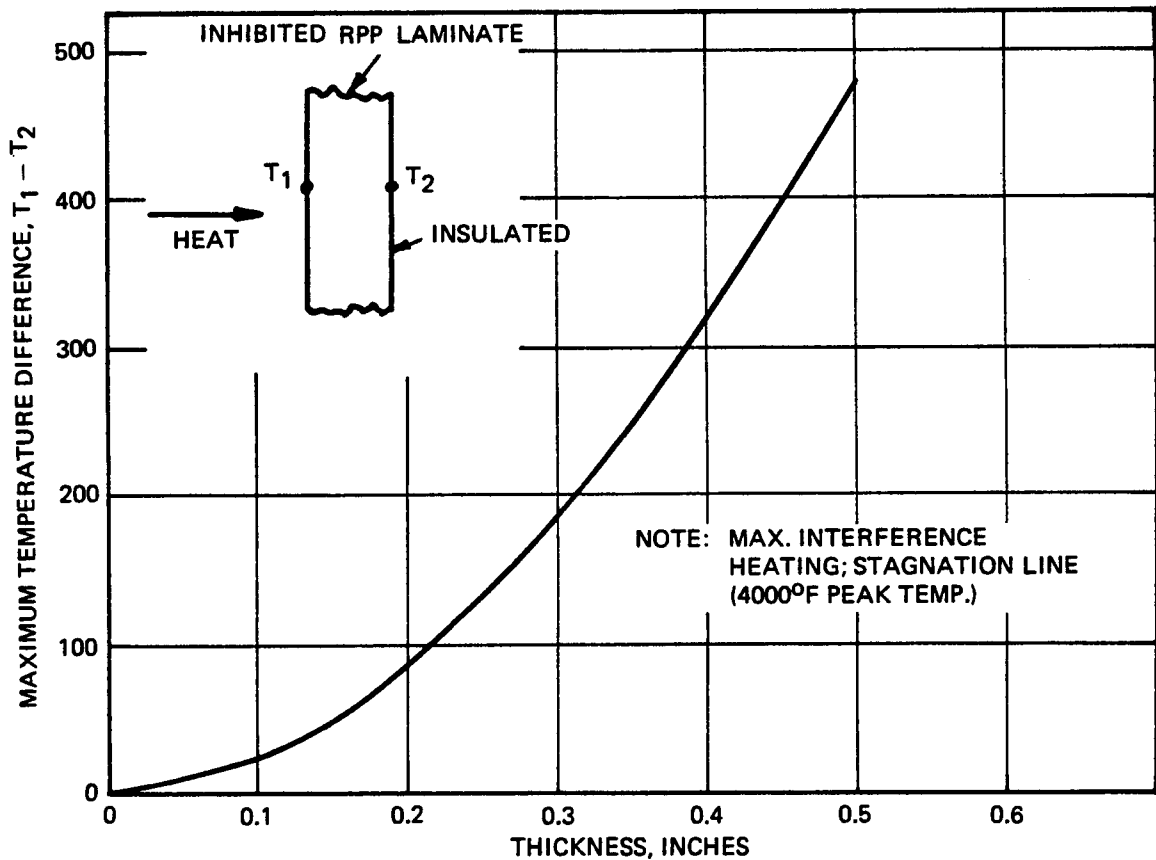


**FIGURE 3-27 MAXIMUM TEMPERATURE DROP ACROSS
RPP LAMINATE**

The maximum temperature difference across the 0.15 inch thick skin is only 46°F, and it occurs at 175 seconds, when the rate of temperature rise is a maximum. A strong variation of temperature gradient with skin thickness is shown on figure 3-27. However, stress analyses indicate the thickness will likely be less than 0.20 inch and therefore a temperature difference of less than 100°F is expected.

It should be noted that analyses in section 3.3.5 indicate that cross-radiation of heat from the back side of the laminate to surrounding structure significantly alters temperature gradients. Since the temperatures in figures 3-26 and 3-27 do not reflect cross-radiation, they apply only to designs in which this radiation is suppressed. Tailoring of skin material for high thermal conductivity across the plies is clearly not justified for such designs, because temperature gradients in that direction will be quite low.

Foam Core Sandwich - The design configuration considered for this analysis consisted of 0.61 inch thick silicon carbide foam with 0.04 inch thick RPP laminate faces bonded to each surface, as shown in figure 3-28. This particular geometry was based on early structural design estimates. One-dimensional analyses were performed to predict maximum temperature gradients for three locations on the leading edge. Intimate thermal contact between the faces and core was assumed.

The variation of maximum temperature difference with the heat flux corresponding to various locations is presented on figure 3-28. Due to the low conductivity of the foam, the temperature difference is much greater than for solid laminates, reaching a maximum of 1497°F at the stagnation line.

Temperature-time response of the faces and foam at the stagnation line is given on figure 3-29. At the time of peak temperature difference, 175 seconds, the temperature on the back side is low, relative to that on a solid laminate. Back side cooling by cross-radiation will therefore be much lower than for a solid laminate by a factor of about 6.2. Maximum temperature gradients in figure 3-28 which are based upon an insulated back face, should therefore be realistic.

Honeycomb Sandwich - This concept consists of 0.61 inch thick bare RPP honeycomb with 0.04 inch thick inhibited RPP laminate faces bonded to each surface, as shown in figure 3-30. The honeycomb bulk density was 17 lb/ft³ with 0.25 inch cells. One-dimensional analyses were performed to predict maximum temperature gradient at the stagnation line. Intimate thermal contact between the faces and core was assumed, and heat transfer across the honeycomb included both

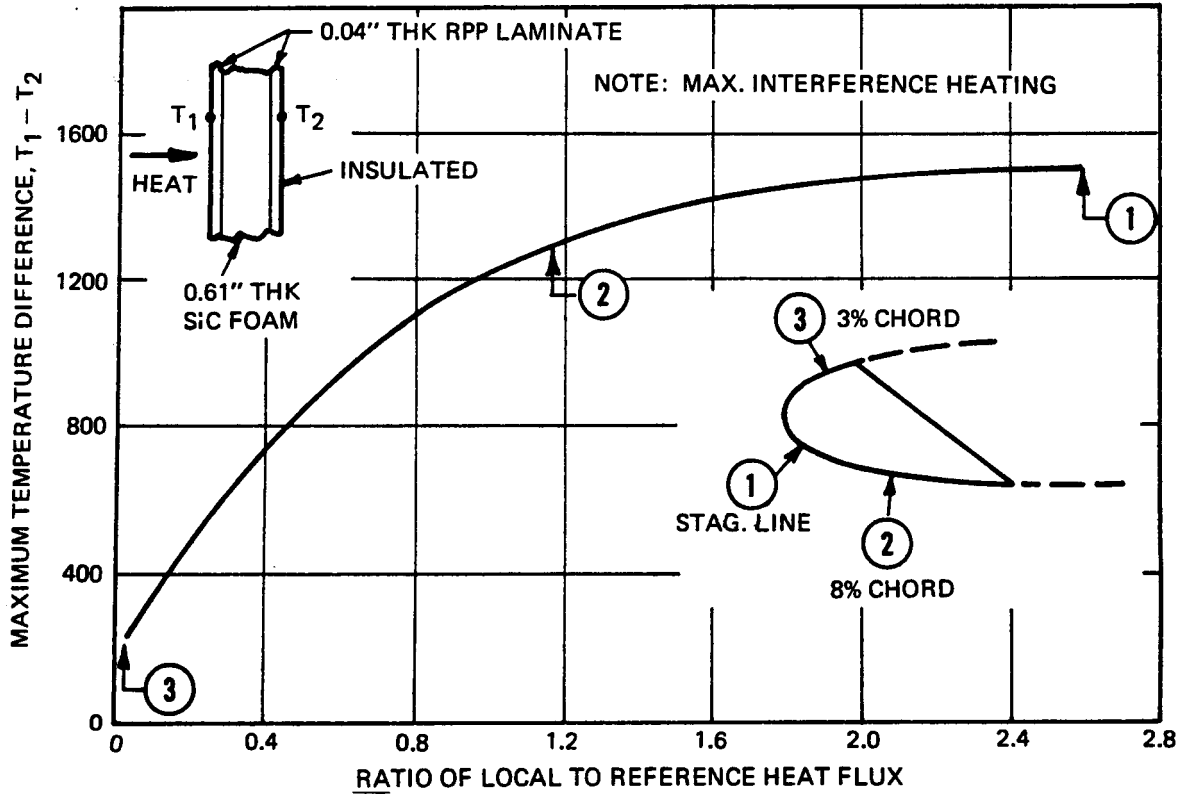


FIGURE 3-28 MAXIMUM TEMPERATURE DROP ACROSS RPP FOAM CORE SANDWICH

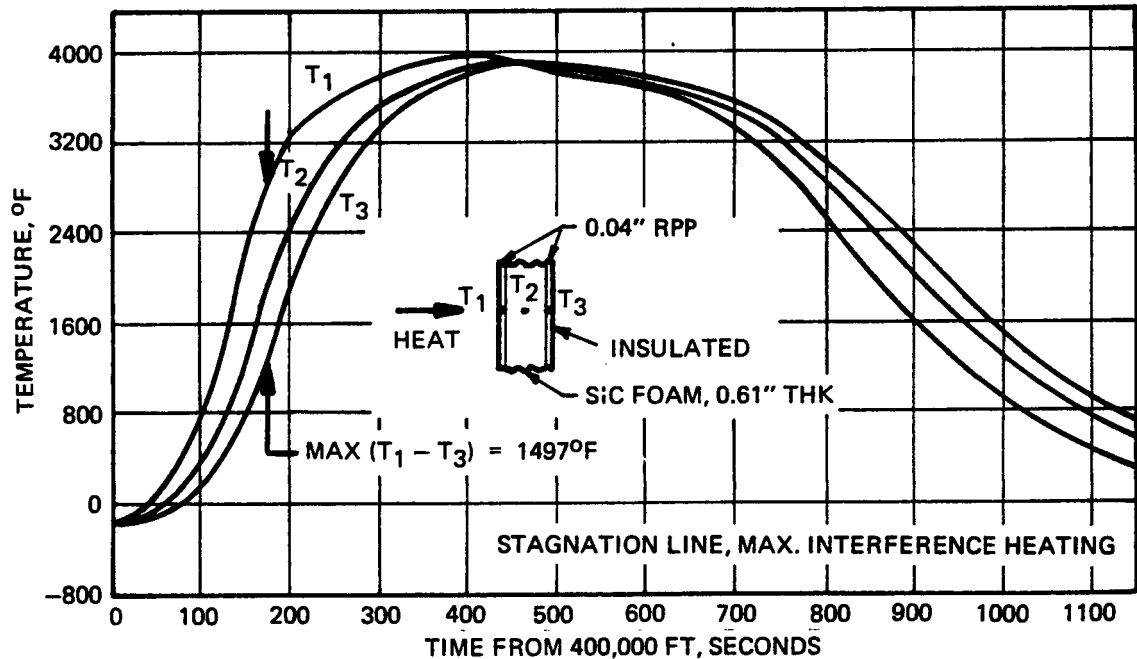


FIGURE 3-29 THERMAL RESPONSE OF FOAM CORE SANDWICH

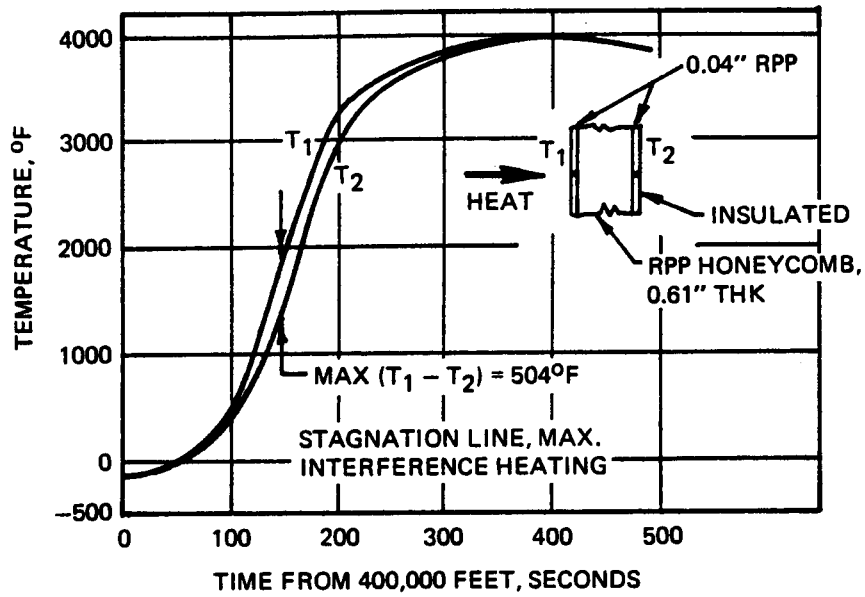


FIGURE 3-30 THERMAL RESPONSE, HONEYCOMB SANDWICH

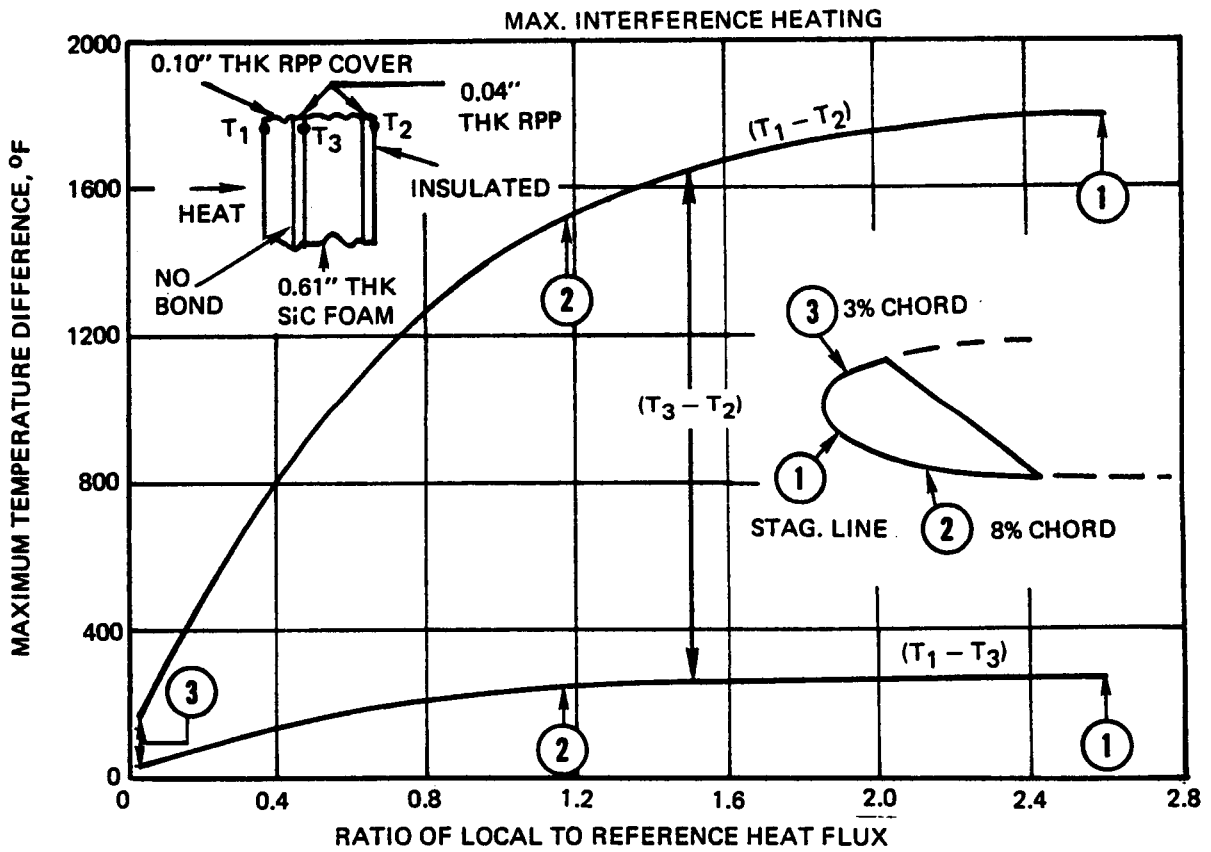


FIGURE 3-31 MAXIMUM TEMPERATURE DROP ACROSS COVER/SANDWICH COMBINATION

conduction and radiation modes. Radiation heat transfer included interchange between faces and cell walls, as well as direct radiation from face to face.

The maximum temperature difference between the sandwich faces is 504°F and occurs at 150 seconds. This temperature difference is lower than that for foam core sandwich, and occurs slightly earlier, due primarily to the radiation heat transfer across the honeycomb. It is still much higher, however, than the temperature difference across 0.15 inch thick solid laminate. It will be noted that cross-radiation from the front to back face did not reduce the peak front face temperature. This is due to the fact that the backface does not constitute an appreciable heat sink, because it is thin and was assumed insulated on the back side.

Cover on Foam Core Sandwich - In this concept the foam core sandwich analyzed previously is covered by a 0.10 inch thick layer of RPP laminate. The cover was planned to serve as both an oxidation and thermal barrier and could be replaced after a limited number of flights. It is retained mechanically, rather than bonded to the foam core sandwich.

Analyses were performed to predict maximum temperature gradients for three locations on the leading edge and the reduction in temperature of the sandwich due to the cover. Thermal contact between the cover and sandwich is imperfect, so it was necessary to estimate the thermal conductance across the interface between these two elements.

Heat is transferred across the interface, or joint, by conduction and radiation. The conduction component was estimated from measurements in reference (10) using the joint coefficient between silicon carbide coated RPP and pyrolytic graphite at 700°F, with no contact pressure at the joint. A computed radiation component of 7 BTU/HR-FT²°F at 700°F, was subtracted from the measured total coefficient of 100 BTU/HR-FT²°F to yield a conduction component of 93 BTU/HR-FT²°F. Joint coefficient as a function of temperature was estimated by summing radiation and conduction contributions, the latter being assumed invariant with temperature. Results indicate that at the lower temperatures of interest, conduction and radiation are of the same order of magnitude, whereas at higher temperatures radiation dominates.

Figure 3-31 presents the variation of maximum temperature differences with the heat flux at various locations. The temperature difference across the sandwich ($T_3 - T_2$) is essentially the same as it is without the cover. The temperature difference between the cover front face and the sandwich front face ($T_1 - T_3$) is a maximum of 280°F.

Since the computed joint coefficient is not precise, limited analysis was performed to determine sensitivity of computed temperatures to variation in joint coefficient. As a lower limit the joint coefficient was assumed to be equal to radiation component alone. Results are shown in figure 3-32 which presents temperature at the time of maximum gradient, 175 seconds. The effect of reduced joint coefficient is to reduce sandwich temperatures by 230°F, with little effect upon gradients within the cover or sandwich.

The effect of the cover in reducing the maximum temperature reached by the back face of the sandwich is given in figure 3-33. Without the cover the back face reaches a maximum temperature 75°F lower than the maximum reached by the front face at the stagnation line. With the cover the temperature reduction from cover front face to sandwich back face is 86°F. Hence, the cover reduces maximum sandwich back face temperature only 11°F. With reduced joint coefficient a further reduction of 5°F was obtained. The cover is therefore ineffectual as a thermal barrier and would serve only as an oxidation barrier.

Overlay on Solid Laminate Skin - This concept consists of an overlay of zirconia bonded to a 0.15 inch thick RPP laminate, as shown in figure 3-34. The overlay was planned to function as both an oxidation and a thermal barrier. The purpose of the analysis was to determine the reduction in maximum RPP laminate temperature which could be achieved with various thicknesses of zirconia.

One-dimensional analyses were performed for the stagnation line, with the overlay and laminate being considered in intimate thermal contact. Only a 52°F reduction in laminate temperature can be achieved with a 0.16 inch thick overlay, the maximum thickness considered. Thus, the overlay is ineffectual as a thermal barrier and could serve only as an oxidation barrier.

Structural Rib - The type of skin support rib being considered as the prime candidate for the leading edge is integrally laid up with a solid laminate skin as shown in figure 3-35. The purpose of this analysis was to predict maximum temperature gradients across the rib, as a function of location on the leading edge and design dimensions for use in rib thermal stress analysis.

A two-dimensional analysis was performed which considered heat conduction along the skin and across the rib vertical member, as well as cross-radiation from the skin to the rib web and upper flange. In the actual design two ribs will be mated as shown in figure 3-17. Since thermal response of the ribs will be similar, the mating surface was assumed to be

COVER/SANDWICH CONCEPT
 HIGH INTERFERENCE HEATING, STAGNATION LINE
 TIME OF MAXIMUM GRADIENTS, 175 SEC. FROM
 400,000 FT.

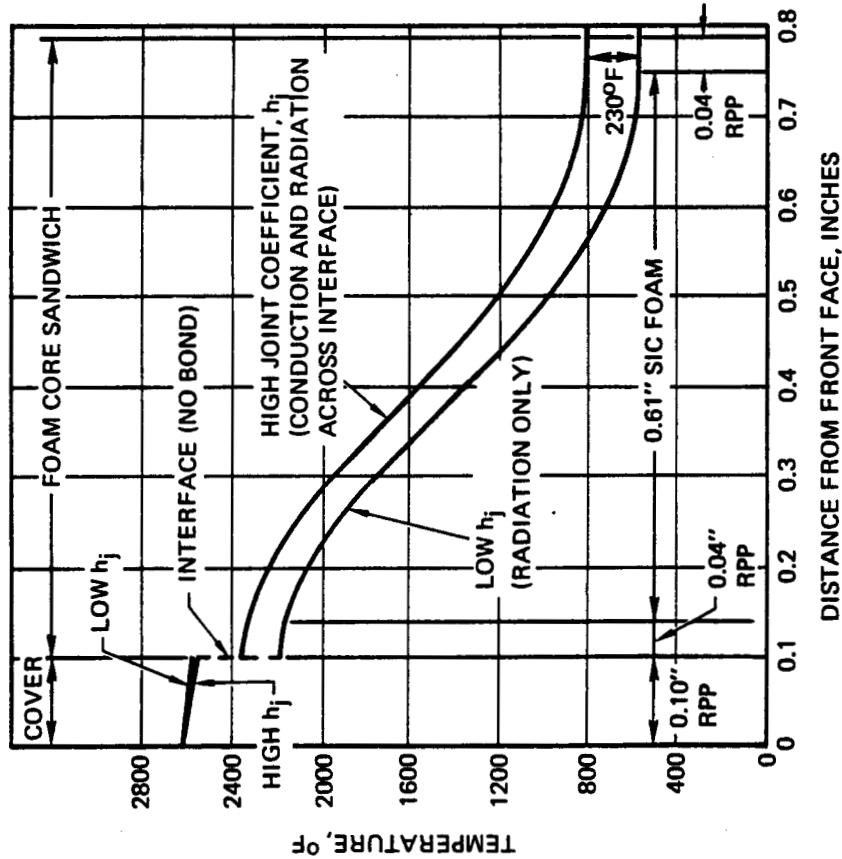


FIGURE 3-32 EFFECT OF JOINT COEFFICIENT UPON TEMPERATURE GRADIENTS

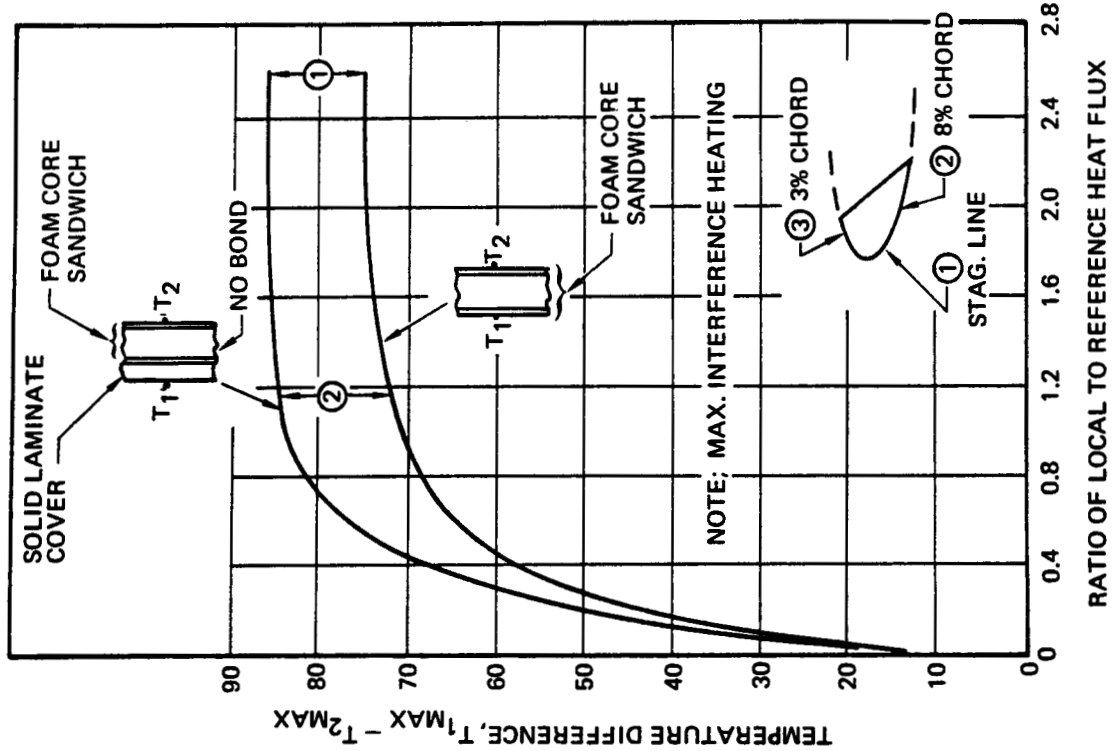


FIGURE 3-33 TEMPERATURE REDUCTION ON BACK SIDE FOAM CORE SANDWICH

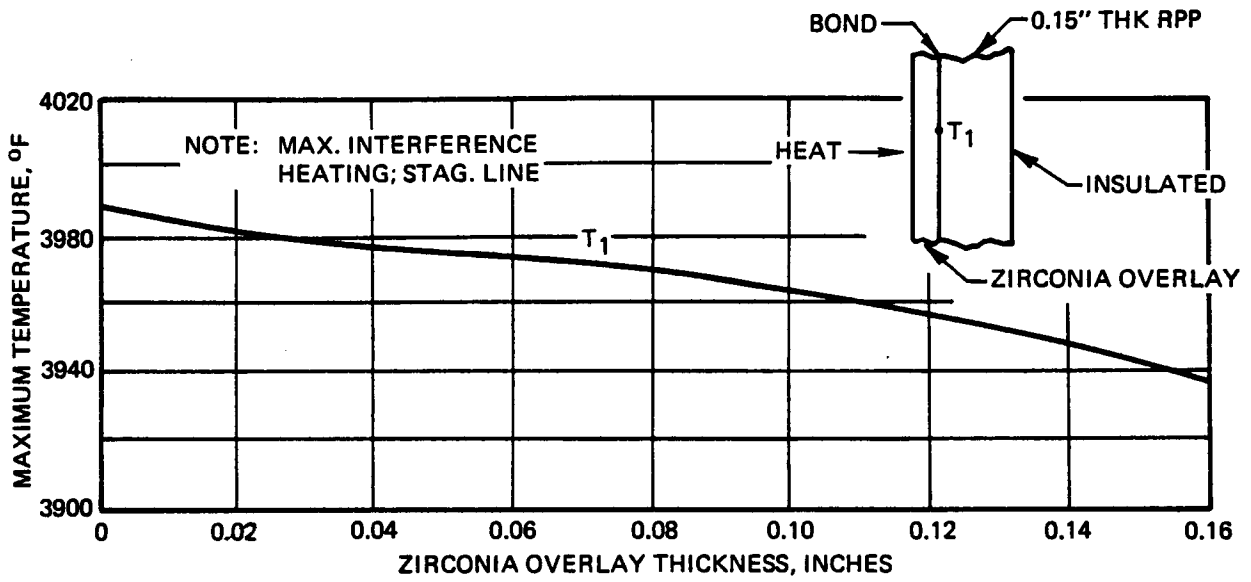


FIGURE 3-34 MAXIMUM TEMPERATURE OF RPP WITH OVERLAY

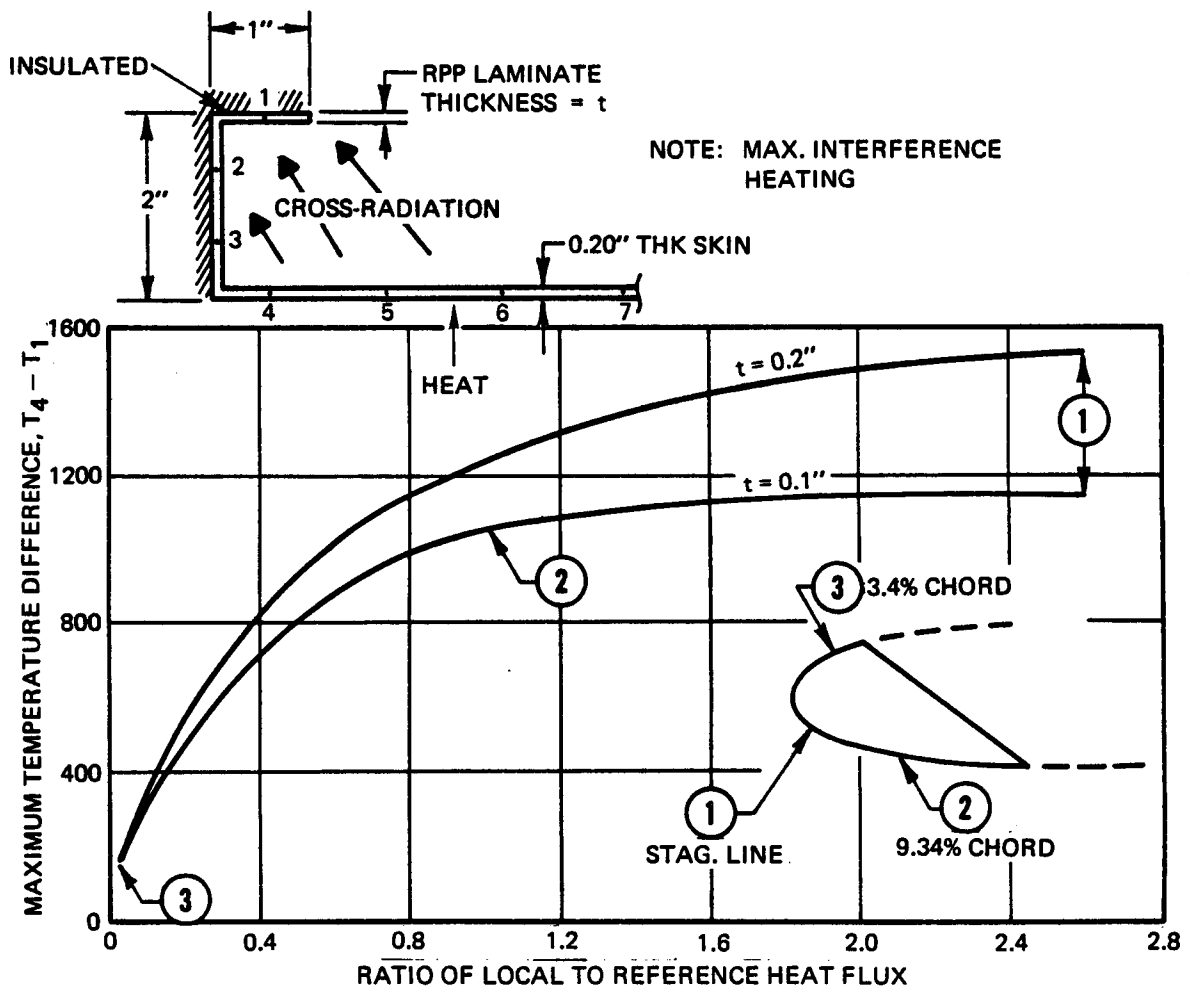


FIGURE 3-35 MAXIMUM TEMPERATURE DROP ACROSS RIB

insulated. The top surface of the upper flange was also assumed to be insulated. Cross radiation from this surface to surrounding structure is possible; however, this analysis indicates that at the time of maximum gradient the surface temperature is relatively low, precluding appreciable radiation cooling.

The surface of the rib web which receives radiation from the skin also views surrounding structure. This was included in the analysis, with the surrounding structure temperature being computed from radiant interchange with the skin and rib.

Maximum temperature difference across the rib as a function of the heat flux at various locations is given in figure 3-35. Rib thicknesses of 0.10 inch and 0.20 inch were considered with skin thickness of 0.20 inch. A severe gradient was developed, with temperature differences of 1140°F and 1530°F for thickness of 0.10 and 0.20 inch, respectively at the stagnation line. The higher gradient for the greater thickness is due to the greater rib heat capacity which delays heat up of the upper flange.

It will be noted that the rib temperature difference is about the same as that across the foam core (figure 3-28). This was surprising since cross-radiation at elevated temperatures is a better heat transfer mode than conduction across foam. Figures 3-36 and 3-37 which present temperature-time response curves for the 0.20 inch thick rib at three locations, show that at the time of peak gradient, 175 seconds, the skin temperature is far below its peak value, limiting the cross-radiation heat transfer. The relatively low temperature at node 2 in figures 3-36 and 3-37 is due to radiant interchange between the web and surrounding structure. Temperature of the surrounding structure was somewhat lower than that of the skin. At node 3 this effect was overridden by conduction.

Sensitivity analyses were performed to assess methods of minimizing the rib temperature gradient, since preliminary stress analyses indicated high resultant stresses. Three approaches were investigated,

- o Reduce rib height to enhance conduction
- o Increase thickness of web to enhance conduction
- o Increase skin thickness locally near rib to reduce rate of temperature increase

MAX. INTERFERENCE HEATING, STAGNATION LINE

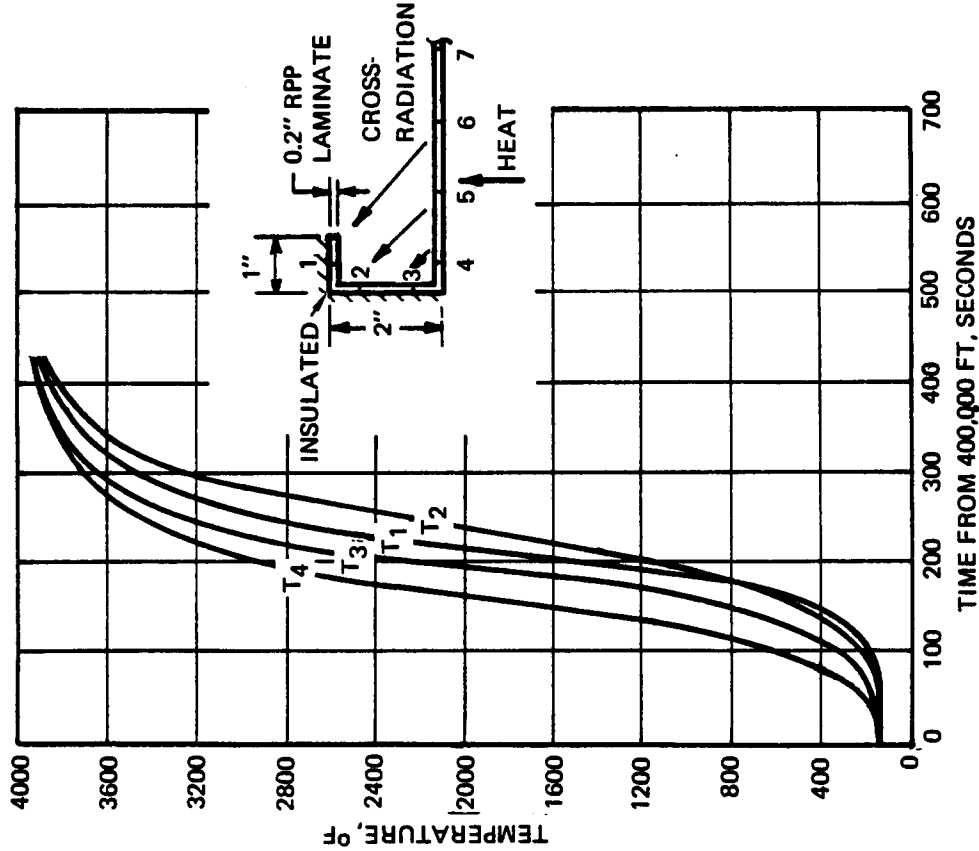


FIGURE 3-36 THERMAL RESPONSE OF RIB

MAX. INTERFERENCE HEATING

0.20" THK RPP RIB AND SKIN
2" RIB HEIGHT
SEE SKETCH IN FIGURE 36 FOR LOCATIONS OF POINTS 1 - 4

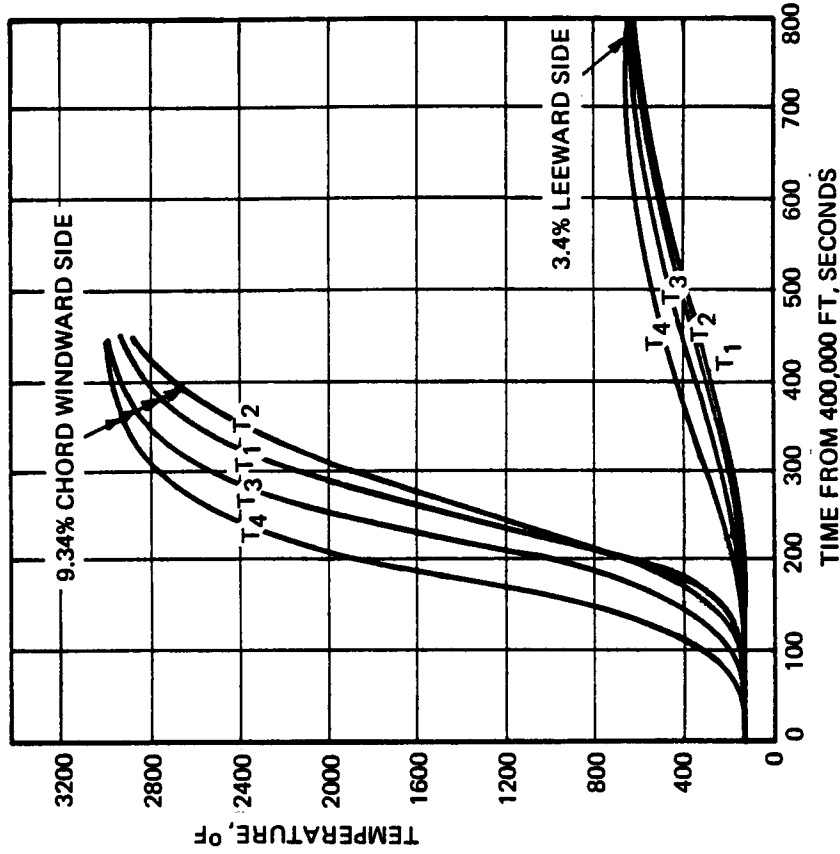


FIGURE 3-37 THERMAL RESPONSE OF RIB

Heating rates corresponding to a peak radiation equilibrium temperature of 3600°F were used, based upon results of cross-radiation analyses in section 3.3.5 which indicated this to be a realistic peak stagnation line temperature for solid laminate skin construction. The sketch below and table 3-3 show the rib and skin dimensions considered.

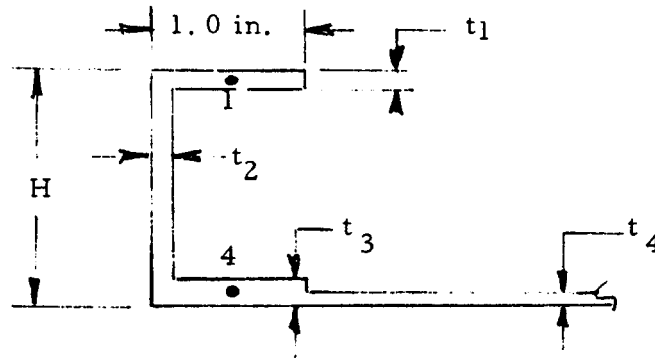


TABLE 3-3 RIB ANALYSIS SUMMARY

Configuration	H"	t ₁ "	t ₂ "	t ₃ "	t ₄ "	(T ₄ -T ₁) _{max} °F	
1	2.0	0.2	0.2	0.2	0.2	1450	Results from Figure 3-35 q/q _{REF} = 1.74
2	2.0	0.1	0.1	0.2	0.2	1130	
3	1.5	0.1	0.1	0.22	0.12	850	Sensitivity analyses q/q _{REF} = 1.74
4	1.5	0.1	0.2	0.22	0.12	862	
5	1.0	0.1	0.1	0.22	0.12	766	

Table 3-3 summarizes maximum temperature differences from figure 3-35 (Configurations 1 and 2) and the sensitivity analyses (Configurations 3-5). Reducing the rib height, H, and increasing the local skin thickness, t₃, relative to the nominal skin thickness, t₄, reduces the temperature difference significantly, from 1130°F (Configuration 2) to 766°F (Configuration 5). Increasing the thickness of the web is ineffective, as seen by comparing Configuration 3 and 4. This is evidently due to the increased heat capacity of the rib, which offsets the increased conduction. It should be noted that the dimensions used in the most favorable configuration (5) are considered sound from a structural viewpoint.

Attachment Between Skin and Titanium Bean - The leading edge is attached to titanium brackets bolted to the wing box as illustrated in figure 3-38. Analyses were performed to determine the insulation required to protect the titanium brackets and steel bolt from overheating for

aerodynamic interference heating conditions which result in a peak radiation equilibrium temperature of 3290°F at the stagnation line. The investigation of insulative heat shield attachment systems in reference (10) indicates that for temperatures of interest in the attachment area (2000°F maximum) fused silica insulator, or its equivalent, will be required.

A number of insulation concepts and dimensions were analyzed, resulting in selection of the configuration shown in figure 3-38. This provides a 1.0 inch diameter by 0.7 inch thick insulator to protect the bolt, plus one inch diameter by 0.2 inch thick washers and bushings to protect the titanium brackets. A two-dimensional, 50 node thermal model was used for analysis of this configuration and included heat conduction along the skin and flanges, across the insulators, and into the bolt and titanium brackets. Cross radiation from the skin to the RPP flanges and 0.2 inch thick washer was included, while other surfaces were assumed to be insulated.

Bolt temperature on figure 3-38 is shown to peak at 1170°F , late in reentry, while the titanium bracket temperature reaches 680°F during subsonic cruise. Nickel alloy steel bolts can operate at temperatures in excess of 1200°F , hence their predicted temperature is acceptable. Predicted peak titanium temperature is only slightly above the value of 650°F given as a limit in reference (4). If necessary, the insulator thickness can be increased slightly to eliminate the small predicted over-heat.

3.3.5 Reduction of Skin Temperature Gradients

The circumferential temperature gradients based on radiation equilibrium temperatures, presented in figure 3-21 result in high thermal stresses. Two modes of heat transfer, not accounted for in the radiation equilibrium analysis, which tend to reduce these gradients are conduction along the skin in the circumferential direction and internal cross-radiation. Analyses were therefore performed to assess the magnitude of these effects. Solid RPP laminate skin was considered in all analyses.

Circumferential Heat Conduction - A two-dimensional analysis was conducted to determine the effect of conduction on circumferential gradients in the area near the stagnation line. Internal cross-radiation was not included in this analysis. Figure 3-39 shows the resulting skin temperatures in the region of the stagnation line at the time of peak gradients, 400 seconds, for maximum interference heating. Temperatures are shown for three skin thicknesses, 0.2, 0.3, and 0.5 inch. Only a 7.5 percent reduction in maximum temperature gradient from the radiation equilibrium value was achieved with the thickest skin. At 175 seconds,

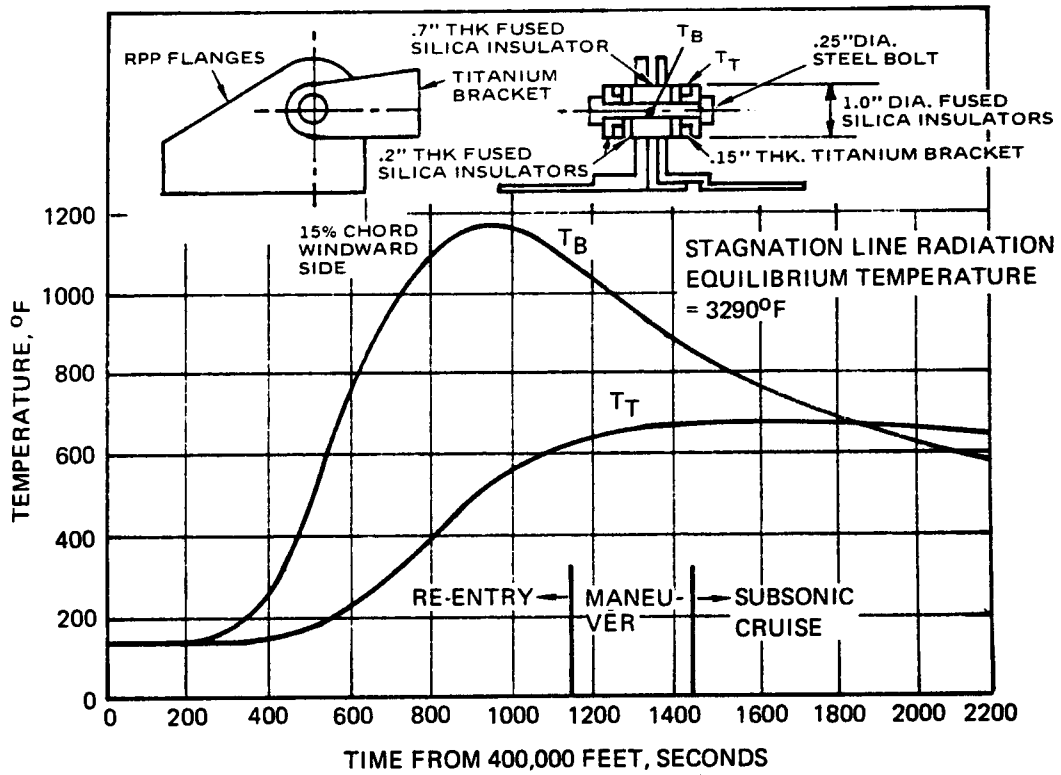


FIGURE 3-38 ATTACHMENT THERMAL RESPONSE

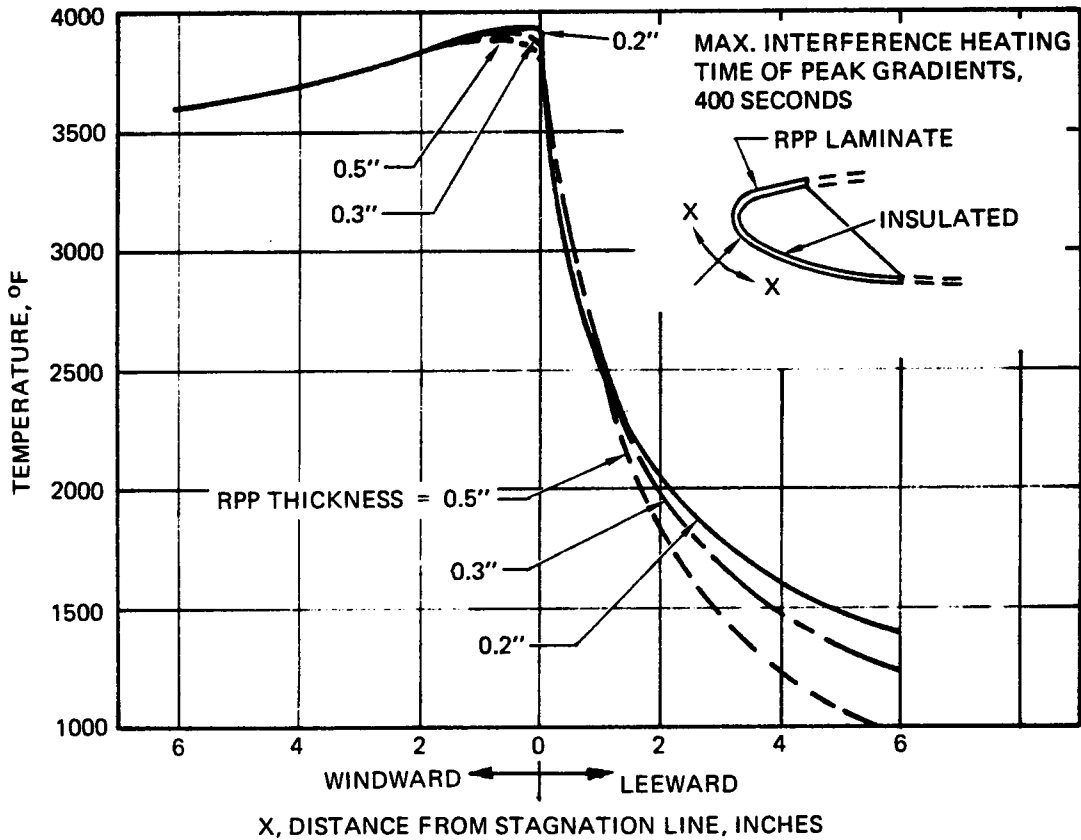


FIGURE 3-39 EFFECT OF CIRCUMFERENTIAL HEAT CONDUCTION UPON TEMPERATURE GRADIENTS

however, when heating rates are 35% of those at 400 seconds, the gradient was reduced 44% with a 0.5 inch skin. The efficiency of conduction in reducing circumferential gradients is therefore highly dependent upon the degree of interference heating. Only if this heating is minimal will local increases in skin thickness and tailoring of skin material for high conductivity be warranted. This is the case at the 175 second time point, where maximum gradients have been computed.

Cross Radiation - A two-dimensional analysis was conducted to determine the effect of cross radiation within the leading edge upon temperature gradients. Heat conduction through the skin in both circumferential and thickness directions was included in the analysis. Figure 3-40 shows the 43 node thermal model which was employed. A constant 0.20 inch thick RPP laminate skin was considered. The aft surface of the enclosure was assumed to be adiabatic to represent insulation over the wing support structure. All 24 interior nodes were permitted to participate in the cross radiation.

Radiation view factors between nodes were computed using Hottel's "crossed string method" from reference (11).

Numerical calculations were performed using a VMSC computer routine, which calculates coefficients for cross-radiation from the view factors and emittance using an exact net radiation method, rather than an approximation technique involving only a small number of reflections. All surfaces are assumed to be gray and diffuse reflectors, which is reasonable for the materials of interest.

Temperatures were computed for maximum interference heating and for a nominal interference heating condition which results in a peak radiation equilibrium temperature of 3290°F at the stagnation line. Results are shown in figures 3-40 to 3-42 for maximum interference heating and a preliminary heating distribution. Figure 3-40 presents temperatures at each node location at the time of peak heating (400 seconds), while figure 3-41 shows temperature-time response at selected points. Temperatures as a function of location at 175 and 400 seconds, compared with radiation equilibrium temperatures at 400 seconds are shown in figure 3-42. Calculations were made later for a refined heating distribution, and those results are summarized in Table 3-4 for both maximum and nominal heating. The temperatures discussed hereafter are all based upon the refined analysis, but they differ only slightly from those shown in figures 3-40 to 3-42.

Of considerable significance is the fact that the stagnation line temperature peaked at 3630°F for maximum heating, 370°F below the

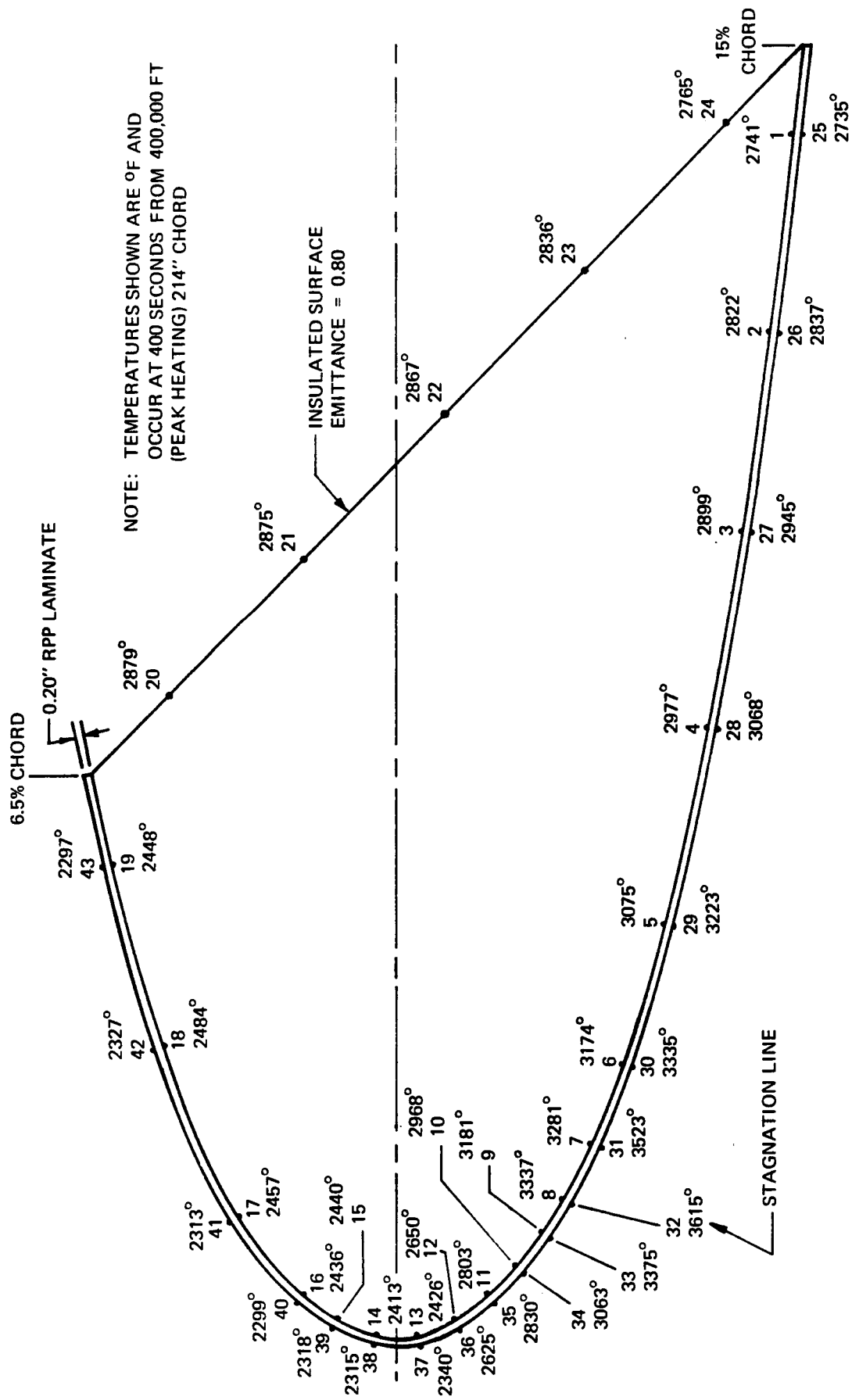


FIGURE 3-40 THERMAL MODEL, LEADING EDGE WITH INTERNAL CROSS-RADIATION
MAXIMUM INTERFERENCE HEATING CASE

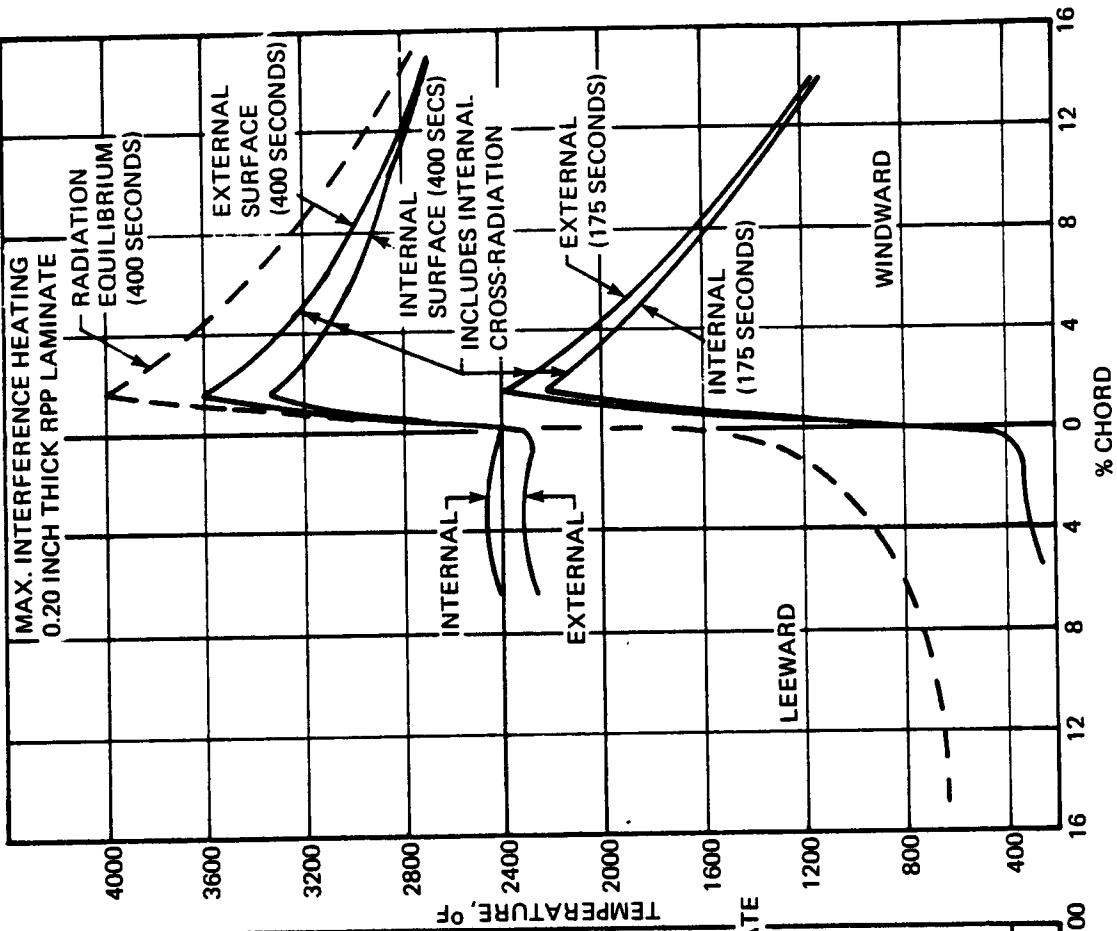


FIGURE 3-41 THERMAL RESPONSE OF RPP LAMINATE WITH INTERNAL CROSS-RADIATION

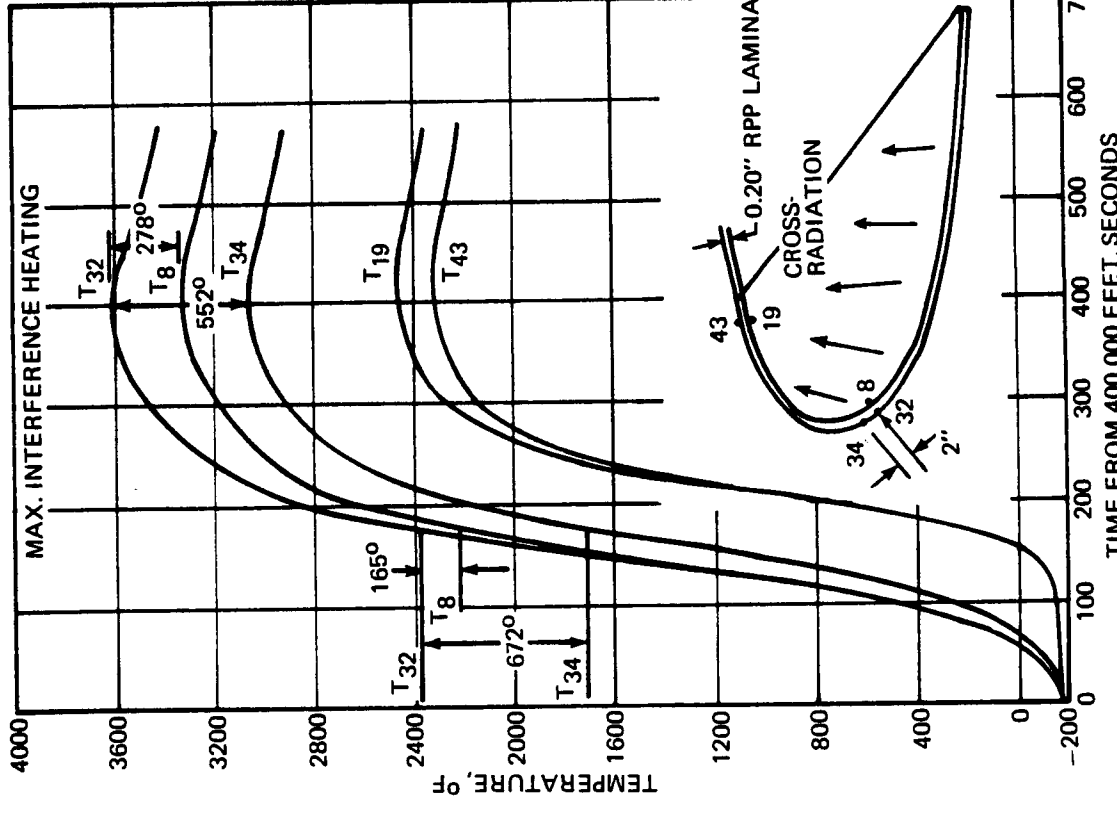


FIGURE 3-42 EFFECT OF INTERNAL CROSS-RADIATION UPON PEAK TEMPERATURES

radiation equilibrium value. For nominal heating the peak temperature was 2910°F, 380°F below radiation equilibrium. The reduction in peak temperature for nominal heating, as compared with maximum heating, was higher than expected. This is due to the greater importance of circumferential heat conduction at the lower heating rates, as was discussed in the previous section.

TABLE 3-4 CROSS RADIATION ANALYSIS SUMMARY

Heating Condition	Peak Stagnation Line Temperature °F	Maximum Circumferential Temperature Gradient °F/inch	Time of Maximum Gradient Seconds	Maximum Gradient Occurs Between Nodes	Maximum Canted Heatshield Insulation Temperature °F
Maximum (4000°F peak radiation equilibrium temperature)	3635	380	205	36 & 37	2914
Nominal (3290°F peak radiation equilibrium temperature)	2900	338	215	36 & 37	2394

Cross radiation also resulted in a reduction in circumferential temperature gradient which is important from a thermal stress standpoint. The peak gradient for maximum heating was 380°F/inch compared to a radiation equilibrium value of 900°F/inch. The time of peak gradient was also shifted from 400 seconds to 205 seconds. The peak gradient at 400 sec with cross radiation was only 228°F/inch. For nominal heating the peak gradient was 338°F/inch at 215 seconds and 208°F/inch at 400 seconds. The maximum circumferential gradient does not occur at the stagnation point, but occurs near the geometric leading edge between the nodes indicated in Table 3-4 and figure 3-40. The reduction in temperature gradient for the nominal heating case, as compared with maximum interference heating is less than might be anticipated based upon the difference in peak stagnation line temperatures. This is due to the fact that in the region of peak gradients the interference heating effect is much lower than that at the stagnation line.

The peak temperature gradient across the skin thickness occurred at 400 seconds and was 280°F at the stagnation line for maximum heating. This compares with 87°F for an internally insulated skin (figure 3-27), the increase being due to the cross radiation cooling effect on the back side. For nominal heating the peak gradient was only 150°F. On the leeward side the inside surface is hotter than the outside due to the dominant effect of cross radiation. The net effect of the reduced circumferential gradient with increased thickness gradient is a substantial reduction in thermal stress.

The aft surface in the thermal model, which represents insulation on the wing structural front beam, reached 2914°F for maximum heating conditions, indicating a stringent temperature requirement for the insulating material. For nominal heating conditions the insulation temperature was reduced to 2394°F.

There are a number of methods by which the beneficial effects of cross-radiation could be enhanced or insulation temperature reduced, including optimizing orientation of the canted insulation barrier, increase of RPP thermal conductivity, and incorporation of fins, baffles or low emittance coatings. Evaluation of these methods and of effects of interior components should be accomplished in future analyses.

3.3.6 Surface Recession of Bare RPP

In order to provide a basis for evaluating effectiveness of the oxidation protection systems in terms of number of missions capability, calculations were made to predict surface recession of bare, uninhibited RPP during reentry. A VMSC computer routine was utilized with RPP oxidation characteristics based upon plasma arc tests. Reaction rate control, transition and diffusion control oxidation regimes are accounted for in the routine.

Figure 3-43 presents the computed surface recession as a function of reentry time for RPP with a density of 1.4 gm/cm³. This density is achievable if desired. Computer runs were made for the stagnation line and geometric leading edge with maximum interference heating. Recession for intermediate heating conditions was scaled from the stagnation line results, based upon diffusion control for which recession is proportional to heat flux rate. Since reaction rate control is important at the lower heating rates, this procedure is slightly conservative.

Peak recession rate occurs at 700 seconds and is 4.97×10^{-4} in/sec at the stagnation line. Total recession is 0.274 inch at the

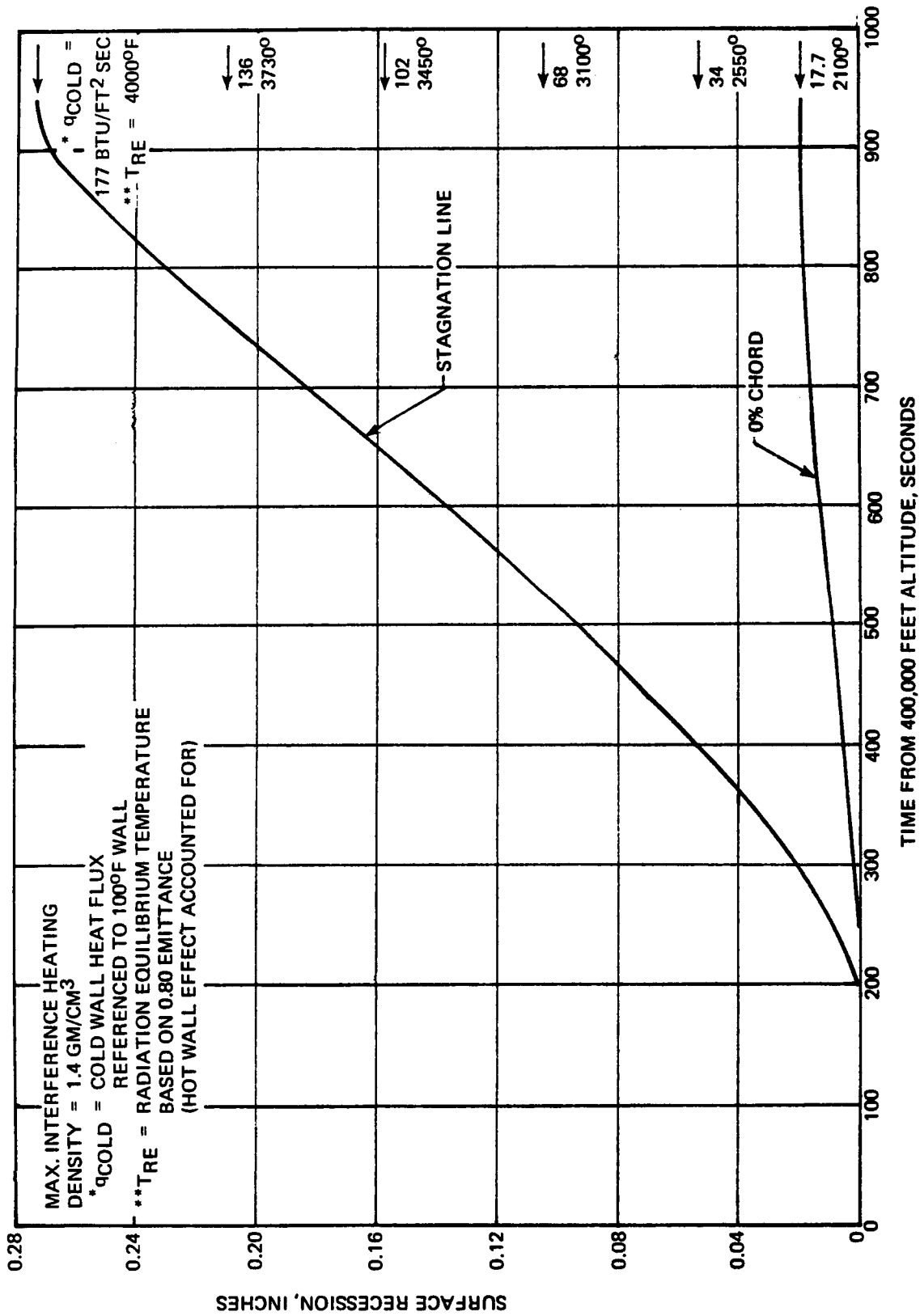


FIGURE 3-43 RE-ENTRY SURFACE RESSION OF BARE RPP

stagnation line and 0.019 inch at the geometric leading edge. This indicates single mission capability for bare RPP near the stagnation line and multimission capability on the leeward side or in low heating rate regions of the leading edge, outboard of the maximum interference heating zone. This indicates that coated RPP must have multi-mission capability in excess of two or three missions to be cost effective.

3.3.7 Conclusions and Recommendations

The following conclusions are drawn from the foregoing analyses:

(1) Emittance of RPP should be maximized with a value of 0.80 being a development goal.

(2) Thermal conductivity is of lesser importance, but should also be high, with the values in figure 3-23 being a development goal.

(3) Solid laminate skin construction is favored over foam core or honeycomb sandwich to minimize temperature gradients and peak stagnation temperature.

(4) The overlay and solid laminate thermal cover concepts are ineffective as thermal barriers, and could provide only oxidation protection.

(5) Temperature gradients across support ribs will be large, but can be minimized by proper design.

(6) Cross-radiation provides an effective method of reducing circumferential temperature gradients and reducing peak stagnation line temperatures.

(7) Conduction can also be used to reduce circumferential gradients when heating rates are low.

(8) Front beam insulation will require 2914°F temperature capability for maximum interference heating, but this can probably be reduced by optimized design. A requirement of only 2394°F exists for nominal reentry trajectory conditions.

(9) Bare, uninhibited RPP would be capable of multimission reuse in low heating regions and single mission use with maximum interference heating.

Additional thermal analyses considered desirable, but outside the current scope of activity, are as follows

(1) Evaluate methods of optimizing effects of cross-radiation on leading edge gradients and heatshield insulation temperature by:

- o Heatshield orientation
- o Application of low emittance coating to local areas on inside of skin
- o Tailoring skin thickness

(2) Determine effect upon cross-radiation of skin thickness and interior components, such as support ribs and intercostals.

3.4 STRUCTURAL ANALYSIS

Structural analyses of the leading edge were performed to establish realistic directions for materials property goals and structural configurations; to determine feasibility of an RPP leading edge; to determine significant design factors; and to establish approximate sizing and weights for consideration in Shuttle trade studies. The parametric analyses performed permit the evaluation of specific materials systems once firm material properties are established. Some of the analyses reported herein were conducted prior to obtaining test data on the candidate material systems, but final leading edge sizing and weight data were analyzed using mechanical property data approximating the siliconized RPP material system.

Optimization analyses were performed to determine optimum leading edge segment span based on weight considerations. Other analyses examined thermal stresses induced in solid laminates, sandwich skin panels, and support ribs to establish their significance in leading edge design. It was determined that thermal stresses can be the most sensitive factor in the design of oxidation inhibited RPP and these stresses favor the use of solid laminates over sandwich designs. With low elastic modulus and/or low expansion coefficient thermoelastic stress problems are relieved.

Those conditions employed in the analysis of the leading edge functional elements are as follows:

(1) The boost condition (figure 3-1) was used in the loads analysis of the leading edge skin panels.

(2) The cruise maneuver condition (figure 3-5) is critical for rib bending moment analysis.

(3) The worst case radiation equilibrium and cross radiation temperature distributions of figure 3-42 were used as a basis for thermo-elastic analysis.

Since maximum thermal gradients or maximum temperatures do not occur simultaneously with maximum airloads, the airloads and thermal stress conditions were analyzed separately. In fact, at the time of maximum airloads the leading edge temperatures have cooled below 500°F.

Material properties upon which initial analyses were based are listed in Table 3-5. These were obtained from very limited test data, available at the outset of the program. It was assumed that for material design thickness anticipated (0.10 - 0.20 inches), coated RPP strengths would exceed the 10,000 psi noted for the siliconized RPP and a value of 15000 psi, equivalent to bare RPP, was used. This produced a realistic target for development of materials properties since initial test data obtained on this program showed that strength could vary from 8400 psi to 21,100 psi, depending upon the particular coating system selected. However, recent characterization data for siliconized RPP shows that an average strength of approximately 10000 psi is more realistic. Final weight and sizing were therefore based on the lower value.

TABLE 3-5 MATERIAL PROPERTIES ASSUMED FOR ANALYSIS

		Room Temperature			
		E	ρ	CTE	F _{bu}
		10 ⁶ PSI	$\frac{LB}{FT^3}$	10 ⁻⁶ IN/IN/°F	$\frac{F_{tu}}{PSI}$
	Bare RPP	1.8	80	1.7	15000
	WCA Graphite				
Initial	Siliconized RPP	12	123	2.9	15000
Analyses	WCA Graphite		(Faces)		
Final ⁽¹⁾	Siliconized RPP	2	88	1.6	10000
Sizing	WCA Graphite				

(1) Composite values including bare core and coated face contributions

Further, for thermoelastic analyses using temperature dependent properties it was assumed that modulus of elasticity for coated material would be reduced at elevated temperature. Based on various literature data on carbides, a temperature variation that produces a modulus reduction of 50% at 3000°F was used. There is some evidence that bare RPP will also exhibit a modulus reduction in the 3000-4000°F range even though strength continues to increase above room temperature values. Other analyses were conducted assuming stiffness properties invariant with temperature, i. e., room temperature properties remain constant. This produces substantially higher stresses. It is significant to note that the elastic modulus achieved in flexure testing of the siliconized RPP is significantly less than the initially assumed value and results in thermal stresses lower than anticipated.

3.4.1 Element Analysis

Two bending optimization analyses were performed on ideal panel elements. One was done on sandwich material to determine the optimum proportions between core and face for weight analysis. The other was done on diffusion coated solid laminates, where the composite is, in effect, a sandwich construction of coated faces and bare core. Both analyses assume that face density and stiffness are greater than for the core, and the face material controls initiation of failure. Optimization for bending as opposed to tension or compression was conducted because that is the manner in which the skin panels are primarily loaded. These analyses were used as guides to materials development by establishing idealistic coating depth goals.

For the sandwich design, where all the bending load is carried by the faces, it can be shown that the face weight (total of two faces) equals the core weight for a minimum weight design (reference 35).

If, however, a solid laminate with coated outer plies and bare inner plies is optimized, a different equation is obtained. In this case a linear strain distribution is assumed and the optimum proportions are a function of the densities and the elastic moduli of the layers (reference 35).

Typical results of this analysis are illustrated on figure 3-44. Taking for example $\frac{\rho_f}{\rho_c} = 1.55$ and $\frac{E_f}{E_c} = 10$, it is found that the optimum

depth of coating is 31% per face (or 62% of the total thickness should be coated). If a higher density coating material were to be used, the depth of coating would optimize at a lower percentage. Similarly, with a lower ratio of elastic moduli like that obtained on siliconized diffusion coated specimens, the optimum would occur at a lower coating depth.

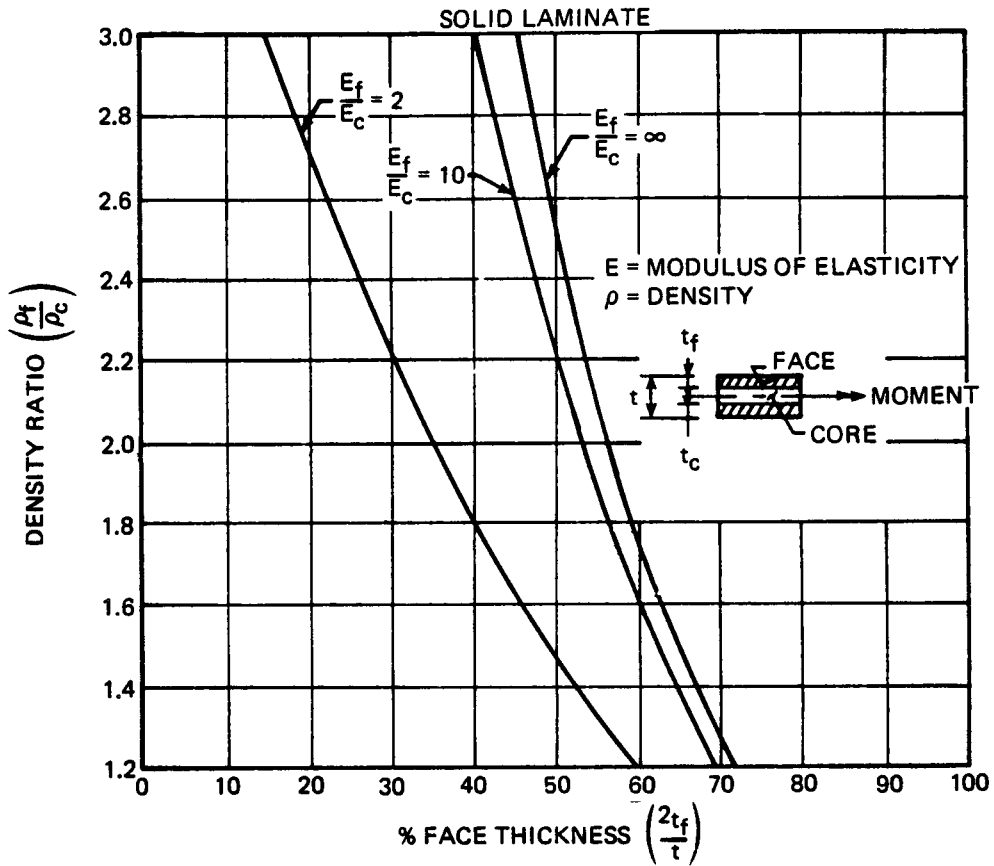


FIGURE 3-44 OPTIMUM FACE THICKNESS

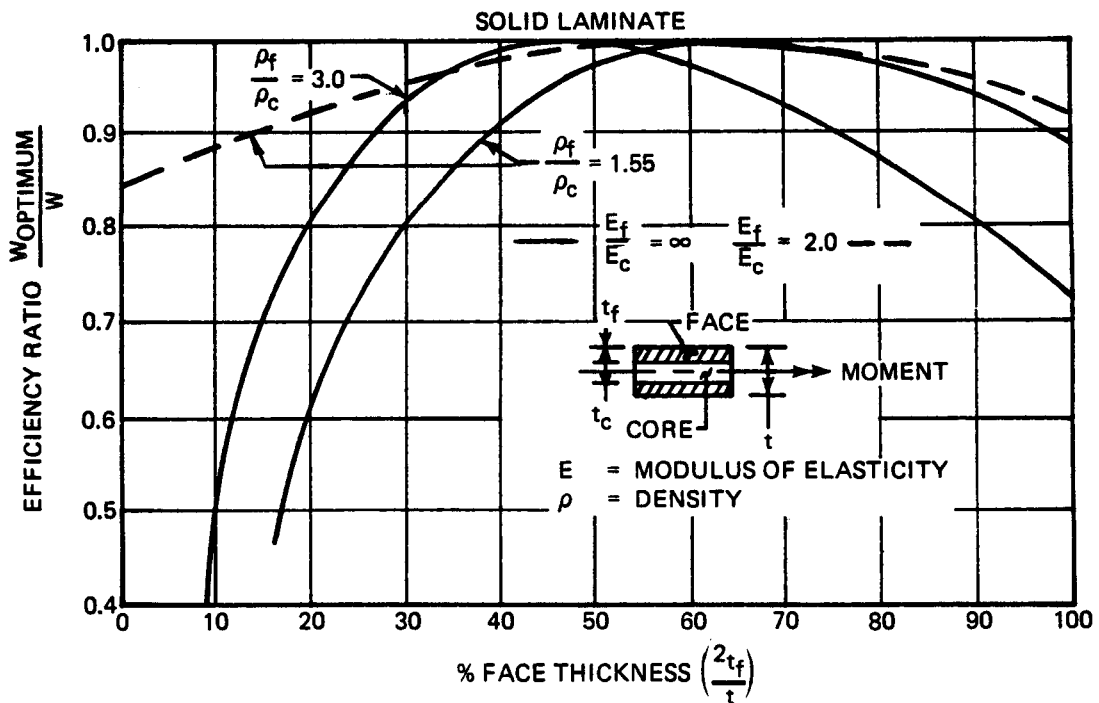


FIGURE 3-45 WEIGHT SENSITIVITY

The sensitivity of coating depth on laminate weight is illustrated on figure 3-45, where $\frac{\rho_f}{\rho_c} = 1.55$ and $\frac{E_f}{E_c} = \infty$ is taken as an example. For

this case there is a broad range of coating depth over which little efficiency is lost. Even if full coating depth is considered, only a 10% decrease in efficiency is realized. As coating density is increased, optimum weight is more sensitive to coating depth and a large weight penalty would exist if the coating were full depth. As the ratio of elastic moduli decrease, like with the current coatings, the laminate weight is relatively insensitive to coating depth. The curve for $\frac{E_f}{E_c}$ illustrates this.

$$\frac{E_f}{E_c} = 2.0$$

Once minimum coating depth is established, it is necessary that coating depth equal or exceed that limit to avoid a possible overstress situation. This is shown in figure 3-46 where the ratio of actual to optimum stress is plotted against core thickness. For example, if the optimum core thickness were 50% (corresponding to a coating depth of 25% per face) but the actual bare core was 60% (face thickness = 20%) the face stress would be 11% greater for a given moment. This can be controlled by establishing realistic coating minimums and adequate inspection techniques.

The weight sensitivity of sandwich construction to variations in core thickness was also determined and is shown in figure 3-47 for a 300 inch pound/inch moment, typical of the leading edge strength requirement. This shows fairly insensitive response to large variations in core depth. This could be important where core shear is the limiting design constraint. In this case core depth could be increased 50% with only 7.2% weight penalty over an optimum weight design.

3.4.2 Initial Airloads Analysis

Initial analyses of the leading edge were conducted using a critical loading condition produced during cruise maneuver. The pressure distributions for this case are given in figure 3-48. In addition, as noted above, computations were based on a bending strength allowable of 15000 psi, an elastic modulus of 12×10^6 psi, and an average density of 107 lb/ft³. Current test data indicates material properties for the siliconized RPP are closer to 10000 psi bending strength, 2×10^6 modulus of elasticity, and 88 lb/ft³ density. The leading edge design was updated using these properties and is covered in section 3.4.3. However, weight and thickness calculations for the initial assumed allowables are documented herein for reference.

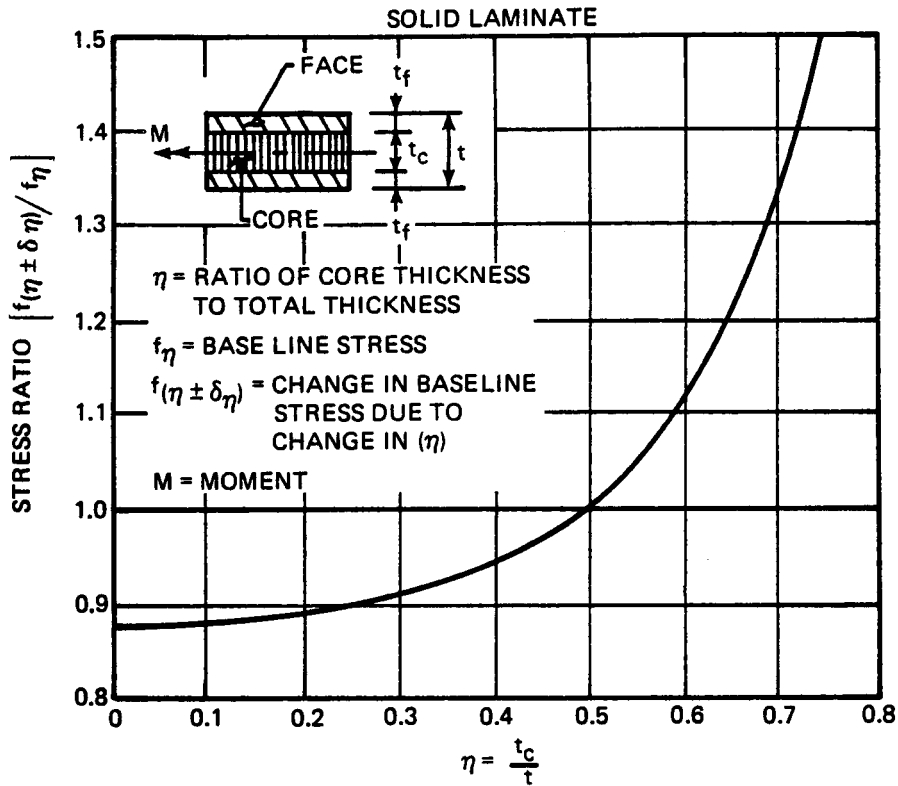


FIGURE 3-46 STRESS SENSITIVITY

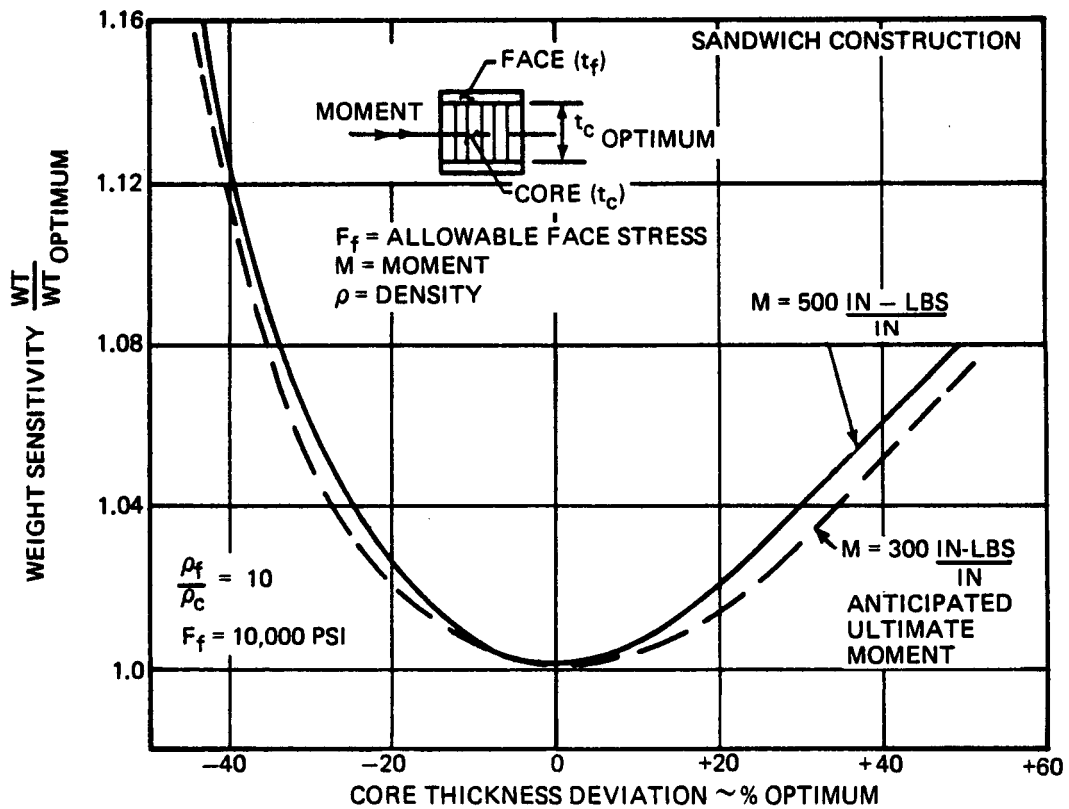


FIGURE 3-47 OPTIMUM WEIGHT SENSITIVITY

Panels - The airload panels were analyzed as plates under uniform pressure loading. Initially, the lower panel was analyzed for a uniform pressure of 2.1 psi ultimate. Without intercostal it was assumed simply supported on all four sides. The chordwise dimension was fixed at 33 inches, while the span was varied. Under these conditions the panel thickness was deflection limited, where the limit was set at one thickness (1.0 t). With an intercostal installed at the mid-chord point the panel became stress limited and the thickness and weights were reduced accordingly. Thickness results are given on figure 3-48 and the overall leading edge weight is summarized in figure 3-49.

An arbitrary panel thickness limit of 0.10 inch has been used based on current best estimates for fabrication of large unstiffened panels.

The upper panel was analyzed for 6.15 psi ultimate assuming a 16 inch fixed chord and simple supports on all sides. Thickness requirements are given on figure 3-48 where a lower limit of 0.10 inch is indicated as explained above. Both the upper and lower panel thicknesses are based on a 15,000 psi allowable and an optimum diffusion coating depth for the assumed RPP properties.

Ribs - The ribs distribute the loads from the airload panels into the support structure attach fittings. The design bending moments on each rib is a function of panel span, and is composed of two components. One is the edge loading from each panel, which has a distribution and resultant moment shape similar to that shown for the unit width sandwich panel on figure 3-50. The other component is from the leading edge radius (forward 2% of chord), which acts as a support for the upper and lower panels and subsequently beams the panel reaction loads to the ribs, and from the intercostal end loads.

For weight analysis the ribs were assumed to be back-to-back "C" sections, having a minimum thickness of 0.10 inches and an outstanding leg of 1.0 inches. The height of the rib section was varied with panel span to meet the bending moment requirements as shown in figure 3-51. Rib height was assumed constant around the leading edge but improved efficiency would result from varying the height as required. This is particularly important where thermal stresses are significant as discussed below. The "T" section seal strip shown in figure 3-49 is included as non-optimum or nonstructural weight.

Leading Edge Radius - The leading edge radius was examined for resistance to collapse pressures during boost. Using the assumed properties and 0.10 inch thickness material, a collapse pressure of 40 psi was obtained which is more than 7 times the requirement. The significance is that this portion of the leading edge should present no difficulties.

- ASSUMPTIONS:**
- ALLOWABLE STRESS = 15,000 PSI
 - ALLOWABLE DEFLECTION = 1.0 t
 - MINIMUM THICKNESS = 0.1 LOAD CARRYING MEMBERS
 - SOLID LAMINATE:
 - FACES ARE COATED RPP, DENSITY = 0.0711 #/IN³
 - CENTER IS BARE RPP, DENSITY = 0.0462 #/IN³
 - SANDWICH CORE THICKNESS = 3PLY (.042)
 - CENTER IS 38% OF TOTAL THICKNESS
 - SANDWICH FACES ARE COATED RPP, DENSITY = 0.0711 #/IN³
 - MINIMUM FACE THICKNESS = 3PLY (.042)

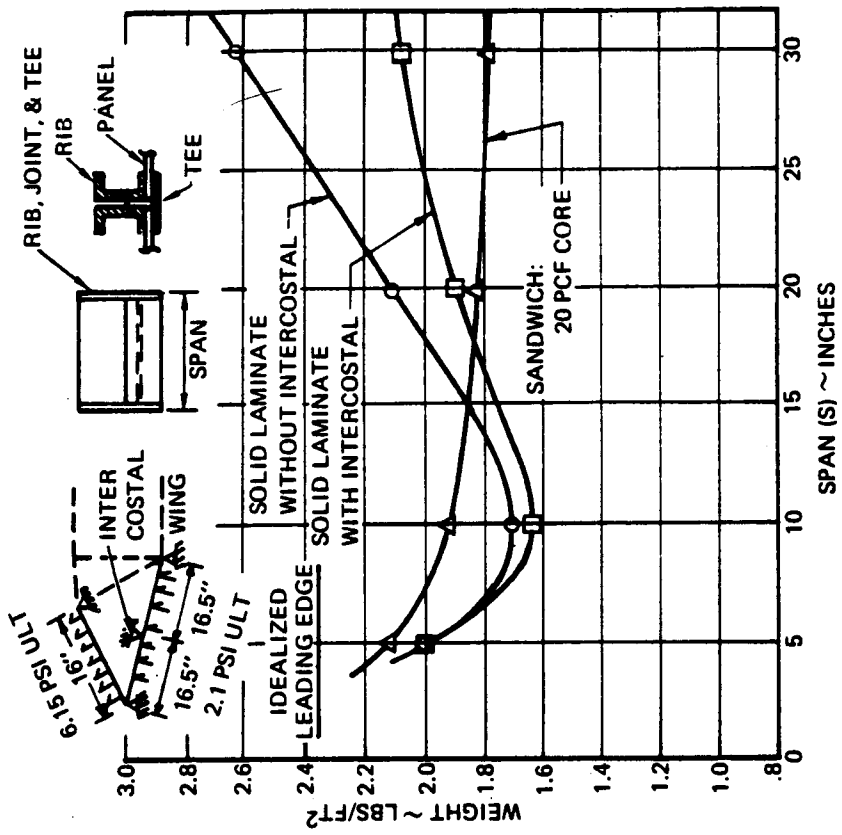


FIGURE 3-49 LEADING EDGE WEIGHT INITIAL MATERIAL ASSUMPTIONS

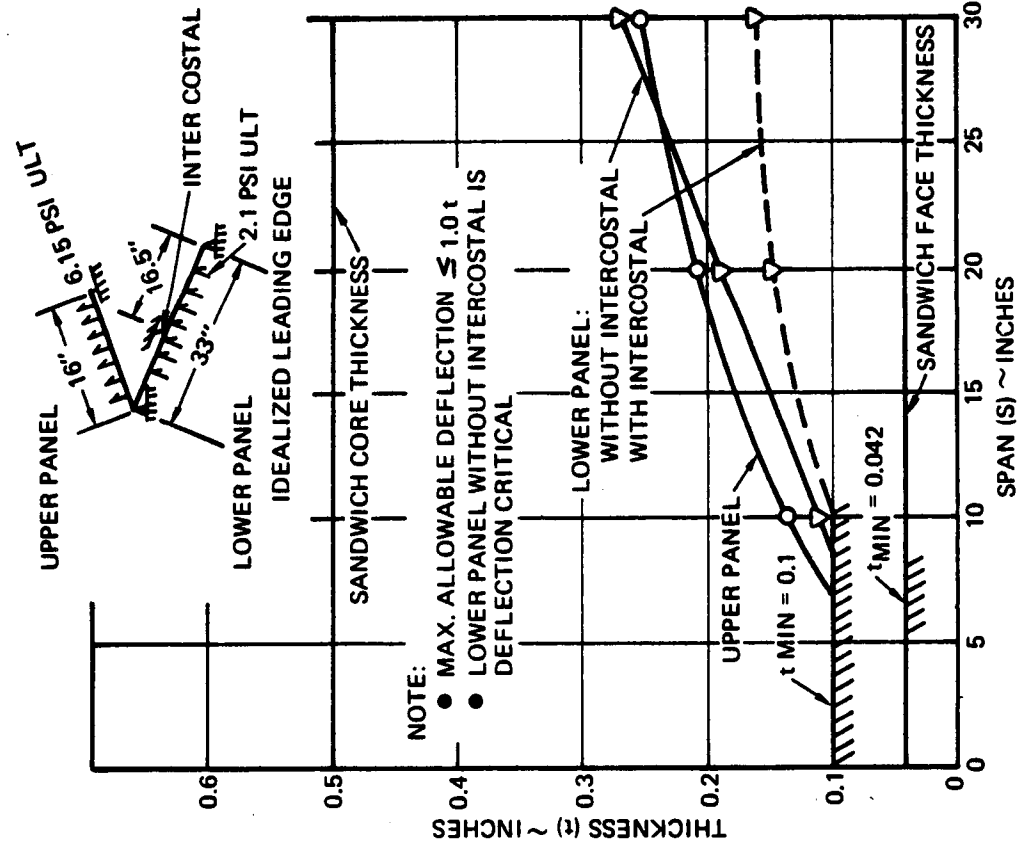


FIGURE 3-48 PANEL THICKNESS INITIAL MATERIAL ASSUMPTIONS

NOTE: ALL LOADS ARE FOR 1.0 IN
OF SPAN

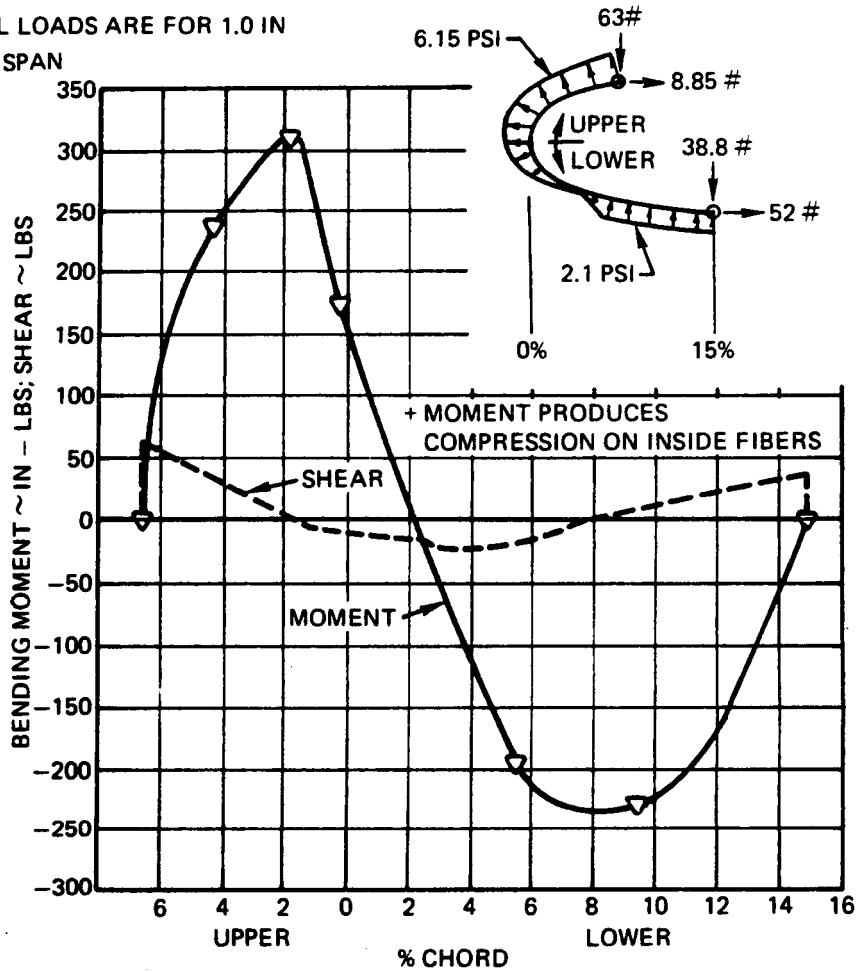


FIGURE 3-50 ULTIMATE MOMENT AND SHEAR, SANDWICH DESIGNS

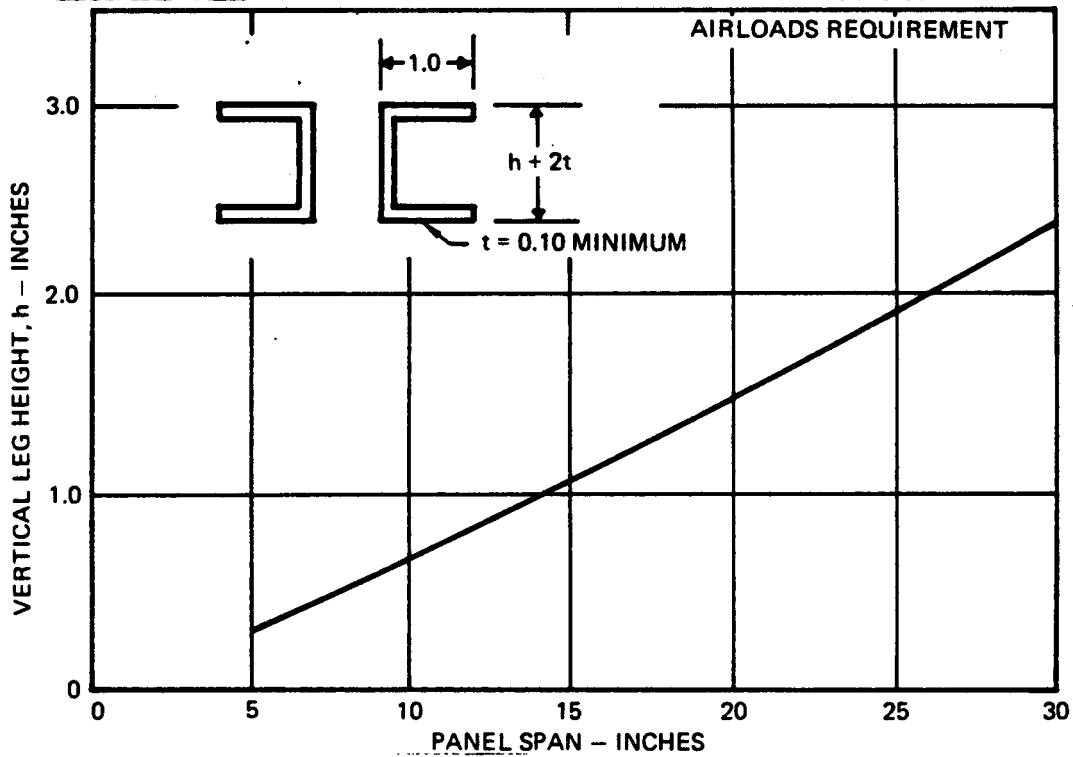


FIGURE 3-51 RIB GEOMETRY

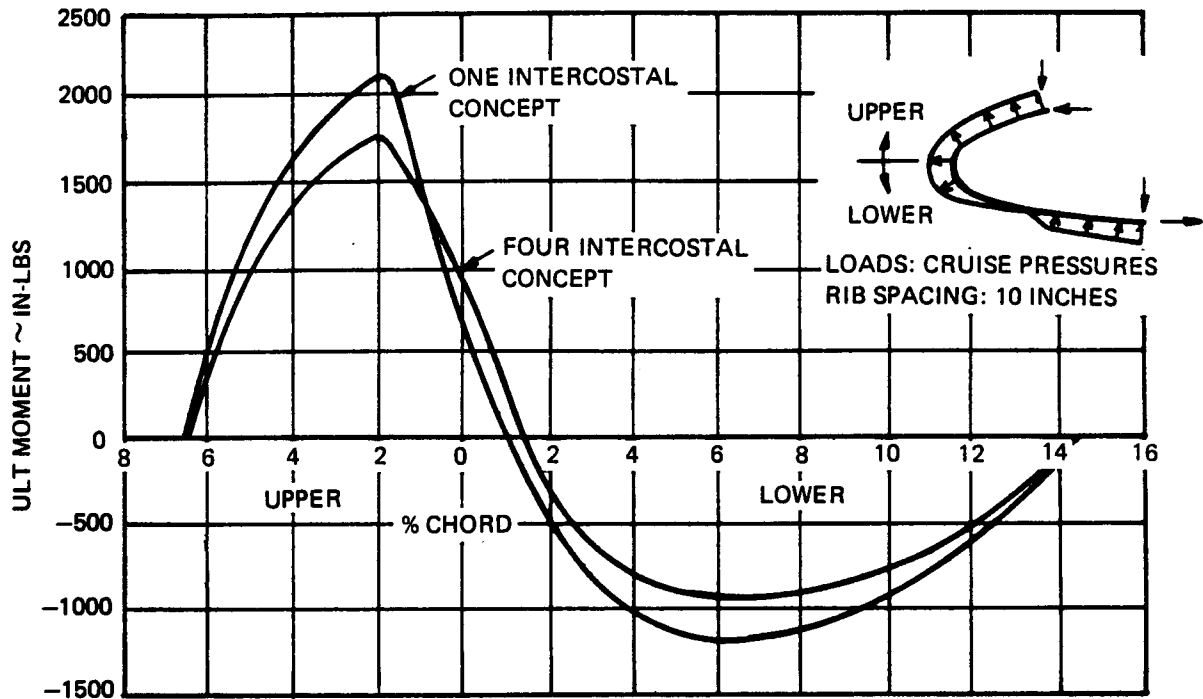


FIGURE 3-52 RIB MOMENT

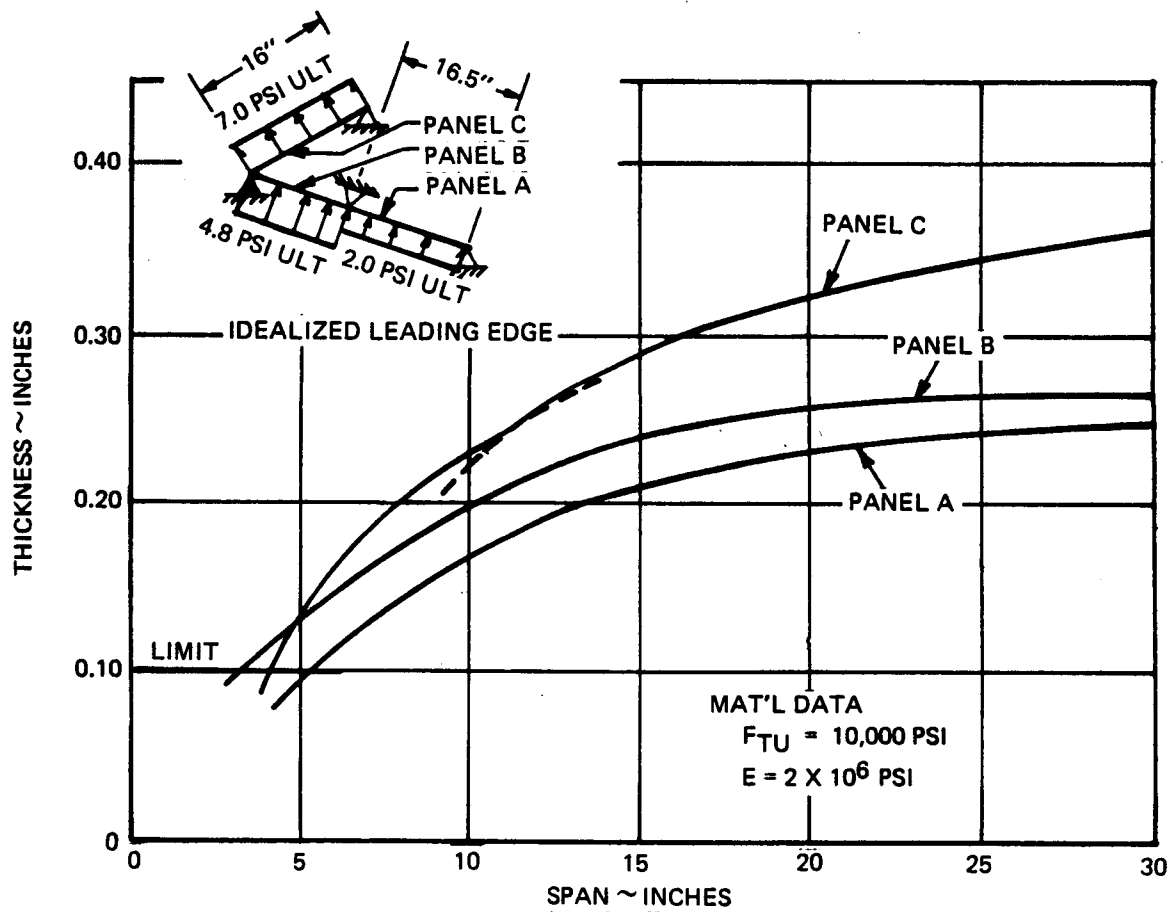


FIGURE 3-53 PANEL THICKNESS - ONE INTERCOSTAL

Sandwich Panel - The sandwich design requires no ribs because each strip of panel acts as a rib in supporting the airloads acting on that strip. The ultimate unit width bending moment of 310 inch - pound/inch is shown in figure 3-50. For an optimum sandwich design employing a 20 pound/foot³ core and a minimum of 3-ply faces the dimensions become: core height equals 0.50 inches and face thickness equals 0.042 inches. The resultant ultimate shear stress requirement is 125 psi. A nominal shear strength of 171 psi was obtained on a test of 20 pounds/foot³ RPP foam. This would probably reduce to 150 psi or less as a reliable design value, so that the use of a foam density less than 20 pounds/foot³ is probably not structurally feasible. The weight of this system is given on figure 3-49. Honeycomb core could be used in lieu of foam. VMSC fabricated RPP honeycomb panels, having constructed the honeycomb core from graphite cloth, and found that a satisfactory bond between the honeycomb and the faces was difficult to achieve. In addition, the RPP core tended to be relatively heavy. It was projected to weigh 14 pounds/foot³ in a reimpregnated condition and 21 pounds/foot³ if siliconized. Strength data was not obtained, but it is felt that the weight data on figure 3-49 for a sandwich design is a reasonable projection for production designs.

3.4.3 Final Airloads Analysis

Two design approaches were examined using reduced mechanical property allowables more typical of current siliconized RPP. A bending strength of 10000 psi and a modulus of elasticity of 2×10^6 psi was used in these analyses, which were done prior to obtaining final characterization data on either the siliconized RPP or the Zr-B-Si system.

A design using one intercostal to break up the lower airload panel like Concept No. 1, figure 3-16, was compared against Concept No. 3, figure 3-17, which employs three intercostals on the lower panel and one on the upper panel. The additional intercostals enable the ribs to be more widely separated, the main advantage being lower cost through reduced tooling requirements. Lower weight through more efficient use of rib material is also obtained.

The upper airload panel and ribs are designed by cruise maneuver loads, while the lower airloads panels are critical for boost pressure. Design pressures are indicated on the various figures. Bending moment for the ribs are given in figure 3-52 for a 10 inch span. These values were scaled linearly with variations in span. Ribs were configured as "C" sections with 0.10 inch minimum thickness.

Air load panel thickness requirements for the two design approaches are given in figures 3-53 and 3-54. With the one-intercostal

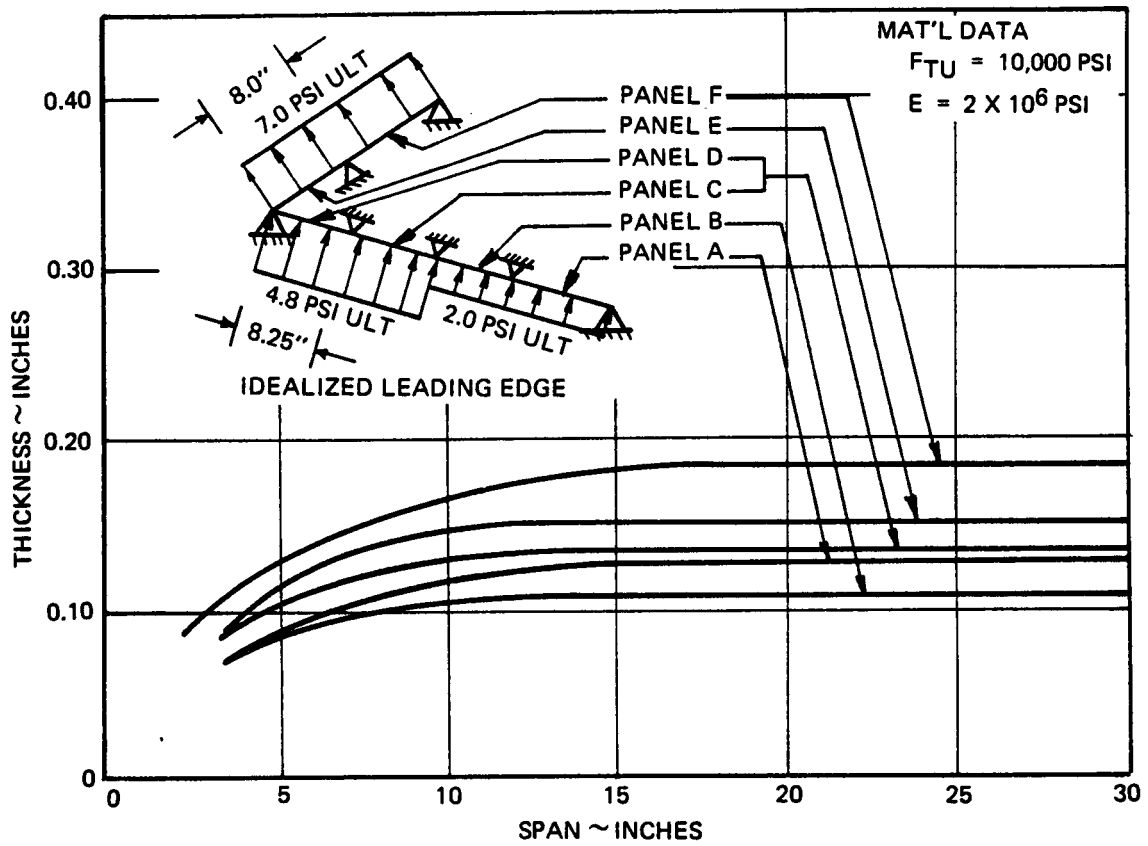


FIGURE 3-54 PANEL THICKNESS - FOUR INTERCOSTALS

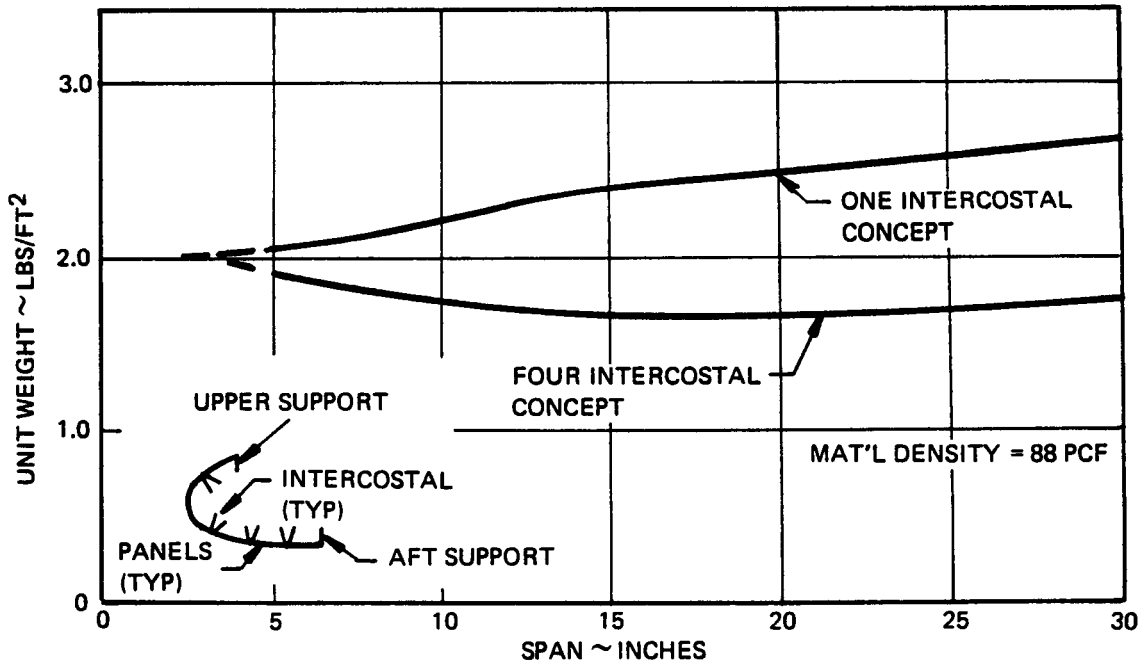


FIGURE 3-55 LEADING EDGE UNIT WEIGHT

design the lower panel is deflection limited (deflection equal to thickness) as is the upper panel below a span of 13 inches. With four intercostals the upper panels are stress limited but the lower panels are still deflection limited. No attempt has been made to optimize either the number or location of the intercostals to maintain more uniform distribution of air-load panel material. Obviously, this can be done and should result in a slight weight reduction.

Final leading edge weight in terms of lb/ft^2 of leading edge surface area is shown in figure 3-55. The unit weight includes airload panels, ribs, overlap seal strip, intercostals, insulators at the rib support points and the rib support bolts. The overall efficiency in the use of intercostals is evident in comparing unit weights of the two design approaches. Minimum weight for the four-intercostal design is at approximately 20 inches span but little loss of efficiency is realized for segment spans beyond 30 inches. Concept No. 3 in figure 3-17 shows a 30 inch segment size but this may be increased, being determined by weight, cost and thermal expansion compromises. The current large spans are made possible through the use of low modulus, low expansion coefficient material. Thus, thermal stress ceases to be the dominant factor in establishing rib geometry, and deeper ribs with the greater load carrying capability necessary for wide spacing are permitted.

With one intercostal minimum weight occurs at rib spacing below 5 inches. However, the large number of ribs required with each one slightly different from any other forbodes high tooling costs and is therefore an unattractive approach.

3.4.4 Thermoelastic Analysis

Thermal stress analysis was performed on both solid laminates with coated faces and solid laminates coated throughout, with both temperature dependent and constant modulus of elasticity; sandwich panels; ribs; and radiation equilibrium and cross radiation temperature distributions. Each of these is discussed below. Resultant stresses were plotted parametrically so that temperature and material property variations could be assessed for significance on design.

Solid Laminate Panel - The Levy method was used in the thermoelastic analysis of the panels. This is a simplified thermal stress technique, restricted to infinite span and constant spanwise temperature. Temperatures may, however, be varied through the thickness and also chordwise around the section. The approach assumes sections remain plane (i. e., no warpage) although extension and rotation are permitted. Neither interlaminar shear, nor shear lag at the panel edges is assessed

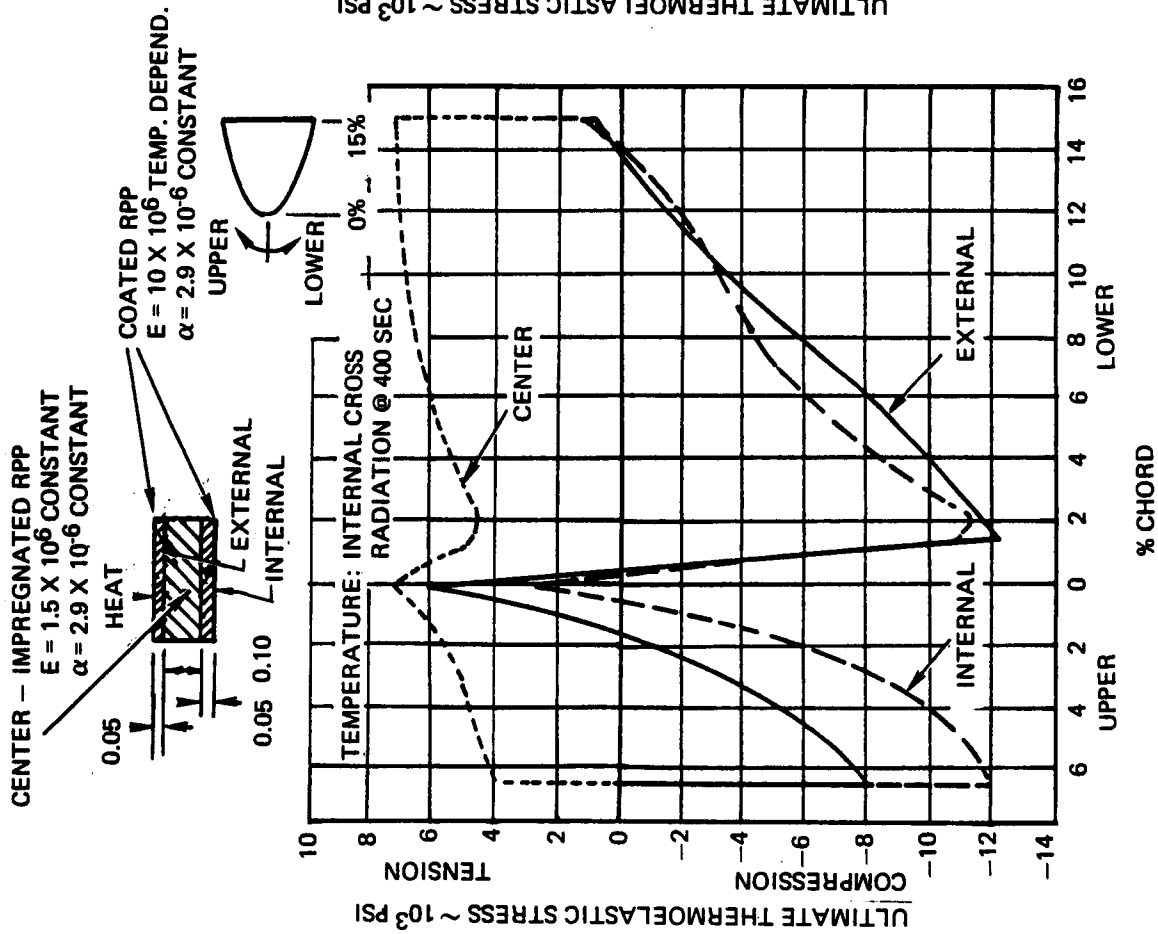


FIGURE 3-56 ULTIMATE THERMOELASTIC STRESS

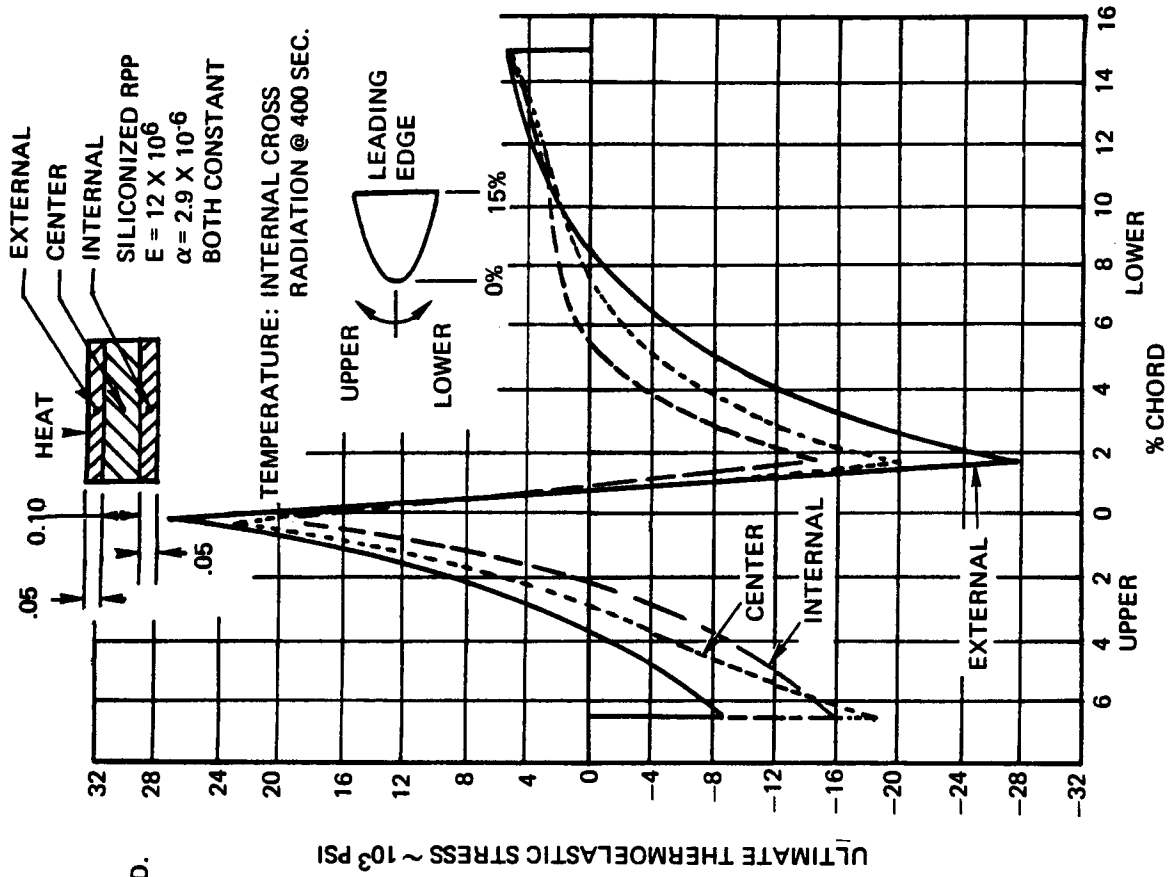


FIGURE 3-57 ULTIMATE THERMOELASTIC STRESS

by the method. As a result, the computed tension and compression stresses may be overstated. The advantage of using this approach is that analyses can be conducted quickly and inexpensively. This enables one to determine the magnitude of the thermal stress problem and establish direction for design improvement before resorting to more sophisticated and costly computational techniques.

For all solid laminate analyses a panel thickness of 0.2 inches was assumed. Temperature was varied through the thickness and around the leading edge. Panels with coated faces and panels with uniform properties throughout were analyzed. Typical resultant stress distributions are given in figures 3-56 and 3-57. In figure 3-56 it will be noted that the center bare material resists a significant portion of the face loads. This results in reduced face tensile stresses, while compression stresses tend to be highest. One would also anticipate interlaminar shear stress between the coated and bare layers. With uniform properties tensile and compressive stresses are approximately equal as noted in figure 3-57, but tensile stresses are increased over the previous results. This indicates that a certain amount of "tailoring" of the panel configuration is possible. The employment of such a technique would depend on specific material properties, such as tensile, compression and interlaminar shear allowables.

The maximum tensile and compression stresses obtained from these analyses are plotted on figure 3-58 and 3-59 respectively. The stresses are plotted using a convenient parameter, $E \alpha \Delta T$, where E is the room temperature elastic modulus in psi, α is the coefficient of thermal expansion in inches/inches/ $^{\circ}\text{F}$, and ΔT represents the panel stagnation temperature in $^{\circ}\text{F}$. For example, taking a cross-radiation case with temperature dependent E , having a room temperature value of 12×10^6 psi, $\alpha = 2.9 \times 10^{-6}$ inches/inches/ $^{\circ}\text{F}$, and 400 seconds into the entry phase, where ΔT is 3600°F , a value of 12.5×10^4 psi is obtained for $E \alpha \Delta T$. The resultant tensile stress (figure 3-58) is found to be about 8800 psi. If however, the maximum stagnation temperature is reduced to 3200°F (ΔT value) the $E \alpha \Delta T$ parameter becomes 11.1×10^4 and the maximum tensile stress is 7800 psi. This assumes all temperatures around the leading edge remain proportional to the stagnation temperature. While this is not an exact technique for determining the thermoelastic stress at other temperatures, it is sufficiently accurate at this point to gage the severity and sensitivity of thermal stress to various influencing factors.

An examination of bare RPP indicates thermal stress to be no problem. To clarify, using the properties in table 3-5 and a $\Delta T = 3600^{\circ}\text{F}$ for the cross-radiation case, $E \alpha \Delta T = 1.1 \times 10^4$, and the corresponding maximum tensile stress is only 780 psi. This is exceedingly small compared with an allowable stress of over 15,000 psi.

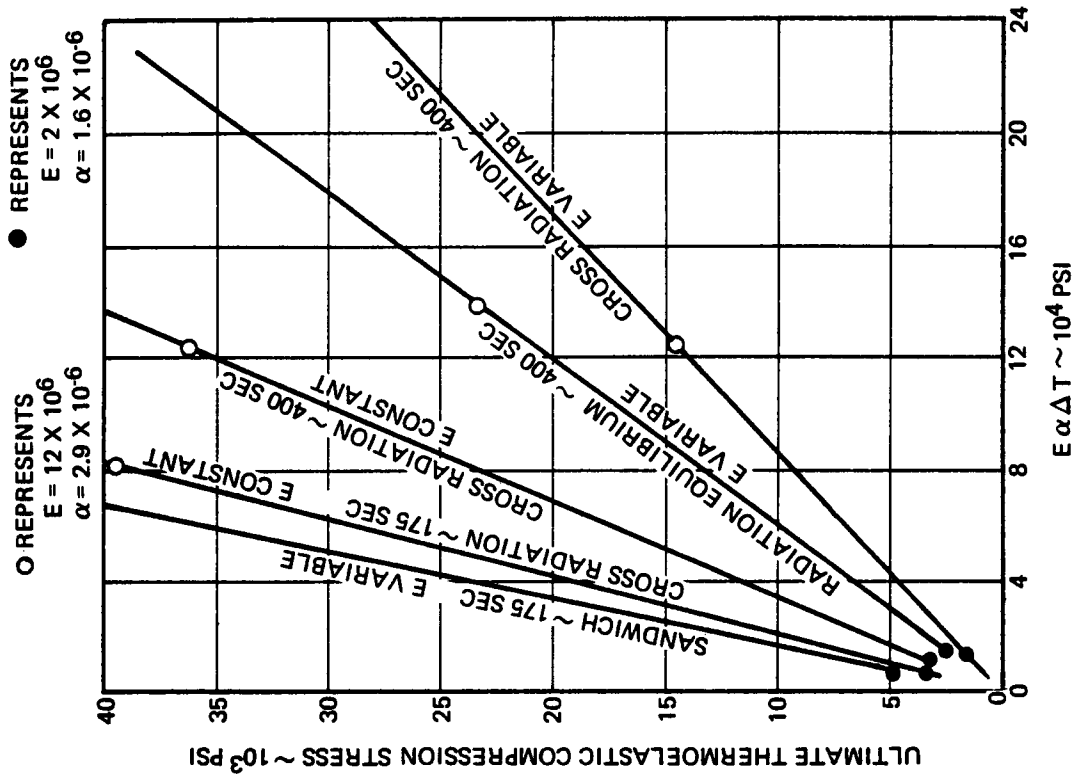


FIGURE 3-59 THERMOELASTIC COMPRESSION STRESS

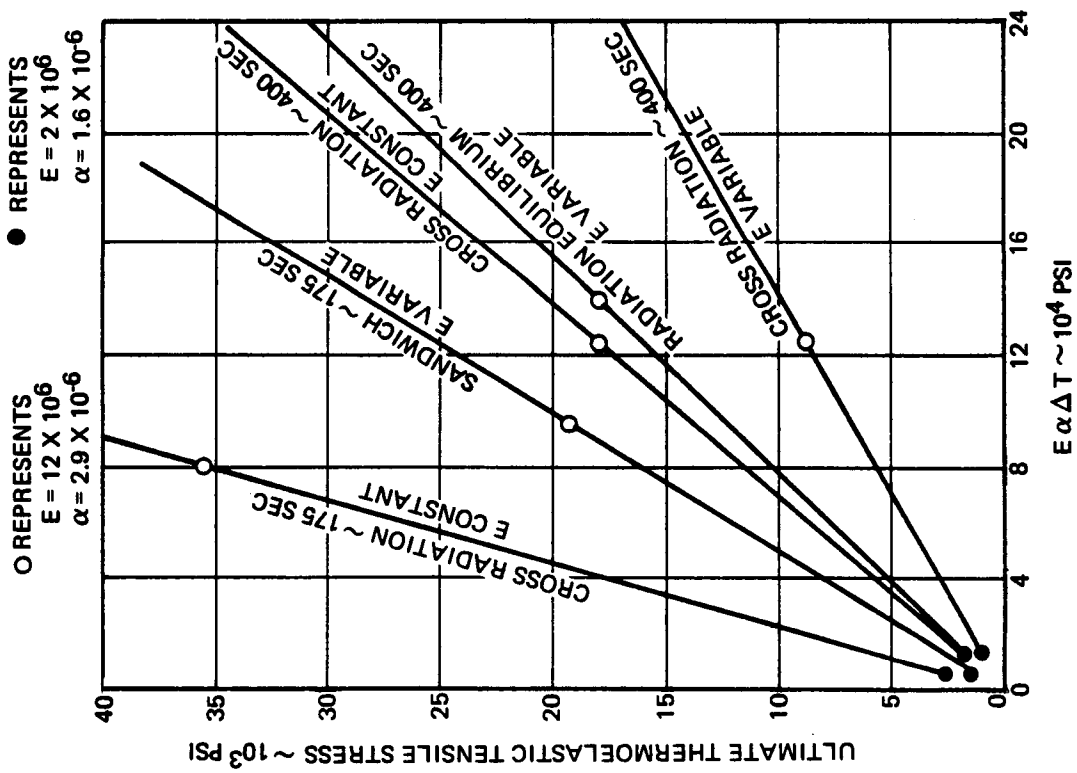


FIGURE 3-58 THERMOELASTIC TENSILE STRESS

Recent test data obtained for siliconized RPP also shows that thermal stresses should be low. Points for this material are indicated on the figures by closed circles ().

An examination of figure 3-58 reveals some interesting results. Focusing on the circled points, representative of a system having room temperature face modulus of 12×10^6 psi and $= 2.9 \times 10^{-6}$ inches/inches/ $^{\circ}$ F an estimate of the effect on stress of certain factors can be seen. The stress difference between a cross radiation system and one based on radiation equilibrium is a factor of two at the maximum temperature (at 400 sec), worst interference heating conditions. The same factor on stress is evident between constant E and the cases in which E is reduced to half at 3000° F.

Note that the thermal gradients and stresses at 175 seconds are more severe than at 400 seconds. This is due to the fact that the full benefit of cross radiation is not obtained at the lower temperatures associated with 175 seconds. A comparison with the equivalent 400 seconds show that stresses are twice the magnitude of those at 400 seconds.

Tensile stresses developed in solid and sandwich designs at 175 sec are approximately equal, but compression stresses in the sandwich panel exceed those in the solid laminate by a factor greater than two.

Some reduction in the stresses of a solid laminate at the 175 second point are believed possible by local thickening around the nose to sink or conduct heat from the hotter region. This is more feasible at lower heating rates, typical of those with nominal rather than maximum interference heating. Nominal conditions have been analyzed (ref section 3.3.4) and have shown an 11% reduction of temperature gradient around the nose region over worst case conditions. The nominal shuttle trajectory, coupled with reduced elastic modulus for the selected coating systems indicates that thermal stress should not be severe.

In general the compression stresses exceed the tensile stresses for the configuration analyzed. As stated previously tensile and compression stresses can be better equalized if uniformity of properties is produced through the laminate or alternately as differences between coated and uncoated material properties become small. This appears to be the case for the selected coating systems.

The conclusions to be reached from this analysis are that bare RPP or coated material with low elastic modulus are not subject to significant thermal stresses, but coated material with high modulus of elasticity

can produce high stresses. Maximum thermal stress occurs early in the entry phase before cross radiation becomes powerful as a heat transfer mechanism. None-the-less, gradients employing cross radiation are less than those based on radiation equilibrium and therefore utilization of this fact in design remains important. Of course, the most important advantage of designing to permit cross radiation is the large reduction in stagnation temperature.

Rib - The rib was analyzed for thermal stresses assuming a linear gradient between inner and outer flanges. That is, the thermal stresses computed occur because of the restraint of the support points, as opposed to stresses produced by possible non-linear gradients within the rib. The approach to rib analysis was to determine the deflection of the rib support points as if the rib were completely free and subjected to the thermal gradients computed and shown in section 3.3. Restoring loads required to return the support points to the undeflected position were computed. These support loads in turn produce the rib bending moments and stresses. Maximum stresses resulting from this analysis are shown in figure 3-60 where they are plotted against maximum temperature gradient at the stagnation point.

This solution assumes uniform stiffness around the rib, but an overall reduction in support load and bending stress could be achieved if the rib stiffness were varied judiciously. The optimum stiffness distribution is one that is proportional to the thermal stress bending moment curve. Thus rib height would be greater at the stagnation region and lower near the support points.

Since thermal stresses are proportional to thermal gradients and thermal gradients are reduced for lower rib height (section 3.3) it follows that thermal stresses can be reduced by reducing rib height. This is illustrated in figure 3-60. Here again the effect of elastic modulus on thermal stress is apparent. Initial assumptions of an $E = 12 \times 10^6$ psi indicate a potential thermal stress problem, but the more recent estimates of 2×10^6 psi modulus of elasticity for coated RPP show that a substantial margin of safety exists if the allowable stress is in the 10000 psi range. With the lower modulus material there is no apparent restriction on rib height and therefore increased rib spacing is permissible for reduced fabrication cost. However, as rib spacing increases the number of intercostals must increase to maintain the airload panels within acceptable deflections and low weight. The latest design concept in figure 3-17 reflects this approach, where a 30 inch span, or twice that of the initial design, is illustrated.

The data on figure 3-61 shows that large panel span is acceptable from a thermal expansion standpoint. The total expansion of the leading

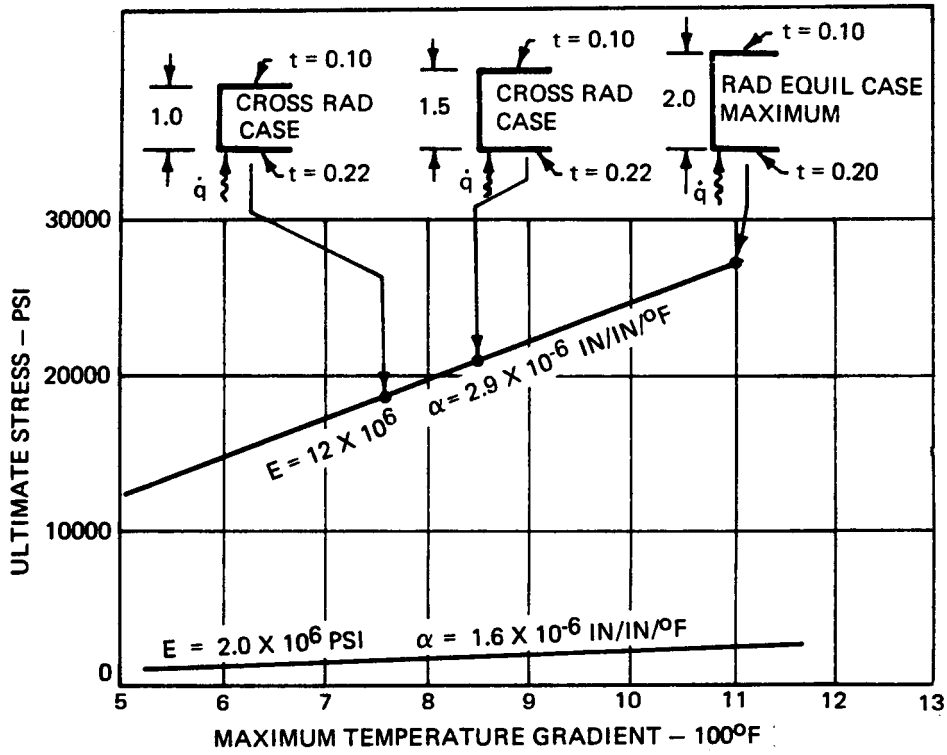


FIGURE 3-60 RIB THERMAL STRESS

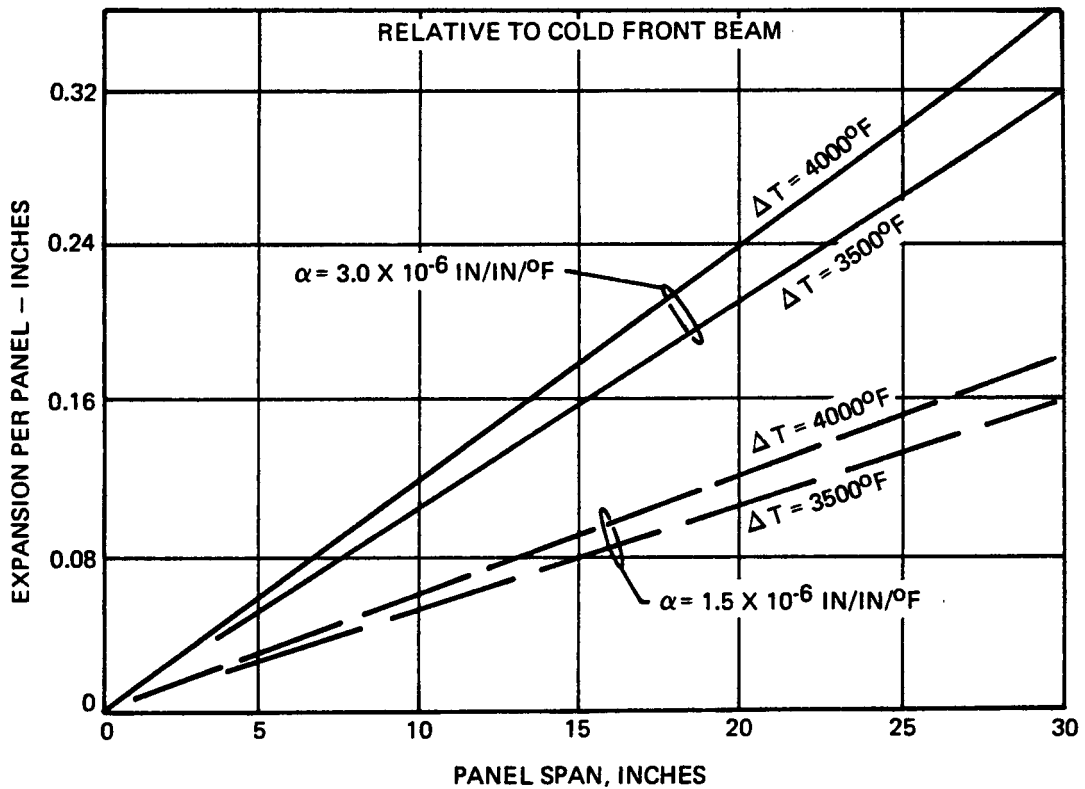


FIGURE 3-61 THERMAL EXPANSION RELATIVE TO COLD FRONT BEAM

edge at the stagnation point has been related to a 0°F front beam and supporting structure. The assumption here is that with a cold soak in orbit and temperature lag of the front beam during entry, the leading edge will be at its maximum value (at 400 sec from start or entry) while the front beam is still cool. This is illustrated by the titanium temperature in figure 3-38. With the 30 inch span and cross radiation design total expansion would be 0.16 in. for 1.5×10^{-6} in/in/°F expansion coefficient. This would be reduced 15% with the lower operating temperature of siliconized RPP.

In summary the thermal stresses induced in the rib can be significant with coated RPP having a high modulus of elasticity. However, the stress magnitude is not severe for the lower elastic modulus obtained on the current candidate coating systems for RPP.

3.4.5 Conclusions and Recommendations

As a result of the airloads stress and thermal stress analyses, a number of conclusions have been drawn as follows:

(1) Where a solid laminate has coated outer plies, the depth of coating can be optimized for maximum moment per unit weight. Likewise, a sandwich design can be optimized in a similar fashion. In the region of expected properties for oxidation inhibited material the sensitivity of coating depth on optimum weight is small.

(2) RPP structural thickness requirements for realistic leading edge segments will range between 0.10 inch and 0.20 inch. Local thickening for heat transfer around the nose region may exceed these limits. Panel span for the baseline leading edge geometry is expected to be at least 30 inches, based on weight, cost and thermal expansion trade-off.

(3) Anticipated unit weight of RPP leading edge segments is expected to be about 2 pounds/foot², which includes airload panel, ribs, integral seal strip at expansion joints, and support point fastener and joint insulation.

(4) Thermal stresses for coated material having high elastic moduli produce the most sensitive design condition and would appear to preclude sandwich design from consideration. For bare RPP or with low modulus coatings, airloads and not thermal stresses establish design constraints.

(5) Thermal stresses in solid laminates can be "tailored" to a certain extent by controlling coating depth but this is not necessary where coating and bare RPP properties are not significantly different.

(6) Maximum thermal stresses occur during heat up (approximately 205 seconds after start of entry), but it is believed that the gradients can be controlled to a certain extent by material distribution shaping.

3.5 CONCLUSIONS

Conclusions reached from an evaluation of the concept design work, thermal analysis, and the loads and thermoelastic stress analyses are summarized below. Additional conclusions and recommendations concerning materials will be found in section 5.0, Testing.

(1) Solid laminate designs are favored over sandwich designs for several reasons. Among these are:

- (a) The benefits derived from cross radiation in a solid laminate permit a significant reduction in the maximum temperature requirements for oxidation inhibited RPP. This can be reflected as increased service life, temperature margin or reliability.
- (b) The inherent simplicity and lower cost (in terms of development and production costs) of solid laminates over their sandwich counterparts.
- (c) The lower thermal stresses developed in solid laminates which should result in increased reliability and service life.
- (d) Solid laminate designs are weight competitive with sandwich designs.
- (e) Solid laminates appear to be inherently more easily inspected between missions which can be translated into cost or reliability.

(2) Both bare and coated RPP appear feasible for the shuttle. The bare material would require replacement each flight in those areas subjected to the maximum interference heating. The greater portion of the leading edge could be designed for bare RPP with a life of at least two or more missions prior to replacement.

Coated materials exhibiting a tensile strength/expansion parameter, $\frac{F}{E\alpha}$ in excess of 600, should readily sustain the thermal gradients imposed on the leading edge and provide reliable design.

(3) Laminated or shingled designs are ineffectual as insulators and could only serve to provide an oxidation barrier. The overall benefit of low cost replacement shingles is questionable when compared with initial cost and weight penalties.

(4) The selected solid laminate design concept which is relatively simple, appears to be readily fabricable and can employ existing RPP fabrication techniques.

(5) For oxidation-inhibited RPP systems, having a modulus of elasticity in the 10×10^6 psi range or above, thermal stresses present the most significant design factor. Bare or coated RPP with low modulus of elasticity experiences low thermal stress, and airloads become the designing factor.

(6) Although VMSC has not computed leading edge unit weights for other material concepts, it is understood that the weights predicted for the VMSC RPP concept is competitive.

4.0 MATERIALS DEVELOPMENT

Materials development for the Shuttle Leading Edge consisted of the evaluation of RPP substrates and the formulation and evaluation of oxidation inhibitor compounds for the protection of RPP. Selection of substrates, inhibitor systems, and fabrication methods to be examined was made using best technical judgment amassed from past experience, test data from past programs, literature surveys, and technical discussions with consultants expert in the field of high temperature oxidation protection. Evaluation and selection of best material systems was made on the basis of oxidation inhibitor performance, strength properties and fabricability.

Substrates examined included graphite and carbon cloths and filaments of high and low modulus with high and low strength. Seven materials have been examined. WCA graphite cloth has remained the best substrate tested thus far, because of better compatibility when used with the VMSC processing and coating systems. However, improvements with coating compatibility are still desired. Carbides or oxides of titanium, tantalum, zirconium, silicon, hafnium, aluminum, boron, and tungsten were compounded with the RPP material in four different processing techniques in an effort to produce an oxidation inhibited system capable of providing multi-cycle protection under reentry conditions producing temperatures up to 4000°F.

Add-mixture, diffusion, add-mix and diffusion combined, and overlay coating approaches were the techniques considered in combining oxidation inhibitors with the RPP substrate. The add-mix system is one in which the oxidation resistant refractory materials in the form of fine powders are introduced into the organic resin binder during buildup of the individual graphite cloth plies. Further thermal processing produces insitu reaction of the oxidation resistant constituents. Diffusion coating employed primarily the pack cementation technique although some work was also performed using chemical vapor deposition. These processes diffuse the metallic constituents into the RPP substrate where they are reacted. The combined coating approach consisted of adding one of the metallic ingredients into the resin during laminate buildup, as in the add-mix system, while the second constituent was diffused into the laminate. Overlay coatings were applied by plasma spraying, cementing, or melting a layer of oxidation resistant materials ovetop of another coating system.

These inhibitor fabrication techniques were selected on the basis that each had distinct attributes to contribute to the laminates. The diffusion system was felt to be able to provide high strength through a controlled gradation of inhibitor material that would tie the outer coated fibers into the RPP core material. A dense outer surface and a progressively less dense or soft diffusion zone was predicted to give a transition between the outer surface and the RPP core to provide better strength and coating compatibility.

The add-mix system permitted controlled depth of penetration and controlled composition for protective metal powders. A distinct advantage was the possibility of gaining the option of having a large surface recession before replacement of leading edge segments was required, although weight would suffer from this approach. The combined system afforded the opportunity to enhance laminate integrity by lowering the quantity of metal powder additions to the binder resin. Another aspect was the possibility of tailoring a laminate to optimize strength and oxidation resistance where bare RPP is located at the center of the laminate and the inhibitor is graduated toward the outside. Also, better control was predicted for the siliconizing process to gain the desired depth of silicon carbide penetration. The overlay coatings were envisioned as providing an oxide layer as an oxygen barrier to enhance the performance of the coating system beneath.

In plasma arc and flexure testing the add-mix systems failed to provide the strength or oxidation resistance demonstrated by the diffusion coated systems. While it was felt that continued development of the add-mix approach may prove fruitful, there was little justification to select any of these systems over their diffusion coated counterparts and, therefore, further development was discontinued.

The combined systems failed to survive the final diffusion coating process step. Like the add-mix systems, further development may have proven productive, but compared to the diffusion coated systems there was little to recommend their continuance and they were dropped.

The diffusion coated systems, therefore, emerged as the most promising approach to achieving the desired oxidation resistance within the laminate at strength levels acceptable for leading edge design. Evaluation of five basic diffusion coatings with a large number of variations yielded two coating systems, siliconized and zirconium-boron-silicon, with good plasma arc performance that can be developed for the shuttle leading edge application.

Overlay coatings employing hafnia or hafnium and tantalum have shown potential for extending the temperature limits of the diffused coatings and their evaluation continues.

This section of the report discusses the basis for selection of initial candidate material systems, documents the processing and in-process evaluations performed in the modification and development of the coatings and substrates, and draws general conclusions relative to environmental and fabrication performance achieved.

Substrate evaluation is covered first and then the coatings work is discussed in chronological order beginning with the initial screening of systems, continuing through the modification trials of the best of these, and finally documenting the results of the final stage of development in Phase I. It may be concluded that high temperature oxidation resistance performance of the selected coating systems is good and will meet shuttle leading edge requirements. However, additional development is considered desirable to improve strength and develop a better balance with oxidation resistance. Specific flexure, furnace and plasma arc test data, evaluation, and discussion of results are included in Section 5.0.

4.1 SUBSTRATES

Seven different substrate materials were evaluated on the program. Flexure strength, fabricability and coating compatibility were the main factors to be examined. Cost/weight trade-offs require analysis at the system level and were not specifically a consideration in this evaluation. Material candidates were selected that would provide a representative cross-section of the carbonaceous filamentary products available. Cloth and filament forms of carbon and graphite in both high and low modulus of elasticity varieties were examined. In the final analysis it is the properties in the coated and not the bare condition that determines acceptability of a particular substrate for shuttle application. VMSC, therefore, elected to evaluate substrate performance with the siliconized coating system since this system had been established as a prime coating candidate and was developed further than any of the others.

Two of the substrates (VYB and KGF-200) were not received in time to complete their evaluation through siliconizing and flexure test, since it takes approximately one month from virgin panel availability to siliconized flexure bars. Any remaining process steps can be completed in Phase II.

Several of the panels fabricated from filaments developed some degree of delamination during the densification and strengthening process. These panels were molded by vendors using their resins and molding techniques, while pyrolysis and strengthening were performed by VMSC. VMSC uses furfuryl alcohol for reimpregnation and usually requires three reimpregnation and repyrolysis cycles to obtain maximum strength without risking delamination. However, the panels in question delaminated after only one or two reimpregnations. The reasons for this are not clear. Perhaps the reimpregnation fluid is not compatible with the resin, the pyrolysis cycle may be too severe, or more probable the cross-ply laminates are more susceptible to delamination than the unidirectional laminates usually evaluated for the filament materials. Cross laminated material was tested because this was believed to be a more efficient layup for leading edge airload panels, and therefore, would be a more realistic configuration to evaluate. Of the four high modulus panels processed, all experienced some degree of delamination, but it was encouraging that the Modmor II system appeared compatible with siliconizing. No coated

flexure strength data could be obtained on this panel, however, because prior delamination precluded meaningful results. It is felt that the delamination problem could be solved by optimizing resin volume and molding pressure during virgin panel fabrication.

At this point WCA graphite cloth remains the only acceptable substrate tested and, although this is not a high strength, high elastic modulus material, analysis shows that leading edge unit weights of less than 2 lb/ft² can be achieved with coated WCA. In addition the low elastic modulus of WCA minimizes thermoelastic stresses and permits designing for lower cost structure than possible with the high elastic modulus material.

Valid flexure data obtained on candidate substrates in comparable laminates is summarized in Table 4-1. Data on low quality material (except for the delaminated Hyfil panels) or data on small unidirectional layups has not been included, although it is discussed in the following paragraphs. All except the KGF-200 data was obtained using four-point loading and a 4.2 in. overall span. KGF-200 was tested with three point loading and 3.5 inch span. Specimens ranged from 0.7 to 1.0 inch wide and were nominally 0.18 to 0.30 thick. For comparative purposes, typical load-deflection curves are shown in Figure 4-1, simply to illustrate the shape of the curves obtained. Most of the materials exhibit some degree of yielding except the siliconized VCA, which shows greater brittleness.

Each of the substrate materials investigated are discussed below.

WCA Graphite Square Weave Cloth - This Union Carbide material has become a standard with VMSC because it has good strength, is easy to handle, is relatively inexpensive (in the range of \$40/lb), and has approximately equal properties in both the warp and fill directions. The material is procured to VMSC specifications. Substantial mechanical property improvement is obtained with reimpregnation with furfuryl alcohol. All coatings work done to date has been conducted with this material to ensure that substrate performance was not an initial variable in coating evaluation. VMSC obtains strengths of 16,600 psi in flexure, 3,250 psi in shear, and elastic modulus of 1.8×10^6 psi at a density of 1.27 gm/cc with laminates of this material. Higher strengths between 21,000 and 23,000 psi were obtained on 0.18 in. thick material used for coatings characterization. This material had an apparent density of 1.35 gm/cc. The supplier reports filament strengths typical of that which forms the cloth, of 90,000 psi (WYB graphite yarn) and elastic modulus of approximately 6×10^6 psi.

WCA has demonstrated reasonable compatibility with the oxidation inhibitor coatings and has, therefore, remained the baseline substrate. Even though strength diminishes when siliconized, and suggests that improvements need be made, strength remaining is satisfactory for leading edge design. Except for Supertemp's substrate where conclusions cannot yet be drawn, no

TABLE 4-1
SUMMARY OF FLEXURE STRENGTH COMPARATIVE RESULTS -
SUBSTRATE EVALUATION

Specimen	Spec. No.	Condition	No. of Reimpreg.	Bend. Stress F _B psi	Elastic Modulus		Remarks
					F _B psi	E 10 ⁶ psi	
Super-Temp	14-2-1(1)	CVD SiC	-	16100		2.9	
	14-2-1(2)	CVD SiC	-	16800		2.7	
	14-2-1(3)	CVD SiC	-	16900		2.6	
Bristol Hyfil	A4	Bare	3	17000		10.0	0, 45°, 90°
	B1	Bare	3	16100		10.7	layup delaminated 0, 30°, 60°, 90° layup de-laminated
Kreha KGF-200	—	Bare	1	8400		1.7	0°, 90°
	—	Bare	3	16200		2.3	layup
Modmor II	—	Bare	0	6600		9.8	0, 90° layup
	—	Bare	0	6600		9.8	0, 90° layup
VCA	VCA-1	Bare	3	21800		3.2	
	VCA-2	Bare	3	20700		2.8	
	VCA-3	Bare	3	20200		2.3	
WCA	WCA-1	Bare	3	16800		2.9	
	WCA-2	Bare	3	15100		2.6	
	WCA-3	Bare	3	15800		2.5	

TABLE 4-1 (continued)

Specimen	Spec. No.	Condition	No. of Reimpreg.	Bend. Stress F_B psi	Elastic Modulus $\frac{E}{10^6}$ psi	Remarks
VCA	M12-1	Siliconized	3	7100	3.3	Bare Panel
	M12-2	Siliconized	3	8400	3.3	Heat treated at 3400°F
WCA	M12-3	Siliconized	3	12600	1.8	Bare Panel
	M12-4	Siliconized	3	11700	1.9	Heat treated at 3400°F

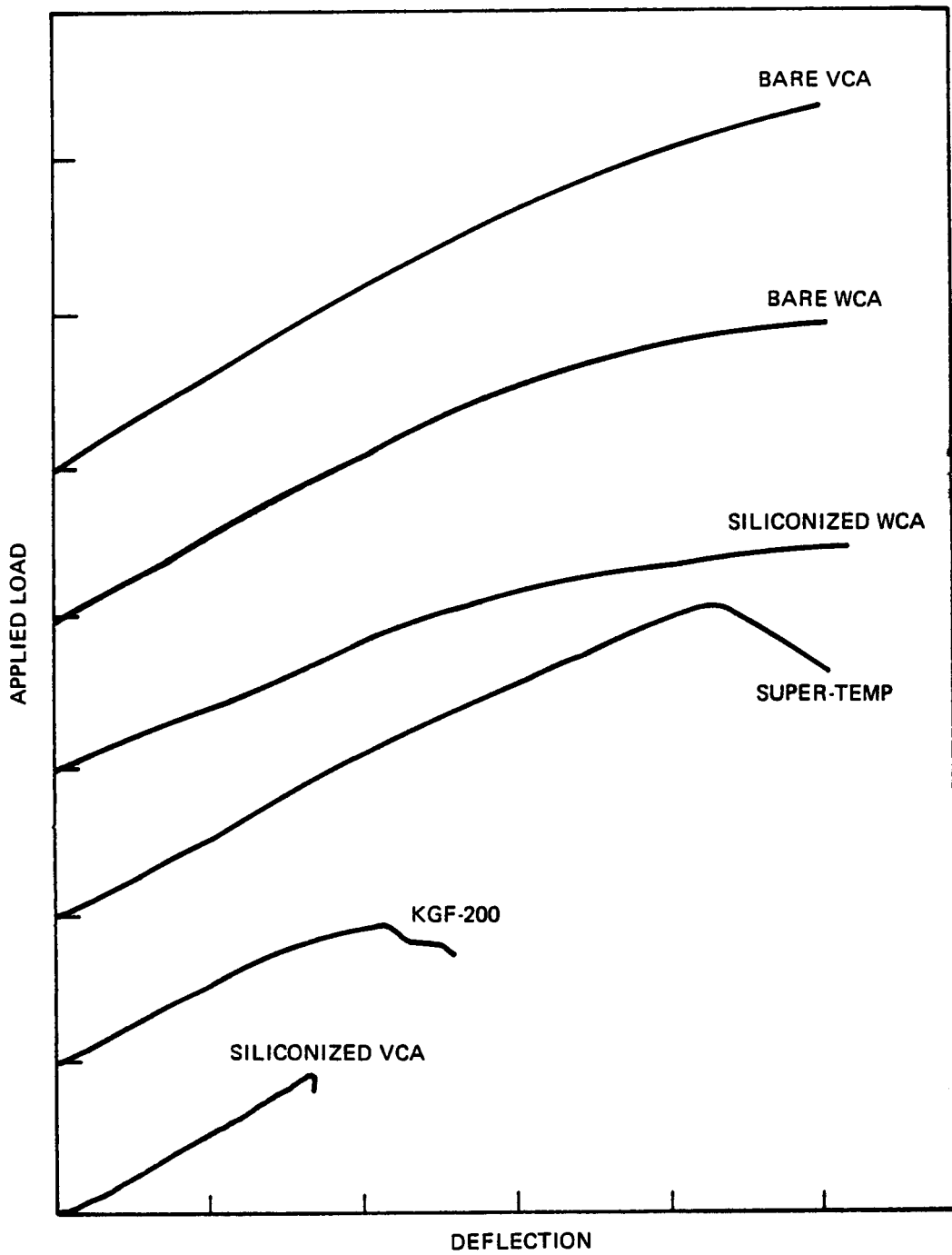


FIGURE 4-1 TYPICAL LOAD DEFLECTION CURVES FLEXURE SPECIMENS

0

other coating has withstood either reimpregnation or siliconizing without delamination or producing lower strength than the WCA.

VCA Carbon, Square Weave Cloth - This material was selected for evaluation because of its slightly higher filament strength (120,000 psi VYB carbon yarn) than WCA and the potential for higher laminate strength due to better expansion match with the pyrolyzed, carbon resin. Panel stiffness and cost are about equivalent to WCA laminates. VCA material was procured from Union Carbide to a modified WCA cloth procurement specification.

In a comparative evaluation bare VCA showed a 31% strength improvement over WCA, the stresses being 21,000 psi for VCA compared to 16,000 psi for WCA. Elastic moduli were roughly equivalent at 2.8 and 2.9×10^6 psi, respectively. However, siliconized test results were reversed. In this condition, siliconized WCA averaged 56% higher stress than siliconized VCA (12,200 psi versus 7,800 psi), although elastic modulus was lower at 1.9×10^6 psi compared to 3.1×10^6 psi. Since the strengths were lower than WCA and there was no apparent advantage of pursuing VCA, it was dropped from the program.

VYB Carbon Yarn - Although not specifically identified in the Program Plan, VMSC attempted to evaluate a cross-ply unidirectional filament layup of Union Carbide's VYB carbon yarn. The objective was to provide direct comparison data between the straight run filaments of this panel and the curved path filaments in the VCA woven cloth laminate. Strength and stiffness were expected to exceed those of VCA, while costs would be in the same range. A 90° layup was selected because, for the leading edge design, good strength in both directions is desired.

The first panel fabricated from this material proved to have low strength, averaging 1600 psi after pyrolysis, evidently due to the fact that the protective finish on the filaments had not been removed prior to layup. A replacement panel was not received from the vendor in sufficient time to complete all processing and evaluation prior to program completion. This work could continue in Phase II.

Modmor II High Modulus Fibers - A typical high modulus, high strength fiber material was selected to ascertain the potential benefits to be derived from this class of materials. Modmor II, marketed by Narmco/Whittaker, was selected because it has excellent fiber strength of 350,000 psi with a 35×10^6 elastic modulus. The Modmor II sacrifices modulus to gain strength compared to the Modmor I material. Cost of the raw material is an order-of-magnitude higher than the other test materials, being in the \$400/lb. class.

The prime questions for the high strength materials are (1) will a significant percentage of the strength be retained after coating, and (2) is it cost-effective?

A small pyrolyzed specimen of Modmor II unidirectional layup with epoxy resin produced a strength of 38,200 psi in flexure and an elastic modulus of 19.1×10^6 psi. These may be expected to be reduced to at least half in a cross-ply layup but the results were encouraging. These values were obtained after initial pyrolysis which would indicate that considerably higher values are potentially achievable with reimpregnation and repyrolysis. Another sample of this material delaminated severely during pyrolysis, but these laminates were fabricated using epoxy resin in a proportion designed for application in the virgin and not pyrolyzed state. VMSC's experience has been that phenolic resins produce better RPP laminates than the epoxy resins, so it was expected that Modmor II/phenolic laminates would solve the delamination problem.

The first Modmor II/phenolic cross-ply laminate fabricated by Whittaker delaminated at various levels during the pyrolysis and reimpregnation processing, and was unusable. A replacement panel using higher molding pressure proved stronger but eventually delaminated at the mid-layer. Strength after initial pyrolysis was 6640 psi and elastic modulus was 11×10^6 psi. Siliconizing did not appear to significantly aggravate the delamination and is encouraging for this material. Delamination prevented meaningful strength data from being obtained so it is still not clear if coated Modmor II or similar should be a candidate for shuttle application. It is recommended that evaluation continue in Phase II. A promising application for the high modulus, high cost fibers is in a "sandwich" construction with lower cost WCA as the core material. The objective would be to obtain a better balance of weight and cost.

In terms of cost-effectiveness, the weight optimization technique discussed in Section 3.4 for solid laminates with coated outer layers can also be employed in cost optimization. If it is assumed that a low modulus, low cost material such as WCA cloth is used as middle laminates and a high modulus, high cost Modmor II type material is used for face layers, the distribution between the two materials can be optimized on a materials cost basis. This results in an indication that the high cost material should make-up 10% of the total thickness. At this point, these results are inconclusive and it is still not clear that the high strength, high modulus material will ultimately be a suitable selection.

The high modulus material could produce a thermoelastic problem if the ratio of strength to the product of elastic modulus and expansion coefficient ($F/E\alpha$) does not exceed a value of 600. This is covered in Section 3.0. Data is not available on coated material to make this evaluation.

Hyfil 2710 - This material made by Rolls Royce from PAN fibers is another example of the high modulus, high strength fiber materials available. Fiber strength is about 350,000 psi and elastic modulus is 27.6×10^6 psi. Strength of a unidirectional laminate of 39,000 psi was obtained as pyrolyzed with a density of 1.38 gm/cc.

Panels fabricated for VMSC evaluation were layed up 0.25 inch thick in 0° , 45° , 90° and 0° , 30° , 60° , 90° orientations. Molding pressure was over 100 psig. Strength was reduced significantly with the cross-oriented plies compared to unidirectional layup to produce under 3700 psi after first pyrolysis. Three reimpregnations and repyrolysis cycles boosted flexure strength to 17,000 psi with modulus of elasticity of 10×10^6 psi, but these results were obtained on delaminated material and are meaningless.

Siliconizing of a flexure bar specimen resulted in additional and severe delamination and cracking. Continued exploration of this material is not recommended.

KREHA KGF-200 - A panel of this Japanese material was provided by Whittaker Corporation, for comparison with and as a possible alternate to the VYB. KGF-200 fibers are fabricated from pitch and spun into yarns. Fiber strength is reported at 160,000 psi with elastic modulus of 10×10^6 psi. A cross-ply laminate has been evaluated through the third repyrolysis cycle and produced flexure strength of 16,200 psi and an elastic modulus of 2.3×10^6 psi. This is approximately equivalent to WCA cloth laminates. Data on siliconized specimens has not been obtained but evaluation should be continued in Phase II to determine compatibility with VMSC coatings.

Super-Temp - Laminates applied by Super-Temp were machined from a composite layup of fabric, which had been infiltrated by carbon vapor deposition to a density of 1.6 gm/cc. Reported strengths of bare laminates are in the 19,000 to 25,000 psi range. VMSC tests of 0.25 inch thick material with Super-Temp's silicon carbide coating produced an average flexure strength of 16,600 psi. However, coating thickness was only 3 to 4 mils. Initial attempts to siliconize bare laminates with the VMSC coating proved unsuccessful since penetration was not achieved. Additional trials may be conducted in Phase II to determine substrate compatibility with VMSC coatings. VMSC coatings show better stability in plasma arc testing than the Super-Temp coating, hence, the desire to investigate this combination.

4.2 OXIDATION INHIBITORS

Oxidation inhibitors for RPP substrates to be applied in the form of add-mixtures, diffusion, combined systems, and overlays were selected on the basis that protection could be achieved either by formation of an inert

inhibitor system (stable at all air temperatures) or one that would show little noticeable response to the test environment. Inert oxidation resistant systems to near 3,000°F are possible for the add-mix, combined or diffusion system if the correct material combinations are obtained in the inhibitor fabrication process. This fact is shown in the fabrication of inhibited RPP specimens and test results of reference 14. Inert systems for above 3,000°F service are possible if barriers can be provided to impede or attenuate oxygen flow to the underlying inhibited substrate. This oxygen barrier might be accomplished by a secondary diffusion treatment or by an overlay treatment of a dense oxidation resistant material.

4.2.1 Candidate Oxidation Inhibitor Systems

The selection of candidate oxidation inhibitor systems was based on past demonstrated performance as well as theoretical predictions. Rationale used in this initial selection of material constituents and the protective devices for each is discussed in the following paragraphs.

Silicon System - Silicon metal reacts readily with carbon to form silicon carbide in two crystal structures: cubic, the beta form; and hexagonal, the alpha form (reference 15). The alpha form has many polymorphs and is considered to have a greater stability when heated in air. Formation of alpha silicon carbide initiates at temperatures above 3,400°F, while the beta phase is formed at lower temperatures. RPP specimens inhibited with beta silicon carbide had shown excellent oxidation resistance in plasma tests at temperatures to 2,700°F (reference 16). Tests at 3,010°F showed a slight recession and modest weight loss while tests at near 4,000°F caused severe recession and weight loss. RPP specimens inhibited with alpha silicon carbide had not been tested. It was speculated that a greater resistance to air oxidation could be achieved if the more stable alpha phase fraction could be incorporated into the beta phase. This was accomplished by processing RPP in the silicon pack at a temperature of 4,000°F, but performance of these systems in plasma arc testing proved inferior to siliconized RPP processed at 3,400°F.

Zirconium Diboride-Silicon System - The ZrB₂/Si system has been investigated by several persons (references 13, 14, 17, 18, 19) for its resistance to oxidation under varied test conditions. Reference 14 describes the preparation and test of RPP specimens inhibited with ZrB₂ and tested to 4,800°F for ten seconds in the AVCO-RAD plasma with no recession observed. Tests on additional specimens at above 5,500°F for 20 seconds had recession rates of 0.600 inch/min. and 0.270 inch/min. Kaufman of Manlabs (reference 18) demonstrated the superiority of a hot-pressed ZrB₂-SiC-C system to withstand plasma arc test conditions to above 4,000°F. Very little surface recession was recorded, but in-depth loss of the SiC phase was noted for multiple test recycles. The Manlabs composites contained a high ZrB₂ loading near 80 weight percent. The RPP specimens of reference 14 contained 36

weight percent. From the previous test results, it was concluded that RPP specimens containing a higher concentration of ZrB_2 than those of reference 14 and close to reference 18, while still retaining the silicon carbide phase, would appear to enhance oxidation resistance. Processing techniques or strength deficiency would provide limits to the loadings achievable with the RPP system.

Zirconium/Silicon System - Zirconium/silicon inhibitor combinations applied to RPP substrates have been shown to be resistant to oxidation to temperatures near $4,000^{\circ}F$ (reference 14). Weight losses to slightly larger than 20 weight percent were recorded for tests to five minutes duration; weight gains of one to two percent were recorded for tests at $3,000^{\circ}F$ for 15 minutes. A low temperature problem existed at $1,400^{\circ}F$ in the form of delaminations of the RPP substrate plies. The theory was advanced that this problem could be minimized by increased proportion of the silicon carbide constituent to better balance the high and low temperature performance.

Tantalum-Silicon System - Tantalum and silicon form carbides that have melting points above $4,000^{\circ}F$. The tantalum reaction with carbon according to Campbell (reference 12) can initiate and become appreciable above $2,300^{\circ}F$, while silicon and carbon react very readily at near the melting point ($2,500^{\circ}F$) of silicon. There is no evidence currently available which predicts the preferential reaction of one of these refractory materials in the presence of the other or that formation of binary compositions of TaC-SiC cannot be made. In the presence of excess carbon, no silicides of tantalum should be evident if heat treatment temperature is sufficient. Rates of diffusion for each binary pair, when applied together on a graphitic body such as RPP are unknown. Should this vary greatly between components at the temperature level selected, a diffused zonal system could occur. The level of oxidation resistance of a TaC-SiC system would depend largely on the vitreous film of silica which forms and provides a protective layer over the somewhat less oxidation resistant, but more refractory tantalum carbide. The data of reference 14 shows that tantalum and silicon systems provide oxidation resistance to $4,000^{\circ}F$ for five minutes with weight loss at 11%. At $3,000^{\circ}F$ for fifteen minutes the weight loss was slightly over one percent. The system was composed of a 90 w/o tantalum • 10 w/o silicon applied to an RPP substrate.

Titanium-Silicon System - The Titanium and Silicon binary carbide system was explored and reported by Dr. E. Rudy, reference 13. The oxidation potential of titanium/silicon carbides was evaluated by specimen fabrication and elevated temperature test in the work of reference 14. Inhibitor compositions of 90% titanium and 10% silicon were applied to RPP substrates by a silicon pack cementation method. Test results in air at $4,000^{\circ}F$ showed as little as 10% weight loss when tested for five minutes.

Similar specimens when tested at 3,000°F for fifteen minutes gained slightly more than one percent in weight. The weight lost at 4,000°F was attributed to the formation and subsequent loss of a volatile oxide of titanium. Control of the oxide formation was deemed feasible by increasing the silicon content of the inhibitor, thus shifting the Ti-Si-C phases to a silicon carbide rich system. It was assumed the silicon carbide oxidation product during air heating would provide a protective vitreous silica film and an oxide "sink" for the smaller amount of titania formation.

Hafnium-Tantalum System - Evaluations at the LTV Research Center several years ago showed that a hafnium-tantalum refractory metal coating system protected bulk graphite from air oxidation at temperatures up to 3300°F. The protective system, comprised of 80 weight percent hafnium and 20 weight percent tantalum, had been applied by a multiple melt impregnation process. This composition takes advantage of the low (3800°F) melting point of the alloy for application to graphite substrates. The process which is applicable to RPP, combined with the oxidation test results of reference 36 clearly indicate the potential of this system as a candidate for RPP. Weight gains of slightly more than 1% were recorded for specimens held at 3,330°F for three minutes in air. The oxide film formed during the test was self-supporting and firmly attached to the underlying substrate. A mismatch of thermal coefficients of expansion between the substrate and the resulting oxide caused some spallation, but the failure was in the graphite and not in the oxide nor at the oxide/graphite interface. It was concluded that with better expansion match a highly oxidation protective coating would result. Rudy in reference 37 recognized the wide interest and oxidation promise of the hafnium-tantalum system, where the alloy is in direct contact with carbonaceous materials, and speculated that the nature of the equilibria occurring in the system was conducive to producing one of the best thermal-shock resistant metal-carbide composite structures. The indication was that a chemically graded system from carbon to metal carbide to metal oxide was possible, which would have merit as an oxidation protective device for RPP.

Zirconia and Hafnia - The oxides of zirconium and hafnium have been studied extensively for use at high temperatures above 4,000°F and consequently, an abundance of literature is available for review. The final materials report for the X-20 Dyna-Soar nose cap program shows clearly the use potential of zirconia to protect siliconized bulk graphite to temperatures in the range between 3500°F and 4000°F.

Stabilization studies to minimize crystal transformation and inversions with heating were successful and accompanied by a welcomed increase in thermal shock resistance. Uniform thermal expansion of stabilized zirconia was obtained and reported by the National Bureau of Standards in Washington and by references 38 and 39. Cambell (reference 40) reports that hafnia is similar to zirconia and would be expected to show the same stability and

chemical inertness at high temperatures and suggests that it would probably be preferred to zirconia for most refractory applications. The scarcity of pure hafnium compounds precludes its wide use and dictates the use of the more commercially available hafnia which contains 2 to 3 percent zirconia and is entirely acceptable for the present Shuttle Leading Edge Program.

4.2.2 Add-Mix Systems

For the purposes of this report, the term add-mix is defined as a fabric reinforced laminated construction with metal powder additive(s) dispersed, bound, and reacted in the interlaminar zone with binding matrix carbon. Add-mix systems were evaluated by plasma arc and flexure strength. In each case they were inferior to the diffusion coated systems and were ultimately rejected for continuance on the program.

The add-mix systems utilized two metal powders applied to the individual plies of resin impregnated graphite fabric. Silicon metal was common in all panels. The principal metals were ZrB_2 , Ta, ZrH and Ti. The add-mix systems fabricated and the composition goals for each of the panels in its cured state are presented in Table 4-2.

Reinforcement for the inhibited RPP composites utilized a square weave graphite cloth, WCA. This material was preimpregnated with phenolic resin in accordance with VMSC Materials Specification 307-7-7, "Phenolic Impregnated Graphite Fiber Cloth." An impregnated fabric was preferred to assure a thorough wetting of the fabric by the powder resin slurry. Additional resin was incorporated in the composite as required. Experience had shown that impregnation of dry fabric with a powder loaded resin resulted in a filtration effect where the powders were partitioned at the weave surface while the resin permeated the fabric. This resin starved powder zone was accompanied by lower strength and caused this method to be discontinued.

The reinforcement was cut into 6" x 7" sizes, with the number of plies for a given panel being varied to achieve the desired thickness. A dry powder mixture of the various inhibitors was prepared using the goals of Table 4-2 as a guide. Metal powders were weighted out in sufficient quantities to satisfy the total composite requirement. Mixing of the powders was achieved by rolling the container and contents on a ball mill for two hours. The Fiberite panel, supplied by the Fiberite Corporation for evaluation, was in the cured state when received.

The required quantity of inhibitor and resin mixture was divided into equal increments to coat the surface of each ply. Isopropyl alcohol was added as required to reduce the slurry viscosity to a spreadable consistency. This mixture was then applied to a pre-weighed ply of pre-impregnated reinforcement and the mixture spread to a uniform thickness. These coated plies were air dried at room temperature one hour to allow solvent evaporation.

TABLE 4-2
Add-Mix Composites Data
Cured Panel Composition Goals
Volume Percent

Constituents	PANEL NO.						
	3	4	5	7	8	10	5A Fiberite ⁽¹⁾
ZrB ₂			8.6	23.5			6.3
ZrH					8.5		
Ta	4.1	1.6					
Ti						17.7	
Si	43.3	16.3	5.6	11.0	15.5	28.4	4.0
Fiber Reinforcement	20.1	41.6	40.0	25.5	30.7	20.8	39.0
Resin Solids	32.5	40.5	45.9	40.0	45.7	33.1	50.7
No. of Plys	7	16	15	12	13	9	14

(1) Ply count was made visually and powder loading calculated from Fiberite inputs that the panel consisted of 25 w/o of a 4/1 mixture of ZrB₂ to Si.

TABLE 4-3
Add-Mix System Process Data
Weight Changes Due to Processing

Panel No.	Initial Weight	Wt. % Loss Initial Pyrolysis	Wt. % Carbon ⁽¹⁾ Gain w/Re-impregnation	3400°F Heat ⁽²⁾ Treat Wt. Loss
3	358.0	30.7	--	--
4	397.1	28.2	--	--
5	302.5	16.0	18.4	14.8
7	463.8	7.3	17.5	14.8
8	338.1	17.5	19.8	13.4
10	414.2	5.1	19.0	14.3
5A Fiberite	317.9	8.2	10.8	11.5

(1) Based on initial pyrolyzed weight

(2) Based on fourth pyrolysis weight

Subsequently, the coated plys were further heated in an air circulating oven for five minutes at 240°F to complete solvent removal and to advance the phenolic resin cure. The weight of the coated plys was checked to establish the total weight pickup.

The prepared plys of reinforcement were laid up into a laminate and cured using a vacuum bag autoclave, pressure augmentation technique in accordance with VMSC process specification 308-7-10A, "Fabrication of Reinforced Pyrolyzed Plastics." The time-temperature cycle was as follows: 180° ± 10°F for two hours, 240° ± 10°F for one hour, and 300°F ± 10°F for one hour. The autoclave was cooled to 180°F before removing the panel and the vacuum bag.

Post cure and pyrolysis of the panels was performed in a stainless steel retort where the panels were restrained between flat graphite plates. Retort void space was packed with calcined petroleum coke powder to preclude oxidation of the panels. The temperature cycle was performed in a Huppert Electric Furnace in accordance with VMSC specification 308-7-10A. Significant changes experienced by the panels during processing are noted in Table 4-3. The net weight losses resulting from first pyrolysis are shown in the column headed "Weight % Loss Initial Pyrolysis". For comparison purposes, standard uninhibited RPP normally experiences approximately 25% loss by virtue of the resin conversion to carbon. Of the panels described under add-mix, all survived this processing point with the exception of the tantalum loaded composites. Both panels 3 and 4 failed by delamination during pyrolysis. Powder loading alone was not the cause of failure, since panel number 10 with titanium and silicon inhibitor, was similar in total composition to panel 3, but produced a sound laminate.

Calculated pyrolyzed composition of the panels on a volume basis, given in Table 4-4, are based on the known pyrolyzed weight and the fact that pyrolysis weight changes are essentially due to the resin conversion only. This calculation was not made for panels 3 and 4 since their condition after first pyrolyzation did not warrant further processing.

Densification was the next process step and was intended to increase interlaminar and intralaminar strength of the RPP. The intent is to place additional carbon in the porosity of the inhibitor filled area. Subsequent heat treatment of the panels was designed to promote reaction of the metal powders with resin carbon to form carbides. Densification was accomplished by successive cycles of furfuryl alcohol impregnation followed by cure and pyrolysis. A tabulation of the net weight increase due to carbon pickup by virtue of the multiple impregnation is given in Table 4-3.

Following pyrolysis, test specimens were cut from the add-mix RPP panels. The use of diamond and carbide tip tools were necessary to minimize the chance of damaging the specimens which had hardened considerably due to sintering in the pyrolyzation treatment.

The RPP specimens cut from the add-mix panels were heat treated to advance the reaction state of the inhibitor powders and form carbide products with the available carbon of the laminate. The specimens were packed for heat treatment between layers of carbon felt, placed in a graphite

TABLE 4-4
Add-Mix Composites Data
Pyrolyzed Panel Composition
Volume Percent

Constituents	PANEL NO.								
	3(1)	4(1)	5	7	8	10	5A Fiberite		
ZrB ₂	Panel Lost in Pyrolysis	Panel Lost in Pyrolysis	9.6	29.4			6.7		
ZrH					9.2				
TA									
Tl							22.0		
Sl					7.1	13.8	16.8	35.2	5.0
Fiber Reinforcement					44.7	31.9	32.9	26.0	48.7
Resin Carbon					39.5	24.9	41.1	16.8	39.7
No. of Plys					15	12	13	9	14

(1) Not calculated due to panel condition after pyrolyzation.

retort, and heat treated for four hours at 3,400°F under an inert atmosphere. Average weight loss data for the various inhibitor systems is given in Table 4-3. In all cases, a weight loss was experienced due to the heat treatment. The loss was attributed to the vaporization of the free metal fractions at the high temperature. Some slight loss of carbon content was probably also experienced. Typically, RPP experiences a weight loss of 2.1% when heat treated to 3400°F.

Strength of the add-mix panels was very low being less than half of their diffusion coated counterparts. This indicated a system with possible low reliability. Plasma arc performance at the screening heat flux level of 160 Btu/ft²-sec showed mass loss rates only 2 to 5 times better than bare RPP and an order of magnitude worse than siliconized RPP. For these reasons, the add-mix systems were dropped from further consideration.

4.2.3 Combined Systems

The combined system approach utilizes the processing of add-mix fabrication followed by silicon diffusion coating. The non-silicon oxidation inhibitor constituent is mixed with the resin and applied to the composite outer plies. The silicon metal constituent is added by diffusion processing to generate SiC within the inhibited RPP.

The laminate design was such that a three-layer construction resulted. The middle layer was uninhibited RPP, while the outer two layers were coated with the principal metal inhibitor as described previously. The cured panel ingredient goals for the combined panels are listed in Table 4-5.

The reinforcement coating, layup, cure and pyrolysis was the same as described for add-mix systems in Section 4.2.2. The gross response of weight change for the panels numbered 1, 2, 9 and 11 is shown in Table 4-6 while Table 4-7 lists the results following pyrolysis. Examination of the panels revealed surface attack, which was attributed to chemical attack of the substrate filler by the impregnating solution.

Specimen preparation and heat treatment were performed as described in Section 4.2.2. Following heat treatment the specimens were siliconized in a standard pack treatment at 3400°F for four hours. The results of this treatment were catastrophic (reference 35) and no acceptable test specimens were recovered. For each of the four combined process systems delamination occurred at the interface between the bare center plies and the coated outer plies, indicating a gross mismatch in expansion coefficient. Deep cracking of flexure bars and surface spalling prevailed. Siliconizing penetrated unexpected deep and the loading was undesirably heavy. The reasons for this are unclear. The gross delamination problem could probably be corrected by introducing the add-mix constituent throughout the laminate rather than confining it to the outer plies. The siliconizing problem may be correctable through reduced loading

TABLE 4-5
 Combined Composites Data
 Cured Panel Composition Goals
 Volume Percent

Constituents	PANEL NO.			
	1	2	9	11
ZrB ₂	26	13.6		
ZrH			6.9	
Ti				11.2
Fiber Reinforcement	24	38.7	31.1	41.4
Resin Solids	50	47.2	62.0	47.5
No. Plys Bare	5	5	4	4
No. Ply Coated	8	8	10	10

TABLE 4-6
 Combined System Process Data
 Weight Changes Due to Processing

Panel No.	Initial Weight	Wt. % Loss Initial Pyrolysis	Wt. % Carbon ⁽¹⁾ Gain w/Reimpregnation	3400°F Heat ⁽²⁾ Treat Wt. Loss
1	458.3	9.6	13.4	10.7
2	92.5	13.3	9.2	17.2
9	256.8	21.0	21.1	11.1
11	248.6	11.3	26.2	20.9

(1) Based on initial pyrolyzed weight

(2) Based on fourth pyrolysis weight

or process change. In any event it was felt to be unlikely that the combined system would perform better than the diffusion systems as evidenced by the inferior performance of the add-mix systems. Therefore, work was discontinued on this approach.

TABLE 4-7
 Combined Composites Data
 Pyrolyzed Panel Composition
 Volume Percent

Constituents	PANEL NO.			
	1	2	9	11
ZrB ₂	67.5	46.5		
ZrH			20.0	
Ti				37.4
Fiber Reinforcement	16.2	24.0	44.8	28.5
Resin Carbon	16.4	29.4	35.1	34.1

TABLE 4-8
Preliminary Diffusion Coating Experiments

Exp. Run	System	Slurry Composition (Wt. Percent)	Pack Composition (Wt. Percent)	Reaction Temp.	Time at Temp.	Specimens Coated 1/4" Thick	Avg. Wt. Gain %	Coating Thickness (inches)	Oxidation Test 2300°F Wt. Loss %
1	ZrB ₂ /Si/C	68.2 ZrB ₂ 17.2 Si 14.6 C	30 Al ₂ O ₃ 70 Si	2900°F	4 Hrs.	6-3/4" Disks	30 ⁺	0.015	Not Tested
2	Ta/Si	86.7 Ta 13.3 Si	70 Al ₂ O ₃ 30 Si	3400°F	4 Hrs.	6-3/4" Disks	22	0.020	Not Tested
3	Si	33.3 Si 33.3 SiC 33.3 Al ₂ O ₃	30 Al ₂ O ₃ 70 Si	2900°F	4 Hrs.	6-3/4" Disks	28 ⁺	0.014	1
4	Ti/Si	65 Ti 35 Si	30 Al ₂ O ₃ 70 Si	2000°F 2500°F 2900°F	2 Hrs. 1 Hr. 4 Hrs.	6-3/4" Disks	*	Not Determined	Not Tested
5	ZrH/Si	78 ZrH 22 Si	30 Al ₂ O ₃ 70 Si	2000°F 2500°F 2900°F	2 Hrs. 1 Hr. 4 Hrs.	6-3/4" Disks	*	Not Determined	None
6	ZrB ₂ /Si/C	68.2 ZrB ₂ 17.2 Si 14.6 C	70 Al ₂ O ₃ 30 Si	3400°F	4 Hrs.	4-3/4" Disks (from Run #1)	Total 46 ⁺	0.015	None
7	Ta/Si	86.7 Ta 13.3 Si	70 Al ₂ O ₃ 30 Si	3400°F	4 Hrs.	4-3/4" Disks (From Run 2)	Total 17 ⁺	0.018	None
8	Si	33.3 Si 33.3 SiC 33.3 Al ₂ O ₃	70 Al ₂ O ₃ 30 Si	3400°F	4 Hrs.	4-3/4" Disks (from Run #3)	Total 36 ⁺	0.040	None
9	Si	33.3 Si 66.7 SiC	70 SiC 30 Si	3400°F	4 Hrs.	2-3/4" Disks	29	0.018	3
10	ZrH/Si	78 ZrH 22 Si	70 Al ₂ O ₃ 30 Si	2000°F 2900°F	2 Hrs. 4 Hrs.	6-3/4" Disks	*	Not Determined	Not Tested

TABLE 4-8 (continued)

Exp. Run	System	Slurry Composition (Wt. Percent)	Pack Composition (Wt. Percent)	Reaction Temp.	Time at Temp.	Specimens Coated 1/4" Thick	Av. Wt. Gain %	Coating Thickness (inches)	Oxidation Test 2300°F Wt. Loss %
11	Ti/Si	65 Ti 35 Si	70 Al ₂ O ₃ 30 Si	2000°F 2900°F	2 Hrs. 4 Hrs.	6-3/4" Disks *	*	Not Determined	Not Tested
12	Ti/Si	65 Ti 35 Si	100 Al ₂ O ₃ 100 SiC	2000°F 2900°F	2 Hrs. 4 Hrs.	3-3/4" Disks 3-3/4" Disks	0.4 5	Not Determined	Not Tested
13	ZrH/Si	78 ZrH 22 Si	100 Al ₂ O ₃ 100 SiC	2000°F 2900°F	2 Hrs. 4 Hrs.	3-3/4" Disks 3-3/4" Disks	2 0.6	.002 Not Deter.	Not Tested
14	Ti/Si	65 Ti 35 Si	90 Al ₂ O ₃ 10 Si 90 SiC 10 Si	2000°F 2900°F	1 Hr. 4 Hrs.	3-3/4" Disks 3-3/4" Disks	8 6	.005 Not Deter.	Not Tested
15	ZrH/Si	78 ZrH 22 Si	90 Al ₂ O ₃ 10 Si 90 SiC 10 Si	2000°F 2900°F	1 Hr. 4 Hrs.	3-3/4" Disks 3-3/4" Disks	15 30	.012 Not Deter.	Not Tested
16	Ti/Si	65 Ti 35 Si	85 Al ₂ O ₃ 15 Si 85 SiC 15 Si	2000°F 3400°F	1 Hr. 5 Hrs.	1-3/4" Disk (new) 2-3/4" Disks (from 14) 3-3/4" Disks (from Run 14)	13 20 Total 12 Total	Not Determined	6 11
17	ZrH	78 ZrH 22 Si	85 Al ₂ O ₃ 15 Si 85 SiC 15 Si	2000°F 3400°F	1 Hr. 5 Hrs.	1-3/4" Disk (new) 2-3/4" Disks (from 15) 3-3/4" Disks (from 15)	40 70 Total + 18 Total	Not Deter.	None 5

+Pack material or metal adhering to specimens

*Specimens covered with excessive metal

TABLE 4-9
Diffusion Coating for Characterization Specimens

Experiment Run	18	19	20	21	22
System	Si	ZrB ₂ /Si C	Ta/Si	Ti/Si	ZrH/Si
Slurry Composition (Wt. Percent)	33.3 Si 33.3 SiC 33.3 Al ₂ O ₃	68.2 ZrB ₂ 17.2 Si 14.6 C	86.7 Ta 13.3 Si	65 Ti 35 Si	78 ZrH 22 Si
Pack Composition (Wt. Percent)	70 Al ₂ O ₃ 30 Si	70 Al ₂ O ₃ 30 Si	70 Al ₂ O ₃ 30 Si	85 SiC 15 Si	85 SiC 15 Si
Reaction Temperature	3400°F	3400°F	3400°F	2000°F 3400°F	2000°F 3400°F
Time and Temperature	4 Hours	4 Hours	4 Hours	1 Hour 4 Hours	1 Hour 4 Hours
Specimens Coated	10-3/4" Disks 1-3" Disk 2-1" x 5"	10-3/4" Disks 1-3" Disk 2-1" x 5"	10-3/4" Disks 1-3" Disk 2-1" x 5"	10-3/4" Disks 1-3" Disk 2-1" x 5"	10-3/4" Disks 1-3" Disk 2-1" x 5"
Average Weight Gain (Percent)	14	11	9	13	16
Coating Thickness (inches)	21 on 3/4" Disks 0.020	12 on 3/4" Disks 0.010	10 on 3/4" Disks 0.015	20 on 3/4" Disks 0.012	18 on 3/4" Disks 0.007
Oxidation Test * 2300°F Weight Loss Percent	1	3	4	No Change	10
X-ray Diffraction	α SiC β SiC	α SiC β SiC ▽ ZrC	α SiC β SiC ▽ TaC	Not determined	α SiC β SiC ▽ ZrC
Emission Spectrograph Analysis	Si	Si, Zr No Boron	Si, Ta	Si, Ti	Si, Zr,

* Weight loss on bare substrate material was 11%

▽ Tentative, positive identification not possible as tested

4.2.4 Initial Diffusion Systems

Five oxidation inhibitor systems listed in Tables 4-8 and 4-9 were applied to the densified pyrolyzed substrates. Pack composition and furnace reaction temperature were varied in an effort to maximize diffusion depths into the substrate. A final series of diffusion coatings with the selected pack composition and furnace reaction temperature was made with the five oxidation inhibitor systems to produce specimens for initial screening testing.

Oxidation inhibitor systems were applied after the specimens had been machined to finished dimensions. Specimens were cut from 10" x 12" flat laminates produced to 0.25 in. thickness. Inhibitor systems were applied by VMSC's pack cementation process using the inhibitor system compounds in a combination slurry pack-cementation technique. The slurry was prepared by stirring the mixture of ingredients listed in Table 4-8 in isopropyl alcohol to a consistency sufficient to provide a smooth, uniform coat when applied to a dry specimen. The slurried specimens were then placed in a pack for processing.

The pack consisted of a graphite retort and pack material, which was a uniformly blended mixture of silicon metal powder and inert filler. Pack composition for each diffusion system experiment is listed in Table 4-9. A cover layer of carbon black was used to isolate the system and a graphite lid, containing an aperture, permitted escape of volatiles. The retort was placed in an air circulating oven at 300°F and held overnight to drive out all moisture and residual isopropyl alcohol.

The still hot retort was then placed in the VSMC high temperature diffusion furnace and the system was evacuated three times and back filled with argon to a final pressure of 3 - 5 psig. A 3 - 5 SCFH flow of argon was maintained during the processing. The temperature of the retort was raised to the desired temperature and held for a pre-determined time as noted in Table 4-8. Some of the experiments were reacted at more than one temperature during the same furnace run.

Specimens, upon removal from the pack, were brushed and scraped to remove adhering pack and slurry residues. This was followed by washing with isopropyl alcohol.

During the preliminary experiments, runs 1 through 17, evaluation of the effectiveness of the oxidation inhibition process was made by calculation of the weight gain and measurement of penetration depth of the diffused coating. These results are included in Table 4-8 for each experiment.

Depth of penetration was defined as the continuous ring effect on the specimen as measured using photomicrography. The surface was examined at 50 X magnification. A typical photomicrograph of an area of a coated specimen is shown in Figure 4-2. The darker area is the coating and the

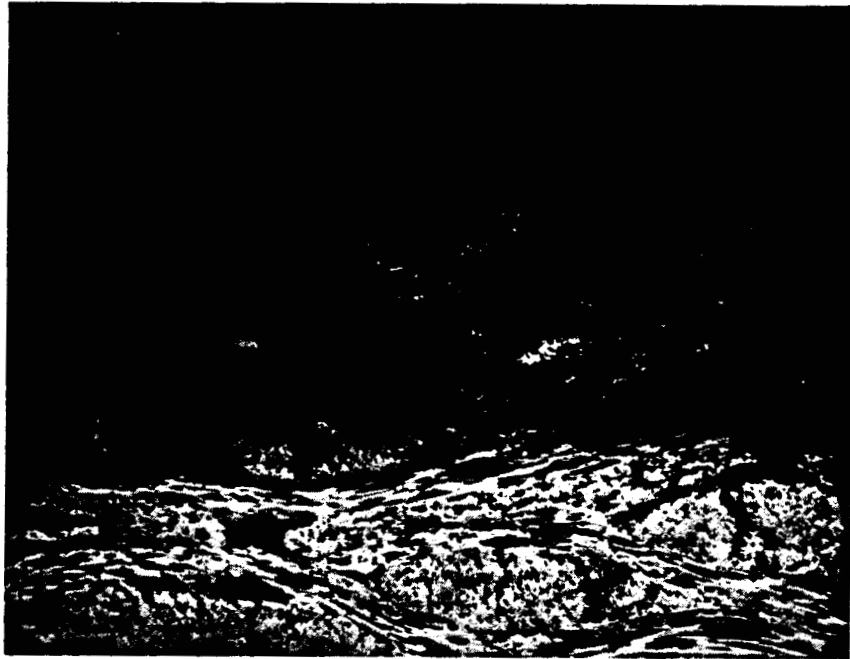


FIGURE 4-2 TYPICAL PHOTOMICROGRAPH OF DIFFUSION COATED SPECIMEN (50X). SPECIMEN FROM EXPERIMENTAL RUN NUMBER 8

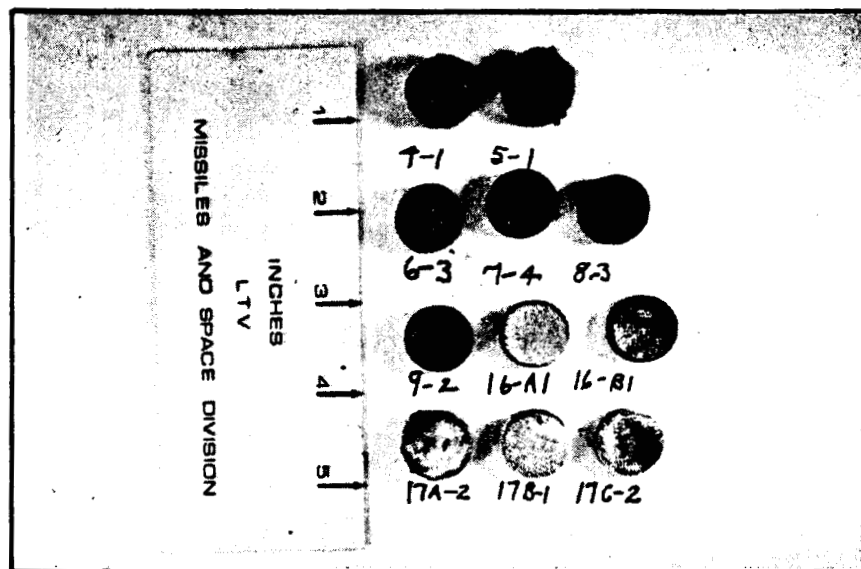


FIGURE 4-3 PHOTOGRAPH OF SELECTED SPECIMENS DIFFUSION COATED DURING PRELIMINARY EXPERIMENTS AFTER STILL AIR OXIDATION TEST AT 2300°F

lighter area is the RPP substrate material. The deep diffusion illustrated by the photograph shows that the coating has penetrated into the porosity of the substrate and reacted with the cloth fibers. The coating thickness of this specimen as shown from experimental run 8, was 0.040 inch.

Still-air oxidation testing was utilized on selected specimens during the preliminary experiments as an additional method of determining processing effectiveness. Weight loss results are shown in Table 4-8 and Figure 4-3 is a photograph of the specimens after testing.

Based on these results, specimens for characterization tests of the five oxidation inhibitor systems were prepared using the procedures established by the trials. Slurry compounds, pack compounds, reaction temperatures and time at temperature used are listed in Table 4-9. Evaluation of these specimens for processing effectiveness included coating thickness and weight gain measurements, which are listed in Table 4-9.

After test, flexure bars of the five final coating systems were sectioned and fired at 1,500^oF in an air furnace for nearly fifteen hours. The results of this exposure are shown in Figure 4-4. Two specimens each of the five inhibitor types are shown. Of particular interest is the remaining inhibitor of the ZrB₂/Si, ZrH/Si and silicon systems. The silicon system clearly shows its ability to resist low temperature oxidation. The diffused portion of the silicon carbide inhibitor can be clearly seen. The ZrB₂/Si shows a weakening and collapse of the inhibitor. The ZrH/Si system has undergone a definite volume change which is probably due to the lack of oxidation resistance of zirconium carbide when silicon carbide is not present in sufficient amount. There appears to be a tendency for one surface of the specimens to have a heavier inhibitor layer, which indicates a preferential inhibitor formation in the pack treatment. It has been found that the upper surface is more deeply coated. This can be taken advantage of in flight hardware by orienting the stagnation heating region upward.

Chemical analysis of the coating material employed a nondestructive x-ray diffraction method, which scanned the surface of 3/4-inch diameter specimens. The main constituent in all five systems was found to be silicon carbide. Indications of other compounds were noted and are listed in Table 4-9. The x-ray diffraction line peaks attributed to the silicon carbide were of high intensity due to the preponderance of this compound in the specimens. This caused superimposing of silicon carbide diffraction peaks over the angular range for some of the diffraction peaks of other possible compounds and prevented their positive identification. In all specimens, emission spectrographic analysis found silicon and all other applied elements except boron, which had been applied as a zirconium diboride. These analyses tended to substantiate the finding of the x-ray diffraction analysis.

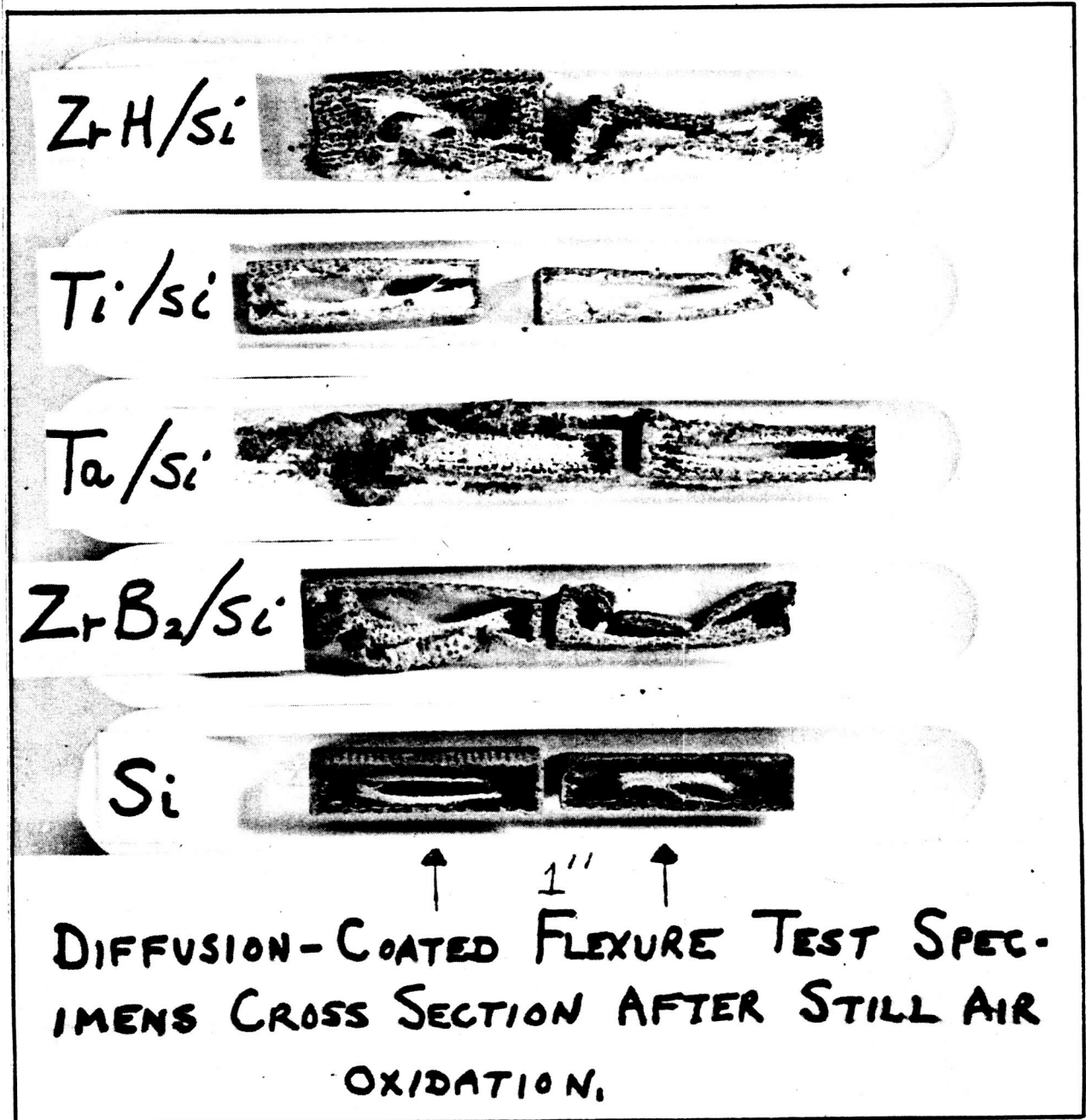


FIGURE 44 PHOTOGRAPH OF SECTIONED FLEXURE BARS AFTER CARBON BURNOUT AT 1500°F

Powder techniques were used in subsequent analyses to better determine the chemistry and assist in developing the coating systems. The present data indicates that the silicon metal at temperatures to 3,400°F is not a suitable carrier for the other metals or compounds for deep diffusion. It would appear that the small amount of the compounds found on the specimens is a result of high temperature solid-state reaction or physical bonding of the compound by the silicon carbide formed on the surface of the specimens.

4.2.5 Modified and Final Diffusion Systems

Two oxidation inhibitor systems were selected from the preliminary diffusion coating experiments results for further development. The primary selection was a siliconized RPP diffusion system which exhibited low surface loss and low mass loss when tested in the plasma arc. The second was the zirconium-boron-silicon diffusion system. This system, although not as uniform nor as well developed as the primary selection did show encouraging results.

A total of 43 development diffusion coating experiments (Tables 4-10 and 4-11) were made to improve performance and determine best processes for shuttle application.

Siliconized System Trials - The siliconized system exhibited several processing problems requiring correction. The primary problem, as noted in Table 4-8, was the difficulty in recovering test table specimens from the diffusion pack. Even though much improved for the preliminary characterization of specimens listed in Table 4-9, the problem persisted. Ease of clean-up of specimens and excessive vaporization during processing were other problems requiring attention.

Processing parameters investigated included slurry compound composition, pack compound composition, processing temperature and time at temperature. Each resultant coating system was reviewed for improvement with step-wise process changes being made when justified. Plasma arc testing was utilized to ascertain that the resultant coating system either improved or retained the preliminary siliconized systems performance of low mass loss and low surface loss.

The alpha form of silicon carbide was expected to have a higher temperature capability in air than the beta form which is obtained during siliconizing at 3400°F and below. It was hoped that the alpha form would show even better performance in the plasma arc than previous siliconized coatings had shown. Two approaches were taken to achieve the alpha phase: (1) siliconize at 3400°F to develop beta silicon carbide and subsequently heat treat to 4000°F to convert to the alpha phase, and (2) siliconize at 4000°F to obtain the alpha form directly. In each case the alpha phase was indeed formed as determined by x-ray diffraction analysis, but plasma arc data showed each system to have lower performance than the beta variety. Accordingly, further development effort of alpha silicon carbide was discontinued.

TABLE 4-10

DIFFUSION COATING EXPERIMENTS
SILICONIZED SYSTEM

Experiment	System	Slurry Compound Composition (Weight Percent)	Pack Compound Composition (Weight Percent)	Furnace Temperature (°F)	Time At Temperature (Hours)	Specimens Coated	Additional Processing
23	SiC	33.3 Si	30 Si	3400	4	1/4" Thick 3/18" Thick	
		33.3 SiC	70 Al ₂ O ₃				
		33.3 Al ₂ O ₃					
M-5	SiC	50 Si	30 Si	3200	4	6-3/4" Disks	Disks preheat treated 3400°F
		50 SiC	70 SiC	3400	1		
M-10	SiC	33.3 Si	30 Si	3400	4	4-1"x5"	Disks preheat treated 3400°F 3 disks post heat treated to 4000°F
		33.3 SiC	70 Al ₂ O ₃				
		33.3 Al ₂ O ₃					
M-12	SiC	33.3 Si	30 Si	3400	4	4-1"x5"	Pre heat treated at 3400°F
		33.3 SiC	70 Al ₂ O ₃				
		33.3 Al ₂ O ₃					
M-18	SiC	33.3 Si	30 Si	3200	4	6-3/4"disks	Pre heat treated 3400°F 4 hrs.
		66.7 SiC	70 SiC	3400	1		
M-19	SiC	33.3 Si	30 Si	3400	4	2-1"x5"	Pre heat treated 3400°F 4 hrs.
		33.3 SiC	70 SiC				
		33.3 Al ₂ O ₃					
M-20	SiC	33.3 Si	30 Si	3400	4	5-3/4"disks	
		33.3 SiC	70 SiC				
		33.3 Al ₂ O ₃					
M-25	SiC	33.3 Si	30 Si	3400	4	2-1"x2" 5-3/4"disks	
		33.3 SiC	70 Al ₂ O ₃				
		33.3 Al ₂ O ₃					

TABLE 4-1Q(Continued)

DIFFUSION COATING EXPERIMENTS
SILICONIZED SYSTEM

Experiment	System	Slurry		Pack		Furnace Temperature (°F)	Time At Temperature (Hours)	Specimens Coated	Additional Processing
		Compound Composition (Weight Percent)	Compound Composition (Weight Percent)	Composition (Weight Percent)	Composition (Weight Percent)				
M-26A	SiC	33.3	30 Si	30 Si	3400	4	5-3/4" disks		
		33.3 SiC	70 SiC	70 SiC					
		33.3 Al ₂ O ₃							
M-26B	SiC	40 Si	30 Si	30 Si	3400	4	5-3/4" disks		
		40 SiC	70 SiC	70 SiC					
		20 Al ₂ O ₃							
M-28	SiC	33.3 Si	30 Si	30 Si	3200	4	10-3/4" disks	5-3/4" disks	
		33.3 SiC	70 Al ₂ O ₃	70 Al ₂ O ₃				post heat treated 4 hrs. @ 4000°F	
		33.3 Al ₂ O ₃						Pre heat treated 4 hrs. - 3400°F	
M-30	SiC	40 Si	30 Si	30 Si	3400	4	*35-3/4"x5"		
		40 SiC	70 SiC	70 SiC			4-3" disks		
		20 Al ₂ O ₃					16-3/4" disks		
M-31	SiC	40 Si	30 Si	30 Si	3400	4	*10-1"x5"	Pre heat treated	
		40 SiC	70 SiC	70 SiC			8-3/4" disks	4 hrs. 3400°F	
		20 Al ₂ O ₃					6-3" disks		
M-40	SiC	40 Si	30 Si	30 Si	3400	4	*3-1"x6"		
		40 SiC	70 SiC	70 SiC			1-1"x5"		
		20 Al ₂ O ₃					4-3/4" disks		
M-36	SiC	40 Si	30 Si	30 Si	3400	4	*2-1 1/2" disks		
		40 SiC	70 SiC	70 SiC					
		20 Al ₂ O ₃							

TABLE 4-11

DIFFUSION COATING EXPERIMENTS
ZIRCONIUM-BORON-SILICON SYSTEM

Experiment	System	Slurry Compound Composition (Weight Percent)	Pack Compound Composition (Weight Percent)	Furnace Temperature (°F)	Time At Temperature (Hours)	Specimens Coated 1/4" Thick *.18" Thick	Additional Processing
M-1	B ₄ C	33.3 B 33.3 SiC 33.3 Al ₂ O ₃	30 B 70 Al ₂ O ₃	2900	4	3 3/4" disks	
M-2	B ₄ C	50 B 50 SiC	30 B 70 SiC	2900	4	3-3/4" disks	
M-3	B ₄ C	50 B 50 SiC	30 B 70 SiC	3400	4	3-3/4" disks	
M-4	B ₄ C	100 B	100 B	3400	4	3-3/4" disks	
M-6	B ₄ C	100 B No slurry on one disk	100 B	3400	4	21-3/4" disk	Overcoated in runs - M-7, M-8, M-13, M-14, M-15, M-16, M-17 & M-21
M-7	ZrB ₂	100 ZrH	30 ZrH 70 Al ₂ O ₃	2800	4	3-3/4" disks	Pre treated in run M-6
M-8	ZrB ₂	100 ZrH	30 ZrH 70 SiC	2800	4	3-3/4" disks	Pre treated in run M-6
M-9	ZrC	100 ZrH	30 ZrH 70 SiC	2800	4	3-3/4" disks	
M-11	B ₄ C	100B	100 B	3400	4	5-3" disks	Over coated in run M-41

TABLE 4-II(Continued)

DIFFUSION COATING EXPERIMENTS
ZIRCONIUM-BORON-SILICON SYSTEM

Experiment	System	Slurry		Furnace Temperature (°F)	Time At Temperature (Hours)	Specimens Coated	Additional Processing
		Composition (Weight Percent)	Compound Composition (Weight Percent)				
M-13	ZrB ₂	100 ZrH	100 Al ₂ O ₃	2800	4	2-3/4" disks	Pre treated M-6
M-14	ZrB ₂	100 ZrH	100 SiC	2800	4	2-3/4" disks	Pre treated M-6
M-15	ZrB ₂	100 ZrH	15 ZrH 85 Al ₂ O ₃	2800	4	2-3/4" disk	Pre treated M-6
M-16	ZrB ₂	100 ZrH	15 ZrH 85 SiC	2800	4	2-3/4" disks	Pre treated in run M-6
M-17	ZrB ₂ SiC	77.6 ZrH 22.4 Si	100 SiC	2800	4	2-3/4" disks	Pre treated in run M-6
M-21	ZrB ₂ SiC	77.6 ZrH 22.4 Si	100 SiC	3400	4	2-3/4" disks	Pre treated in run M-6
M-22	B ₄ C	None	100 B	3400	4	20-3/4" disk	Over coated M-27, M-29, M-32A, M-32B M-33A
M-23	ZrC	None	99 ZrH 1 C	3400	4	5-3/4" disks	Over coated M-35
M-24	B ₄ C	None	100 B	3400	4	11-3/4" disks	Over coated M-32A, M-32B, M-33A, M-33B
M-27	ZrB ₂	97.1 ZrH 2.9 Si	100 SiC	3400	4	5-3/4" disks	Pre treated in run M-22

TABLE 4-11(Continued)

DIFFUSION COATING EXPERIMENTS
ZIRCONIUM-BORON-SILICON SYSTEM

Experiment	System	Slurry Compound Composition (Weight Percent)	Pack Compound Composition (Weight Percent)	Furnace Temperature (°F)	Time At Temperature (Hours)	Specimens Coated 1/4" Thick *.18" Thick	Additional Processing
M-29A	ZrB ₂	97 ZrH 3 Si	100 SiC	3000	4	5-3/4" disks	Pre treated M-22
M-29B	ZrB ₂ SiC	25 ZrH 75 Si	100 SiC	3000	4	5-3/4" disks	Pre treated M-22
M-32A	ZrB ₂ SiC	25 ZrH 75 Si	100 SiC	3000	4	5-3/4" disks	Pre treated M-22, M-24
M-32B	ZrB ₂ SiC	12.5 ZrH 87.5 Si	100 SiC	3000	4	5-3/4" disks	Pre treated M-22, M-24
M-33A	ZrB ₂ SiC	25 ZrH 75 Si	100 SiC	3400	4	3-3/4" disks	Pre treated M-22, M-24
M-33B	ZrB ₂ SiC	12.5 ZrH 87.5 Si	100 SiC	3400	4	3-3/4" disks	Pre treated M-24
M-34	B ₄ C	None	100 B	3400	4	*49- 3/4" disks	Over coated M-38, M-39, M-41
M-35	ZrB ₂	None	100B	3400	4	5-3/4" disks	Pre treated M-23
M-37	ZrC	None	99 ZrH 1 C	3400	4	* 13 - 3/4" disks	Over coated with Boron Pack M-37A
M-37A	ZrB ₂	None	100 B	3400	4	* 13 - 3/4" disks	Pre treated M-37

TABLE 4-11 (Continued)

DIFFUSION COATING EXPERIMENTS
ZIRCONIUM-BORON-SILICON SYSTEM

Experiment	System	Slurry		Pack Compound Composition (Weight Percent)	Furnace Temperature (°F)	Time At Temperature (Hours)	Specimens Coated		Additional Processing
		Compound Composition (Weight Percent)	Weight Percent)				1/4" Thick	*.18" Thick	
M-38	ZrB ₂ SiC	50 ZrH	100 SiC	3000	4		*5 -	Pre treated	M-34
		50 Si					3/4" disks		
M-39	ZrB ₂ SiC	50 ZrH	100 SiC	3400	4		*5 -	Pre treated	M-34
		50 Si					3/4" disks		
M-41	ZrB ₂ SiC	25 ZrH	100 SiC	3400	4		1-3" disk	Pre treated	3" disk M-11
		75 Si					3-3/4" disks	3/4" disks M-34	
M-42	B ₄ C	None	100 B	3400	2 1/2		6 - 3" disks	Over coated	M - 43
							35-3/4"x5"		
							2- 1/2" disks		
							1-1/4"x3"		
M-43	ZrB ₂ SiC	25 ZrH	100 SiC	3000	4		13-3/4" disks	Drg Treated	M-42
		75 Si					3-3"x6"		
							2-1/2"x4"		
							20-1/2"x1/2"		

In an effort to optimize performance in the plasma arc and at the same time improve coatability, several variations in the coating process were examined. Changes in the pack compound composition by replacing the aluminum oxide with silicon carbide greatly improved the ease of removal of specimens. Replacing the aluminum oxide with silicon carbide in the slurry mix, although improving the ease of cleaning the specimens, did not yield a good coating when judged by plasma arc test results. Lowering the percent composition of aluminum oxide in the slurry compound with increases in the percent silicon and silicon carbide improved the cleanup of the specimens without detrimental effect on the coating system.

The final selection of a siliconized diffusion coating system yielded uniform specimens which were easily removed from the pack and cleaned up satisfactorily. Plasma arc results on this coating system showed high temperature oxidation protection better than any other siliconized coating previously tested.

Final Siliconized Diffusion System Process - The siliconized diffusion system was applied after the specimens had been machined to finished dimensions and heat treated for four hours at 3400°F in an argon atmosphere. This heat treatment aided in stabilizing the RPP and removed volatile products retained after pyrolysis. Limited flexure data indicated higher coating strength would be obtained and the coating appeared more uniform. Additional experimentation with heat treating is believed desirable to better optimize coating substrate compatibility. The coating system was applied by a pack cementation process using the inhibitor system compounds in a slurry pack cementation technique.

The slurry was prepared by stirring a uniform blend of slurry compound containing 40% by weight of silicon metal powder, 40% by weight of silicon carbide powder and 20% by weight of aluminum oxide powder in isopropyl alcohol. Sufficient isopropyl alcohol was added to obtain a consistency which when applied to a dry specimen yielded a smooth uniform coating, approximately 1/16-inch thick.

The pack consisted of a graphite retort in which the slurry coated specimens were completely surrounded by pack material. Pack material was a uniform blend of 30% by weight of silicon metal powder and 70% by weight of silicon carbide powder. A cover layer of carbon black was used to isolate the system. The retort graphite lid contained an aperture to permit escape of volatiles.

The packed retort was placed in an air circulating oven at 300°F and held overnight to drive out moisture and residual isopropyl alcohol. Final processing of the pack was conducted in a high temperature diffusion furnace.

The retort, still hot from the drying operation, was placed in the diffusion furnace, where the system was evacuated and back filled with argon three times to a final pressure of 3 - 5 psig. A 3 - 5 SCFH flow of argon was maintained while the temperature of the retort was raised to 3400^oF, as measured by an optical pyrometer, and held at temperature for four hours.

Upon removal from the pack, the specimens were brushed and scraped to remove adhering pack and slurry residues.

Zirconium-Boron-Silicon System Trials - The zirconium-boron-silicon system selected for further development had shown encouraging test results during the screening phase and was thought to have the potential for superior performance. One of the primary problems had been insufficient coating penetration depth into the carbon-carbon substrate. It appeared that neither zirconium nor zirconium diboride were being diffused or carried in by the other reactants, but were being held on the surface by the silicon carbide formed during processing.

To obtain deeper penetration into the substrate the best approach appeared to be the insitu formation of zirconium diboride, even though two processing cycles would be required. Two approaches were investigated; one in which the zirconium in the form of zirconium hydride was reacted first, followed by reaction with boron, and the other in which the opposite order was tried, boron reacted with the substrate first, followed by the zirconium reaction. These experiments are included in Table 4-11.

The reaction of the zirconium hydride with the substrate did not provide satisfactory penetration although zirconium carbide was formed. The silicon, used to assist as a carrier, did not improve penetration significantly. These primary diffusion coatings were overcoated with boron as a reactant and although powder x-ray diffraction showed the presence of zirconium diboride, zirconium carbide, silicon carbide and boron carbide, the coating was unsatisfactory when plasma arc tested.

The opposite method in which the boron was reacted with the substrate first gave better results. X-ray diffraction analysis found both silicon carbide and boron carbide (silicon from impurities in the boron) in the initial coating. The penetration depth desired was obtained by varying the compositions of the slurry and pack compounds, and the process heating cycle. The primary coating system was then overcoated with zirconium and silicon.

Problems of obtaining specimens suitable for testing were encountered. X-ray diffraction powder camera analysis confirmed the presence of the desired zirconium diboride along with zirconium carbide, boron carbide and silicon carbide. Again the process parameters were varied to obtain a process which yielded specimens suitable for testing and also gave satisfactory plasma arc test results.

The zirconium-boron-silicon system, produced to meet the requirements, is appropriately called a zirconium diboride-silicon carbide system and is so noted in Table 4-11 (ZrB_2-SiC). The developed process, although producing specimens suitable for testing, requires additional development experiments for more uniform penetration depths and better repeatability.

Final Zirconium-Boron-Silicon Diffusion System Process - The zirconium-boron-silicon diffusion system was applied after the specimens had been machined to finished dimensions. The system was applied by a two-cycle method consisting of a boron carbide system over coated to form the zirconium diboride-silicon carbide system.

The boron carbide coating was applied by the pack cementation process in the same manner as discussed for the siliconized system, except that the pack material was boron metal powder and no slurry coating was employed. Coating temperature was $3400^{\circ}F$, but hold time at temperature was limited to 2-1/2 hours, rather than the customary four hour cycle, in an effort to limit depth of diffusion. The time reduction proved ineffective because coating depth varied greatly, penetrating deeply in some areas and shallow in others. Another method of reducing coating depth by dilution of the pack with boron carbide was subsequently tried and proved feasible. This could be incorporated into additional coating improvements in Phase II.

The zirconium-silicon coating was overlaid by the slurry-pack cementation process described previously. Slurry composition consisted of 75% by weight of silicon metal powder and 25% by weight of zirconium metal powder. Pack material was silicon carbide powder, and coating was conducted at $3000^{\circ}F$ with a four hour hold at temperature.

4.2.6 Overlay Systems

Overlay systems, comprised basically of thin metal oxide layers, were applied over diffusion coated RPP, (1) to increase the operational temperature of the composite; (2) to limit the oxygen available to the diffused coating; (3) to develop a method which would lend itself to local hot spot application and possibly mission refurbishment, and (4) as an alternate approach to the protection of bare RPP.

Plasma spray, refractory bonding, and melt impregnation were the three techniques explored in the overlay concept. Siliconized and Zr-B-Si coated RPP were considered the prime candidates for overlay coatings. Trial applications of the first two approaches were limited to siliconized RPP on the basis that this coating was further developed at the time of investigation. Promising overlay systems would ultimately be evaluated with the Zr-B-Si diffusion coating. Melt impregnation was examined on bare RPP, as well as boronized, siliconized, and Zr-B-Si diffusion coated RPP.

Plasma spray of the hafnia refractory oxide appeared to have the potential for raising operating surface temperature of the siliconized system by 200-300°F with additional development but refractory bonding proved unsatisfactory. Melt impregnation of a hafnium-tantalum coating was the most impressive system evaluated in terms of achieving multi-mission performance at 4000°F surface temperature. Continued evaluation of this system is strongly recommended for 4000°F applications.

Evaluations of the three application techniques are discussed below. Specific plasma arc data on each coating system tested and a discussion of results is provided in section 5.2.

Plasma Spray Technique - Plasma spray applications were performed at Georgia Tech under the direction of Mr. J. Walton and Mr. A. Sales. One set of five siliconized RPP specimens (Set 1), 3/4 inch diameter, were plasma sprayed with a powder mixture consisting of 80% alumina and 20% chromia. The alumina was chosen to provide high temperature (3700°F) capability and because of its close matched thermal expansion characteristics with RPP. The addition of chromia served to increase surface emittance. A second set of siliconized RPP specimens (Set 2) were also coated with alumina and chromia. However, this system differed from the first set in that the alumina was applied as a single layer with an overspray of chromia. This method concentrated the chromia at the surface where emittance properties are critical.

A third plasma sprayed system (Set 3) over siliconized RPP included hafnia, which has the temperature capability to meet a 4000°F requirement. Although hafnia undergoes a phase change within the temperature range between room temperature and 4000°F which effects thermal expansion characteristics, hafnia is still more compatible with RPP than unstabilized zirconia which passes through two crystalline phase changes within these temperature limits. A metal powder mixture of 2% silicon and 15% tungsten was added to the hafnia powder prior to spraying to act as a binder and to enhance thermal shock resistance of the hafnia.

The three plasma sprayed overlay coating systems were evaluated by plasma arc test. The Al_2O_3/Cr_2O_3 specimen reached a surface temperature of 3700°F at a cold wall heat flux of 105 BTU/ft² sec. Post examination of the specimen revealed melting and flaking off of the coating at the flame spray to silicon carbide interface. A red color had also formed in the alumina coating. Post examination of the Al_2O_3 coating with Cr_2O_3 overspray appeared about the same as that with the Cr_2O_3 added to the Al_2O_3 . However, at 100 BTU/ft² sec cold wall heat flux a surface temperature of only 3350°F was measured. Because of the melting problem of the alumina coating, no additional work with this system was attempted.

Specimens which had been sprayed with hafnia/tungsten silicon metal reached a surface temperature of 3510°F at 105 BTU/ft² and 3830°F at 160

BTU/ft² sec cold wall heat flux. Neither specimen melted, but a large area of the coating flaked off at the hafnia to silicon carbide interface. The portion remaining after cooldown appeared to have good adherence. The results of these first trial hafnia specimens were encouraging although better overall adhesion of the coating would be required.

Mr. A. Sales of Georgia Tech. suggested treatment of the silicon carbide coated substrate with ethyl silicate to enhance adhesion of the hafnia. Two additional sets of specimens were plasma sprayed at Georgia Tech. using this approach. One system, Set 6, included the previous hafnia/tungsten/silicon coating and the other, Set 7, was hafnia alone. Both types of hafnia coated specimens were tested in the plasma arc at a cold wall heat flux of 140 BTU/ft² sec. where surface temperature of both specimens reached 3640°F. The specimen with the tungsten/silicon overlay developed one large blister having a bluish cast. It is believed that this condition was a result of the formation of tungsten silicate. The adherence in the remaining portion of the sample appeared to be satisfactory. Blistering also occurred on the specimen having only hafnia as the overspray material. Microscopic examination revealed a clear glassy melt between the hafnia and the silicon carbide indicating an excess of silica. Areas which had not blistered had good adhesion. Continued modification and evaluation of these coatings could prove fruitful. However, schedule and budget constraints, coupled with the more promising hafnium/tantalum system precluded further exploration of these systems.

Dr. E. Rudy of the Oregon Graduate Center defined a coating system based on chemical compatibility of all constituents. This coating system requires a surface layer of zirconium diboride in the RPP substrate and a metallic diffusion barrier overcoated with a refractory oxide of zirconia or hafnia. Although the recommended system requires the zirconium diboride to be reacted or diffused in-depth into the RPP it was considered worthwhile to use plasma spray application for early compatibility evaluation.

Specimens of bare RPP were sent to Georgia Tech. for plasma spray applications of the proposed coating system. One group of specimens used an overspray of zirconia rich zircon. The zircon, because of the silica present, was added to the zirconia to increase particle adhesion. This system was tested in the plasma arc at 90 BTU/ft² sec. for 300 seconds. The surface temperature reached 3610°F; however, the coating flaked off in many small pieces.

A second group was oversprayed with hafnia. This system was tested in the plasma arc at 140 BTU/ft² sec. for 300 seconds reaching a surface temperature of 3890°F. The bare RPP appeared to have oxidized around the edge of the specimen at the coating to RPP interface. After the test the coating separated at the RPP interface but the multi-layer coating remained flat and intact and appeared to have considerable strength. The results of this

test were encouraging, recognizing that the applications of the zirconium diboride layer by plasma spray techniques would not give the desired penetration into the RPP as recommended by Dr. Rudy. Final results of this coating system will be documented by an inhouse IR and D summary report.

Refractory Bonding - Processing trials were made to bond Union Carbide's ZYW-30 zirconia woven cloth over siliconized RPP as an overlay system. Previous trials using Aremco's Ultra-Temp 516 cement were unsuccessful because of melting which occurred below 3000°F. Additional bonding trials were made using Union Carbide's ZY-2 yttria stabilized zirconia cement and their recommended cure cycle. This included a room temperature air dry, "B" staging at 240 to 300°F for 3 to 4 hours and final cure at 100°F for one hour. Initial trials were made by applying the ZY-2 cement to the zirconia cloth and to the silicon carbide coated specimen. The saturated cloth was then placed on the coated specimen and the excess cement removed with a rubber roller. In all cases, using this application method, "mud" cracking appeared before or during the 240-300°F "B" staging operation. The cloth would also curl or lift from the silicon carbide coated RPP specimens, exhibiting little or no adhesion.

Additional trials were made in a platen press at 50 psi and heated through the "B" stage portion. This application method gave sufficient adhesion to complete the 100°F cure. A specimen with the zirconia cloth overlay was tested in the plasma arc at 160 BTU/ft² sec. cold wall heat flux for 300 seconds with the specimen reaching a surface temperature of 3640°F. No melting of the cloth was observed but at the completion of the test the cloth overlay separated completely from the siliconized carbide RPP specimen. Moreover, chemical attack of the silicon carbide was observed and this approach was discontinued.

Hafnium/Tantalum Coating Melt Systems - Dr. Schwemer of the LTV Research Center had proposed a refractory metallic coating for high density graphite, based on an eutectic mix of hafnium and tantalum. Early work showed that a low melting eutectic was formed at an atomic weight ratio of 80% hafnium and 20% tantalum. This eutectic is confirmed by Rudy (Ref. 37) to have a melting point of 2130°C. The wetting of high density graphite was reported to have been excellent. It was felt that this type of coating would perform quite well on either bare RPP or diffusion coated RPP in an oxidizing atmosphere. The hafnia metal would convert to the hafnia oxide and remain as an oxygen barrier with a melting point above 4000°F.

Specimens were made by melt impregnating a pressure formed wafer of 80% hafnium 20% tantalum atomic weight percent into bare RPP-O. Good wetting and depth of penetration of the metal mix was achieved. One of the specimens, tested in the plasma arc at a cold wall heat flux of 140 BTU/ft² sec. for 300 seconds, reached a surface temperature of 3700°F and formed a strong white oxide layer, which had very good adhesion. An additional

300 seconds exposure to the same conditions produced the same results and a good adhering oxide layer remained. The same specimen, when exposed to a third 300 seconds test at 140 BTU/ft² sec. reached a surface temperature of 4130°F, some 400°F higher than the previous tests. Two additional 300 second tests performed at the same test conditions produced a consistent surface temperature of 4180°F. One additional test was performed on this same specimen at 100 BTU/ft² sec. for 300 seconds in which the surface temperature reached 3780°F. The white oxide layer remained intact, strong, and tightly adherent throughout the entire 30 minutes test exposure.

The results of the repeated exposure of the above specimen to plasma arc tests were extremely encouraging. Examination of the cross-sectioned specimen revealed a coating thickness on the exposed side of approximately 0.030 inches. No subsurface oxidation was observed and penetration of the coating into the RPP was apparent. Though success was achieved with RPP-O, several questions were posed. Would the coating provide suitable protection for the substrate at low temperature but higher pressure conditions? Can the coating be applied to the higher strength RPP-3? Will a diffusion coated substrate (siliconized, boronized, or Zr-B-Si coated) offer greater potential for the Hf-Ta overlay? Fabrication trials, using pressed wafers, dry powder, and slurry techniques, sought answers to these questions. Fabrication successes were evaluated by repeated plasma arc exposure. These trials are discussed in the following paragraphs.

Melt impregnation of the hafnium-tantalum eutectic was made in RPP-O with the metal powder being applied as a slurry mix. The purpose of the slurry was to control depth of penetration and coating uniformity. This specimen was tested in the plasma arc at 140 BTU/ft² sec. for 300 seconds, reaching a surface temperature of 3650°F, which was comparable to the previous specimens tested. An additional 300 seconds exposure at the same test conditions again reached a surface temperature of 3650°F. Cross-sectioning of the specimen revealed a discontinuous coating only 0.005 inches thick and subsurface oxidation. Obviously, a thicker coating is required for RPP protection but perhaps less than the 0.030 inch thick coating on the initial specimen.

Limited melt impregnation experimentation with RPP-3 using thin wafers failed to produce the deep wetting and flow achieved with RPP-O. However, continued examination of RPP-3 with slurry application techniques is recommended.

Hafnium-tantalum applied over boronized RPP, using melts from pressed wafers, showed good surface wetting and good adhesion. However, fracture occurred in the boron diffusion layer due to shrinkage of the hafnium-tantalum, and this approach was abandoned. A similar specimen treated with a light slurry coat, produced a bright, very uniform metallic coating after melt. This specimen was tested in the plasma arc for 300 seconds at

a heat flux of 130 BTU/ft² sec. The surface temperature reached 3700°F; however, the fragile white oxide film failed at the hafnia to boron interface.

The hafnia-tantalum eutectic was also applied to siliconized RPP. After unsuccessful trials with pressed wafers, dry powder mixtures, and heavy slurry applications, a satisfactory coating was formed by three applications and heat melts of thin slurries. This specimen was tested in the plasma arc for 300 seconds at a cold wall heat flux of 130 BTU/ft² sec. The maximum surface temperature reached was only 3000°F, suggesting low-catalytic influence from the silicon coating, although a strong white oxide coating was formed. Additional exposure to the same heating conditions again produced 3050°F surface temperature with hot spots up to 3140°F, but after testing, a small portion of the oxide layer flaked off during handling. Further evaluation was terminated.

The Zr-B-Si coated system was also evaluated with three applications of the thin slurry mix. This specimen was tested at 130 BTU/ft² sec, and surface temperature of 3320°F. However, part of the oxide layer fell off after 180 seconds of testing.

In summary, the hafnium-tantalum wets and flows on and into RPP-O very readily, but in limited examination of bare and coated RPP-3 it was found that deep wetting and flow are restricted. In addition, coating adherence after plasma arc exposure has been a problem. Slurry mix has proven to be a successful application technique but multiple layers are required to build the coating thickness to an acceptable value. A thick coating has protected RPP-O well, while thin (0.005 in.) layers are unsuccessful. Additional experimentation with this coating is recommended in view of the superlative performance in plasma arc testing. Effort should be concentrated on evaluation of RPP-O, RPP-1, RPP-2, and RPP-3, the objective being to obtain the best compromise between substrate strength and coating oxidation resistance performance.

Additional efforts to integrate the hafnium-tantalum coating with a sub-surface oxidation inhibitor may still prove rewarding, although current trials using diffusion coated substrates failed to produce the desired results.

4.3 CONCLUSIONS

(1) Both the siliconized RPP and the Zr-B-Si diffusion coated RPP can be fabricated with a very low specimen rejection rate and offer the best performance of all diffusion systems tested.

(2) A desired 0.015-0.020 inch coating depth can be achieved with both of the diffusion coating systems.

(3) The add-mix and combined process techniques for achieving oxidation resistance for RPP indicate much less promising approaches compared to diffusion coating.

(4) The hafnium tantalum coating can be readily applied to as-pyrolyzed RPP and offers outstanding protection to 4000°F. However, little success has been realized with this system on diffusion coated or bare RPP after densification.

(5) Though processing through diffusion coating has not been completed on all substrates, WCA graphite laminates remain the best of those evaluated. It possesses satisfactory strength and is reasonably compatible with VMSC diffusion coatings.

5.0 MATERIALS TEST EVALUATION

Flexure strength, furnace oxidation resistance, and plasma arc erosion/oxidation resistance were the prime test tools used in the evaluation of candidate materials coating systems. The evaluation was performed in two stages. First, a screening program was conducted to select best systems from the several material constituents and techniques of introducing the oxidation inhibitors into the substrates. The two selected systems were then modified to improve performance. This section of the report describes the testing and results of the screening program, and then covers the testing of the modified systems leading to the final coated RPP formulations. Characterization data on the selected systems is presented and special attention is given to a discussion of low catalytic effects of the VMSC coatings.

5.1 CANDIDATE INHIBITOR SYSTEMS SCREENING

There were some fifteen different material coating systems fabricated as part of the initial group of candidate oxidation inhibited RPP systems. Three major screening tests were conducted to evaluate these systems and select the two best for further development:

- (1) Flexure testing obtained the potential strength capacity of each system to determine weight competitiveness of the composite. Low strengths suggest both high weight and possibly low reliability.
- (2) Furnace testing exposed specimens to temperatures below 2300°F to uncover potential low temperature weakness in the high temperature coatings, such as the "silicon pest problem".
- (3) Plasma arc testing evaluated the oxidation and spallation resistance of candidate systems under heating rates and pressure conditions simulating the shuttle maximum heating environment. Systems with good potential were given multicycle exposure to the environment.

5.1.1 Flexure Screening Tests

Room temperature flexure screening tests were conducted on coated RPP systems to determine the influence of the coating on RPP properties. Previous data on bare WCA graphite cloth laminates indicated a nominal flexure strength of 16,000 psi and interlaminar shear stress of

3250 psi achievable after three re-impregnations and pyrolysis cycles. These values provided a baseline for comparison with coated material.

Room temperature testing of RPP materials was deemed reasonable for screening because maximum airload conditions occur at low temperature. In addition, graphitic materials increase in strength at higher temperature, although stiffness may tend to decrease. On final selected systems flexure and stiffness data were obtained throughout the temperature range of -250°F through 3000°F as part of the characterization test program. Precondition cycling of test bars at elevated temperatures in an oxidizing atmosphere was also part of these tests and is discussed in section 5.4.

The screening test program employed 1.0 inch x 5.0 inch x 0.25 inch (nominal) test bars under four-point loading. Loaded span was 4.2 inches with 1.7 inches between applied loads, and loading rate was 0.05 inches/minute. The four-point loading provides a more realistic failing stress for low elongation materials than a three-point loading because it places a greater volume of material under maximum stress and therefore increases the probability of obtaining a reliable failing stress level.

The add-mix systems proved to have weak interlaminar strength as recorded in Table 5-1. The highest failing stress level for this class of material was attained by a Fiberite ZrB₂-Silicon panel, believed to be compression molded. All other systems were autoclave bonded at 80 psi. Modulus of elasticity values were also very low. All specimens failed by interlaminar shear but a titanium/silicon system also experienced a tensile failure. The poor strength performance of the add-mix systems was a major factor in discarding them from future development.

None of the combined process system specimens were suitable for testing and therefore no data was obtained.

Test results on the diffusion coating systems provided in Table 5-2 were encouraging from two standpoints: first, failing strength reached a maximum of 21,100 psi on a zirconium-silicon system; and two, the failure of all specimens was gradual, as opposed to a completely brittle fracture where both halves of the specimen completely separate. The type failure obtained may be termed "quasi-plastic", and for redundant structure permits some degree of load redistribution. Chances for mission completion are, therefore, enhanced even if failure were initiated. This behavior is similar to that afforded by metal structures.

Typical load deflection curves obtained during test are shown in Figure 5-1 to illustrate the type of failure obtained. Note also that there

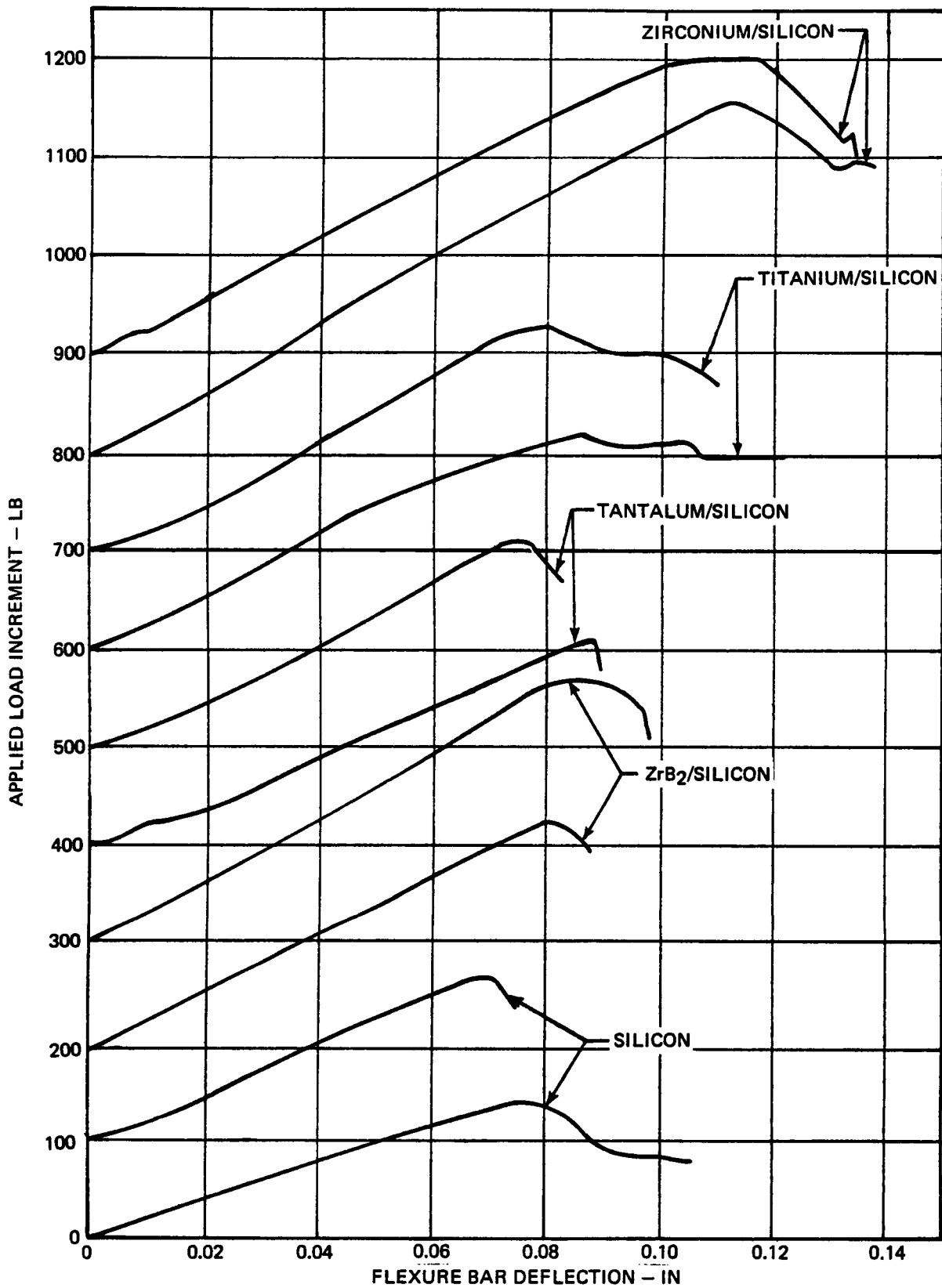


FIGURE 5-1 LOAD-DEFLECTION CURVES DIFFUSION COATED FLEXURE BARS

TABLE 5-1
ADD-MIXTURE SYSTEM FLEXURE DATA

Coating System	Specimen		Failure Condition			
	Width In.	Thickness In.	Total Load, Lb.	Max Deflection 10^{-3} In.	Max Stress PSI	Elastic Modulus, 10^6 PSI
Fibrite	1.006	0.251	79	71.5	4700	1.02
	1.004	0.253	81	68.9	4750	1.06
ZrB ₂ - Silicon System No. 5	1.005	0.272	53	35.1	2690	1.10
	1.004	0.251	49	33.8	2920	1.34
ZrB ₂ - Silicon System No. 7	1.003	0.248	22	29.9	1330	0.70
Zirconium-Silicon	1.019	0.300	111	46.8	4530	1.26
	1.021	0.310	104	52.0	3980	0.96
Titanium-Silicon	1.013	0.392	111	45.5	2700	0.59
	1.013	0.362	108	53.3	3070	0.62

TABLE 5-2
DIFFUSED COATING SYSTEM FLEXURE DATA

Coating System	Specimen		Failure Condition				
	Width In.	Thickness In.	Total Load, Lb.	Max Deflection 10^{-3} In.	Max Stress PSI	Elastic Modulus, 10^6 PSI	
Silicon	1.017	0.248	140	70.2	8400	1.88	
	1.016	0.251	167	65.0	9780	2.33	
ZrB ₂ - Silicon	1.030	0.249	233	83.2	13700	2.57	
	1.026	0.251	274	81.9	15800	2.99	
Tantalum - Silicon	1.009	0.248	210	88.4	12700	2.25	
	1.020	0.245	208	75.4	12800	2.69	
Titanium - Silicon	1.018	0.245	217	86.5	13300	2.44	
	1.020	0.245	228	81.9	14000	2.71	
Zirconium - Silicon	1.018	0.251	360	113.1	21100	2.89	
	1.019	0.243	304	118.3	19000	3.02	

is no obvious indication, such as slope change, that coating failure preceded general failure.

Coating depth on the 0.25 inch thick laminates was of the order of 0.020 inch per face. This was initially believed to be too shallow, based on the optimization analyses of section 3.4, but the low erosion rate obtained in plasma arc testing and the relatively low strength obtained on the siliconized RPP suggest that a shallower coating might prove to be the best approach. This has not been examined experimentally since prime effort has been devoted to obtaining oxidation resistance and no effort has been expended on flexure strength enhancement. This should be done in Phase II.

A point of concern was the relatively low strengths obtained with the silicon coated RPP. While the strength obtained was in the range of previous data (i. e., 10,300 psi on material coated completely through the thickness), 8400 psi is about half of that anticipated for this less brittle system. The reason for the low strength is not clear, but it is believed that the strength should and can be raised by better mechanical match between coating and substrate. As noted above this has not been examined except by substitution of VCA carbon cloth in place of the WCA graphite cloth to vary the coefficient of thermal expansion. This proved unsuccessful.

On each of the coated specimens the average modulus of elasticity was relatively low, compared to that expected. This is satisfactory in that it tends to relieve thermal stresses, which are directly proportional to modulus of elasticity. The separate stiffness contribution of the coated material to the overall flexural stiffness can be ascertained if it is assumed that the elastic modulus of the bare material is known. Assuming that $E_{\text{BARE}} = 1.8 \times 10^6$ psi, it can be computed, for example, that the elastic modulus for the stiffest zirconium/silicon system is 4.4×10^6 psi. This is reasonably low, especially with the high flexure allowable obtained for that coating so that thermal stresses with the proposed design concepts should pose no problem.

5.1.2 Furnace Screening Tests

It is well known that material coating systems resistant to oxidation at high temperatures may not provide the necessary protection at lower temperatures. The silicide "pest" problem is a notable example. Therefore, each coating system was tested for its low temperature performance. The 2300°F temperature achieved was felt to be above that at which the coatings protective mechanism would be expected to take effect.

The test employed was only a screening test, conducted in still air, in which 3 in. diameter x 0.25 inch thick discs were introduced into an oven preheated to 2300°F. The specimens were held in the furnace for 15 minutes, sufficient to reach equilibrium, then withdrawn and allowed to air cool. This constituted one cycle, and effectively subjected the specimens to an incremental time period at each temperature level through the maximum achieved. Heat up and cool down rates were a function of individual specimen properties. However, the cycle time and one-atmosphere pressure conditions were probably conservative relative to the low pressure flight environment, even though the test was conducted in still air.

The weight changes experienced by the add-mix and RPP control specimens are listed in Table 5-3. The surface appearance of the post-test specimens is shown in Figure 5-2. Visual examination of the specimens revealed the following conditions: ZrB₂/Si specimens 5 and 5A were partially coated on the surface with a white, loosely adhering powder, ZrB₂/Si specimen 7 was heavily coated with a loosely adhering white powder; ZrH/Si specimen 8 was coated with a soft brown to grey loosely adhering powder; Ti/Si specimen 10 was covered with a hard brown to white coating which easily flaked from the surface.

Weight changes determined after exposure of the diffusion coated specimens to the 2300°F furnace test are provided in Table 5-4. A photograph of the 3 in. diameter discs following test exposure is given in Figure 5-3. As can be seen only the siliconized coating appears uniform and without visible change. Visual examination of the other systems indicated that the coatings were thin and not well adhering. Coating breakthrough and subsurface oxidation prevailed on all but the siliconized RPP. While powder formations were apparent as noted for the add-mix specimens, it was clear that the zirconium constituent coatings needed better oxidation inhibition, either in the form of greater silicon carbide makeup or in the use of a boron constituent.

TABLE 5-3

WEIGHT CHANGE EXPERIENCED BY ADD-MIX
SPECIMENS AS A RESULT OF 2300°F OXIDATION TEST

Specimen	Weight, gms		Weight Change, %
	Before	After	
ZrB ₂ /Si (5)	47.25	46.41	- 1.78
ZrB ₂ /Si (5A) Fibrite	41.91	41.42	- 1.17

TABLE 5-3 (Continued)

WEIGHT CHANGE EXPERIENCED BY ADD-MIX
SPECIMENS AS A RESULT OF 2300°F OXIDATION TEST

Specimen	Weight, gms		Weight Change, %
	Before	After	
ZrB ₂ /Si (7)	76.26	76.88	+ 0.81
ZrH /Si (8)	51.75	50.73	- 1.97
Ti/Si (10)	66.45	67.92	+ 2.16
RPP 3 Bare Control	36.99	32.78	-11.40

TABLE 5-4

WEIGHT CHANGE EXPERIENCED BY DIFFUSION COATED
SPECIMENS AS A RESULT OF 2300°F OXIDATION TEST

Specimen	Weight, gms		Weight Change, %
	Before	After	
RPP-3 Bare Control	36.99	32.78	-11.4
18-13 Si	44.82	44.24	- 1.3 (1st cycle) - 2.1 (2nd cycle)
19-13 ZrB ₂ /Si	34.97	34.02	- 2.7
20-13 Ta/Si	43.78	42.12	- 3.9
21-13 Ti/Si	45.94	45.88	- 0.1
22-13 ZrH/Si	45.84	41.16	-10.2

5.1.3 Plasma Arc Screening Tests

To support the selection of promising material systems for further development 35 tests were performed on 12 materials systems in the MSD 180 KW plasma arc facility with a 1.5 inch exit diameter, Mach 3 nozzle. The purpose of these tests was to evaluate resistance of the materials to oxidation and other erosion mechanisms under simulated earth atmospheric entry environmental conditions representative of the space shuttle leading edge.

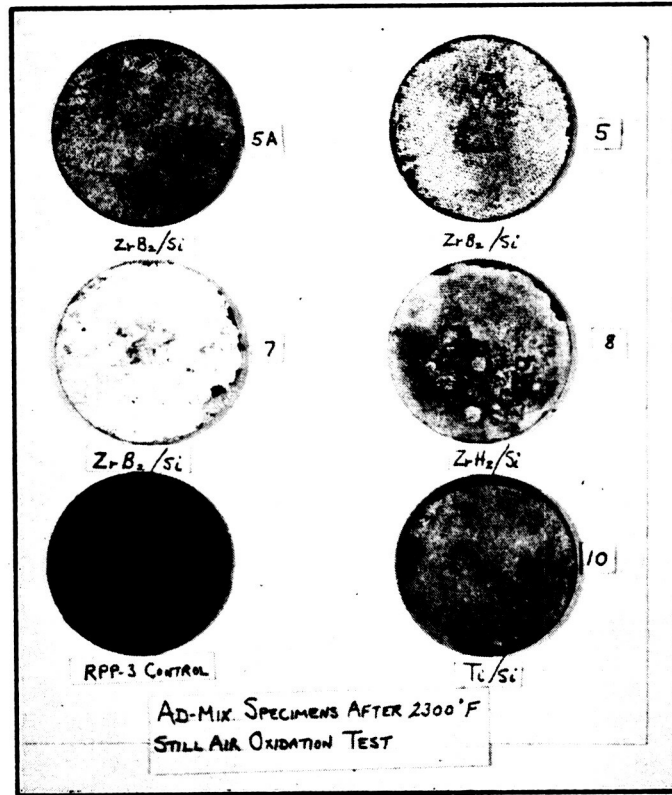


FIGURE 5-2 SURFACE APPEARANCE OF ADD-MIX SPECIMENS AFTER 2300°F STILL AIR OXIDATION TEST

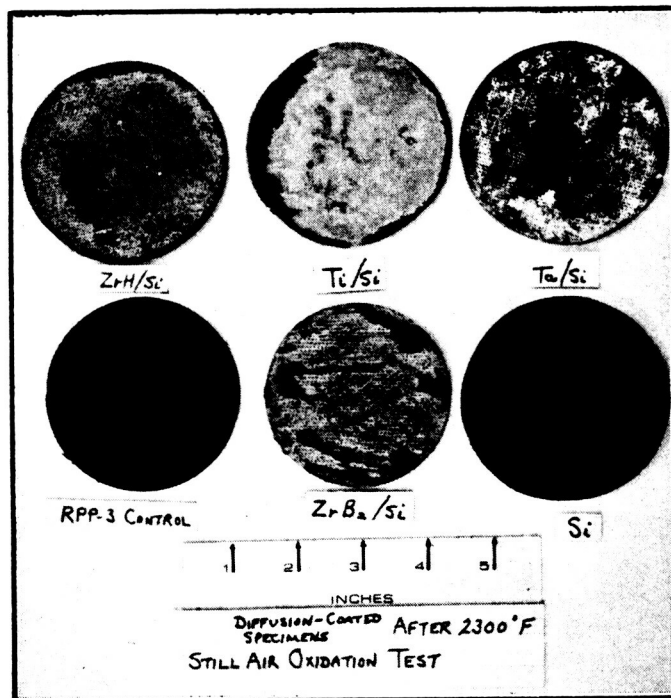


FIGURE 5-3 SURFACE APPEARANCE OF DIFFUSION COATED SPECIMENS AFTER 2300°F STILL AIR OXIDATION TEST

Three cold wall heat flux rates were included in the test series, 100, 160 and 200 BTU/ft² sec, corresponding to radiation equilibrium temperatures* of 3400, 3900 and 4100°F for a surface emittance of 0.80. Actual specimen temperatures were generally lower than radiation equilibrium values, as will be discussed later. All specimens were exposed to the intermediate heating level, and those specimens which demonstrated acceptable performance were evaluated at the lower and higher heating rates. Bare RPP control specimens were evaluated at each heating rate to provide a basis for material performance evaluation. Specimen exposure time was 300 seconds.

The criteria established for determining acceptable performance were as follows:

- o Erosion rate and/or weight loss must be less 0.10 that of the bare control specimen.
- o Specimen must not crack nor experience other mechanical failure.

Subsequent testing in the plasma arc, after making modifications to the plasma arc head, tended to indicate that the screening test heat fluxes were overstated by as much as 30 BTU/ft²/sec at the recorded 160 BTU/ft² sec flux level and 50 BTU/ft²/sec at the recorded 200 BTU/ft²sec flux level. Data at the 100 BTU/ft²sec level appears correct. While this apparent error affects the absolute magnitude of performance, it has no effect upon relative performance between coating systems or bare RPP. Heat flux and performance data on the selected coating systems reported in section 5.2.3 is believed to be correct for the 180 KW plasma arc facility.

On the basis of results of these tests, two material systems were selected for further development, siliconized RPP and zirconium-boron-silicon, both using diffusion processing. These systems were chosen on the basis of meeting or exceeding the above criteria under test conditions where the surface temperature of bare RPP exceeded 3500°F.

Test specimens were 0.75 inch diameter by a nominal 0.25 inch thick and mounted on a stagnation heating specimen holder with a 1.5 inch diameter graphite shroud. The shroud, together with 0.25 inch thick graphite felt insulation behind the specimens, were included to minimize specimen heat losses.

Heating rates were measured with a 0.75 inch diameter, flat face, water cooled calorimeter with a shroud to match the shrouded specimen configuration. Heat flux was measured immediately before and after each specimen exposure. The calorimeter reading q_c was corrected to reflect specimen surface temperature using the following relation.

* Equilibrium temperatures reflect hot wall effects

$$\dot{q}_{\text{HOT}} = \dot{q}_c \frac{i_s - i_w}{i_s - i_c} \quad (1)$$

Where

$$\begin{aligned} \dot{q}_{\text{HOT}} &= \text{hot wall heat flux rate, BTU/FT}^2 \text{ SEC} \\ i_s &= \text{stagnation enthalpy, BTU/LB} \\ i_w &= \text{air enthalpy at specimen temperature and stagnation pressure} \\ i_c &= \text{air enthalpy at calorimeter temperature} \end{aligned}$$

Stagnation enthalpy was determined by the energy balance method and stagnation pressure was determined by prior calibration with a pressure probe. Surface temperature of each specimen was measured with an optical pyrometer and corrected for window absorption and emittance effects. Specimen emittance was estimated from literature data for emittance of material constituents.

Measurements were made of specimen thickness and weight before and after exposure to determine surface recession rates and mass loss.

Method of Data Analysis - Prior evaluations of bare RPP in air plasma arc tests (References 20 - 24) indicated that oxidation was the primary cause of surface recession in the temperature range of interest for the space shuttle leading edge (2300°F - 4300°F). The current program is directed toward providing protection against such oxidation. A brief review of oxidation theory is given below to provide a background for the method used to analyze test results.

Oxidation occurs in three temperature regimes, depending upon the mechanisms controlling mass loss. In the reaction controlled regime at low temperatures the air at the surface is oxygen rich, and oxidation is controlled by surface chemical kinetics. In the transition regime at intermediate temperatures the rate of oxidation is sufficiently high to reduce the concentration of oxygen near the surface. In the diffusion controlled regime at high temperatures the oxidation rate is controlled by the available supply of oxygen diffusing through the boundary layer to the surface.

Theoretical results in Reference 25 show that in the diffusion control regime, the mass loss of carbonaceous materials in air is given by:

$$\dot{M}_D = \frac{C_{\text{oxe}} L_{\text{EFF}} \dot{q}_{\text{BLOW}}}{R_{\text{ox}} \Delta i} \quad (2)$$

- Where:
- \dot{M}_D = mass loss rate of carbon per unit area in diffusion regime, lb/ft² sec.
 - q_{BLOW} = convective heat flux rate corrected for blowing effects, BTU/ft² sec.
 - q_{HOT} = convective heat flux rate without blowing effects, BTU/ft² sec.
 - K = blowing coefficient = 0.67 for stagnation flow
 - Δi = enthalpy difference across boundary layer, BTU/lb
 - C_{oxe} = free stream mass concentration of oxygen in air = 0.23
 - R_{ox} = mass ratio of oxygen to carbon entering the reaction = 1.333 R_c , assuming CO is the only product of the reaction.
 - R_C = proportion of carbon in the total material
 - L_{EFF} = effective Lewis number, assumed equal to unity

Equation (1) can therefore be re-written:

$$\frac{\dot{S}_D}{h_{EFF}} = \frac{0.172}{\rho R_c} \quad (3)$$

Where:

- \dot{S}_D = surface linear recession rate, ft/sec
- h_{EFF} = surface heat transfer coefficient
- ρ = density of material, lb/ft³

Equation (3) suggests the use of S/h_{EFF} as a parameter for correlating plasma arc test recession data. If S/h_{EFF} is independent of surface temperature and equal to the value given by equation (3) the data falls in the diffusion regime. If S/h_{EFF} is temperature dependent and less than the value from equation (3), the data falls in the reaction or transition regime. If values of S/h_{EFF} for oxidation inhibited materials fall below those for bare RPP, the effectiveness of the inhibitor is established.

Test Simulation of Re-entry Conditions - It is apparent from the preceding discussion that in order to properly simulate re-entry heating conditions, plasma arc tests must provide representative surface temperatures and boundary layer oxygen diffusion rates. Figure 5-4 presents a comparison of radiation equilibrium temperature versus oxygen diffusion rate curves for the space shuttle re-entry trajectory and plasma arc tests. The re-entry curves reflect maximum and nominal interference heating rates at the leading edge stagnation line. It is seen that the plasma arc tests provide diffusion rates which simulate maximum interference heating values and are conservative for nominal heating. Temperatures varied from peak values for nominal heating to 150°F below peak values for maximum heating.

Plasma Arc Test Results - Discussion of results of the plasma arc screening tests is presented in two sections. In the next section performance of all material systems is discussed with emphasis upon the material integrity following exposure and the rationale of selection of zirconium-boron-silicon and siliconized inhibited RPP for further development. This section presents a more detailed analysis of performance of the selected materials from a thermomechanics standpoint. Surface temperature response is considered first, followed by a discussion of surface recession.

In the re-entry flight environment inhibited RPP will dispose of the bulk of incident heating by surface re-radiation to space. Hence, it is important to compare the plasma arc specimen re-radiation heat flux rates with the incident convective heating. Re-radiation heat flux q_{RR} was computed from measured surface temperature, T , using the familiar relation.

$$q_{RR} = \sigma \epsilon T^4 \quad (4)$$

Where

$$\begin{aligned} \sigma &= \text{Stefan-Boltzmann constant} \\ &= 0.476 \text{ BTU/ft}^2 \text{ sec } ^\circ\text{R}^4 \\ \epsilon &= \text{surface emittance} \end{aligned}$$

Incident convective heating was assumed equal to the hot wall heat flux q_{hot} . For bare RPP control specimens this neglects blowing effects of ablation products and heat of combustion; however, at the stagnation enthalpies of interest these are very nearly compensating.

Figure 5-5 presents a plot of q_{RR} versus q_{hot} for control and inhibited specimens. Indications were that the control specimens re-radiated about 83% of the incident heat at test points 2 and 3. Heat losses from the back side and circumferential edge of the specimens were calculated to be

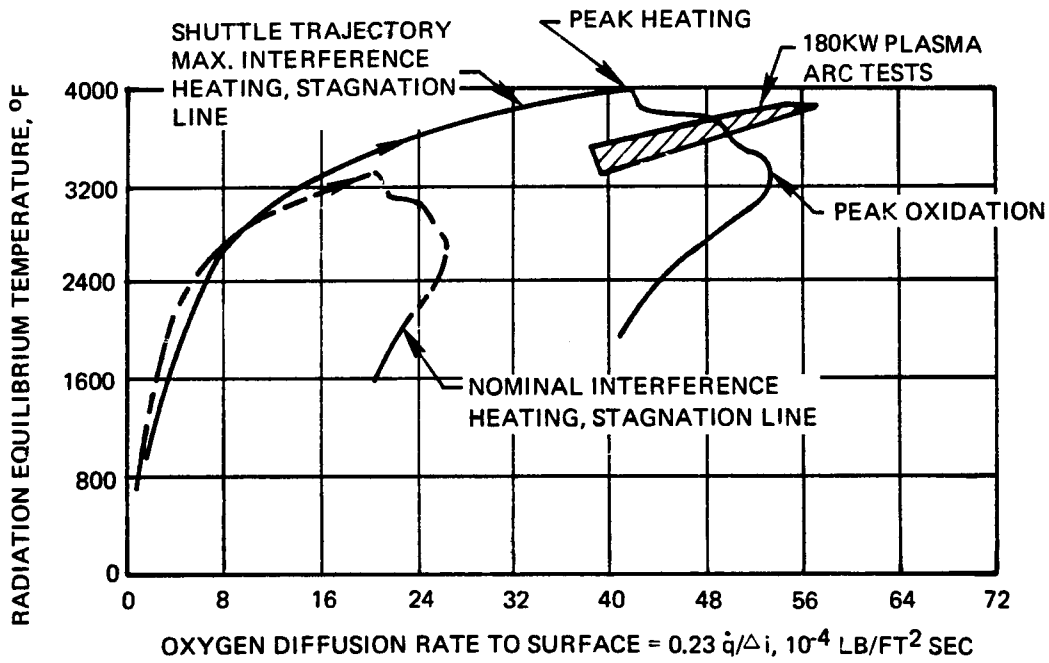


FIGURE 5-4 PLASMA ARC SIMULATION OF RE-ENTRY OXIDATION

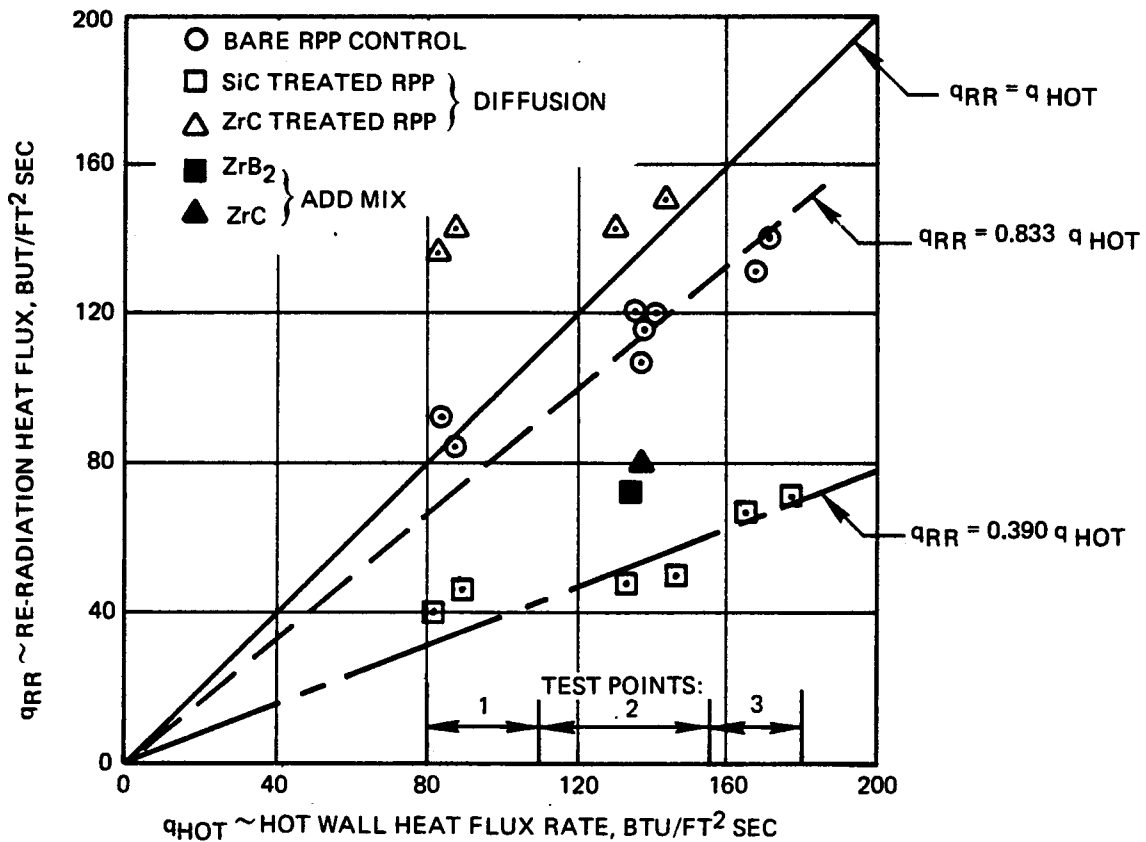


FIGURE 5-5 PLASMA ARC TEST SURFACE HEAT BALANCE SCREENING TESTS

about 25 BTU/ft² sec. which satisfactorily accounted for the remaining 17% of the incident heat. At test point 1 the control specimen data indicated that $q_{RR} = q_{hot}$. Since the calculated heat loss would still be about 16 BTU/ft² sec, it was expected that q_{RR} would be about 83% of q_{hot} , consistent with test points 2 and 3. Since the measured surface recession and mass loss at test point 1 were higher than expected, it was concluded that the discrepancy was probably due to a low heat flux measurement. Later test data indicates that the bare RPP specimens reach radiation equilibrium and the heat flux measurements at test points 2 and 3 were in error. However, since this doesn't change the relative performance of the candidate systems the following discussion of system performance is offered. Data is provided in terms of specimen temperature or bare RPP temperature which are not believed questionable. Bare RPP temperature is now considered to be equivalent to radiation equilibrium temperature.

Re-radiation heat flux for SiC treated RPP at test points 2 and 3 correlated along a line where $q_{RR} = 0.39 q_{hot}$. At test point 1 the data fell about 20% above the correlation line, which is consistent with the control data. The low re-radiation heat fluxes for these specimens correspond to measured surface temperatures 500 to 800°F below measured values for the control specimens. Several possible explanations were considered and were concluded to be unlikely explanations for the reasons summarized below.

<u>Possible Explanation</u>	<u>Critique</u>
Specimen heat losses	Thermal conductivity of diffused coating would have to be twice that of copper to account for difference.
Specimen heat sink effects	All specimens reached equilibrium temperatures.
High surface emittance	Emittance would have to be greater than unity.
Endothermic chemical reaction	Heat of reaction of 10,000 BTU/lb required, even if entire specimen enters the reaction.

Another possible explanation is that SiC treated RPP is non-catalytic with respect to recombination of the dissociated air within the boundary layer. This would result in lower convective heating rates on the specimens than those on the copper calorimeter. This phenomena is

discussed later in Section 5.3 in more detail, with the conclusion that it is the probable explanation for the low surface temperatures on siliconized RPP.

Re-radiation heat flux rates for Zr and ZrB₂ treated add-mix systems were found to lie between those for SiC and those for bare RPP. Non-catalytic effects are again suspected as being the cause of the low re-radiation.

Re-radiation fluxes for diffusion processed Zr specimens are indicated in Figure 5-5 to be higher than the incident heat. This is highly unlikely, and it is probable that the surface emittance for these materials is much lower than the values assumed in computing q_{RR} (0.74 to 0.78 depending upon temperature).

Surface recession rates are presented on Figure 5-6, normalized with respect to the oxidizing potential of the air flow (S/h), for the control material and those materials which have been selected for further development. The recession rates are correlated with measured specimen temperature and are compared with previous plasma arc test data for RPP.

A compilation of prior data for bare RPP ($\rho = 62 \text{ lb/ft}^3$) is indicated by the cross-hatched data band (References 20 - 24). In the temperature range of 2400°F to 4100°F \dot{S}/h is independent of temperature and falls within a + 25% band about the expected value of 0.00278 (ft/sec)/(lb/ft² sec) for diffusion control. It is seen that the bare RPP control specimens used in the current testing and denoted by circles were in generally good agreement with prior data for bare RPP and with theoretical results.

Recession rates of siliconized RPP are compared with NASA-MSC plasma arc test data from Reference 25 on a previous version of SiC treated RPP. In each case recession was negligible below 2750°F. At temperatures between 2750°F and 3130°F, however, the current SiC treated material demonstrated significantly lower recession rates than the previous material. In this temperature range, with up to three exposure cycles, recession rates were 1% or less of that for bare RPP, whereas the previous material experienced recession rates 18.5% of that for bare RPP at 3000°F. At 3250°F the diffusion layer melted, and recession rate was comparable to that for the previous material and for bare RPP.

The add-mix processed Zr and ZrB₂ treated specimens experienced recession rates 3-6% of that for bare RPP in the 3190 - 3300°F temperature range on the first exposure. Better performance was shown by the diffusion processed Zr with recession rates less than 1% of those for

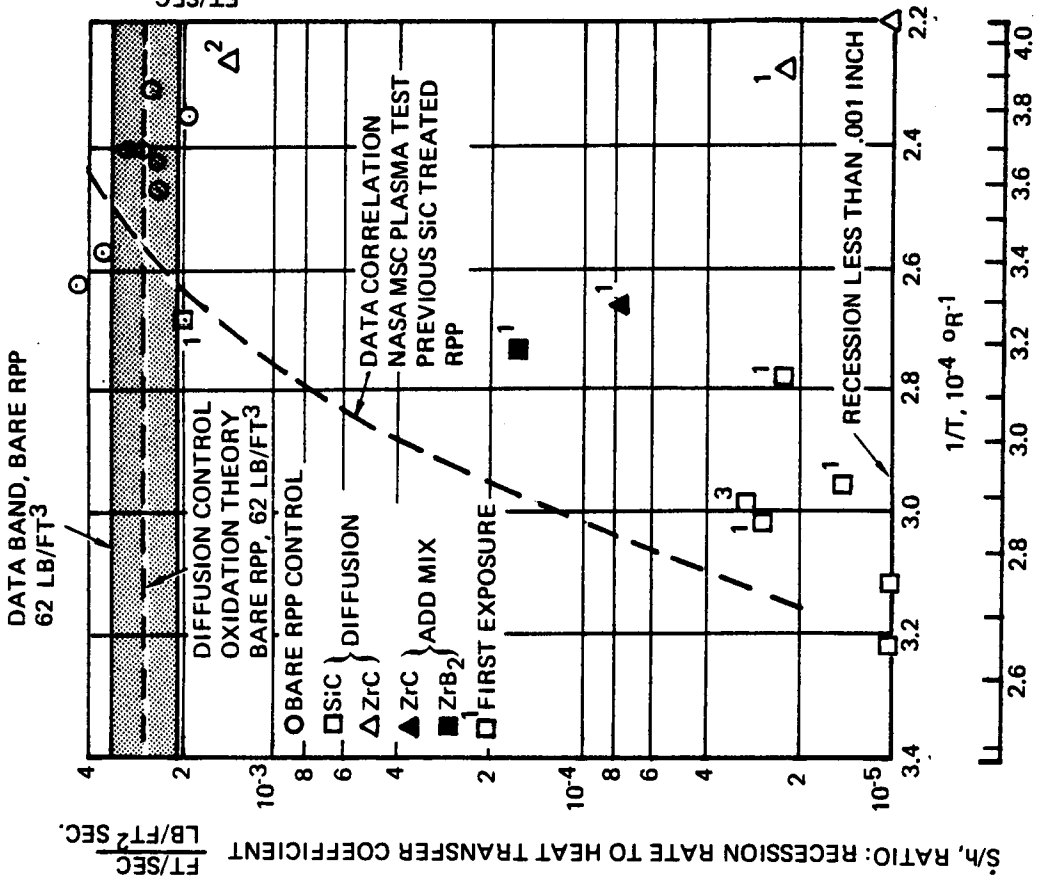


FIGURE 5-6 PLASMA ARC TEST, SURFACE RECESSON DATA RELATIVE TO SPECIMEN SURFACE TEMPERATURE

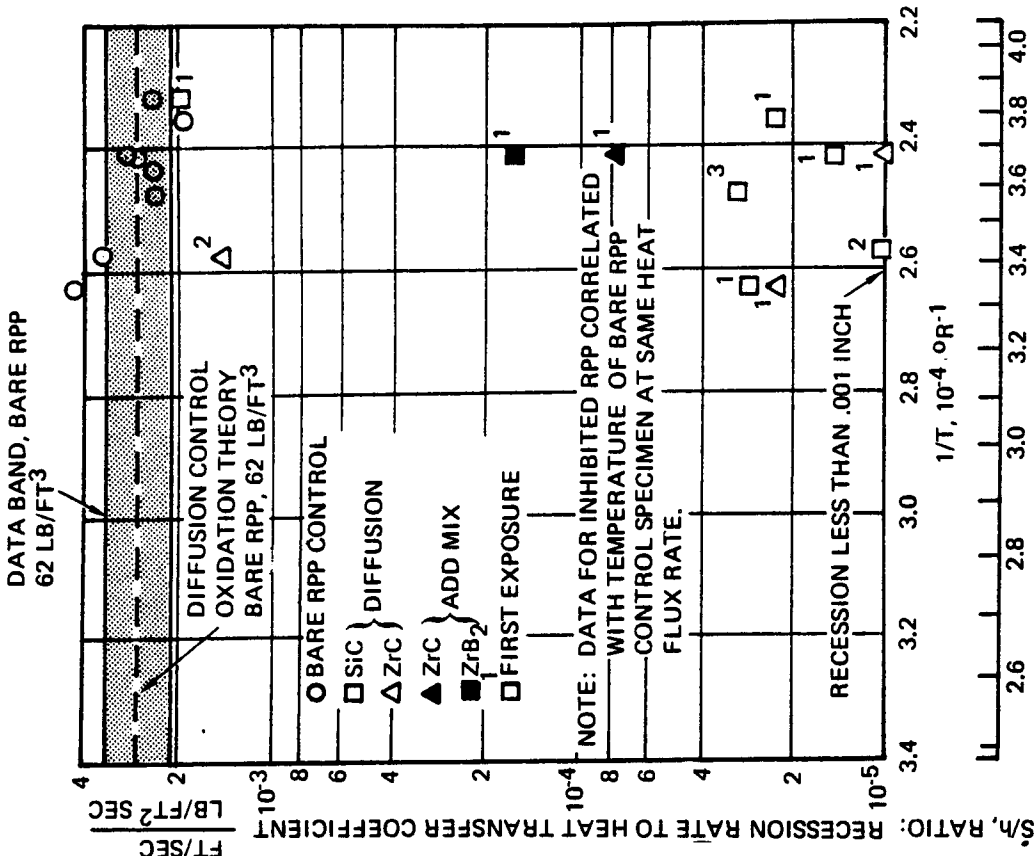


FIGURE 5-7 PLASMA ARC TEST, SURFACE RECESSON DATA RELATIVE TO BARE RPP SURFACE TEMPERATURE

bare RPP at temperatures up to 4090°F on the first exposure. However, on the second exposure erosion was severe, with essentially no oxidation protection.

It was shown previously that silicon carbide treated RPP operates at a significantly lower surface temperature than bare RPP and the other inhibited materials at a given heat flux rate. Preliminary investigation of this phenomena indicates that it is probably not unique to the plasma arc test method, but applicable to the flight environment as well. The presentation of surface recession rates as a function of individual specimen temperature, as in Figure 5-6, does not, therefore, provide a common basis for comparison of materials. A given surface temperature will imply a more severe entry thermal environment for one material than for another.

In order to provide a common basis for material performance comparison, surface recession is presented in Figure 5-7 as a function of the measured temperature of the bare RPP control specimen at the heat flux rate appropriate to each data point. The validity of this presentation is based upon the assumption that any significant factors unique to the test method will similarly affect all materials. It is believed that only specimen heat losses fall in this category and that these will not significantly affect relative material performance. Their affect upon absolute material performance is reflected in Figure 5-7 by using measured control specimen temperatures rather than radiation equilibrium temperatures. Hence, Figure 5-7 should provide a more realistic indication of material temperature capability for the re-entry environment than Figure 5-6.

Material recession rate performance is summarized in Table 5-5, as a function of both individual specimen temperature and equivalent temperatures on bare RPP at the same heat flux rate, as presented in Figure 5-7. Two significant points become apparent when performance is expressed in terms of equivalent bare RPP temperature, as opposed to individual specimen temperature: (1) siliconized RPP has potential application in a much more severe re-entry environment, equivalent to 3780°F rather than 3130°F, (2) the performance potential of SiC relative to Zr is improved significantly. Mass loss rates relative to bare RPP were generally higher than surface recession rates. This effect is much less pronounced for SiC than for the other materials, and SiC has significantly lower mass loss rates than these materials at all equivalent bare RPP temperatures. The relatively high mass loss for Zr and ZrB₂ suggests that there was in-depth mass loss.

TABLE 5-5

PLASMA ARC TEST PERFORMANCE SUMMARY - SCREENING

<u>Inhibitor</u>	<u>Process</u>	<u>No. of Exps.</u>	<u>Indiv. Spec. Temp. °F</u>	<u>Equiv. Bare RPP Temp. °F</u>	<u>Recession Rate % of Bare RPP</u>	<u>Mass Loss Rate % of Bare RPP</u>
C	Diffusion	2	2750	3420	Negligible	0.3%
		1-3	2750-3130	3350-3780	1%	2.7%
		1	3250	3850	74%	62%
r	Diffusion	1	3910-4090	3350-3685	1%	6.5%
		2	4030	3420	52%	Not meas.
r	Add mix	1	3300	3685	3%	18%
rB ₂	Add mix	1	3190	3685	6%	18%

Plasma Arc Testing Material System Performance - Thirty-five plasma arc tests were conducted on the screening program. These included multiple exposure tests and bare controls runs for the diffusion coated and add-mix RPP systems. A summary of results is given in Table 5-6, while pictures of the specimens after test at the 160 BTU/ft.²/sec flux level are shown in Figures 5-8 through 5-11. The performance of each of these systems is briefly discussed below. Initial screening was performed at the 160 BTU/Ft²/sec heat flux level (Test Point No. 2). Promising systems were then tested at 100 and 200 BTU/Ft²/sec corresponding to Test Points No. 1 and 3, respectively. The 160 and 200 BTU/Ft²/sec flux levels are believed to be overstated as previously noted so for discussion purposes, test levels will be indicated by No. 1, 2, or 3.

The titanium/silicon coating in both the diffusion (21-1) and add-mix systems (10-1) performed poorly, having high recession rate and high mass loss. The reason for the difference in surface temperature between the diffusion coating (3420°F) and add-mix coating (4200°F) systems is not clear. However, it may be due to the difference in silicon carbide content, and hence non-catalytic behavior, since the diffusion coated system

TABLE 5-6 PLASMA ARC TEST SUMMARY - INITIAL SCREENING

Test Point	Test Exposure	Specimen		Cold Wall Heat Flux BTU/ft ² Sec (5)	Stag-nation Enthalpy BTU/Lb	Stag-nation Pressure Psia	Time Duration Sec	Radiation Equilibrium Temp °F (1) (ε = 0.80)	Mass Loss 10 ⁻⁴ Lb	Thickness Loss Inch	Average Recession Rate 10 ⁻⁴ In/Sec	True Surface Temp °F
		Process	Inhibi-tion									
2	1	Bare Control	None	160	9410	0.4	100	3900	11.9	0.052	5.2	3690
	1	Diffusion	SIC	160	9260		300		0.4	0.001	0.03	2920
	1		ZrB ₂ /Si	160	10400		300		10.4	0.072	2.4	2920
	2		Ta/Si	160	10200		300		0.8	-0.002	0.000	3050
	1		Ti/Si	160	7500		180		7.0	Coating	-	3420
	1		Zr/Si	169	10040		300		1.6	Burn Thru	-	4090
	1	Bare Control	None	162	8130		100	3880	12.0	0.057	5.7	3685
	1	Add Mix	ZrB ₂ /Si	155	7640		300		13.0(2)	0.046(2)	1.5	3900
	1		ZrB ₂ /Si (Fiberite)	165	8600		300		13.4(2)	0.051(2)	1.7	4040
	1		Ti/Si	160	8270		300		13.1	0.186	6.2	4200
	1		ZrB ₂ /Si	155	7640		300		5.81(2)	0.012(2)	0.4	3190
	1		Zr/Si	160	7370		300		6.19(2)	0.006(2)	0.2	3300
	2	Diffusion	SIC	130	7020		300		10.8	0.000	0.000	2650
	1	Bare Control	None	160	8110		100	3870	0.4	0.050	5.0	3570
	3	Diffusion	SIC	150	8110		300		0.4	0.002	0.067	2890
	2		Zr/Si	160	7680		300		3.25(4)	-0.002(4)	0.000	4030
	(3)		Ta/Si	160	8075		300		0.465	0.005	0.17	2930
	(3)		ZrB ₂ /Si	160	8000		300		15.1	0.081	2.7	2940
	1	Bare Control	None	165	7970		100	3900	11.3	0.053	5.3	3650
	1	CVD	SIC	160	7100		300		21.7	0.116	3.86	3580
	1		SIC	160	8110		300		15.8	0.100	3.33	3610
	1		SIC	160	7750		300		13.7	0.037	1.2	3040
	1	Diffusion	SIC	200	7850		75	4090	9.2	0.04	5.33	3780
	1	Bare Control	None	200	7700		300		1.0	0.002	0.067	3130
	1	Diffusion	SIC	190	7700		300		10.6	0.056	1.87	3230
	1	Diffusion	Ta/Si	200	8660		300		12.7	0.079	2.60	4670
	1	Diffusion	Zr/Si	250	8200		300		9.2	0.042	5.60	3850
	1	Bare Control	None	200	9290		75	4130	20.4	0.134	4.50	3250
	1	Diffusion	SIC	200	9280		300		14.8	0.075	5.00	3350
	1	Bare Control	None	100	8580	0.2	150	3440	1.28(2)	0.001(2)	0.03	3910
	1	Diffusion	Zr/Si	100	8120		300		3.96	0.032	1.07	3040
	1	Diffusion	ZrB ₂ /Si	100	8200		300		0.227	0.001	0.03	2860
	1	Diffusion	SIC	98	9450		300		14.9	0.081	5.40	3420
	1	Bare Control	None	100	6630		150	3390	6.73(4)	0.056(4)	1.87	3970
	2	Diffusion	Zr/Si	105	8780		300		0.0485	0.000	0.00	2750
	2	Diffusion	SIC	90	8800		300					

- (1) Based upon hot wall heat flux.
- (2) Measurements made after removal of fragile surface coating, formed during test.
- (3) Second exposure for this specimen but with back side exposed.
- (4) Measurements made before removal of coating.
- (5) Cold wall heat flux above 100 Btu/ft²-sec is apparently overstated. See text.

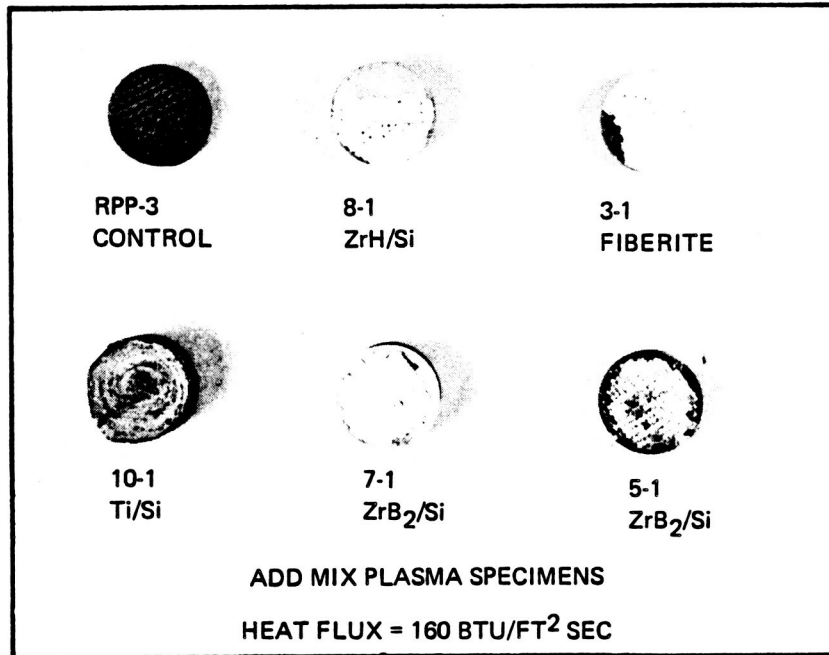


FIGURE 5-8 ADD-MIX SPECIMENS AFTER PLASMA TEST

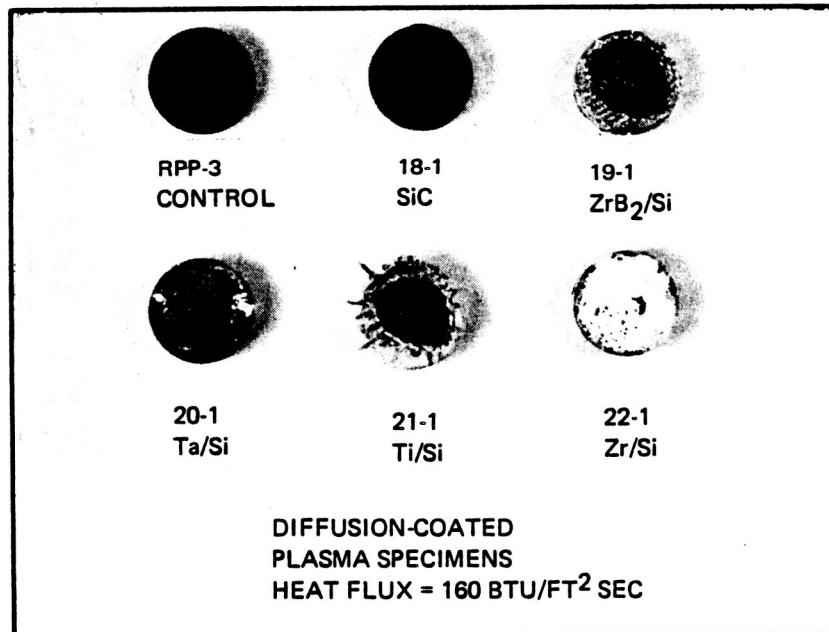


FIGURE 5-9 DIFFUSION COATED SPECIMENS AFTER FIRST SERIES PLASMA TEST

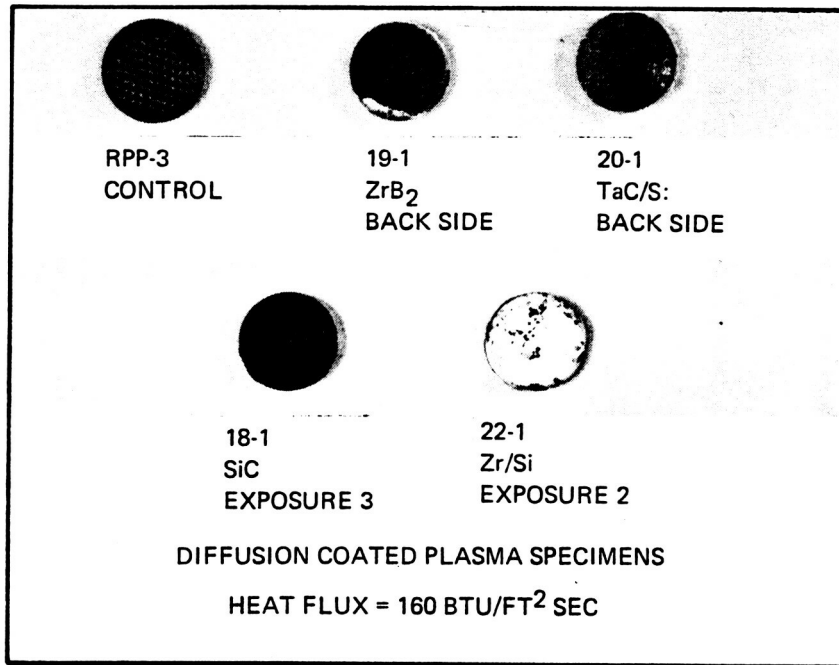


FIGURE 5-10 DIFFUSION COATED SPECIMENS AFTER SECOND SERIES PLASMA TEST

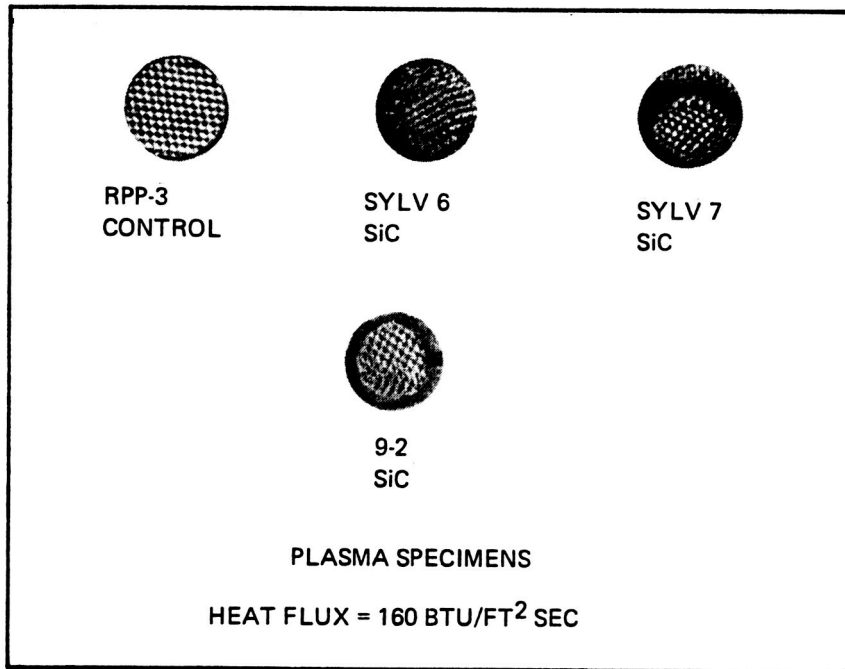


FIGURE 5-11 DIFFUSION COATED SPECIMENS ALTERNATE SILICON CARBIDE COATINGS AFTER PLASMA TEST

theoretically had 70% silicon carbide, while the other had only 25%. In any event, both titanium systems were eliminated from further consideration because of their inability to provide oxidation protection.

The tantalum/silicon system (20-X) was tested only as a diffused coating system because the add-mix approach failed during initial pyrolysis. The first test (20-1) at test point No. 2 resulted in some pitting of the coating that permitted subsurface oxidation. However, it was encouraging that there was no general coating breakdown. Since it was observed that the coating soundness was not uniform between both sides of the flexure bars, when sections were subjected to low temperature oxidation, it was decided to test the backside of the previously tested plasma specimen to ascertain if there was a performance difference. A greater thickness loss was obtained in the second test, but mass loss was less. The thickness loss difference is probably due to the net expansion of the specimen on the initial exposure which makes initial thickness loss measurements unreliable. Surface pitting was the same as before. Surface temperature was low, indicating non-catalytic behavior. When tested to test point No. 3 the tantalum/silicon system (20-4) burned through to the bare substrate. The performance of this system was clearly inferior to the silicon carbide diffusion coating, and therefore, this system was dropped from the program.

The zirconium/silicon diffusion coated RPP showed encouraging first exposure performance but failed upon second exposure. At test point No. 2 the diffusion coated specimen (22-1) increased in thickness after exposure to the plasma. A white powder, possibly zirconia, formed on the surface, part of which was brushed off relatively easily, but some remained firmly attached. A measured 0.004 inch of powder was removed, producing a net specimen growth of 0.010 inch. Part of the surface was uniformly covered with powder of uniform texture but another area showed evidence of a grating effect where the coating material had filled the cavities between the cloth fibers. The surface of this specimen rose to 4090°F, whereas the bare RPP control specimen reached only 3690°F.

Exposure of the Zr/Si diffusion system (22-4) to test point No. 3 levels produced burn through, although part of the white layer remained. Surface temperature for this condition was very high at 4670°F, far behind the required capability. At the lower level, test point No. 1, the results were somewhat different from test point No. 2. The specimen (22-5) reached 3910°F, still quite high and it grew as before, but 0.017 inch thickness of powder was removed this time, although total weight loss was less. Exposure of bare graphite was not apparent. Second exposure of this specimen produced burn through. Lower flux levels were not attempted on the initial screening because test point No. 1 is at the lower limit of the plasmatron with stagnation heating type specimens.

The add-mix system (8-1) produced only 3300°F surface temperature at test point No. 2 in contrast with the 4090°F for the diffusion system, but the surface recession and weight loss were greater. The temperature difference is not readily explained between the two systems. Surface texture showed two distinct zones. One was a dense gray, while the greater area showed the white grating effect, where the graphite cloth was burned out, leaving the coating oxide. The indication is that the coating materials may not have been uniform.

The zirconium diboride/silicon diffusion system (19-X) performed poorly at test point No. 2 level. Both sides of the specimen were tested to verify that coating non-uniformity was not the problem. This system was expected to perform better. Analysis of the coating constituents by X-ray diffraction did not indicate the presence of zirconium diboride in the sample, but this could be expected, since the silicon carbide constituent masks the diboride indicators. Additional analysis by emission spectrography failed to locate boron as well. It is significant that this coating showed non-catalytic behavior with low surface temperature before burn through. However, even at the lower flux level of test point No. 1 the coating did not offer protection.

There were three zirconium diboride/silicon add-mix systems tested. The Fiberite laminate operated at a high surface temperature (4040°F) and developed a white powder layer. After removal of the fragile portion of this layer the recession was 0.051 inches, considered unacceptable performance. Panel number 5, a VMSC system with metal powder proportions similar to the Fiberite panel, performed equivalently.

The third panel specimen tested, No. 7, showed non-catalytic behavior with surface temperature rising to only 3190°F. Performance in both mass loss and surface recession was improved over the other two panels but was not considered good enough. This particular panel had approximately twice the loading of ZrB_2 and Si powders as the others and should account for its better performance.

It is interesting to note that the diffusion coated specimens and the No. 7 specimens, which should have the densest coatings, also operated the coolest.

It was believed that a marriage of the zirconium diboride and zirconium systems would produce an effective oxidation-resistance system. Theoretically this should be the case and is in agreement with the recommendation of Dr. Rudy and Dr. Kaufman, VMSC-T consultants. Accordingly, coating development involving zirconium-boron-silicon constituents were continued.

The VMSC siliconized RPP specimens (Series 18), which by X-ray diffraction produces primarily beta-silicon carbide with a moderate amount of the alpha phase, have shown outstanding performance. While a major factor in the oxidation resistance of this system is the non-catalytic phenomenon, other systems tested exhibiting this feature did not perform as well.

In fact, three other silicon carbide coatings were evaluated during initial screening, two supplied by Sylvania (SYLV 6 & 7) and one VMSC specimen processed differently (9-2) from the prime system. None of these withstood test point No. 2 flux levels without burn through.

The siliconized RPP specimens were tested at test point levels No. 1, No. 2, and No. 3. At the middle flux level, specimen number 18-1 showed surface recessions of 0.001, and 0.002 inches in two exposures. Another exposure of this specimen showed no surface recession at a slightly lower flux level. Surface temperature for the higher of these levels was 2920°F. The corresponding bare RPP control specimen temperature was 3690°F.

Another specimen at test point No. 1 was tested twice. The first exposure netted 0.001 inch recession but the second exposure was not measurable to the thousandths of an inch. Using weight loss as a measure of estimating surface recession, this second test would indicate 0.0002 inch surface recession. Surface temperature peaked at 2860°F while bare RPP temperature was 3350°F, higher than calculations by North American Rockwell of maximum leading edge radiation equilibrium temperature for the straight wing orbitor.

In an effort to determine the maximum flux level and surface temperature that the siliconized RPP will sustain, two specimens were subjected to test point level No. 3. From surface recession and weight loss standpoints, specimen 18-4 did half as well as those tested at the No. 2 flux level, but the temperature was up to 3130°F. Another specimen tested at a slightly higher flux level reached 3250°F temperature, but burned through. The apparent limit of the current coating is between 3130°F and 3250°F, but this is at a temperature at which bare RPP would experience about 3800°F.

In summary, the VMSC siliconized RPP was clearly the superior performer in the plasma tests. If non-catalytic behavior can be realized on the shuttle, and indeed preliminary analyses shows this to be the case, then the siliconized RPP coating system as determined by the screening tests would operate at an equivalent radiation equilibrium temperature of 3800°F with surface recession of only 0.002 inches per mission. In addition, through leading edge designs that utilize cross-radiation to reduce

stagnation temperature, the coated RPP requirement was reduced from 4000°F to 3615°F. This would result in even lower recession for the silicon carbide coating, and a greater temperature margin. For these reasons the siliconized system was the prime candidate selected for additional development.

Because two systems were to be carried for further development, a combination of the zirconium/silicon and the zirconium diboride/silicon system was the second selection made. This choice was based on the potentially good high temperature performance of the Zr/Si and the anticipated performance of the ZrB₂/Si. In addition, this system was expected to produce high strength laminates and low weight leading edges.

5.2 MODIFIED INHIBITOR SYSTEMS TEST

Modifications of the candidate coating systems concentrated primarily on evaluating and improving high temperature oxidation resistance and coating fabricability. It was planned that other properties found deficient would be developed once high temperature performance was secured. Accordingly, test evaluation of the various modified coating systems was limited to plasma arc exposure. Two selected systems, the siliconized RPP and the zirconium-boron-silicon coated RPP, were ultimately tested to determine other physical and mechanical property data. These are documented in Section 5.4.

This section of the report presents the results of all plasma arc test data obtained on both the modified diffusion coating systems and the overlay coating systems. A discussion of the test results, method of data reduction, and the technique by which the data is evaluated in terms of shuttle leading edge mission life is given. NASA-MSD tests on an early VMSC siliconized RPP system are also discussed.

5.2.1 VMSC Plasma Arc Tests

To support the selection of two material systems for Phase II, over 120 tests were performed on at least 10 basic inhibitor systems in the VMSC 180 KW plasma arc facility. These tests were performed in the same manner as the screening tests of Section 5.1.3., except that cold wall heat flux rates were 100, 120, 130, 140 and 160 Btu/ft² sec, corresponding to radiation equilibrium temperatures of 3400, 3580, 3660, 3740, and 3870°F, based upon an 0.80 surface emittance. All specimens were exposed to one of the two higher heating levels, and those specimens which demonstrated acceptable performance were evaluated at one or more of the lower heating rates.

On the basis of results of these tests, two material systems were selected for Phase II evaluation, siliconized RPP and zirconium-boron-silicon (Zr-B-Si) treated RPP. First, performance of these selected materials is discussed in detail from a thermomechanics standpoint. Performance of all material systems is then discussed, with emphasis upon material integrity following exposure and rationale of selection of the siliconized and Zr-B-Si treated RPP for Phase II.

Measured surface temperatures as a function of hot wall heat flux rate, q_{HOT} , correlated with radiation equilibrium relations are presented in Figures 5-12 and 5-13. Data for siliconized RPP and bare control specimens is included in Figure 5-12 while Figure 5-13 includes data for Zr-B-Si treated RPP and bare RPP. Also shown on each figure is the entry cold wall heat flux, q_C , corresponding to q_{HOT} for the air enthalpy at the time of peak entry heating.

For the tests of siliconized RPP the bare control specimen temperatures agreed well with the radiation equilibrium relation. In the screening tests of Section 5.1.3 control specimen temperatures were 4.5% below radiation equilibrium values. The difference is believed to be due to a change in calorimeter operation, rather than the optical pyrometer. In each test series siliconized coating failure occurred at measured temperatures of 3200-3250°F, whereas calorimeter measurements at coating failure were 26% higher in the screening tests (190-200 Btu/ft² sec) than in the later tests discussed herein (150-160 Btu/ft² sec). Agreement of control specimen temperature with radiation equilibrium theory in Figure 5-12 tends to support accuracy of the later calorimeter data. However, due to the question of calorimeter accuracy, material erosion performance is related to control specimen temperature in subsequent discussions, rather than calorimeter measurements. Validity of this approach is supported by recent calibration of the pyrometer, which shows performance within acceptable tolerance.

It is seen in Figure 5-12 that siliconized RPP surface temperatures were 550-630°F lower than control specimen temperatures at the same hot wall heat flux. The temperature data correlates well with a modified radiation equilibrium relation in which the hot wall heat flux is decreased by a factor of one-half. Siliconized RPP and control specimen temperatures were correlated more directly in Figure 5-14, which indicates a ratio of re-radiation heat fluxes of 0.515. As discussed previously for the screening test data, the low temperatures of the siliconized material are believed to be due to low surface catalytic activity, and this phenomena was analyzed in some detail in Section 5.3.

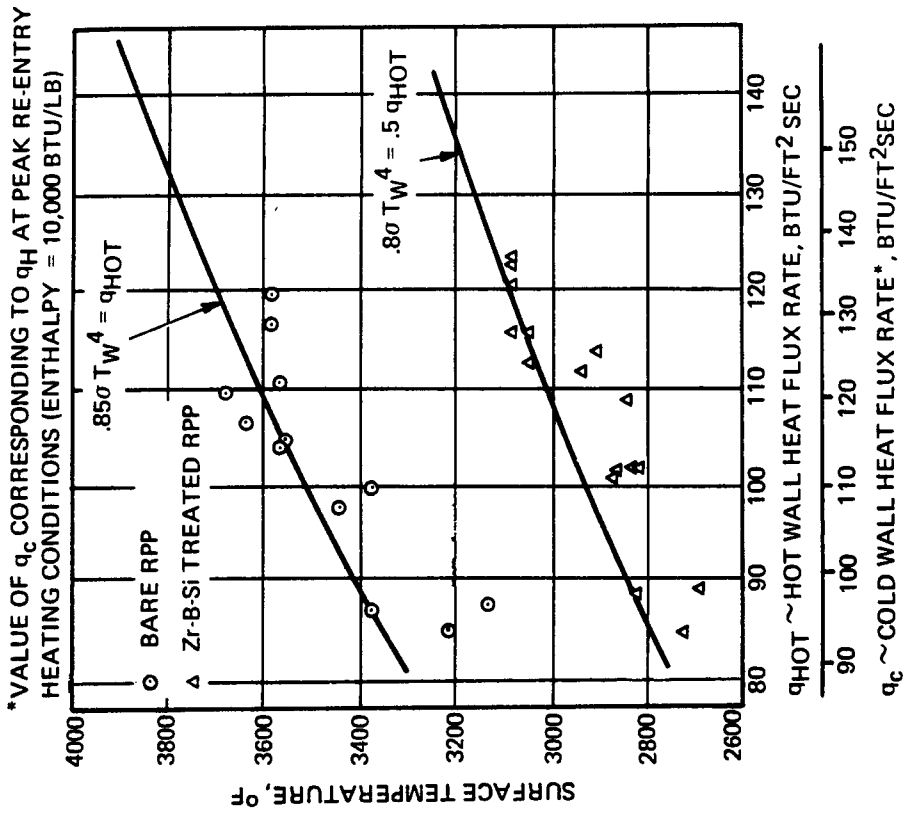


FIGURE 5-13 SURFACE TEMPERATURE OF Zr-Br-Si TREATED RPP

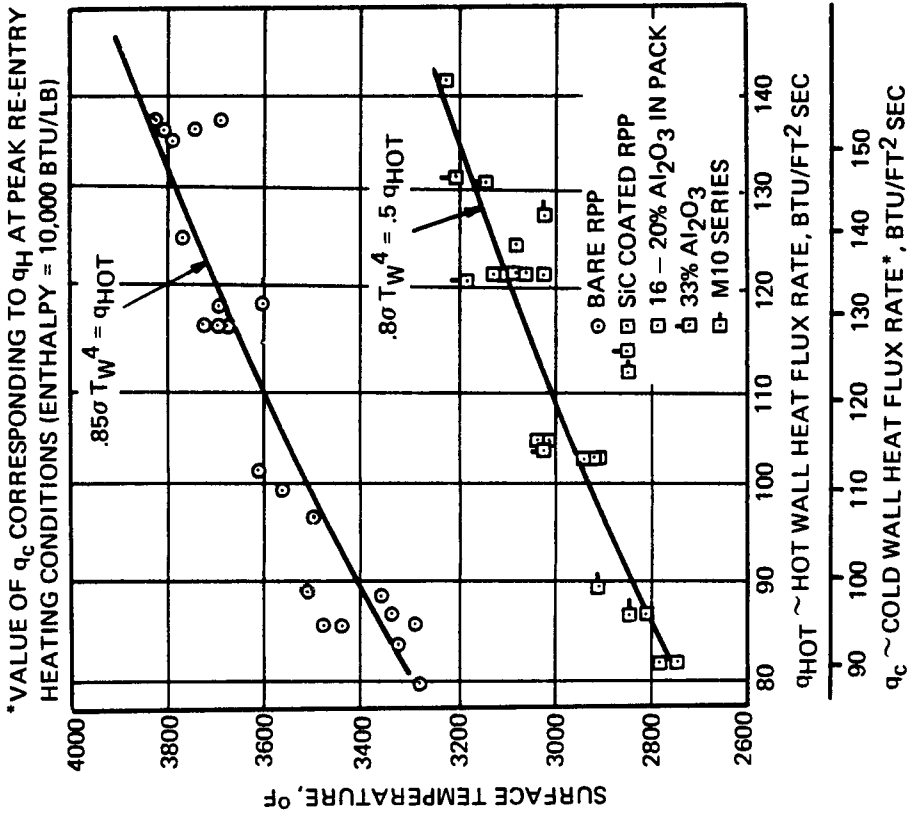


FIGURE 5-12 SURFACE TEMPERATURE OF SILICONIZED RPP

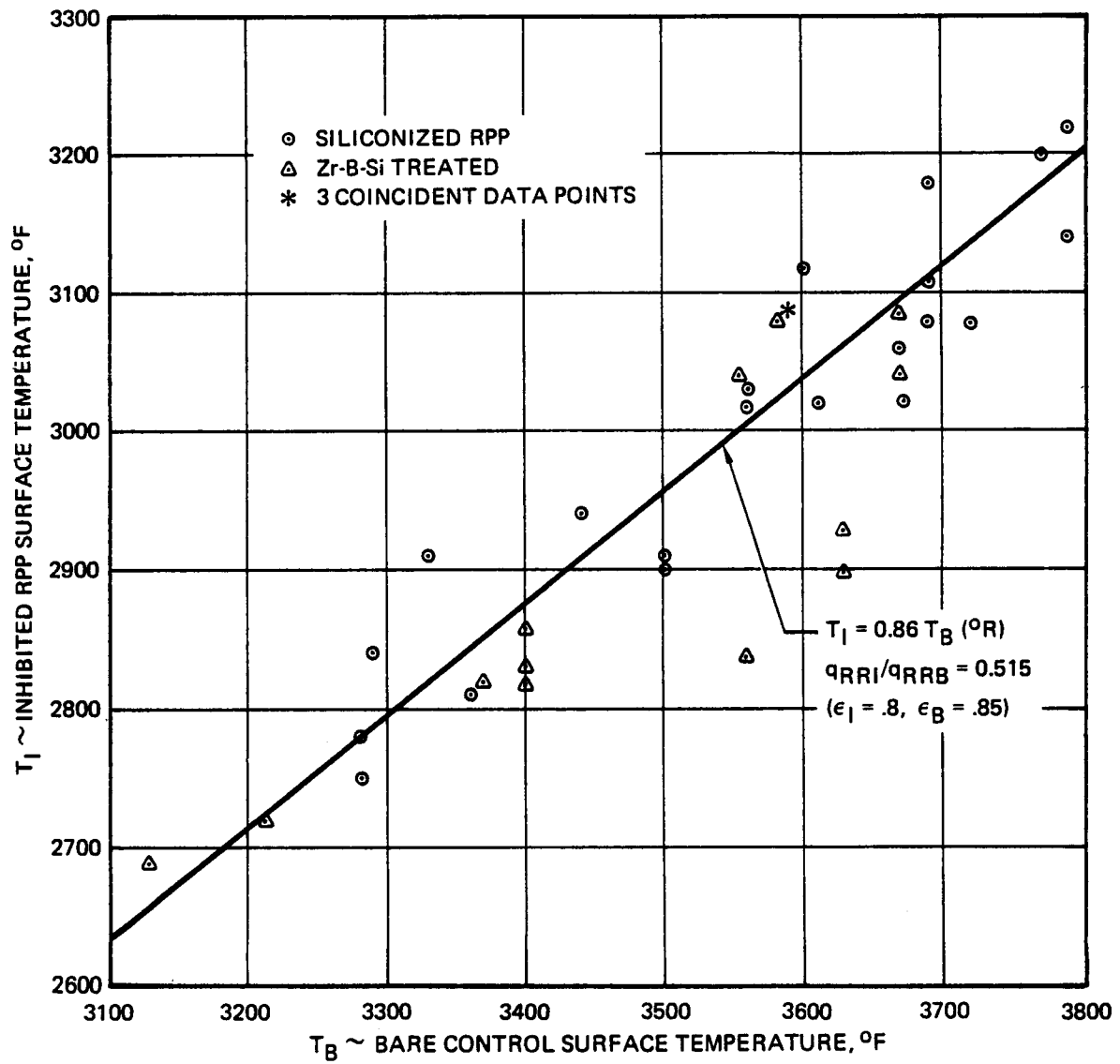


FIGURE 5-14 CORRELATION OF INHIBITED AND BARE PLASMA SPECIMEN TEMPERATURES

Erosion performance of the two selected material systems is presented in Figures 5-15 and 5-16, which present mass loss rates per unit of surface area, normalized with respect to the oxidizing potential of the air flow (\dot{M}/h). Mass loss was chosen as the basis for erosion evaluation, rather than surface recession, because of the much greater accuracy of mass loss measurements. Surface recession was generally on the order of 0.001-inch or less per exposure for siliconized RPP, making an accurate measurement extremely difficult. For those specimens which did recede significantly, it was found that mass loss per unit area could be correlated with surface recession by assuming a coating density of 100 lb/ft³.

Mass loss rates are shown in Figure 5-15 for both siliconized RPP and bare control specimens where they are correlated with both inhibited specimen temperature and control specimen temperature. Mass loss rates of control specimens were generally higher than diffusion control theory values and previous data for bare RPP. Since specimen mass loss, surface area and exposure time can be measured quite accurately, the source of discrepancy is more likely in the normalizing parameter, h , which is the enthalpy based surface heat transfer coefficient. The trend of the control specimen mass loss data suggests that values of h used in computing \dot{M}/h may be too low. This would tend to make the values of \dot{M}/h in Figure 5-15 for siliconized specimens somewhat conservative (high).

The heat transfer coefficient, h , is the ratio of heat flux to enthalpy. Errors in measured heat flux are not a likely source of the postulated low values of h , since the magnitude of the discrepancy is not consistent with the radiation equilibrium correlation obtained between heat flux and control specimen temperature in Figure 5-12. It appears more likely that reported values of enthalpy are somewhat higher than actual values, particularly since this parameter is difficult to measure with high accuracy.

The mass loss data for siliconized RPP was correlated by the empirical relation,

$$\dot{M}/h = 1.123 \times 10^{14} e^{-13.6 \times 10^4/T} \quad (5)$$

where T = temperature of inhibited specimen, °R. This relation provides a reasonable correlation of all data except for the M10 series of specimens. The M10 specimens were processed concurrently with specimens submitted to NASA-MSD for plasma arc evaluation. All other data in Figure 5-15 were obtained for specimens processed later, using improved techniques, and these specimens demonstrated significantly lower mass loss rates than the M10 series. The surface temperature upper limit for siliconized RPP was established to be about 3200 F which corresponds to 3800 F on bare RPP. Below this temperature mass loss rates for siliconized RPP were 0.04% to 4% of those for bare RPP, and in some cases were immeasurably low. The strong dependence of mass loss of siliconized RPP upon surface

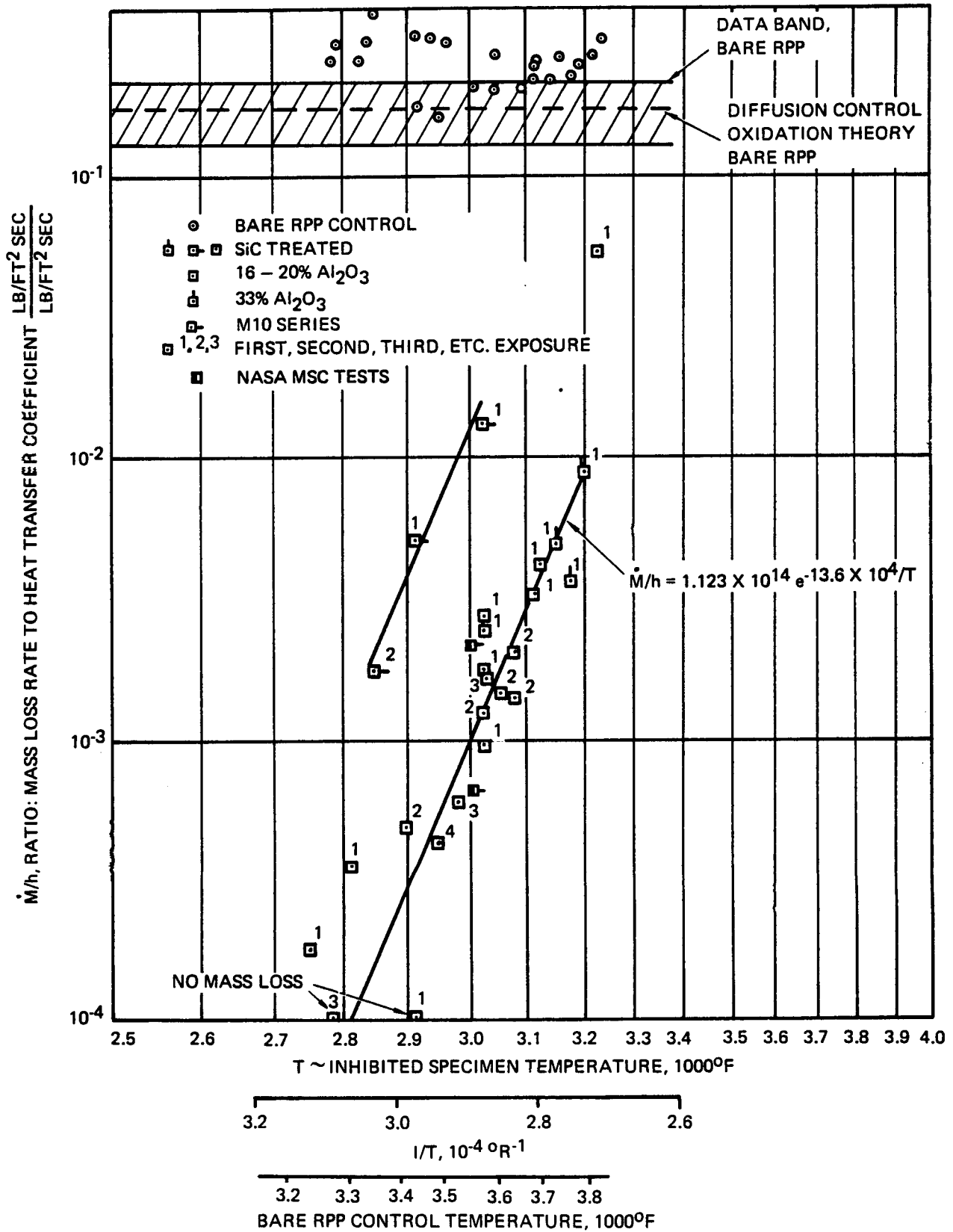


FIGURE 5-15 PLASMA ARC TEST, MASS LOSS DATA SILICONIZED RPP

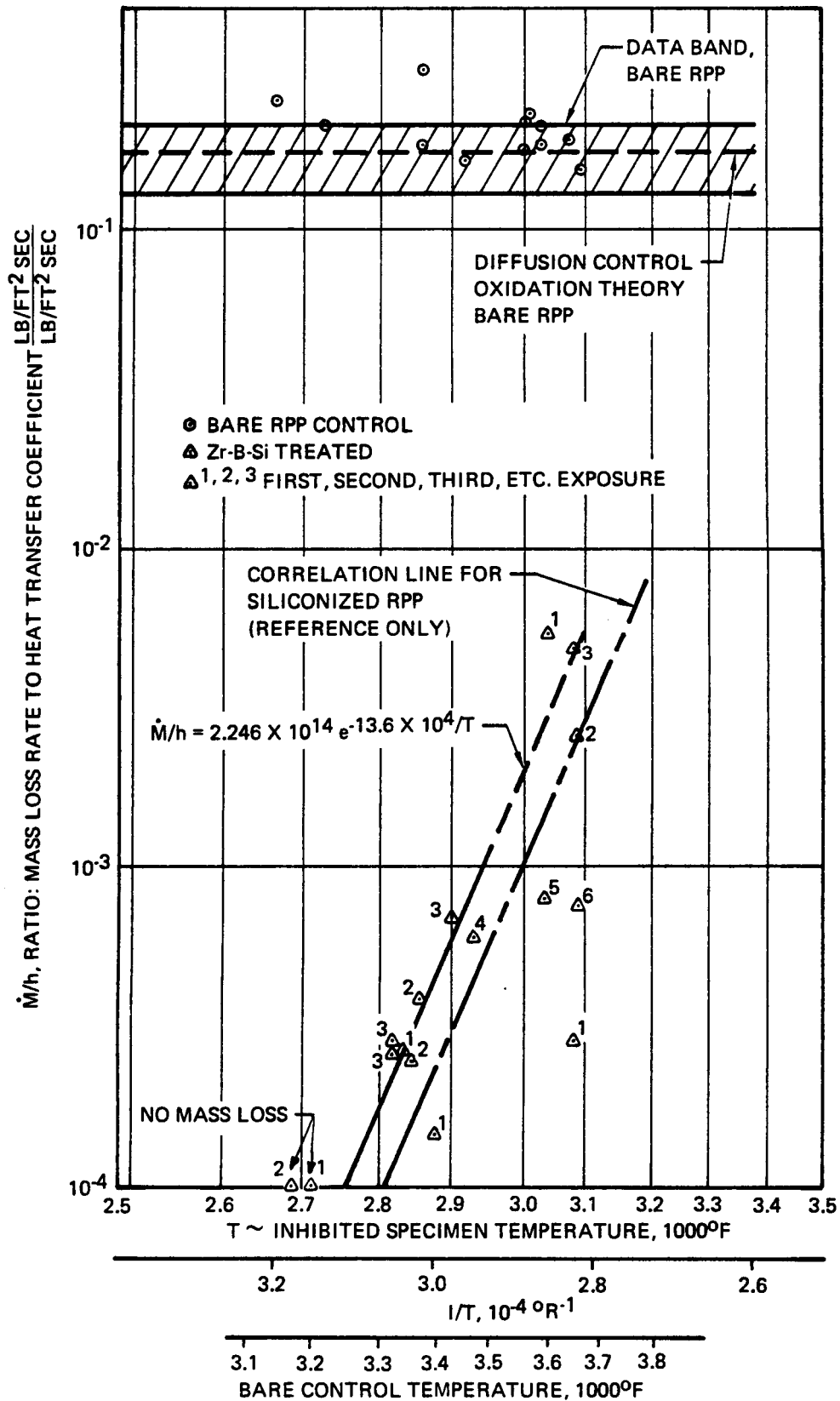


FIGURE 5-16 PLASMA ARC TEST, MASS LOSS DATA Zr-B-Si TREATED RPP

temperature emphasizes the importance of the low temperature operation of this material, as well as the importance of predicted beneficial cross-radiation effects in further reducing surface temperature.

Surface temperatures of Zr-Br-Si treated RPP and associated bare control specimens are shown in Figure 5-13 as a function of hot wall heat flux rate. Temperatures of both control and treated specimens were, on the average, about 100°F or 3% below the values obtained in evaluation of siliconized RPP, at the same values of hot wall heat flux. The calorimeter was reworked between these two test series; which may explain the difference. Figure 5-14 presents a direct correlation of Zr-B-Si treated specimen temperatures with control temperatures. The data generally agrees with the prior correlation obtained for siliconized RPP. Three data points, however, fell well below the correlation line. Since these were all obtained on a single specimen, the correlation line is believed more representative of the relationship between temperatures of Zr-B-Si treated and bare RPP. It should be noted, particularly at the higher heat fluxes, that local areas on the treated specimens ran hotter than the temperatures shown in Figures 5-13 and 5-14. These higher temperatures corresponded to areas of relatively thick coating buildup. Coating stability was poorer in these local areas, and it is believed that this problem can be resolved with improved processing techniques. Hence, the lower temperatures are considered more representative of coating performance.

Mass loss rates of Zr-B-Si treated RPP and associated bare control specimens are presented in Figure 5-16 as a function of both inhibited and bare specimen temperature. Mass loss rates of the control specimens are in much better agreement with diffusion control theory and with previous data for bare RPP than those obtained in the evaluation of siliconized RPP. At surface temperatures up to about 2930°F , corresponding to bare control temperatures up to 3470°F , mass loss rates are correlated reasonably well by a line which parallels that for siliconized RPP, but with higher absolute values by a factor of two. At higher temperatures, it is more difficult to generalize the mass loss rate data, since performance varied from specimen to specimen. However, extrapolation of the lower temperature correlation line to 3100°F appears to provide a conservative representation of material performance.

The plasma arc test data was used in conjunction with computed reentry temperatures and heat transfer coefficients to predict mission life capability of siliconized and Zr-B-Si treated RPP. First, radiation equilibrium temperatures from Section 3.3.3 were used with the correlation in Figure 5-14 of inhibited RPP temperature versus bare control temperature to establish inhibited RPP temperature as a function of reentry time. The validity of this approach is critiqued in Section 5.3 in the light of theory of surface catalytic effects. That analysis suggests that the approach is reasonable, and should yield slightly conservative (high) temperatures of inhibited RPP.

Inhibited RPP temperatures were then used with heating rates and enthalpies from Section 3.3.1 to establish mass loss rate as a function of reentry time for a peak radiation equilibrium temperature of 3576^oF, with the results shown in Figure 5-17 for siliconized RPP. It is seen that mass loss rate drops off rapidly with time from the peak value, due to the strong dependence of M/h upon temperature. The mass loss rate versus time curve was integrated to obtain the total mass loss per unit area for a single mission. The resulting value of 1.2 x 10⁻³ lb/ft² for siliconized RPP was computed to be equivalent to 134 seconds of exposure to the temperature and heat transfer coefficient at the time of peak heating.

These results were used to predict mission capability as a function of peak temperature of bare and siliconized RPP, with the following relation,

$$N = \frac{\Delta L_{\text{Allowable}} \rho}{(\dot{M}/h)_{\text{Max}} h_{\text{Max}} t_{\text{EQ}}} \quad (6)$$

where

N = Number of missions

$\Delta L_{\text{Allowable}}$ = Allowable total surface recession for N missions
 = 0.010 inch = 0.000833 feet

ρ = coating density = 100 lb/ft³

$(\dot{M}/h)_{\text{Max}}$ = value of \dot{M}/h at time of peak reentry heating, dimensionless

h_{Max} = value of surface heat transfer coefficient at time of peak reentry heating, lb/ft² sec

t_{EQ} = equivalent exposure time at $(\dot{M}/h)_{\text{Max}}$ and h_{Max} for single mission = 134 seconds

The allowable total surface recession of 0.010 inch is considered to be a conservative value which would leave about one-half of the initial coating thickness remaining after N missions.

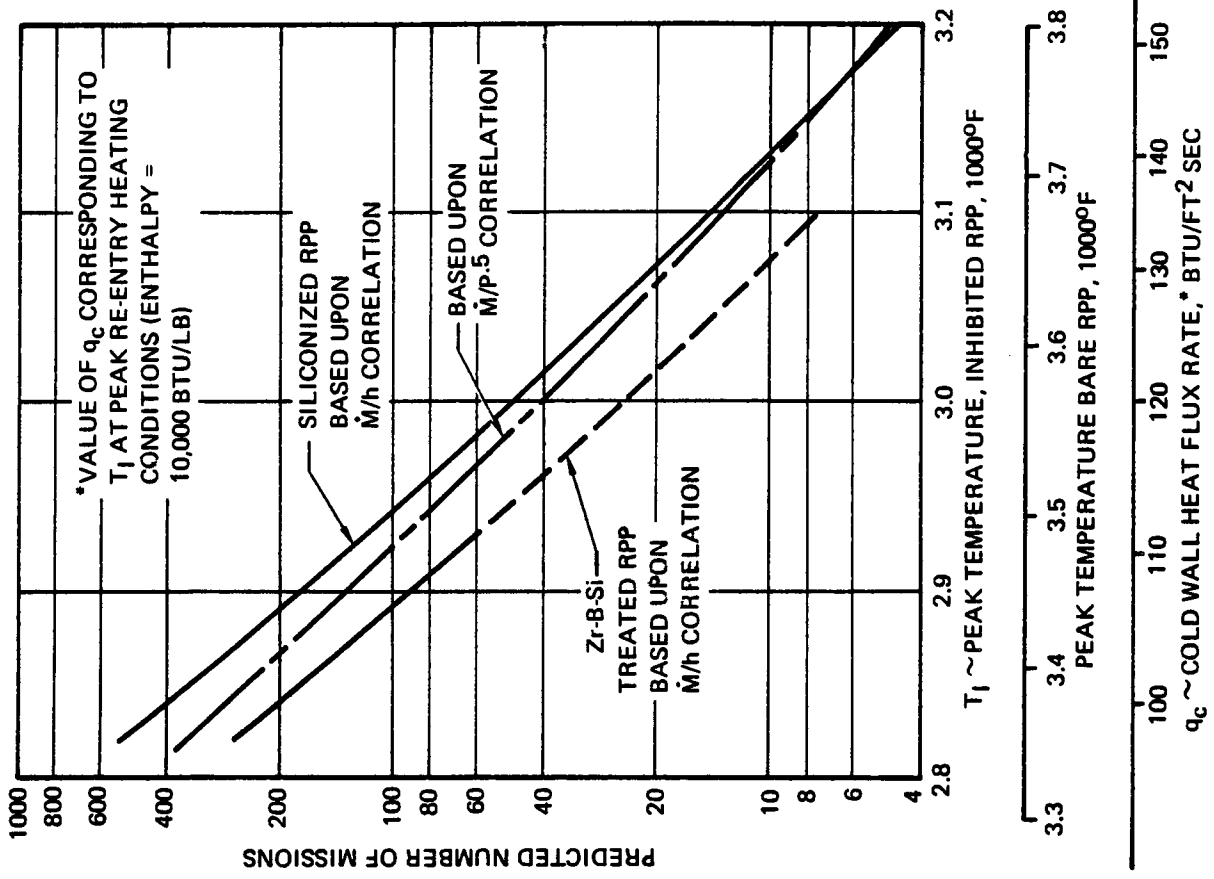


FIGURE 5-18 PREDICTED MISSION CAPABILITY - INHIBITED RPP

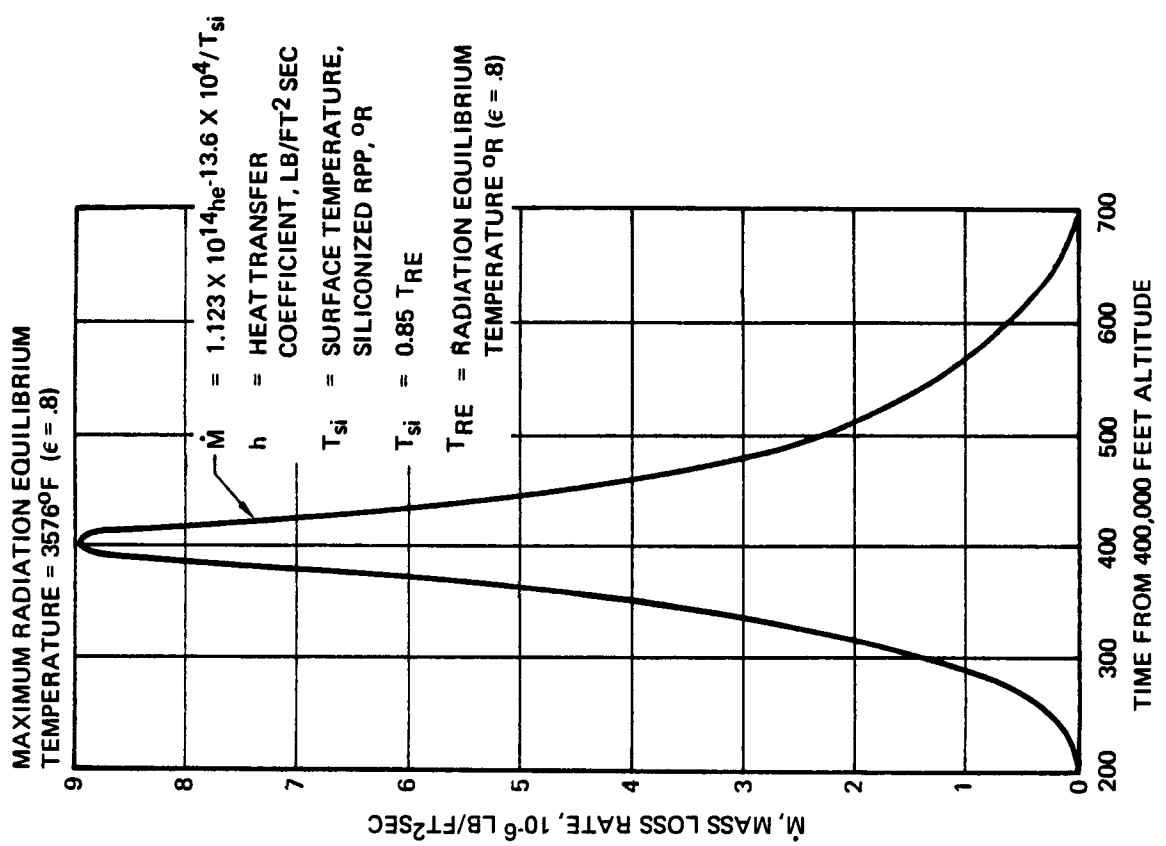


FIGURE 5-17 MASS LOSS RATE VS RE-ENTRY TIME SILICONIZED RPP

The resulting curve of N versus temperature for siliconized RPP in Figure 5-18 indicates capability for 100 missions at heating conditions where bare RPP reaches 3500°F maximum temperature and eleven missions at 3700°F. It is recognized that Figure 5-18 represents a considerable extrapolation of test data to total mission life, particularly at the lower temperatures. However, it will be noted in Figure 5-15 for siliconized RPP that mass loss rate was generally lower on second and third exposures than on initial specimen exposure, suggesting that the extrapolation may be conservative. Furthermore, no allowance is made in Figure 5-18 for beneficial effects of cross radiation in reducing surface temperature.

Mission capability of Zr-B-Si treated RPP was predicted to be one-half that of siliconized RPP for temperatures up to 3100°F, corresponding to bare RPP temperatures up to 3670°F. For temperatures above 2930°F, the predictions are based upon a conservative representation of plasma arc mass loss data, some of which fell well below the mass loss correlation curve.

In order to assess the sensitivity of the mission life prediction in Figure 5-18 to the method of correlating mass loss data, an alternate correlation was obtained in terms of the parameter $\dot{M}/P_S^{0.5}$, as shown in Figure 5-19. Use of stagnation pressure P_S as the normalizing parameter, rather than heat transfer coefficient, is based upon the assumption that mass loss rate is determined by oxygen concentration at the surface, rather than oxygen diffusion rate. The exponent of pressure, 0.5, is somewhat arbitrary, but it has been commonly used for bare carbon. It is seen in Figure 5-18 that use of the alternate correlation has a relatively small effect upon the mission life prediction.

As discussed above, the time integrated erosion environment for shuttle reentry is equivalent to 134 seconds exposure of siliconized RPP to the surface temperature and heat transfer coefficient prevalent at the time of peak heating. For the plasma arc test environment, the equivalent exposure time was computed to be 105 seconds, the difference being due to the higher heat transfer coefficient h at a given surface temperature for the plasma arc tests, as compared with the reentry value at peak heating. This implies that a single 300 second plasma arc test exposure is equivalent to about three reentry missions for siliconized RPP. The three exposure cycles used for final evaluation of siliconized RPP are, therefore, equivalent to about nine reentry missions from an erosion standpoint.

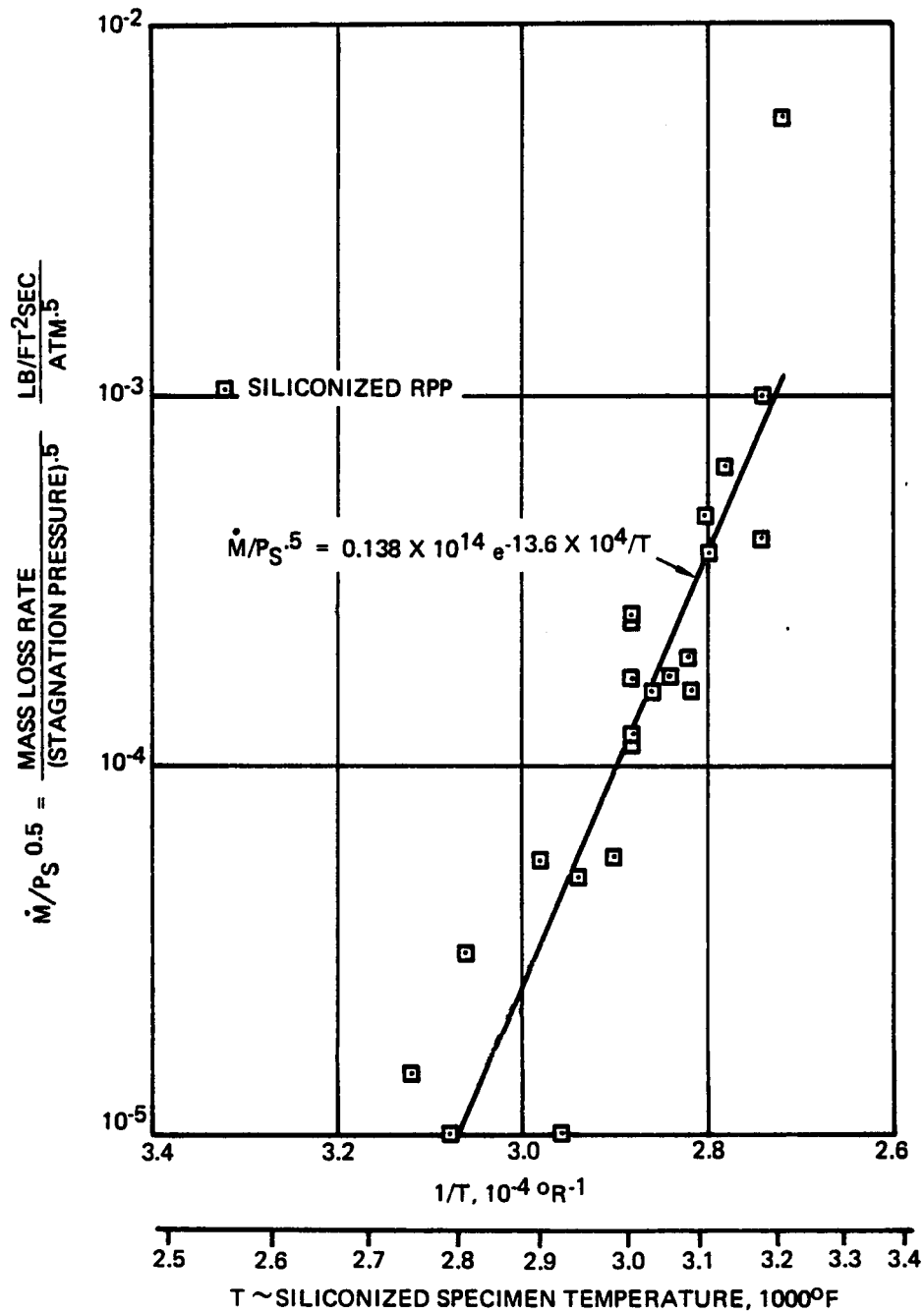


FIGURE 5-19 PLASMA ARC TEST MASS LOSS DATA REACTION RATE CONTROL CORRELATION

Over 120 plasma arc tests were performed on the modified inhibitor systems. These included multiple exposure tests and bare control runs for overspray, overlay, diffusion coated, melt and slurry coated RPP systems. A summary of results is given in Table 5-7 while photographs of selected specimens after tests are shown in Figures 5-20 through 5-22. The performance of each of these systems is briefly discussed below. Initial screening was performed at either the 140 or 160 Btu/ft² sec heat flux level (Test Points No. 5 and 2, respectively) and promising systems were then tested at lower heating rates (100, 120 and 130 Btu/ft² sec corresponding to Test Points No. 1, 4, and 6, respectively).

The alumina/chromia overspray coatings (set Nos. 1 and 2) performed poorly, melting and burning through at 160 Btu/ft² sec heat flux and melting without burnthrough at 100 Btu/ft² sec. Surface temperatures were near bare control specimen levels. These coatings were, therefore, eliminated from further consideration.

Vapor deposited silicon carbide coatings, provided by Super-Temp, burned through at both the 160 and 100 Btu/ft² sec heat flux level. Specimen 2X evidenced low catalytic behavior at the lower heat flux for three minutes, after which it heated up rapidly, indicating coating burnthrough. All other specimens burned through quickly. This system was therefore dropped from the program.

Set No. 4, the zirconia, zirconia-silicon overspray system delaminated at the 100 Btu/ft² sec heat flux level without melting and was eliminated. The coating temperature was above that of the control specimen.

Four hafnia overspray systems were evaluated, all exhibiting relatively poor adherence of the coating to the substrate. The Hf-W-Si system delaminated locally without melting at the 100 Btu/ft² sec heat flux and burned through at 160 Btu/ft² sec. Both the Hf and the Hf-Hf, W, Si oversprays on silicate treated substrate blistered locally without melting. All of the hafnia oversprays reached temperatures near bare control specimen levels. Due to the adherence problem these systems were eliminated; however, because of their good resistance to erosion, further effort was made to obtain a hafnia coating with good adherence. The resultant hafnium-tantalum coating will be discussed later.

Since siliconized RPP demonstrated excellent performance in the initial plasma arc screening tests, considerable effort was devoted to further improvement of this system. Six modifications to the original 18 series system were evaluated, along with duplicates of this system. Modifications included various processing temperatures, and heat treatment. Tests at the 100 Btu/ft² sec heat flux resulted in elimination of M5 (4000°F heat treatment) and M18 (4000°F process temperature) systems on the basis of higher mass loss than the M10 system (process duplication of original 18 series).

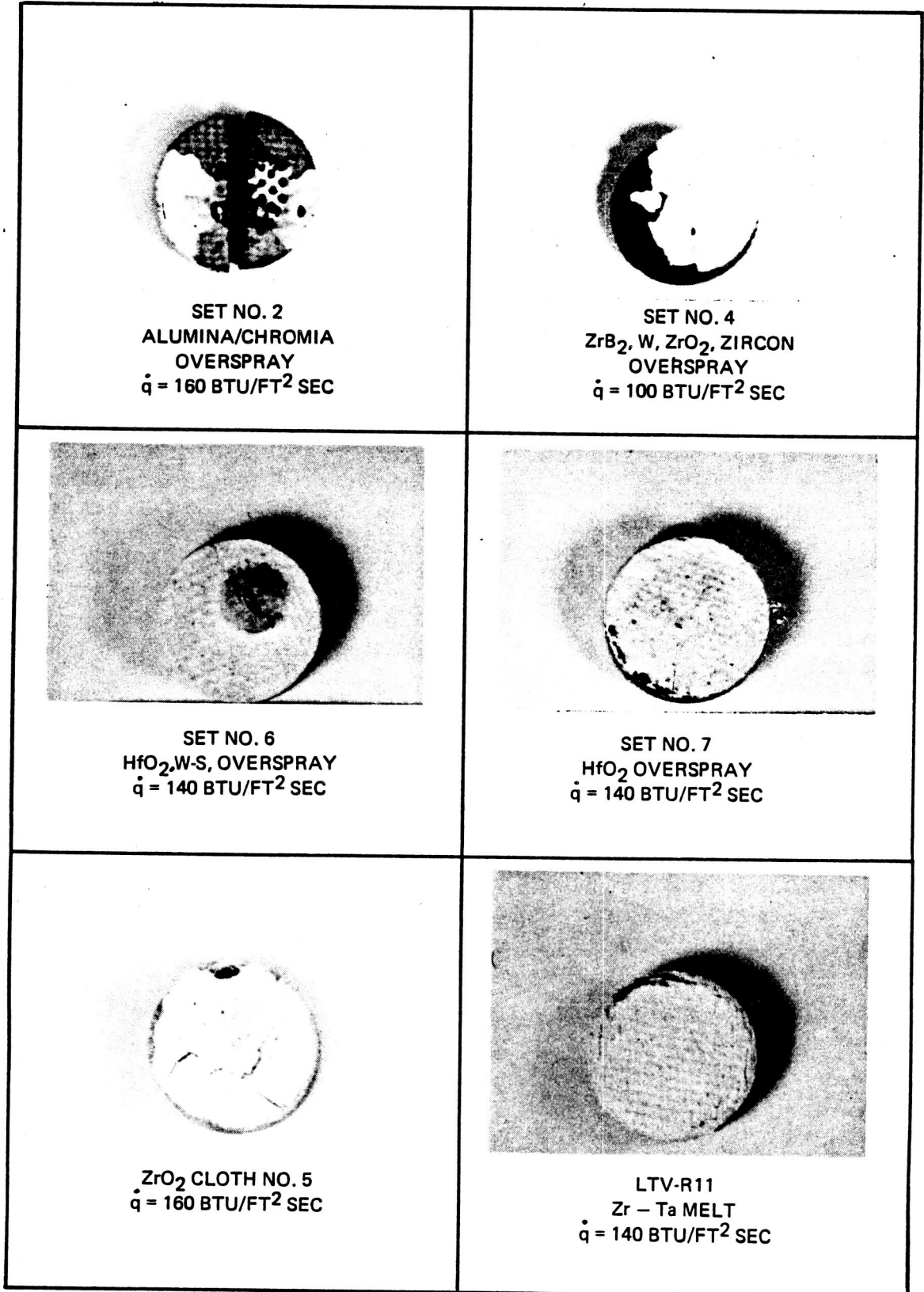
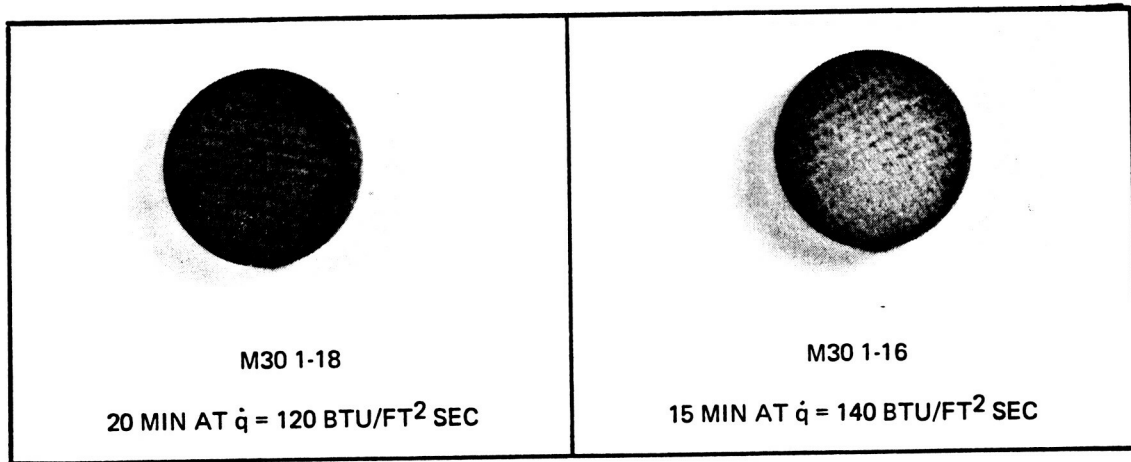
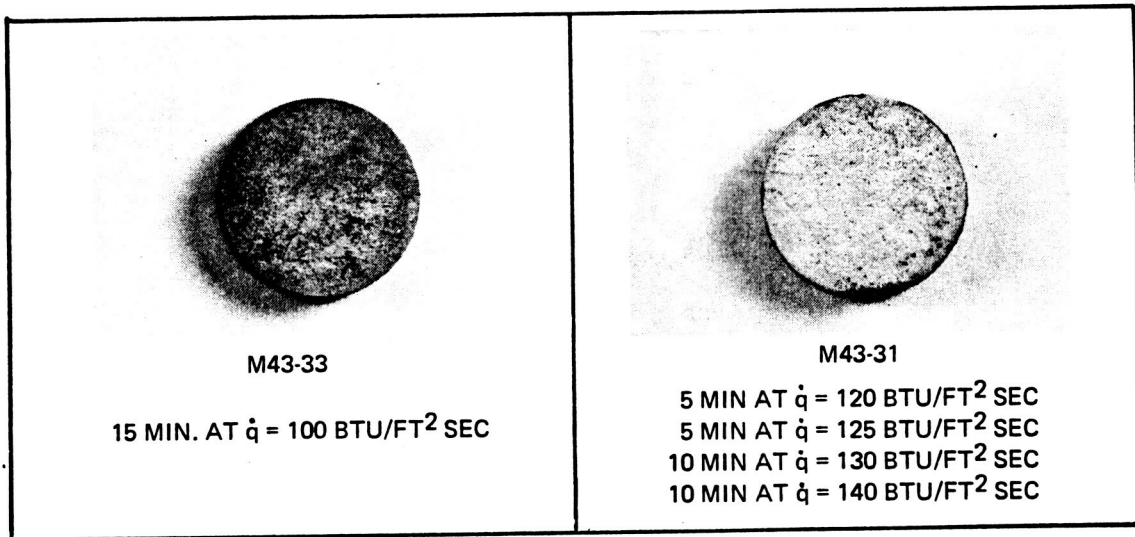


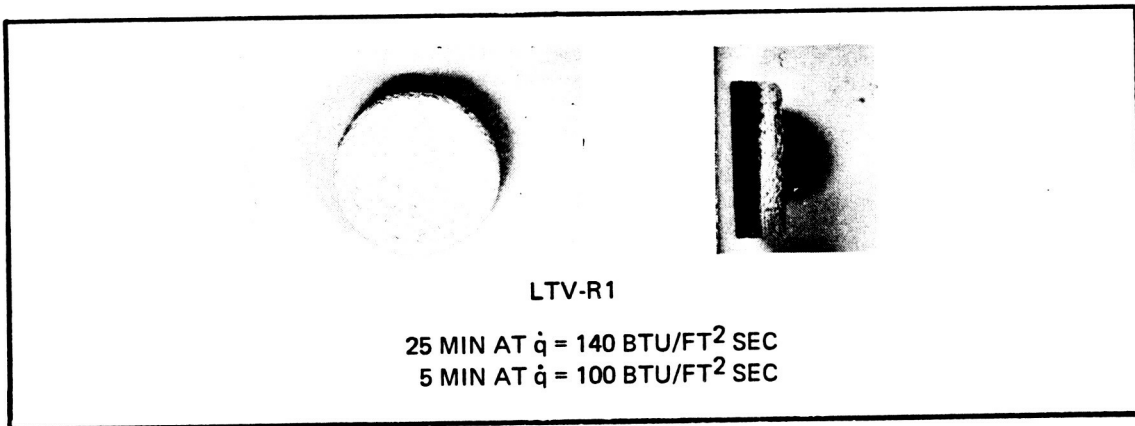
FIGURE 5-20 SELECTED SPECIMENS 3/4" DIA. AFTER PLASMA ARC EXPOSURE



M30 SILICONIZED SYSTEM

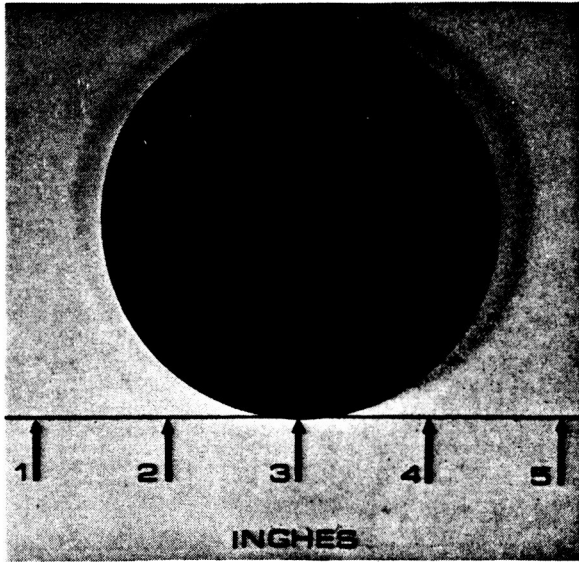


M43 Zr-B-Si SYSTEM



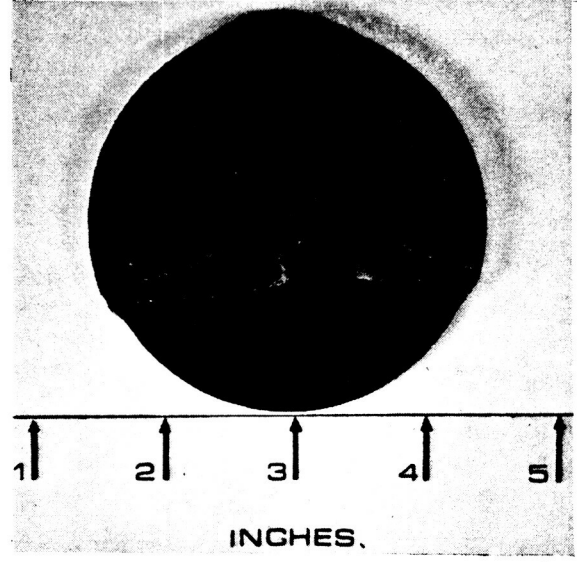
HAFNIUM • TANTALUM • RPP-0 SYSTEM

FIGURE 5-21 CANDIDATE COATING SYSTEMS FOLLOWING PLASMA ARC EXPOSURE 3/4 IN. DIA. SPECIMENS



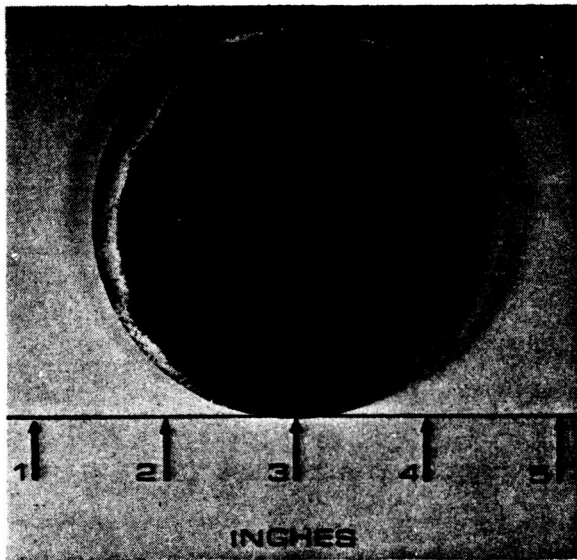
SPECIMEN M10-5 AFTER PLASMA TEST

EXPOSED SURFACE



SPECIMEN M10-6 AFTER PLASMA TEST

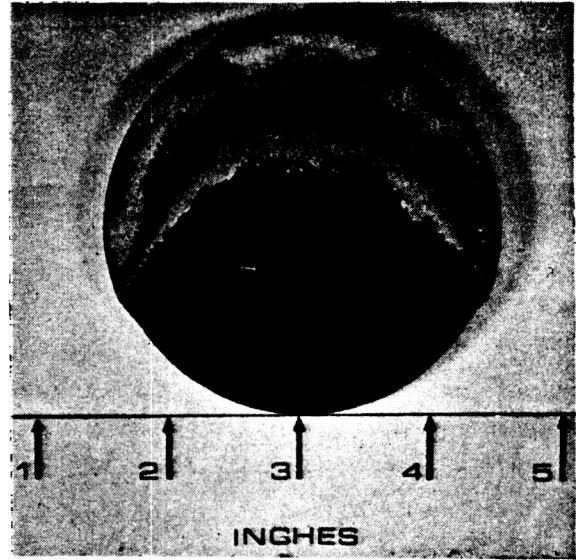
EXPOSED SURFACE



SPECIMEN M10-5 AFTER PLASMA TEST

BACKSIDE

SPECIMEN M10-5 AFTER 40 MINUTES EX-
POSURE AT 100 BTU/FT²-SEC FLUX LEVEL
LOW MASS LOSS
NO SURFACE RECESSION



SPECIMEN M10-6 AFTER PLASMA TEST

BACKSIDE

SPECIMEN M10-6 AFTER EXPOSURE TO
126 BTU/FT²-SEC AND SURFACE TEMP-
ERATURE OF 3220°F

FIGURE 5-22 SILICONIZED SPECIMEN AFTER EXPOSURE TO NASA-MSC PLASMA-ARC

TABLE 5-7
PLASMA ARC TEST SUMMARY

Test Point	Test Expo. Number	Specimen			Cold Wall Heat Flux BTU/ft ² sec	Stag. Enthalpy BTU/lb	Stag. Press. PSIA	Time Duration Seconds	Rad. Equil. Temp. °F(ε=.8)	Mass Loss 10 ⁻⁴ lb	Thick Loss in.	Avg. Recession Rate 10 ⁻⁴ in/sec	True Surface Temp. °F
		Process	Inhibitor	No.									
1	1	Bare Control	None	RPP3-10	105	7807	0.2	150	3440	14.9	0.076	5.06	3510
1	1	Over-spray	[Al ₂ O ₃ Cr ₂ O ₃]	Set 1-2	105	8522	→	300		0.558	-.002	0.000	3710
1	1	Over-spray	[Al ₂ O ₃ Cr ₂ O ₃]	Set 2-2	100	8522	→	300		0.660	-.007	0.000	3350
1	1	Over-spray	Hf, W, Si	Set 3-1	105	8740	→	300		0.194	-.001	0.000	3510
1	1	CVD	SiC	14-4-3	100	7915	→	300		24.7	0.112	3.73	3310
1	1	CVD	SiC	2X	105	8522	→	300		9.26	0.054	1.80	3020
1	1	Bare Control	None	RPP3-13	100	7630	→	150	3415	14.53	0.068	4.53	3290
1	1	Over-spray	ZrB ₂ , W, ZrO ₂ , ZrO ₂ , SiO ₂	Set 4-1	90	8730	0.2	300		Coating Delaminated			3610
2	1	Bare Control	None	RPP3-9	160	8920	0.4	100	3890	11.72	0.056	5.60	3690
2	1	Over-spray	[Al ₂ O ₃ Cr ₂ O ₃]	Set 1-1	160	8700	→	300		13.4	0.079	2.63	3800
2	1	Over-spray	[Al ₂ O ₃ Cr ₂ O ₃]	Set 2-1	160	10400	0.4	300		5.31	0.009	0.300	3560

Table 5-7
PLASMA ARC TEST SUMMARY (Cont'd.)

Test Point	Test Expo. Number	Specimen			Cold Wall Heat Flux BTU/ft ² sec	Stag. Enthalpy BTU/lb	Stag. Press. PSIA	Time Duration Seconds	Rad. Equil. Temp. °F(ε=.8)	Mass Loss 10 ⁻⁴ lb	Thick Loss in.	Avg. Recession Rate 10 ⁻⁴ in/sec	True Surface Temp. °F
		Process	Inhibitor	No.									
2	1	Over-spray	ZrO ₂	5	160	8980	0.4	300		2.18	-0.009	0.000	3640
	1	Over-spray	Hf, W, Si	Set 3-2	160	7735	→	300		18.20	0.09	3.00	3830
	1	CVD	SiC	IX	160	9290	→	300		26.1	0.106	3.52	3700
2	1	CVD	SiC	14-4-1	160	9120	0.4	300		30.1	0.132	4.40	3620
5	1	Bare Control	None	RPP3-23	140	7490	0.4	120	3715	13.1	0.064	5.33	3720
	1	Over-spray	ZrB ₂ , W, Hf	Set 5-1	140	7490	→	300		--	-0.013	0.00	3890
	1	Bare Control	None	RPP3-27	140	7840	→	120		11.8	.061	5.08	3600
	1	Over-spray	Hf; Hf, W, Si	Set 6-2	140	8860	→	300					3640
5	1	Over-spray	Hafnia	Set 7-1	140	8860	0.4	300					3640

Table 5-7
PLASMA ARC TEST SUMMARY (Cont'd.)

Test Point	Test Expo. Number	Specimen		Cold Wall Heat Flux BTU/ft ² sec	Stag. Enthalpy BTU/lb	Stag. Press. PSIA	Time Duration Seconds	Rad. Equil. Temp. °F(ε=.8)	Mass Loss 10 ⁻⁴ lb	Thick Loss in.	Avg. Recession Rate 10 ⁻⁴ in/sec	True Surface Temp. °F
		Process	Inhibitor									
1	1	Bare Control	None	100	6670	.2	150	3390	15.05	.067	4.47	3330
	1	Diffusion	SiC	100	8957	—	300		0.514	0.001	0.03	2910
	2	Diffusion	SiC	97	8500	—	300		0.181	.000	.000	2840
	1	Diffusion 4000°H. T.	SiC	90	6670	—	300		1.035	.001	0.03	2860
	1	Diffusion 4000°	SiC	100	5050	—	300		1.872	.002	0.06	2910
	1	Bare Control	None	100	9680	—	150	3440	14.3	.077	5.13	3360
	1	Diffusion 20% Al ₂ O ₃	SiC	100	6880	—	300		0.046	0.001	.033	2810
	1	Bare Control	None	94	6900	—	150	3350	13.6	0.067	4.47	3280
	2	Diffusion 20% Al ₂ O ₃	SiC	94	6900	.2	300		0.022	0.000	0.000	2750
	3	"	"	"	"	"	"		0.000	0.001	0.033	2780
	1	Bare Control	None	160	8920	.4	100	3890	11.72	0.056	5.6	3690
	1	Diffusion	SiC	140	10950	—	300		1.525	0.008	0.266	3020
	1	Diffusion	SiC	160	8699	—	300		15.3	0.112	3.73	3460
	1	Bare Control	None	160	8640	—	300	3880	11.9	0.054	5.40	3790
	1	Diffusion 33% Al ₂ O ₃	SiC	150*	7650	.4	300		.968	.001	0.03	3140

Table 5-7
PLASMA ARC TEST SUMMARY (Cont'd.)

Test Point	Test Expo. Number	Specimen			Cold Wall Heat Flux BTU/ft ² sec	Stag. Enthalpy BTU/lb	Stag. Press. PSIA	Time Duration Seconds	Rad. Equil. Temp. °F(ε=.8)	Mass Loss 10 ⁻⁴ lb	Thick Loss in.	Avg. Recession Rate 10 ⁻⁴ in/sec	True Surface Temp. °F
		Process	Inhibitor	No.									
2	1	Bare Control	None	RPP3-19	160	9010	.4	100	3890	12.1	0.053	5.3	3810
2	1	Diffusion	SiC	18-6	160	9010	.4	300		10.25	0.072	2.4	3140
4	1	Bare Control	None	RPP3-20	120	7990	.4	120	3580	12.4	0.059	4.92	3610
	1	Diffusion 33% Al ₂ O ₃	SiC	M26-2	119	7240		300		0.36	.000	.000	3020
	1	Diffusion 16% Al ₂ O ₃	SiC	M26-10	120	7740		300		0.386	.000	0.00	3020
	1	Diffusion 3200°F	SiC	M28-2	120	7740		300		0.952	.001	0.03	3010
	1	Diffusion 3400°F H.T.	SiC	M19-6	122	6440		300		0.428	.001	0.03	3040
	1	Bare Control	None	RPP3-22	120	7070		120	3555	11.3	0.058	4.83	3560
	1	Diffusion 20% Al ₂ O ₃	SiC	M30, 1-18	120	7640		300		0.260	0.000	0.000	3020
	2	Diffusion 20% Al ₂ O ₃	SiC	M30, 1-18	120	7640		300		0.180	0.001	0.03	3020
	3	Diffusion 20% Al ₂ O ₃	SiC	M30, 1-18	120	7640		300		0.234	0.001	0.03	3030
4	1	Bare Control	None	RPP3-36	120	5940	.4	150	3520	13.23			3500

Table 5-7
PLASMA ARC TEST SUMMARY (Cont'd.)

Test Point	Test Expo. Number	Specimen		Cold Wall Heat Flux BTU/ft ² sec	Stag. Enthalpy BTU/lb	Stag. Press. PSIA	Time Duration Seconds	Rad. Equil. Temp. °F(€- 8)	Mass Loss 10 ⁻⁴ lb	Thick Loss in.	Avg. Recession Rate 10 ⁻⁴ in/sec	True Surface Temp. °F
		Process	Inhibitor									
4	4	Diffusion	SiC	120*	6290	.4	300		0.075	0.000	0.000	2940
	1	20% Al ₂ O ₃										
	2	Diffusion	SiC	120*	6290		300		0.000	0.000	0.000	2910
4	2	Diffusion	SiC	120	6290	.4	300		0.084	0.000	0.000	2900
5	1	Bare	None	140*	7500	.4	120	3715	13.2	.063	5.25	3690
	1	Control										
	1	Diffusion	SiC	140*	7500		300		.615	.002	0.066	3180
	1	33% Al ₂ O ₃										
	1	Diffusion	SiC	140*	7490		300		.578	-.001	0.000	3100
	1	3400° II. T.										
	1	Diffusion	SiC	140*	7490		300		.662	.001	0.03	3100
	1	Type 18										
	1	Diffusion	SiC	140*	7490		300		.560	.002	.066	3110
	1	16% Al ₂ O ₃										
	1	Bare	None	140	7490		120	3715	13.1	.064	5.33	3720
	1	Control										
	1	Diffusion	SiC	140	7490		300		0.24	-.001	0.00	3080
	1	16% Al ₂ O ₃										
	1	Bare	None	140	7840		120	3725	11.8	.061	5.08	3600
	1	Control										
5	1	Diffusion	SiC	140	7560	.4	300		0.71	0.002	0.067	3120
	1	20% Al ₂ O ₃										

Calorimeter inoperative, based upon subsequent calibration of heat flux versus amperage.

Table 5-7
PLASMA ARC TEST SUMMARY (Cont'd.)

Test Point	Test Expo. Number	Specimen			Cold Wall Heat Flux BTU/ft ² sec	Stag. Enthalpy BTU/lb	Stag. Press. PSIA	Time Duration Seconds	Rad. Equil. Temp. °F(°C)	Mass Loss 10 ⁻⁴ lb	Thick Loss in.	Avg. Recession Rate 10 ⁻⁴ in/sec	True Surface Temp. °F
		Process	Inhibitor	No.									
5	1	Bare Control	None	RPP3-29	140	8210	.4	120	3730	13.12	0.065	5.41	3690
	2	Diffusion 20% Al ₂ O ₃	SiC	M30, 1-16	140	8860		300		0.291	.002	.067	3080
	3	Diffusion 20% Al ₂ O ₃	SiC	M30, 1-16	140	8860		300		0.086	-.001	.000	2980
	1	Bare Control	None	RPP3-35	140	7290		150	3710	15.76	0.079	5.26	3670
	1	Diffusion	SiC	M31-15	140	7290		300		0.170	0.000	0.000	3020
5	2	Diffusion	SiC	M31-15	140	7410	.4	300		0.258	0.001	0.033	3060

Table 5-7
PLASMA ARC TEST SUMMARY (Cont'd.)

Test Point	Test Expo. Number	Specimen			Cold Wall Heat Flux BTU/ft ² sec	Stag. Enthalpy BTU/lb	Stag. Press. PSIA	Time Duration Seconds	Rad. Equil. Temp. °F(ε=.8)	Mass Loss 10 ⁻⁴ lb	Thick Loss in.	Avg. Recession Rate 10 ⁻⁴ in/sec	True Surface Temp. °F
		Process	Inhibitor	No.									
1	1	Bare Control	None	RPP3-12	100	6670	.2	150	3390	15.05	.067	4.47	3330
	1	Diffusion 2750°, 22% Si	Zr, B, Si	M6-16 M17-1	98	8980		300		0.552	.002	0.06	2965
	1	Bare Control	None	RPP3-24	100	7800		150	3420	15.3	.076	5.07	3440
	2	Diffusion 2750°, 22% Si	Zr, B, Si	M6-16 M17-1	100	7650		300		0.181	.003	0.10	2955
	1	Diffusion 3000°, 75% Si	Si, Zr	M29-9	100	7800		300		0.002	0.001	0.03	2860
	1	Bare Control	None	RPP3-26	100	8020		150	3420	14.2	.076	5.07	3340
	2	Diffusion 3000°, 75% Si	Si, Zr	M29-9	100	8020		300		.0485	-.002	0.000	2840
	1	Bare Cont.	None	RPP3-46	100	6970		150	3400	12.51	0.064	4.30	3210
	1	Diffusion B+Zr	B+Zr	M43-33	100	5750		300		-.123	.000	.000	2720
	1	Bare Cont.	None	RPP3-47	100	8150		150	3420	12.35	.062	4.13	3130
	2	Diffusion B+Zr	B+Zr	M43-33	100	7950		300		-.042	.0005	0.016	2690
	1	Bare Cont.	None	RPP3-48	100	8670		150	3430	14.1	.0735	4.9	3370
1	3	Diffusion B+Zr	B+Zr	M43-33	100	7850	.2	300		.0308	.000	0.000	2820

Table 3-1
 PLASMA ARC TEST SUMMARY (Cont'd.)

Test Point	Expo. Number	Specimen			Cold Wall Heat Flux BTU/ft ² sec	Stag. Enthalpy BTU/lb	Stag. Press. PSIA	Time Duration Seconds	Rad. Equil. Temp. °F (ε=.8)	Mass Loss 10 ⁻⁴ lb	Thick Loss in.	Avg. Recession Rate 10 ⁻⁴ in/sec	True Surface Temp. °F
		Process	Inhibitor	No.									
5	1	Bare Control	None	RPP3-23	140	7490	.4	120	3715	13.1	.064	5.33	3720
	1	Diffusion 3400°, 2.9% Si	Zr, B	M27-3	140	7490		300		20.2	.124	4.13	3770
	1	Diffusion 2750°, 22% Si	Zr, B	M21-1	140	7490		300		14.9	.103	3.43	3810
	1	Diffusion 3000°, 75% Si	Si, Zr	M29-8	140	7490		300		2.85	.01	0.30	3750
	1	Bare Control	None	RPP3-27	140	7840		120	3725	11.8	.061	5.08	3600
	2	Diffusion 3000°, 75% Si	SiZr	M29-8	140	7840		300		1.93	.004	0.133	3350
	1	Diffusion 3000°, 87-1/2% Si	ZrSi	M32B-1	140	7560		300		0.778	0.005	0.1667	3150
	1	Diffusion 3400°, 100% Br	Zr+B	M35-2	140	7560		300		9.58	0.05	1.667	4050
	1	Diffusion 3400°, 75% Si	B + Zr	M33A-1	140	7560	.4	300		0.080	0.003	0.10	3020

Table 5-7
 PLASMA ARC TEST SUMMARY (Cont'd.)

Point Number	Test Expo. Number	Specimen			Cold Wall Heat Flux BTU/ft ² -sec	Stag. Enthalpy BTU/lb	Stag. Press. PSIA	Time Duration Seconds	Rad. Equil. Temp. °F (€=.8)	Mass Loss 10 ⁻⁴ lb	Thick Loss in.	Avg. Recession Rate 10 ⁻⁴ in./sec	True Surface Temp. °F
		Process	Inhibitor	No.									
4	1	Bare Control	None	RPP3-32	120	7070	.4	120	3555	11.3	0.058	4.83	3560
	1	Diffusion 75% Si	B + Zr	M33A-3	120	7640		300		--	0.001	0.033	3040
	1	Diffusion 75% Si	B + Zr	M33A-2	120	7640		300		Coating Burned Through			3200
	1	Bare Control	None	RPP3-36	120	5940		150	3520	13.23			3500
	1	Diffusion 75% Si	B + Zr	M32A-2	120	5940		300		-.020	--	--	2770
	2	Diffusion 75% Si	B + Zr	M32A-2	120	6290		300		0.092			2770
	1	Bare Cont	None	RPP3-42	120	6300		150	3540		.067	4.46	3370
	1	Diffusion	B+Zr	M43-20	120	5940		300		0.048	.000	.000	2830
	2	Diffusion	B+Zr	M43-20	120	5940		300		0.072	.000	.000	2860
	3	Diffusion	B+Zr	M43-20	120	5940		300		0.053	.0005	0.017	2820
	1	Bare Cont	None	RPP3-43	120	5940		150	3520	13.95	.069	4.60	3440
	1	Diffusion	B+Zr	M43-31	120	5575	.4	300		0.028	.0015	0.050	2870
4	1	Bare Cont	None	RPP3-49	130	7950	.4	150	3650	15.2	0.076	5.10	3560
6	1	Diffusion	B+Zr	M43-34	130	7110		300		0.908	0.002	0.083	3040
	1	Bare Cont	None	RPP3-50	130	6090		150	3600	15.7	0.074	4.93	3550
	1	Bare Cont	None	RPP3-52	130	6820		150	3620	14.9	0.072	4.83	3420
	3	Diffusion	B+Zr	M43-31	130	7300		300		.114	.0005	0.017	2900
6	4	Diffusion	B+Zr	M43-31	130	6690	.4	300		.1100	0.000	0.000	2930
7	1	Bare Cont	None	RPP3-51	125	7075	.4	150	3610	15.9	0.078	5.22	3560

Table 5-7
PLASMA ARC TEST SUMMARY (Cont'd.)

Test Point	Test Expo. Number	Specimen			Cold Wall Heat Flux BTU/ft ² sec	Stag. Enthalpy BTU/lb	Stag. Press. PSIA	Time Duration Seconds	Rad. Equil. Temp. °F(ε=.8)	Mass Loss 10 ⁻⁴ lb	Thick Loss in.	Avg. Recession Rate 10 ⁻⁴ in./sec	True Surface Temp. °F
		Process	Inhibitor	No.									
5	1	Diffusion 3400°, 87-1/2% Si	B + Zr	M33B-1	140	7560	.4	300		15.0	0.078	2.60	2990
	1	Diffusion 3000°, 75%Si	ZrB ₂	M32A-1	140	7560		300		1.38	.003	0.10	3170
	1	Bare Control	None	RPP3- 35	140	7290		150	3710	15.76	0.079	5.26	3670
	2	Diffusion 3000°, 75% Si	ZrB ₂	M32A-1	140	7290		300		0.990	0.009	0.300	3430
	3	Diffusion 3000°, 75% Si	ZrB ₂	M32A-1	140	7410		300		0.97	0.001	0.033	3470
	1	Bare Control	None	RPP3- 27		7840		120	3725	11.8	.061	5.08	3600
	1	Diffusion 50% Si	B + Zr	M38-1	140	8860		300		4.43	-.008	0.000	3740
	1	Bare Control	None	RPP3- 29	140	8210		120	3730	13.12	0.065	5.41	3690
5	1	Diffusion 50% Si	B + Zr	M39-1	140	8210	.4	300		10.30			3630

Table 5-7
 PLASMA ARC TEST SUMMARY (Cont'd.)

Test Point	Test Expo. Number	Specimen		Cold Wall Heat Flux Btu/ft ² sec	Stag. Enthalpy Btu/lb.	Stag. Press. PSIA	Time Duration Seconds	Rad. Equil. Temp. °F (±.8)	Mass Loss 10 ⁻⁴ lb	Thick Loss in.	Avg. Rec. Rate 10 ⁻⁴ in/sec	True Surface Temp. °F
		Process	Inhibitor									
5	1	BareCont.	None	140	7190	.4	150	3705	15.0	.074	4.93	3580
	1	Diffusion	B+Zr	140	7190		300		0.051	.0005	0.000	3080
	2	Diffusion	B+Zr	140	8250		300		0.395	.001	0.030	3080
	1	Bare Cont.	None	140	8040		150	3730	14.8	.073	4.87	3580
	3	Diffusion	B+Zr	140	8080		300		0.785	.0005	0.016	3080
	1	Bare Cont.	None	140	5625		150	3650	15.8	.0775	5.16	3670
	5	Diffusion	B+Zr	140	5625		300		.1804	.0005	0.016	3040
5	6	Diffusion	B+Zr	140	5625	.4	300		.172	.001	0.03	3080

Table 5-7
 PLASMA ARC TEST SUMMARY (Cont'd.)

Test Point	Test Expo. Number	Specimen			Cold Wall Heat Flux BTU/ft ² sec	Stag. Enthalpy BTU/lb	Stag. Press. PSIA	Time Duration Seconds	Rad. Equil Temp. °F(ε=.8)	Mass Loss 10 ⁻⁴ lb	Thick Loss in.	Avg. Recession Rate 10 ⁻⁴ in/sec	True Surface Temp. °F
		Process	Inhibitor	No.									
1	1	Bare Control	None	RPP3-33	100	8150	.2	150	3420	14.3	0.079	5.26	3480
1	6	Melt	Hf, Ta	LTVR1	100	7383	.2	300		0.575	0.000	0.000	3780

Table 5-7
PLASMA ARC TEST SUMMARY (Cont'd.)

Test Point	Test Expo. Number	Specimen			Cold Wall Heat Flux BTU/ft ² sec	Stag. Enthalpy BTU/lb	Stag. Press. PSIA	Time Duration Seconds	Rad. Equil Temp. °F (€-.8)	Mass Loss 10 ⁻⁴ lb	Thick Loss in.	Avg. Recession Rate 10 ⁻⁴ in./sec	True Surface Temp. °F
		Process	Inhibitor	No.									
5	1	Bare Control	None	RPP3-27	140	7840	.4	120	3725	11.8	.061	5.08	3600
	1	Melt	Hf, Ta	LTVR1	140	8860		300		-0.424	-.006	0.000	3700
	2	Melt	Hf, Ta	LTVR1	140	8860		300		0.148	-.003	0.000	3700
	3	Melt	Hf, Ta	LTVR1	140	8860		300		0.220	-.003	0.000	4130
	1	Bare Control	None	RPP3-29	140	8210		120	3730	13.12	0.065	5.41	3690
	4	Melt	Hf, Ta	LTVR1	140	8860		300		0.167	-.001	.000	4180
	5	Melt	Hf, Ta	LTVR1	140	8860		300		0.388	-.001	.000	4180
	1	Bare Control	None	RPP3-35	140	7290		150	3710	15.76	0.079	5.26	3670
	1	Slurry	Hf, Ta	LTVR6	140	7290		300		-1.165	-.007	0.000	3650
	2	Slurry	Hf, Ta	LTVR6	140	7290		300		0.430			3740
	1	Melt	Zr, Ta	LTVR11	140	7290		300		-.754	-.005	0.000	3860
5	2	Melt	Zr, Ta	LTVR11	140	7290	.4	300		0.551	-.011	0.000	3920
6	1	Bare Control	None	RPP3-52	130	6825	.4	150	3620	14.9	.0725	4.83	3420
	1	Melt on Silc. RPP	Hf, Ta	HT-9	130	6825		300		-1.6	-.027	0.000	3310
	1	Salted on Silc. RPP	Hf, Ta	HT-8	130	6825		300		-.291	0.000	0.000	2960
	1	Slurry on Boron	Hf, Ta	HT-11	130	6825		300		Coating Burned Thru			3700
	1	Slurry on Silc. RPP	Hf, Ta	HT-12	130	6500		300		-1.03	0.022	0.75	3000
	2	" "	" "	" "	130	6500		300		-0.108	-0.001	0.000	3050
	1	Slurry on											

Tests at 120 Btu/ft² sec eliminated the M28 system (3200° F process temperature) on the basis of relatively high mass loss. Tests at 140 Btu/ft² sec resulted in selection of the M26 system (16% alumina in pack), based upon its low mass loss at this heat flux relative to the remaining systems coupled with greater ease of fabrication. The selected system demonstrated low mass loss rates at 100, 120, and 140 Btu/ft² sec heat flux rates with three exposures per specimen. Only slight surface degradation was evident at the highest heating rate, with some discoloration at the lower levels. Based upon these results, siliconized RPP was selected as the prime candidate for Phase II effort.

Final evaluations were performed on the M30 and M31 series of siliconized RPP specimens to determine mass loss rates for multiple cycle exposures. Two to four cycles were included in these tests, which were equivalent to six to twelve reentry missions, respectively. At the lower heat flux rates, 100 and 120 Btu/ft² sec, exposed surfaces of the specimens were only discolored and at the highest heat flux, 140 Btu/ft² sec, only slight surface degradation was experienced. In general, mass loss rates decreased from cycle to cycle, and non-catalytic behavior was observed in all tests. Mass loss rates were similar to those obtained in previous tests of the M26 series of specimens.

Zirconia-Boron-Silicon Treated RPP was selected during the screening tests as a second system for further development. Nine modifications to this system were evaluated, primarily at the 140 Btu/ft² sec heat flux level. These modifications included various process temperatures, percentages of silicon in the pack and percentages of boron. The M32A system (3000° process temperature, 75% silicon in pack) was selected on the basis of low mass loss and low surface recession in these tests. The M32A system was subjected to three cycles at 140 Btu/ft² sec and two cycles at 120 Btu/ft² sec heat flux. Mass loss and recession were low in both tests. A uniform adherent yellow-gray coating was formed at the lower heating rate and the surface temperature was about equal to that of siliconized RPP. At the higher heating rate, the coating was formed only in local areas where the temperature was near bare control specimen levels. In the uncoated areas temperatures were about equal to that of siliconized RPP.

Final evaluations of Zr-B-Si treated RPP were performed on the M43 series of specimens to assess multiple cycle performance. Specimens were exposed to three to four exposure cycles at heat flux rates from 100 to 140 Btu/ft² sec. A yellow-gray coating was formed on the surface of all specimens. This coating was generally quite thin. However, in local areas at the higher heating rates (130-140 Btu/ft² sec) a relatively thick coating was formed. Temperatures of the thin coating were about equal to those for siliconized RPP, and coating stability was good under multiple exposures in these areas. The thickly coated areas ran considerably hotter, near radiation equilibrium, and degraded under multiple exposures. Mass loss rates were generally slightly higher than those for siliconized RPP.

The hafnium/tantalum melt coatings represented an attempt to duplicate the excellent erosion resistance of hafnia overspray coatings while achieving a more adherent coating. This effort was successful for a coating applied to RPP-0, a 62 lb/ft³ density substrate (no reimpregnation). The metal coating converted to an oxide upon initial exposure to a heat flux rate of 140 Btu/ft² sec, with some gain of weight and thickness. One specimen was cycled five times at this heating rate and once at 100 Btu/ft² sec with no surface recession and only small mass loss. The white oxide coating was strong and adherent following these exposures. An anomaly was observed in the surface temperature, which was near the bare control specimens level for the first two exposures and 450 to 500°F higher than the control specimen for subsequent exposures at 140 Btu/ft² sec. At 100 Btu/ft² sec coated specimen temperature was 300°F higher than the control level. There was no visible change in the coating corresponding to the increased temperature, and control specimens confirmed that the heat flux rate had not increased. There was no evidence that the increased temperature degraded coating performance. This coating was not selected as the primary candidate because of limited evaluation and difficulties in application to the high strength reimpregnated substrate, RPP-3, but it is considered an excellent candidate for further development effort.

The hafnium/tantalum slurry coated RPP-0 was cycled twice at 140 Btu/ft² sec and demonstrated low mass loss rates with temperatures near control specimen level. There was evidence of sub-surface oxidation attack, however. Cross-sectioning revealed only a thin 5 mil coating whereas the above melt coating had a 30 mil coating. Multi-application of slurry layers may solve the thickness problem.

The zirconium/tantalum melt coating was also cycled twice at 140 Btu/ft² sec with low mass loss and temperatures about 200°F above the control specimen. Again, there was evidence of sub-surface oxidation attack and the zirconium/tantalum oxide is weaker than the corresponding hafnium/tantalum oxide. For these reasons continued emphasis should be placed on the hafnium rather than the zirconium.

Hafnium/tantalum coatings over siliconized RPP were evaluated as an approach to solving the problem of sub-surface oxidation. Three coating approaches were evaluated, melt, salt, and slurry. The melted on coating, HT-9, formed a hard coating which blistered and fell off after test. Surface temperature was near the bare control level. The salted, or sprinkled on, and melted coating, HT-8, formed a thin uneven grey coating which ran well below the bare control temperature level, supposedly due to presence of silicon in the coating causing non-catalytic behavior. The slurry coating, HT-12, formed a light grey surface coating which held up well for one exposure but locally chipped off after the second exposure. There was evidence of substrate degradation. Weight increase due to oxidation was experienced on all three coatings and surface recession was generally nil.

Hafnium/tantalum slurry coatings over boronized and ZR-B-Si treated RPP were evaluated as alternate solutions to the sub-surface oxidation problem. The slurry coating on boronized RPP became very fragile and degraded during testing. Surface temperature was well above that of the bare control specimen. The slurry coating on Zr-B-Si treated RPP formed a very uneven surface coating, which peeled off locally at the edge during test. Surface temperature was well below that of the bare control specimen.

Only limited experimentation was conducted with hafnium/tantalum overlaying diffusion coated RPP. The exceptional performance of the hafnium/tantalum coating does, however, suggest continued exploration of this system on diffusion coated as well as on the bare RPP.

5.2.2 NASA-MSC Evaluation of Siliconized RPP

Fourteen tests were performed on the M10 series of siliconized RPP specimens in the NASA-MSC 10 MW plasma arc facility. These were performed on 3-inch diameter by 0.25-inch thick discs in a 4-inch diameter graphite shroud holder. The backsides of the specimens were insulated by 0.75 inch thickness of graphite felt insulation to minimize heat losses. A summary of the test conditions and results obtained to date is given in Table 5-8.

It is seen that no surface recession and very slight mass loss was obtained in 40 minutes of exposure of specimen M10-5 at a heat flux rate of 100 Btu/ft² sec, corresponding to a surface temperature of 3450° F on bare RPP. The computed value of \dot{M}/h for these tests (1.21×10^{-3}) is an order of magnitude lower than that obtained in VMSC tests of the M10 material at the same temperature, and agrees well with values obtained in VMSC tests for later modification of siliconized RPP. As in the VMSC tests, surface temperature of the siliconized material was well below that of the control specimen. Computed surface re-radiation heat flux was 0.578 of that for the bare RPP control specimen, compared to 0.543 for the M10 material at the same heat flux in the VMSC tests. The M10-5 specimen was in good condition following test as shown in the photograph in Figure 5-22. The only surface change was discoloration.

On specimen M10-7 there was no surface recession and very low mass loss after 10 minutes of exposure to a heat flux of 100 Btu/ft² sec, corresponding to 3600° F on the bare control specimen, and 5 minutes exposure at 115 Btu/ft² sec. A value of \dot{M}/h could not be computed due to lack of a value for enthalpy, however, mass loss rate for M10-7 appears to be in better agreement with VMSC results for the M10 material than that obtained on specimen M10-5. Surface temperature of M10-5 was 750° F below that of the control specimen. Re-radiation flux was 0.414 of that for the bare control specimen, considerably lower than the value for M10-5 and values obtained by VMSC. The value of \dot{M}/h for the control specimen (0.262) was in good agreement with values obtained in VMSC tests.

TABLE 5-8
PLASMA ARC TEST SUMMARY, NASA-MSC TESTS

Test Facility	Specimen Number	Cold Wall Heat Flux Btu/ft ² sec	Stagnation Enthalpy Btu/lb	Stag. Press. PSIA	Time Duration per Expos. Seconds	Number of Exposures	Surface Temp. °F	Mass Loss lb	Surface Recession Inch
10 MW	Bare Control	100	12000	.25		1	3450	} .932x10 ⁻³ cumulative	0.000
	M10-5	63	6100	.207	300	1	2600		0.000
	M10-5	100	12000	.25	300	5	3000		0.000
	M10-5	100	12000	.25	900	1	3000	0.798x10 ⁻³	0.000
	M10-6	50		.207	300	1		0.000	0.000
	M10-6	126		.379	300	1	3250	Coating Burned Thru	
1.5 Mev	Bare Control	100	17000	.101	120	1	3600	7.72x10 ⁻³	.013
	M10-7	100			300	2	2850	} 1.59x10 ⁻³ cumulative	0.000
	M10-7	115			300	1	2950		0.000
	M10-7	>100			780	1			
	M10-7	>100			1200	1	2995 (3300 on hot spot)	4.07x10 ⁻³	0.003

Additional 13 minute and 20 minute tests were performed on specimen M10-7 at a heat flux rate greater than 100 Btu/ft² sec. Data obtained to date for these tests is incomplete; however, it is known that the specimen was in good condition following the 13 minute exposure. Centerline surface temperature on the 20 minute run was 2995°F and surface recession was slight (0.003"). The mass loss measurement is not meaningful since part of the specimen was heated to about 3300°F due to erosion of the holder, resulting in local coating burn through.

Specimen M10-6 was exposed to 5 minutes at a heat flux of 50 Btu/ft² sec followed by 5 minutes at 126 Btu/ft² sec. Coating failure was obtained at the 126 Btu/ft² sec level, Figure 5-23, compared to 155 to 160 Btu/ft² sec for siliconized RPP in the VMSC tests. Since only one specimen was tested to failure, further evaluation will be required to determine if this difference between NASA-MSD and VMSC test results is repeatable, and if so, to establish the reason for the difference. The temperature at coating failure, which occurred after 4 minutes exposure, was 3250°F, which is in agreement with VMSC test results. Coating burnthrough occurred on only one-half of the specimen surface, as shown in Figure 5-23. The reason for this peculiar behavior is not known. Degradation of the coating on the backside of the specimen is undoubtedly due to high temperatures obtained on the bare carbon following coating failure (3500°F).

In summary, the NASA-MSD plasma arc tests confirmed the very low mass loss rates and surface recession for siliconized RPP that were obtained in VMSC tests. Excellent coating performance was demonstrated at heat flux rates in excess of 100 Btu/ft² sec, corresponding to bare carbon temperatures of 3450-3600°F. Coating temperature limit of 3200-3250°F was also confirmed, as were the low surface temperatures of siliconized RPP at a given heat flux rate, relative to bare RPP. Heat flux rate required to cause coating failure, as obtained on a single specimen, was about 20% below the value established in VMSC tests.

5.3 SURFACE CATALYTIC EFFECTS

Plasma arc tests of inhibited RPP in the NASA-MSD 10 MW facility and the MSD 180KW facility have resulted in measured surface temperatures significantly lower than both radiation equilibrium values and values for uninhibited RPP. Calculations indicate that neither heat leakage to the holder, endothermic chemical reactions, specimen heat sink effects nor high emittance fully explain the low measured temperatures, examples of which are shown in Table 5-9.

TABLE 5-9
TYPICAL PLASMA ARC TEST RESULTS FOR RPP

<u>Test Facility</u>	<u>Material</u>	<u>Hot Wall Heat Flux, Btu/ft² sec</u>	<u>Surface Temp °F</u>	<u>Re-radiation Heat Flux Btu/ft² sec</u>
NASA 10 MW	Bare RPP	90	3450	95
	Siliconized RPP	92	3000	55
MSD 180KW	Bare RPP	119	3690	120
	Zr-B-Si Treated RPP	121	3080	60
	Siliconized RPP	122	3110	62

For bare RPP, re-radiation heat flux based upon measured surface temperature agrees reasonably well with measured convective heating rates. For Zr-B-Si treated and siliconized RPP, re-radiation flux is only 50% of measured incident heating. It has further been observed for diffusion systems, when melt-through of the oxidation inhibited layer occurs, exposing bare RPP, a sharp rise in surface temperature occurs.

One possible explanation is that inhibited RPP is non-catalytic with respect to recombination of air atoms at the surface. For non-equilibrium boundary layers the convective heating rate to non-catalytic materials is substantially lower than that to highly catalytic materials, such as bare carbon and copper used in heat flux probes. A short review of the physical phenomena which lead to this heating reduction is given below to indicate important parameters involved.

5.3.1 Review of Surface Catalytic Effects

At the high temperatures and low densities characteristic of air behind the shock wave of earth entry vehicles and plasma arc test models, the air is highly dissociated, with as much as 12,000 Btu/lb. of the total enthalpy being dissociation energy. The influence of this dissociation energy upon convective heating rates is dependent upon the state of the boundary layer, equilibrium or non-equilibrium, and the catalytic efficiency of the heated surface. Investigations in references 26 - 29 indicate that if the catalytic efficiency of the surface is high, there is little difference between the convective heat transfer rate when the flow is in equilibrium, partly out of equilibrium, or frozen. For high catalytic efficiency, all of the atoms that reach the surface recombine upon it and yield their heat of recombination to the surface (Ref.30).

If the surface is non-catalytic and does not promote recombination reactions, and if the boundary layer is frozen or out of equilibrium, a large decrease in the convective heating rate can result, as much as 75%. When the boundary layer is frozen, the time required for an atom to recombine is long compared to the time for it to diffuse through the boundary layer. Large numbers of atoms reach the surface where, if the wall is non-catalytic, no recombination occurs. Hence, a large fraction of the energy normally available for heat transfer to the surface is not transferred. (Reference 30).

The magnitude of the heating rate reduction is a function of three factors:

- . Fraction of total energy in dissociation
- . Extent of non-equilibrium effects
- . Surface catalytic efficiency

Dissociation energy is relatively straightforward and can be related to density and temperature of the air behind the shockwave. For low densities and high temperatures it can constitute as much as 75% of the total stream energy.

Non-equilibrium effects are measured by a recombination rate parameter, which is basically the ratio of the time for atom diffusion across the boundary layer to the time for atom recombination. For low values of the parameter the boundary layer is frozen, whereas for high values it is in equilibrium. In Reference 30, it was shown that this parameter is mainly a function of free stream air density and nose radius for stagnation flow. Low values of density ρ and radius R result in low values of recombination parameter as shown by the approximate relation,

$$\Gamma = R \left(274 \frac{\rho}{\rho_{SL}} \right)^{1.777} \quad (7)$$

where

$$\rho_{SL} = \text{sea level air density}$$

Surface catalytic efficiency is a function of the surface material, and experimentation is required to determine the efficiency of specific materials. Results in Reference 31 indicate Pyrex glass to have a low efficiency and metals to have high efficiency, and indicate that catalytic efficiency is temperature dependent.

The relationship between surface catalytic efficiency, extent of non-equilibrium flow and dissociation energy will now be considered somewhat more quantitatively as they relate to stagnation point heating. The total heat flux rate to the surface \dot{q} is due to diffusion of dissociation energy \dot{q}_D and convection of the remaining energy \dot{q}_F ,

$$\dot{q}_{\text{TOTAL}} = \dot{q}_D + \dot{q}_F \quad (8)$$

The convection component \dot{q}_F is simply related to the total heat flux for equilibrium flow \dot{q}_E , which is the value computed by conventional methods such as the Fay and Riddell relation. The relation is from Reference 30,

$$\dot{q}_F = \dot{q}_E \frac{\Delta i_f}{\Delta i_t} \quad (9)$$

where Δi_t and Δi_f are enthalpy differences across the boundary layer, with Δi_t based upon total enthalpy and Δi_f based upon total enthalpy less dissociation energy.

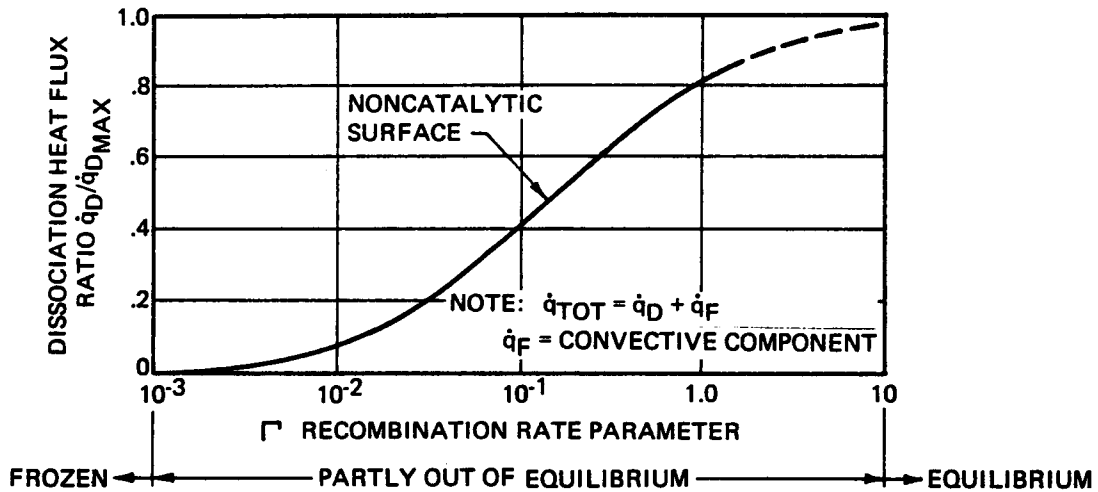
The component of heating due to dissociation energy \dot{q}_D has a maximum value when the flow is in equilibrium. This value is given simply by,

$$\dot{q}_{D\text{max}} = \dot{q}_E - \dot{q}_F \quad (10)$$

The value is very nearly the same in non-equilibrium flow for a catalytic surface. The effect of a non-catalytic surface in combination with non-equilibrium flow in reducing \dot{q}_D is shown in Figure 5-23, which is a correlation of analytical results from Reference 30. The ratio of \dot{q}_D to $\dot{q}_{D\text{max}}$ is plotted versus recombination rate parameter Γ , and it is seen that \dot{q}_D decreases from the maximum value at high values of Γ (equilibrium flow) to zero for low values of Γ (frozen flow).

The total heat flux rate to the surface is therefore a maximum for equilibrium flow or a catalytic surface and is reduced to a minimum value for frozen flow and a non-catalytic surface. The magnitude of the reduction depends upon the degree of dissociation and as noted previously can be as high as 75%. Intermediate values of heat flux occur when the flow is partly out of equilibrium, depending upon recombination rate parameter and catalytic efficiency of the surface.

The preceding discussion was limited to the stagnation point; however analytical results in Reference 30 indicate that heating reductions downstream will be comparable to that at the stagnation point.



RANGE OF APPLICATION OF CORRELATION

VELOCITY = 11,000 – 31,000 FT/SEC
 ALTITUDE = 120,000 – 220,000 FT
 NOSE RADIUS = 1 – 5 FT
 SURFACE TEMPERATURE = 2240°F
 ATOM CONCENTRATION, BOUNDARY LAYER EDGE = 0.075 – 1.0

FIGURE 5-23 EFFECT OF NONCATALYTIC SURFACE UPON STAGNATION POINT HEAT TRANSFER

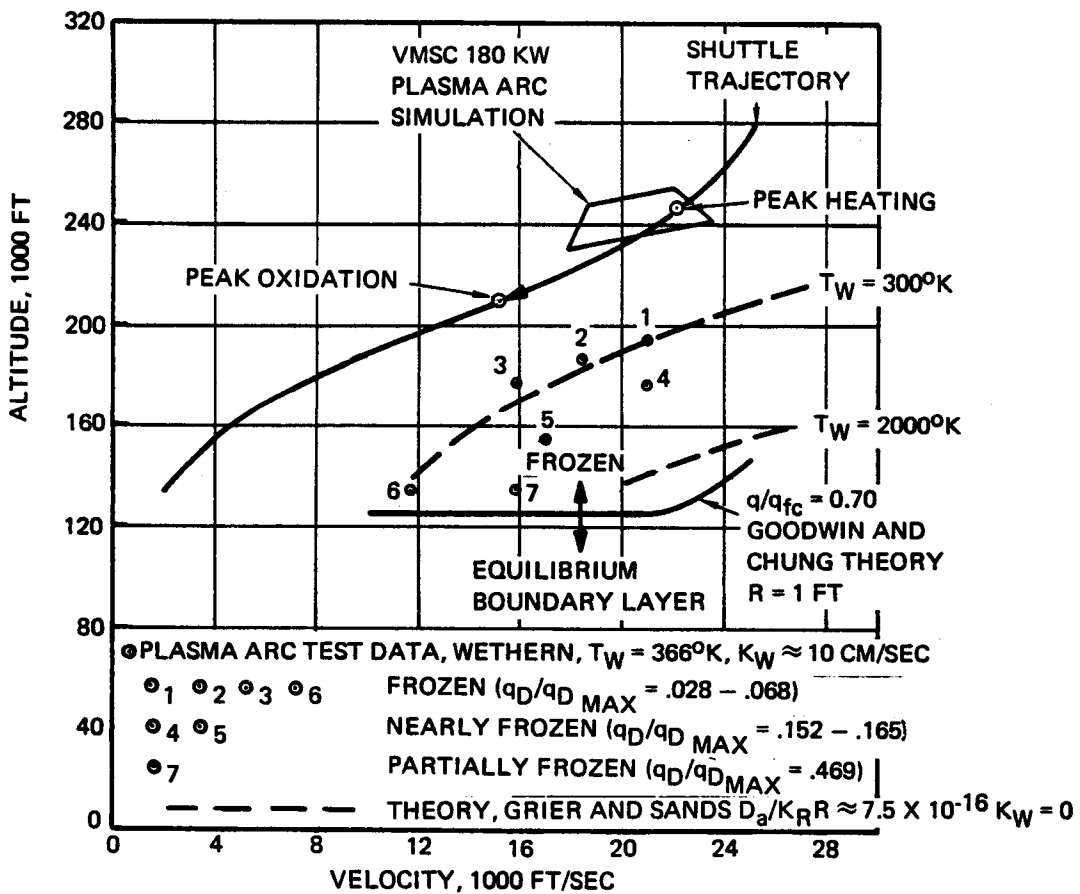


FIGURE 5-24 STATE OF BOUNDARY LAYER FLOW RE-ENTRY AND PLASMA ARC TEST

5.3.2 Frozen Boundary Layer Regime

It is of interest now to assess the potential importance of surface catalytic effects to space shuttle reentry heating on the leading edge as well as the degree to which plasma arc tests simulate these effects. Figure 5-24 shows the boundary between the equilibrium and frozen boundary layer regimes on an altitude-velocity plot as defined in Reference 30. The shuttle trajectory is shown for comparison, and it is seen that both peak heating and oxidation rates occur at altitudes which are well into the frozen regime, where catalytic effects are important. Also shown is the altitude-velocity curve corresponding to freestream densities, stagnation pressures and stagnation enthalpies produced by the VMSC 180KW plasma arc in the inhibited RPP screening tests. The test specimens would appear to have been subjected to frozen flow conditions. This figure indicates that flow conditions in the tests were reasonably representative of reentry conditions from the standpoint of degree of non-equilibrium effects and dissociation energy level.

There is a scale effect which affects the simulation due to the fact that the recombination rate parameter Γ is proportional to nose radius. The effective nose radius of the leading edge is highly dependent upon degree of interference heating, varying from about 1.86 inches for maximum interference heating to 31.3 inches for no interference heating. The effective radius of the shrouded plasma arc specimens is about 2.5 inches, based upon the velocity gradient correction of Reference 33. This is about right for simulation of the maximum interference heating conditions. For lower interference heating, it tends to magnify the heating reduction due to catalytic effects. However, Figure 5-23 indicates that for a non-catalytic surface the scale effect has an important effect upon heating reduction only for greater than about 10^{-3} . For both plasma arc test conditions and reentry conditions at the time of peak heating Γ was computed to be less than 10^{-3} , hence, the scale effect may not be significant, at least for a completely non-catalytic material.

One difficulty in defining the boundary between equilibrium and frozen boundary layer flow is that the recombination rate parameter is a function of the recombination rate constant for air. This constant has not been well defined, a wide range of values having been reported in the literature as reviewed in Reference 34. While the value used in Reference 30 to define the boundary in Figure 93 appears reasonable, it was desirable to confirm the boundary using an approach which did not rely upon an assumed value for air recombination rate constant.

In Reference 34 heat flux rates measurements were reported by Wethern for a plasma arc facility which provided boundary layer flows ranging from partially frozen to essentially completely frozen. Measured heating rates were correlated in Reference 34 with theoretical values for both an equilibrium boundary and a frozen boundary layer with non-catalytic wall.

From these results the fraction of dissociation energy transferred to the calorimeter $\dot{q}_D/\dot{q}_{D_{max}}$ was determined. Test points were plotted on Figure 5-24, where it is seen that points 1, 2, 3 and 6 represented essentially complete frozen flow ($\dot{q}_D/\dot{q}_{D_{max}} = 0.028$ to 0.068). Other test points correspond to nearly or partially frozen flow. A direct comparison of the Wethern test points with the shuttle trajectory and VMSC plasma arc test regime indicates that both should be well into the frozen boundary layer regime.

According to the theory of Grier and Sands in Reference 35, there are three parameters which affect the boundary between equilibrium and frozen boundary layer flow which are not reflected in the altitude-velocity plot of Figure 5-24. It is necessary to determine the effect of these parameters, wall catalytic reaction rate constant, K_W , surface temperature and nose radius upon the comparison between the Wethern test points and the shuttle trajectory and VMSC plasma test regime.

Grier and Sands theory indicates that high values of K_W reduce the altitude required for frozen flow. Wethern's test data was analyzed in Reference 36 by Rosser who estimated a value of recombination coefficient $\gamma = 10^{-3}$ for Wethern's calorimeter surface, which is equivalent to $K_W = 10$ cm/sec. As will be discussed later, it appears that K_W for siliconized RPP is at least an order of magnitude higher, hence the application of Wethern's results to siliconized RPP is conservative from the standpoint of effect of K_W .

Grier and Sand's theory further indicates that increasing surface temperature reduces the required altitude for frozen flow. Wethern's data corresponds to a surface temperature of 366°K , whereas siliconized RPP operates at about 1850°K at heating rates of interest. In order to estimate the reduction in altitude for frozen flow due to this temperature difference, Wethern's data was correlated with Grier and Sand's theory in Figure 5-24. A fit between test data and theory was obtained using a value of $Da/K_R R = 7.5 \times 10^{-16}$ where,

Da = Damkohler number (recombination parameter employed by Grier and Sands, dimensionless)

K_R = air recombination rate constant, $\text{cm}^6/\text{mole}^2 \text{ sec}$

R = nose radius, feet

The correlation was obtained for a value of $T_W = 300^\circ\text{K}$, very near the reported value for Wethern's tests. Using the inferred value of $Da/K_R R$, Grier and Sand's theory was used to establish a frozen flow boundary for $T_W = 2000^\circ\text{K}$, near the value for siliconized RPP. Figure 5-24 shows that this boundary falls 54,000 feet in altitude below Wethern's data and 100,000 feet below the shuttle trajectory and VMSC plasma test regime.

Finally, Grier and Sands theory indicates that increasing nose radius increases the altitude required for frozen flow. Wethern's test model was very nearly the same size (one-inch radius, flat face) as that used in the VMSC tests, hence, from the standpoint of scale effect his results are comparable to the VMSC test regime. As discussed previously, the effective nose radius for the shuttle leading edge varies from 1.86 for maximum interference heating to 31.3 inches for no interference heating. Hence, there is a scale difference between Wethern's tests and the shuttle leading edge, at least for low interference heating. However, Grier and Sand's theory indicates that an increase in nose radius of a factor of 100 corresponds to an altitude increase for frozen flow of only 60,000 feet. The scale effect is, therefore, not sufficient to bring the shuttle trajectory below the altitude required for frozen flow. In summary, Wethern's test results, in conjunction with the theory of Grier and Sands, confirms that both the VMSC plasma test regime and the shuttle trajectory are well into the frozen boundary layer regime where surface catalytic effects are important.

5.3.3 Correlation of Plasma Test Data with Theory of Catalytic Effects

Analyses were next performed to determine if the temperature reductions observed in plasma tests of siliconized RPP are consistent with theoretical heating reductions for a material with low catalytic activity. The theory of Goulard from Reference 36 was employed to define, for a fully frozen boundary layer, the heat flux ratio $\dot{q}_S/\dot{q}_{S,fc}$ where,

\dot{q}_S = stagnation heat flux to a wall of finite catalyticity

$\dot{q}_{S,fc}$ = stagnation heat flux to a fully catalytic wall

The comparable values of heat flux ratio for siliconized RPP were inferred from the re-radiation heat flux rates for siliconized and bare RPP using the relation,

$$\frac{\dot{q}_S}{\dot{q}_{S,fc}} = \frac{\sigma \epsilon_{Si} T_{Si}^4}{\sigma \epsilon_B T_B^4} \quad (11)$$

where,

σ = Stefan-Boltzmann Constant = 0.476×10^{-12} Btu/ft² sec⁰R⁴

ϵ_{Si} = emittance of siliconized RPP = 0.80

ϵ_B = emittance of bare RPP = 0.85

T_{Si} = temperature of siliconized RPP, °R

T_B = temperature of bare RPP at hot wall heat flux corresponding to T_{Si} , °R

Equation (11) is based upon the assumption that bare RPP is fully catalytic. Any finite degree of catalycity in bare RPP will result in somewhat high inferred values of $\dot{q}_S/\dot{q}_{S,fc}$. Effects of blowing and heat of combustion on the temperature of bare RPP are neglected in equation (11), but for the enthalpies of interest these two effects are very nearly compensating. Finally, equation (11) assumes that heat losses from siliconized and bare RPP to the specimen holder and shroud are directly proportional to re-radiation heat fluxes from these materials, and will, therefore, not affect the ratio $\dot{q}_S/\dot{q}_{S,fc}$. While this assumption may not be strictly correct, the radiation equilibrium correlation obtained for bare RPP in Section 5.2.3, suggests that heat losses are not large.

Figure 5-25 presents the comparison of theoretical heating reduction due to a low catalytic efficiency surface with the inferred test values for siliconized RPP. The heat flux ratio $\dot{q}_S/\dot{q}_{S,fc}$ is shown as a function of air total enthalpy. It is seen that all test points fall well below the value of unity for a fully catalytic material, but above the theoretical curve for a non-catalytic surface. Hence, the data falls in a regime which is consistent with a postulated low level of surface catalytic activity. As would be expected theoretical values of $\dot{q}_S/\dot{q}_{S,fc}$ for a non-catalytic surface decrease with increasing enthalpy, due to increasing dissociation energy. Unfortunately, the enthalpy range for the plasma arc tests was not sufficient to establish a clear trend of $\dot{q}_S/\dot{q}_{S,fc}$ with enthalpy for the test points.

While the data obtained to date is not adequate for a complete or final characterization of siliconized RPP with respect to surface catalytic effects, it is of interest to determine a value of wall catalytic reaction rate constant K_W which reasonably fits available test data. Figure 5-25 shows two theoretical curves for $K_W = 410$ cm/sec, corresponding to two values of nose radius-stagnation pressure product RP_S which encompass the test range. Considering the fact that the test data includes specimens fabricated using a range of process techniques, the correlation between the theoretical curves and siliconized RPP data is not unreasonable. It will be noted that a K_W value of 410 cm/sec is in the range of values reported for various metal oxides in Reference 37.

5.3.4 Application of Catalysis Theory to Reentry Environment

It is of further interest to determine theoretical values of heating reduction for a surface with $K_W = 410$ cm/sec, representative of siliconized RPP, and with RP_S product and enthalpy variation corresponding to the wing leading edge during reentry. The resulting shuttle trajectory curve in Figure 5-25 is based upon an effective nose radius corresponding to maximum interference heating ($R = 1.86$ inches) and a constant surface temperature of 1850°K (2870°F). The indicated heating reduction at the time of peak heating is somewhat greater than values inferred directly from the plasma tests due to the higher enthalpy at peak heating, as compared with the plasma tests. This is

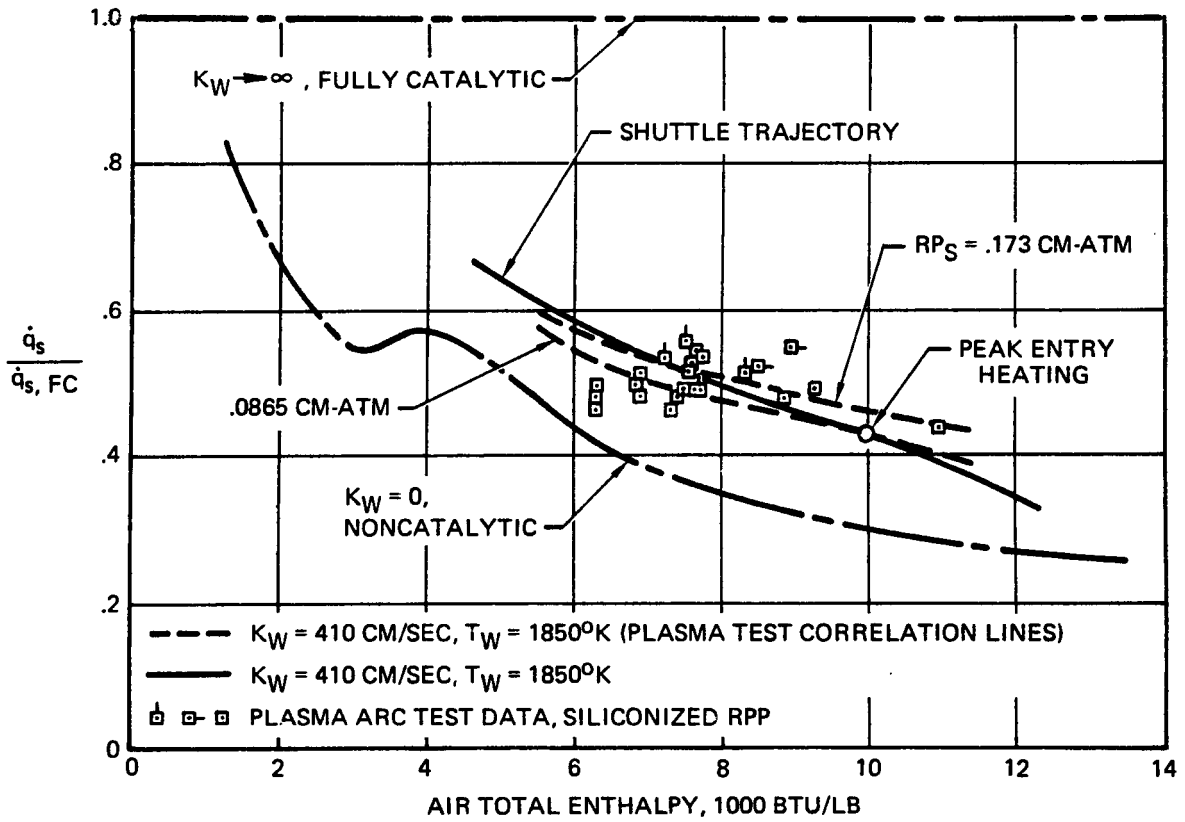


FIGURE 5-25 HEATING REDUCTION DUE TO LOW CATALYTIC EFFICIENCY SURFACE

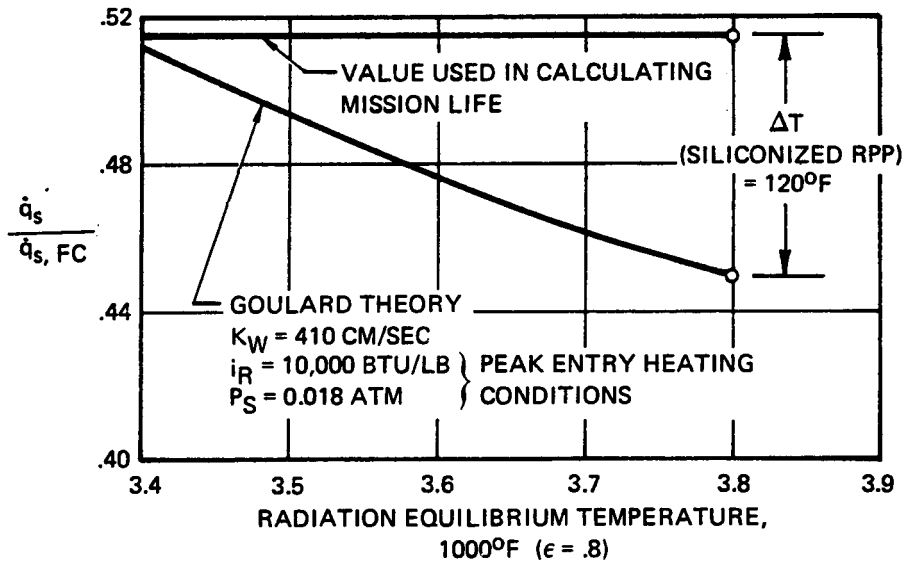


FIGURE 5-26 HEATING REDUCTION COMPARISON

important in that it introduces an element of conservatism into the mission life predictions for inhibited RPP in Section 5.2.3. Those predictions were based upon a direct application of plasma test results to the reentry environment.

Analyses were performed to assess the potential degree of conservatism in the mission life predictions due to the difference in plasma test and peak reentry heating environments. Values of $\dot{q}_S/\dot{q}_{S,fc}$ were computed for conditions at the time of peak reentry heating using Goulard's theory with $K_W = 410$ cm/sec. Calculations were made for a range of radiation equilibrium temperatures using the values of effective nose radius and siliconized RPP temperature appropriate to each degree of interference heating. The results are compared in Figure 5-26 with the value of $\dot{q}_{RRSi}/\dot{q}_{RRB}$ used in predicting mission life of siliconized RPP, where

\dot{q}_{RRSi} = siliconized RPP re-radiation heat flux

\dot{q}_{RRB} = bare RPP re-radiation heat flux

It is seen that Goulard's theory, with the value of K_W inferred for siliconized RPP, indicates a 120°F lower peak temperature for siliconized RPP than the value used in predicting mission life, for a radiation equilibrium temperature of 3800°F. For lower equilibrium temperatures, the difference is less, due to the larger effective nose radii at lower interference heating conditions.

5.3.5 Substantiating Data

The heating reductions due to non-catalytic surfaces discussed above have been verified in plasma arc tests of silicon monoxide and teflon coated calorimeters, as reported in Reference 37. The tests were performed in the NASA Ames Planetary Entry Ablation Facility (PEAF) using frozen nitrogen flows. Results are shown in Figure 5-27 where they are compared with test data for a partially catalytic surface (copper) and with theoretical results from Reference 37. It is seen that heating rates to silicon monoxide and teflon were about one-half that to copper and one-third of the theoretical heating rate to a fully catalytic surface. The heating rates to silicon monoxide and teflon agreed well with theoretical results for a non-catalytic surface.

5.3.6 Effects Upon Downstream Catalytic Material

The theoretical work of Chung, Liu and Mirels in Reference 38 predicts that if a catalytic material is located downstream of a non-catalytic material in a frozen boundary layer, the catalytic material will be subjected to enhanced heating due to the non-catalytic material. This is due to recombination of atoms which would otherwise recombine upstream on a catalytic surface. Since catalytic materials may be used on the shuttle wing

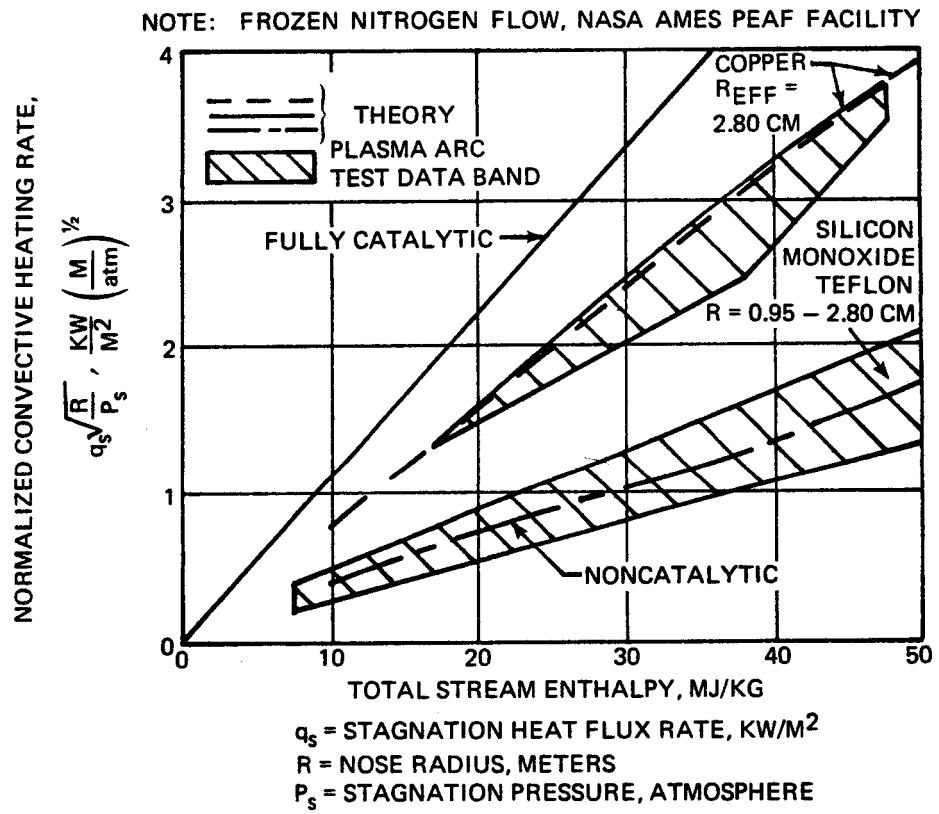


FIGURE 5-27 HEAT TRANSFER TO CATALYTIC AND NONCATALYTIC SURFACES, PLASMA ARC TEST DATA VS THEORY

downstream of the leading edge, it is important to consider potential enhanced downstream heating due to use of a siliconized RPP leading edge.

A detailed investigation of downstream effects was outside the scope of the current effort. However, a review of the literature showed that at least one experimental program has been conducted, which indicates the magnitude of increased heating to be expected on a catalytic material, due to an upstream non-catalytic material. Sheldahl and Winkler reported in Reference 39 the results of plasma arc tests in which heating rates were measured on the side of a copper cylinder downstream of a hemisphere nose which was coated with silicon-monoxide. As shown in the previous Section 5.5.5, copper is a good catalyst, while silicon monoxide is non-catalytic. By performing comparative tests with a copper nose, the increase in heating rate on the cylinder due to the upstream non-catalyst was determined. The results indicated a 50% increase in heat flux rate on the cylinder.

Applying Sheldahl and Winkler's results directly to the leading edge indicates that a catalytic material attached to a siliconized RPP leading edge at the 15% chord location would experience an increase in radiation equilibrium temperature of 300°F, for a stagnation line equilibrium temperature of 3500°F. This 300°F increase could be offset by simply moving the attachment location 12 inches aft, to the 20.6% chord location, where heating rates are 50% lower. It was concluded that further consideration should be given to this effect, but that the increased heating on downstream material can be offset by proper design.

It was concluded that catalytic effects are the probable explanation for the low measured surface temperatures on inhibited RPP, and that they offer potentially important temperature reductions on the space shuttle during reentry. Since the investigations, both experimental and analytical, of these effects on inhibited RPP have been preliminary, they should be pursued further. Possible approaches which are outside the current scope of work include the following:

- Coat the calorimeters used in plasma arc tests of RPP with a thin layer of material of known low catalytic efficiency to confirm that non-equilibrium effects are present.

- Perform plasma arc tests on inhibited RPP in a facility which will provide an equilibrium boundary layer. Tunnels which operate at relatively high pressures, such as those which expand into the atmosphere, would satisfy this requirement. If the low temperatures persist, low catalytic efficiency can be eliminated as a cause.

- If possible, deposit SiC diffusion coating on a calorimeter and test in a non-equilibrium (low pressure) plasma arc tunnel to measure reduction in heating.

- Perform further plasma arc tests on inhibited RPP specimens in a non-equilibrium tunnel in order to measure catalytic reaction rate constant as a function of temperature.

- Perform analyses to determine both stagnation line and downstream heating rates during reentry, including surface non-catalytic effects.

5.4 INHIBITED RPP CHARACTERIZATION DATA

Preliminary characterization data was obtained on the primary and alternate diffusion coating systems to provide additional property data for coating system evaluation and early design values for initiation of Phase II. Only the most significant properties were evaluated at this time because development of more comprehensive design data is a major task of the Phase II program.

Conductivity, thermal expansion, emittance, plasma arc oxidation, furnace oxidation, and flexure properties were obtained. The latter included an evaluation of the effects of both thermal cycling and stress cycling. This was done to determine if potential problems existed on which emphasis should be placed at the outset of Phase II. Plasma arc performance is presented in Section 5.2, while all other tests are reported in this section.

The following agencies were involved in the determination of physical and mechanical properties. Data is given in Tables 5-10 through 5-14 and Figures 5-28 through 5-30.

Battelle - Thermal Conductivity
- Emittance at 3000°F
- Coefficient of Thermal Expansion (-250°F to R. T.)

Southern Research Institute (SRI)
- Flexure Properties (R. T., 2700°F, 3000°F)

Vought Missiles and Space Company -
- Flexure Properties (R. T., -250°F, 1400°F)
- Flexure Properties after Thermal Cycling
- Flexure Properties after Load Cycling
- Coefficient of Thermal Expansion (R. T. to 3500°F)
- Plasma Arc Oxidation Resistance
- Low Temperature Oxidation Resistance

5.4.1 Flexure Tests

The airload panels, which constitute the major portion of leading edge weight, are designed by bending from applied airloads. Flexure strength rather than tensile data was, therefore, obtained in Phase I because for the VMSC leading edge design this is the more important materials property.

Additional property data for tension and compression loading will be obtained in Phase II.

Flexure strength was obtained on specimens 3/4 in. x 5 in. x 0.18 in. using four-point loading. Overall span was 4.2 in. with 1.75 in. between applied loads. Data was obtained in the stronger warp direction, because leading edge design and aspect ratio of airload panels lend themselves to selected orientation of the layup. Thus, the warp direction can be oriented along the maximum stress direction. In addition, the load was applied such that the compression surface was that which is upward during pack cementation coating and should have the thicker coating. This is justified because (1) full-scale leading edges can and should be coated with the stagnation region pointed upward to maximize coating thickness in the most critical area, and (2) airloads on the leading edge place the outer surface of the lower airload panels principally in compression. Load rate was set at 0.05 in/min. and load-deflection curves were obtained. Cryogenic and elevated temperature tests were conducted in an inert atmosphere.

Low cycle flexural fatigue data was obtained at room temperature by loading the specimens ten times to 55% of the average room temperature failing stress before loading to failure. The applied fatigue stress level simulated limit stress and was based on an assumed data scatter of 20% and an ultimate factor of safety of 1.5.

Thermal cycling consisted of subjecting flexure test specimens to furnace oxidation for one, five and ten cycles prior to loading to failure at room temperature. Specimens were inserted into a 2300°F preheated Pereny electric furnace and allowed to remain 10 minutes. They were then withdrawn and aircooled, under stagnant conditions, taking approximately 10 minutes to reach 1000°F. This constituted one cycle. For additional cycles, the specimens, while still at 1000°F, were reinserted into the furnace. The furnace oxidation test is believed to be very conservative relative to actual reentry conditions, but was used to determine potential problem areas requiring closer scrutiny.

Siliconized RPP - Results of flexure testing for siliconized RPP are provided in Table 5-10. Room and cryogenic temperature strength average 12,400 psi in VMSC tests, while elastic modulus varies between 2 and 3 x 10⁶ psi. Two values of elastic modulus are given, because of the characteristic shape of the stress-strain curves obtained by VMSC with the coated material. This is illustrated in Figure 5-28 where an inverse bow is noticed for a typical curve. Accordingly, the secant modulus is given and computed using the maximum failing stress and failure strain. The tangent modulus represents the maximum slope of the stress-strain curve. The curves of Figure 5-28 were computed from load-deflection data using elastic beam equations. The reasons for the inverse bow in the stress-strain curves is not clear. One possible explanation is that if it is assumed that the coating system is crazed or possesses a myriad of fine cracks, mutual bearing of the

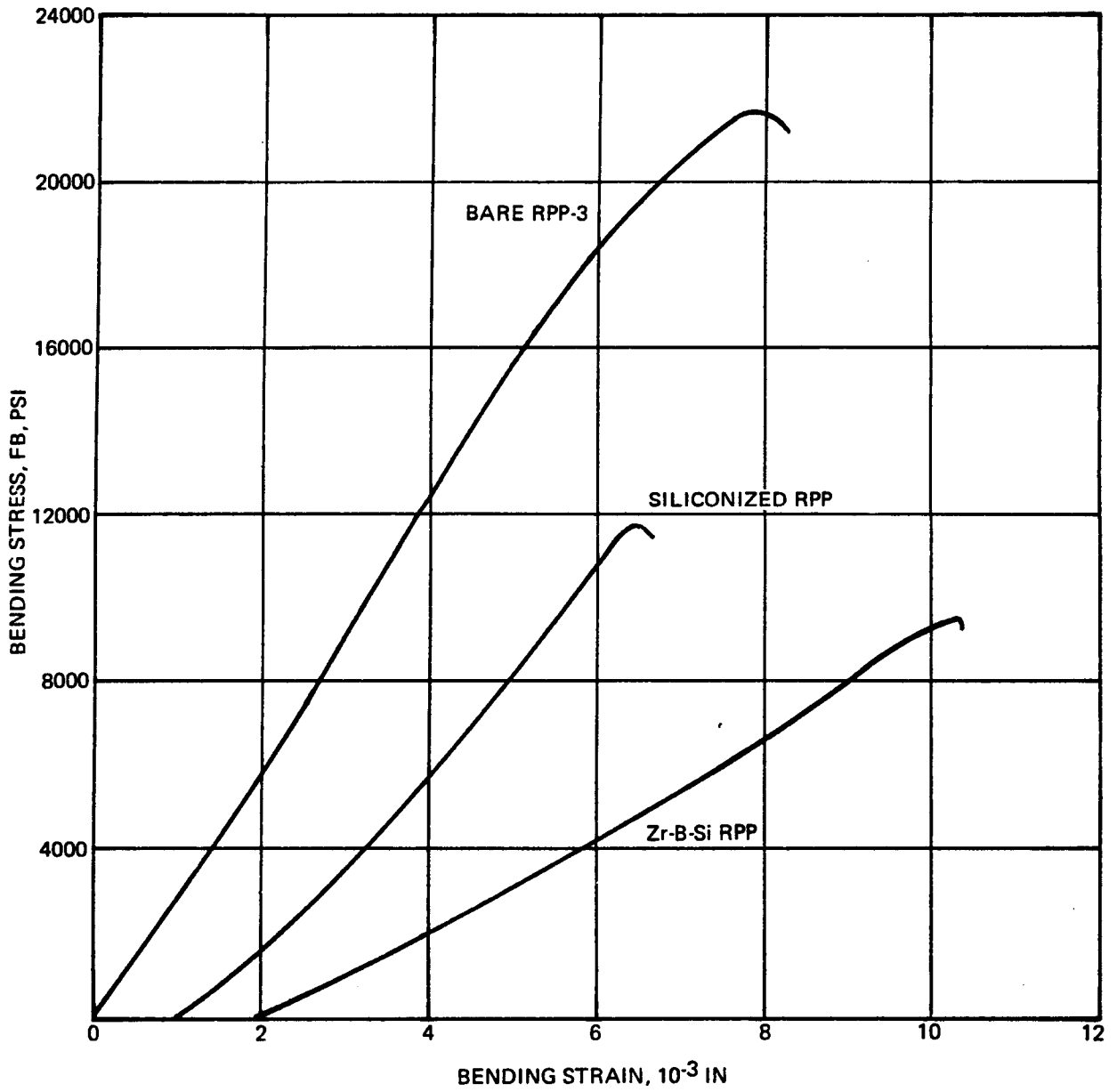


FIGURE 5-28 ROOM TEMPERATURE STRESS-STRAIN CURVES FLEXURE

TABLE 5-10 FLEXURE STRENGTH
AND ELASTIC MODULUS SILICONIZED RPP

Spec.	Treatment	Failure Stress F_b psi	Elastic Modulus, $E_s^{(1)}$	$\frac{6}{10}$ psi $E_t^{(2)}$	Failure Location
<u>VMSC Tests</u>					
33	Room Temp.	12,200	2.26	2.73	Between center load points
34	Room Temp.	11,100	2.03	2.25	Between center load points
40	Room Temp.	14,000	2.50	3.30	Outside of center
41	-250°F	14,500	2.90	3.05	Under upper load point
43	-250°F	11,100	2.54	2.92	Under upper load point
46	10 Cycle Fatigue	12,100	2.52	4.20	Under upper load point
47	10 Cycle Fatigue	11,400	2.79	3.93	Under upper load point
48	10 Cycle Fatigue	9,900	2.50	4.13	Under upper load point
27	One Thermal Cycle	13,400	2.26	2.46	Under upper load point
28	One Thermal Cycle	15,100	2.42	2.83	Under upper load point
29	Five Thermal Cycles	7,000	1.34	2.14	Under upper load point
30	Five Thermal Cycles	6,600	1.28	1.91	Under upper load point
31	Ten Thermal Cycles	4,700	1.0	1.0	Under upper load point
32	Ten Thermal Cycles	1,800	0.6	0.6	Outside of center
44	1400°F	4,700	*	*	
45	1400°F	5,800	*	*	
<u>SRI Tests</u>					
		$E_1^{(3)}$	$E_2^{(4)}$		
39	Room Temp.	6,190	2.0	1.31	Between center load points
37	Room Temp.	10,050	1.35	1.35	Between center load points
42	2700°F	13,780	6.38	2.64	Outside of center
35	2700°F	10,120	6.80	2.85	Under upper load point
38	3100°F	13,340	7.49	2.50	Between center load points
36	3100°F	15,800	7.85	2.46	Between center load points

Notes:

- (1) Secant modulus obtained at maximum stress
- (2) Tangent modulus is the maximum value obtained
- (3) Initial modulus
- (4) Secondary modulus
- * No useable load deflection curve obtained

faying surfaces on the compression side during loading, could tend to stiffen the laminate at higher stresses.

The SRI tests at room temperature produced results significantly lower than those obtained at VMSC and only specimen M30 1-37 produced a stress-strain like that obtained by VMSC and pictured in Figure 5-28. Specimen M301-39 produced an opposite bow with a higher initial elastic modulus and then bending over to a lower secondary modulus. This latter curve shape was typical of all specimens tested by SRI at all temperatures on both coating systems, the lone exception being specimen M30 1-37. Therefore, two moduli of elasticity are reported for the SRI tests, the initial modulus and the secondary modulus. The initial modulus extends over the first 10 to 20% of the stress-strain curve.

It isn't clear why the SRI room temperature data should be low compared to VMSC data nor is it clear (although a theory is postulated) why the VMSC data at 1400^oF should be low compared to SRI data at 2700 and 3100^oF, since all elevated temperature testing was conducted in an inert atmosphere. It is possible that testing technique, warped specimens, or specimen coating non-uniformity could be the influencing factors. These factors must be evaluated thoroughly in Phase II. It is believed, however, that the higher values probably represent the coated system potential and should be achievable with further coating and test technique refinement.

The SRI elevated temperature data is certainly encouraging and indicates that the strength level increases slightly at the higher temperatures. The secondary modulus remains essentially constant and at about the same level as those obtained by VMSC in room temperature tests. The high initial modulus in the SRI tests could possibly be the result of differential expansion between the bare core and the coated faces producing a compression preload in the face material. This would have the effect of increasing the stiffness of the system until the compression preload stress is relieved on the tension side, whereupon the effective thickness of the laminate decreases. Similar results were obtained with the Zr-B-Si system, although not quite as pronounced.

This same postulation could also predict the lower stresses at 1400^oF in the VMSC tests. Referring to the expansion curves of Figure 5-29, it is noted that the maximum differential expansion between siliconized RPP and bare RPP occurs in the region of 1400^oF. This differential expansion could produce high compression stresses in the face material and high tension stresses in the core material. This would effectively reduce the allowable bending stress component carried by the core and result in a lower computed failure stress. This theory must assume that crazing or cracking exists in the coated face material and that it is capable of withstanding compression stresses, but not tensile stress. Unfortunately, load deflection data at the 1400^oF test temperature was unusable for both a comparison with SRI data and to judge the validity of the proposed theory of failure.

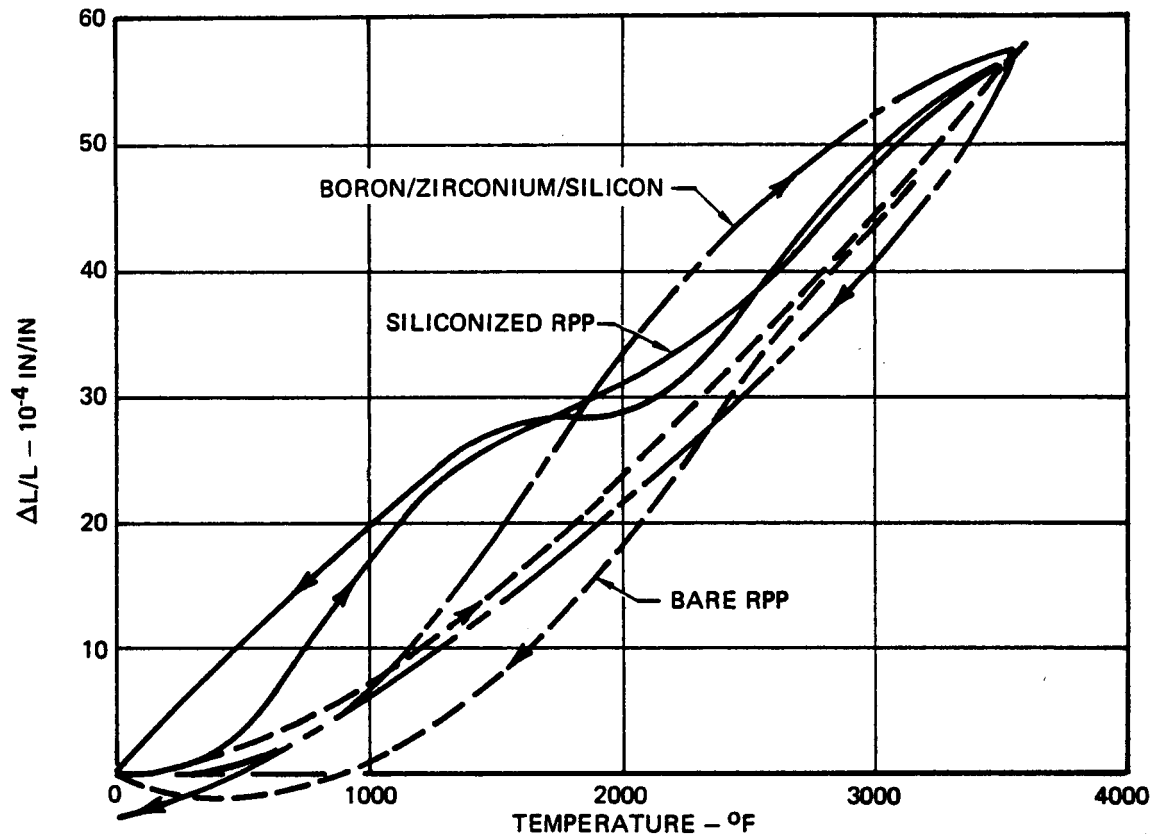


FIGURE 5-29 COEFFICIENT OF THERMAL EXPANSION WARP DIRECTION

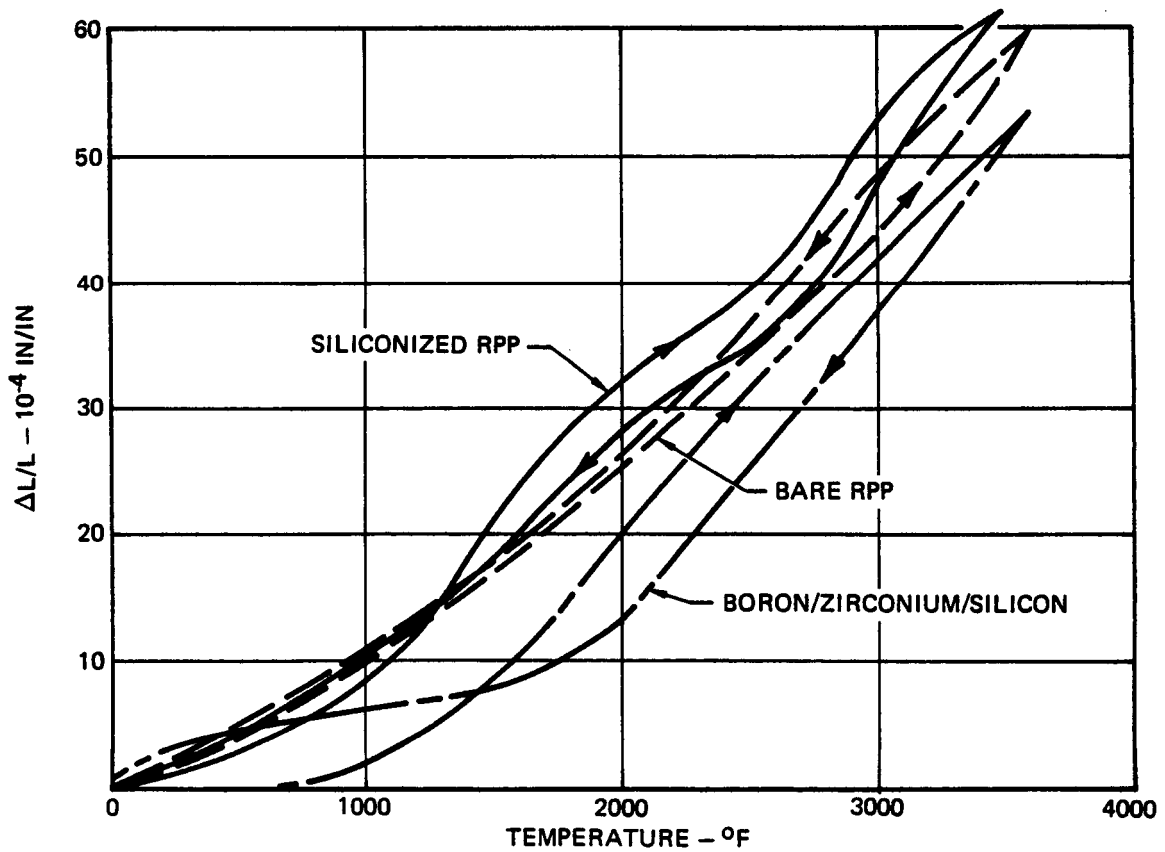


FIGURE 5-30 COEFFICIENT OF THERMAL EXPANSION FILL DIRECTION

Low cycle fatigue data for the siliconized RPP indicates about 10% reduction in failing stress after ten cycles at 55% of the VMSC no-cycle, room temperature, failing stress level. Additional fatigue evaluation should be conducted in Phase II.

Thermal cycling using a furnace test at one atmosphere, even though considered conservative, indicates a possible problem for siliconized RPP that requires additional attention. Data in Table 5-10 shows a strength increase after one 20-minute cycle, but after 100 minutes and 200 minutes (5 and 10 thermal cycles, respectively) strength has decreased considerably. This is evidently due to subsurface (bare RPP) oxidation, as indicated by the weight loss data listed in Table 5-11, since little change in the coating was noted after thermal cycling. Two approaches are open to resolution of this apparent problem: (1) modify the siliconized coating to produce a system insensitive to thermal cycling, possibly through the addition of boron, or (2) devise a rational test technique to conclusively prove or disprove whether a problem does, in fact, exist in the reentry environment for the siliconized system. In view of the remarkable insensitivity of the Zr-B-Si coating to thermal cycling, VMSC elected to pursue the modification of the siliconized coating through the introduction of boron. This effort has not yet been concluded but requires pursuit in Phase II. The second alternative should also be analyzed in Phase II.

Coating thickness determinations were made on the VMSC room temperature tested flexure bars. This data, listed in Table 5-12, indicates coating thicknesses in the 0.020 inch range on the compression side and slightly less on the tension side. The values are within the range expected.

Zirconium-Boron-Silicon Coated RPP - Flexure results for the Zr-B-Si system are listed in Table 5-13. These show that room temperature failing stress averages 8700 psi or 30% less than VMSC siliconized RPP data. However, it is extremely significant that the average failing stress remains essentially constant with thermal cycling or elevated temperature testing up to 1400°F and increases at higher temperature. This would indicate that the coating system is completely insensitive to low temperature oxidation even under conservative conditions.

Weight gain data obtained during thermal cycling is listed in Table 5-11 and shows a weight gain as opposed to a weight loss and indicates the reason for good strength after thermal cycling.

TABLE 5-11
 WEIGHT CHANGE AFTER THERMAL CYCLING
 IN AIR AT 2300°F

Coating System	Spec. No.	No. of Thermal Cycles	Weight, Gm.		Percent Weight Change
			Before	After	
Siliconized RPP	27	1	16.58	16.05	- 3.2
	28	1	16.65	16.20	- 2.7
	29	5	16.74	14.10	-15.7
	30	5	16.92	14.40	-15.0
	31	10	16.83	12.79	-24.0
	32	10	16.69	11.15	-33.2
Zr-B-Si RPP	43	1	18.28	18.80	+ 2.8
	50	1	21.60	21.84	+ 1.1
	11	5	20.22	20.69	+ 2.3
	12	5	19.03	19.90	+ 4.6
	9	10	20.00	20.60	+ 3.0
	10	10	19.17	19.48	+ 1.9
Bare RPP Control	--	1	16.10	15.20	- 5.6
	--	2	16.27	12.62	-22.4

TABLE 5-12 COATING THICKNESSES ON R. T. FLEX SPECIMENS
AT POINT OF FRACTURE

Spec. No.	<u>Siliconized RPP3</u>				t, in.	b, in.
	t_f , in.		t_f , in.			
	Upper	Lower	Right	Left		
33	0.025	0.015	0.015	0.015	0.179	0.746
34	0.020	0.020	0.015	0.015	0.176	0.739
40	0.020	0.015	0.015	0.020	0.183	0.744
Zirconium-Boron-Silicon Coated RPP						
45	0.020	0.015	0.030	0.030	0.179	0.779
48	0.015	0.025	0.030	0.015	0.198	0.788
51	0.015	0.030	0.025	0.030	0.185	0.784

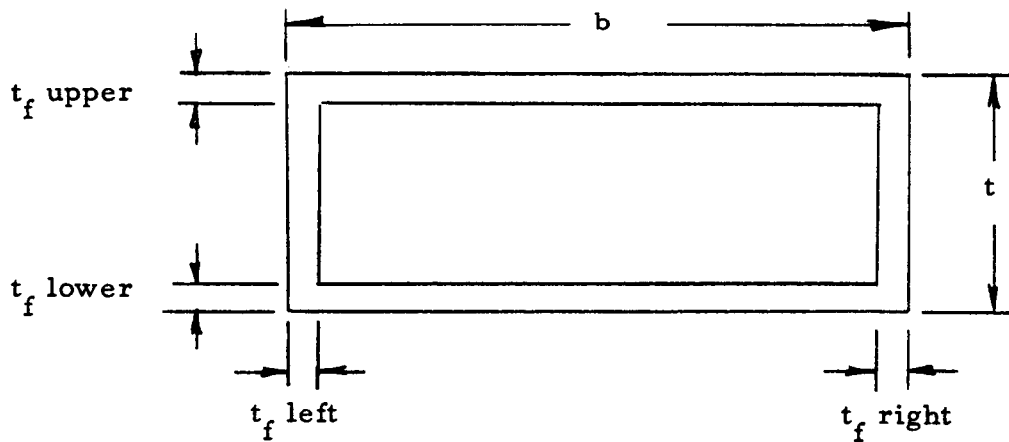


TABLE 5-13 FLEXURE STRENGTH
AND ELASTIC MODULUS ZIRCONIUM-BORON-SILICON COATED RPP

Spec.	Treatment	Failure Stress F psi	Elastic Modulus, $E_s^{(1)}$	10^6 psi $E_t^{(2)}$	Failure Location
<u>VMSC Tests</u>					
45	Room Temp.	10,100	1.25	1.30	Under upper load points
48	Room Temp.	7,200	1.28	1.59	Between center load points
51	Room Temp.	8,700	1.17	1.17	Under upper load points
40	-250°F	15,200	2.30	2.30	Under upper load points
11	-250°F	13,900	2.10	2.10	Between center load points
8	10 Cycle Fatigue	5,700	1.09	1.09	Under upper load points
3	10 Cycle Fatigue	8,800	1.67	1.67	Between center load points
12	10 Cycle Fatigue	9,300	1.69	1.69	Between center load points
3	1 Thermal Cycle	9,000	1.64	1.64	Under upper load points
0	1 Thermal Cycle	8,200	2.10	2.10	Under upper load points
1	5 Thermal Cycles	7,800	1.70	1.70	Under upper load points
2	5 Thermal Cycles	9,700	1.80	1.80	Under upper load points
9	Ten Thermal Cycles	7,900	1.67	1.67	Under upper load points
0	Ten Thermal Cycles	9,400	1.70	1.70	Under upper load points
4	1400°F	9,700	*	*	Under upper load points
5	1400°F	7,700	1.50	1.50	Under upper load points
<u>RI Tests</u>					
			$E_1^{(3)}$	$E_2^{(4)}$	
9	Room Temp.	5,870	2.09	0.72	Between center load points
4	Room Temp.	9,880	1.79	0.96	Between center load points
2	2700°F	12,210	4.97	3.02	Between center load points
5	2700°F	9,780	8.90	3.30	Between center load points
5	3100°F	9,530	3.21	0.70	Outside of load points
3	3100°F	10,010	3.85	1.08	Under upper load point

Notes:

-) Secant modulus is obtained at maximum failing stress
-) Tangent modulus is the maximum value obtained
-) Initial modulus
-) Secondary modulus
-) No useable load-deflection curve

Low temperature (-250°F) strength was surprisingly high and could suggest the potential for this coating. It is difficult to conceive that cryogenic temperature alone could produce the high stresses obtained, but other factors examined, such as location of flexure bars in the pack or different substrate panel from which flexure bars were taken did not provide an explanation.

Low cycle fatigue data showed a 10% reduction in failing stress the same as for the siliconized system. It should be pointed out, however, that more uniform coating can be achieved than that on the tested specimens and more uniformity should improve fatigue strength.

Modulus of elasticity is substantially lower than for the siliconized RPP. This is graphically illustrated by the stress-strain curve plotted on Figure 5-28.

Coating thickness on the Zr-B-Si system given in Table 5-12 show coating depth on the compression side of 0.015 to 0.020 in. while the coating on the tension side averages a little thicker. It was expected that the coating on the upper surface would be more consistently the thicker, but the values obtained are satisfactory.

It is noted that unlike the siliconized system the tangent and secant moduli as determined in VMSC testing are nearly identical through room temperature and 1400°F tests. However, SRI data at room temperature indicates two moduli, the initial one being the greater. At elevated temperature this trend continues and the proposed explanation is the same as that provided in the discussion of the siliconized system.

SRI reports that the failure of the Zr-B-Si specimens was "quasi-plastic" in that failure occurred with a slow, rather than abrupt, loss in load. This is in contrast to the SRI results on the siliconized system, where the failures were more brittle.

The relative constancy of failure stress of the Zr-B-Si system throughout the test range is extremely encouraging and although this system performs only half as well as siliconized RPP under plasma arc test conditions, the Zr-B-Si coating may be the better overall system.

5.4.2 Coefficient of Thermal Expansion

Coefficient of thermal expansion (CTE) was obtained on bare and coated RPP in both warp and fill directions up to 3600°F . The data is plotted in Figures 5-29 and 5-30. Interestingly, the average CTE to 3600°F for bare RPP, siliconized RPP and Zr-B-Si coated RPP all compute to be 1.6×10^{-6} in/in/ $^{\circ}\text{F}$. Slight variations are apparent in the fill direction, but all values are so low as to pose little problem with respect to thermo-elastic

stresses induced by thermal gradients within the overall structure. However, the differences indicated between coated and bare RPP in certain temperature regions, such as that with siliconized RPP around 1400°F, can produce high internal stresses due to temperature alone. These can produce lower allowable stress at these temperatures. It appears that further evaluation of this potential problem is required in Phase II.

Coefficient of expansion data was also obtained from room temperature to -250°F. The values at -250°F were very low and almost insignificant compared to the high temperature end of the spectrum. Preliminary value for siliconized RPP is -0.0125%, while for the Zr-B-Si system it is -0.0200%.

5.4.3 Emittance

Total normal emittance values on the coated materials were obtained at a temperature level of 3000°F, which is near the operational limit of 3200°F for the coatings tested. For siliconized RPP emittance was measured at 0.84, while the Zr-B-Si coating had a value of 0.82. These are consistent with values assumed in the analysis of plasma arc data.

5.4.4 Conductivity

Conductivity was measured both perpendicular and parallel to the laminate. Preliminary data is given in Table 5-14. The siliconized RPP conductivity below 2000°F is lower than that assumed in leading edge analysis, Section 3.0, but above 2000°F the values are higher. The net result is that thermal gradients around the periphery of the leading edge (circumferential gradients) should be higher than those computed. However, cross-radiation relief should be greater than that calculated so stagnation temperatures should be lower than originally anticipated.

5.4.5 Interlaminar Shear Strength

Interlaminar shear strength previously obtained on RPP re-impregnated three times has shown average values of 3250 psi as compared to a design requirement of less than 300 psi. This is considered quite high by industry standards and is obtained on WCA material having a flexure strength of 16600 psi and a density of 1.27 gm/cc. The VMSC 20-mil diffusion coatings on this material should not be expected to alter the interlaminar shear strength capability of the laminate. It is therefore concluded that interlaminar shear strength of VMSC oxidation inhibited material systems is more than adequate for the proposed design.

5.5 CONCLUSIONS

(1) Those coating systems employing silicon have shown pronounced low catalyticity, and in the case of the proposed silicon and Zr-B-Si diffusion coatings, surface temperatures were 14% lower than bare RPP even after multiple cycling.

TABLE 5-14
CONDUCTIVITY OF SILICONIZED RPP

<u>Material</u>	<u>Direction</u>	<u>Temperature, °F</u>	<u>Conductivity Btu/ft-hr-°F</u>
Siliconized RPP	Perpendicular to laminate	R. T.	8.1
	"	1470	8.1
	"	3000	13.3
Siliconized RPP	Parallel to laminate	R. T.	5.8
	"	1470	11.6
	"	3000	13.3
Zr-B-Si RPP	Parallel to laminate	220	5.7
	"	1050	5.6
	"	1980	6.5
	"	2570	5.5
Zr-B-Si RPP	Parallel to laminate	220	11.6
	"	1070	13.2
	"	1980	12.1
	"	2420	13.3

(2) Except for the hafnium-tantalum system which has not been thoroughly evaluated, VMSC siliconized RPP offers the best high temperature oxidation resistance of all systems tested. The Zr-B-Si system, which is second best, has half the mission life capability of the siliconized system.

(3) Plasma spray, refractory bonded, and melt impregnation overlay coating systems did not have good adherence to diffusion coated substrates as evidenced by the results of plasma arc testing.

(4) Hafnium - tantalum coated RPP-O proved to be the best fully catalytic system tested and provided protection to the substrate after repeated exposure at surface temperatures above 4000°F.

(5) Analysis of the low catalytic phenomenon and correlation with test data indicates that the predicted temperature reduction will be achieved by the shuttle during entry and that the VMSC plasma arc test conditions closely simulate the entry environment which is conducive to producing the low catalytic effect.

(6) Zr-B-Si coated WCA laminate strength is unaffected by a one-atmosphere oxidation environment from room temperature to 2300°F.

(7) Siliconized WCA laminates oxidize and lose significant strength upon multiple exposure (100 and 200 minutes) to a one-atmosphere oxidation environment in the range from room temperature to 2300°F. However, this does not necessarily indicate unacceptable performance in the shuttle environment, but requires more thorough evaluation. In addition, siliconized RPP has a potential low strength problem in the 1400°F region requiring additional examination.

(8) Both the siliconized and Zr-B-Si coated RPP have relatively low elastic moduli and low coefficients of expansion. These low values tend to alleviate thermoelastic stresses caused by thermal gradients.

(9) Emittance and conductivity for coated RPP are relatively high. This assists in minimizing both peak temperatures and thermal gradients on the leading edge.

6.0 NONDESTRUCTIVE TESTING (NDT)

The purposes of performing NDT in Phase I were (1) to begin to establish a backlog of data for eventual production use, (2) to support the materials development effort through identification of in-process defects affecting uniformity of coating, constituent distribution, uniformity of depth coating, or delaminations or voids, and (3) to determine which of the various NDT techniques are the most fruitful for each specific defect.

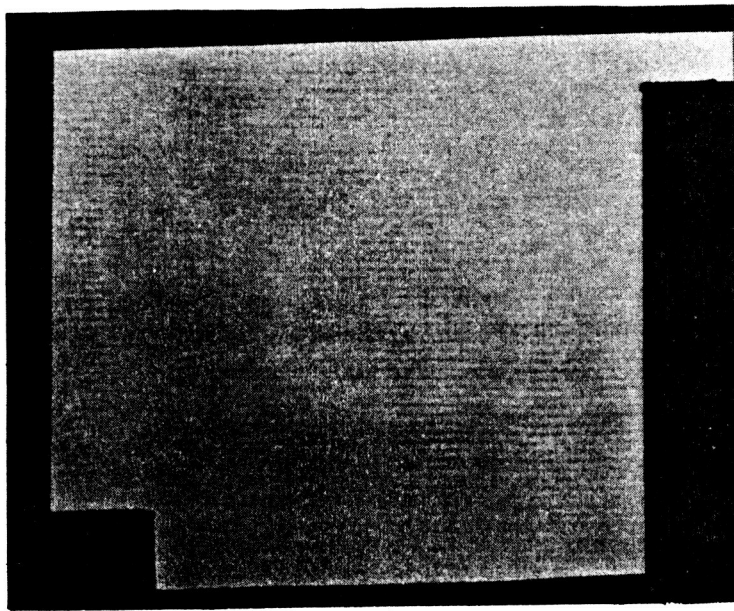
Trial testing of a number of different pieces of test equipment was conducted on bare and coated RPP samples obtained from previous programs. The coated specimens were of the diffusion coated type with silicon, moly/silicon, and tantalum/silicon constituents. X-ray radiography (Norelco-MG50), ultrasonic pulse-echo (magnaflux Model PS900), infrared (Automation Industries Temp-Tester), sonicator-low frequency sound (Automation Industries Model S-1), and eddy current (Magnaflux Corporation) techniques were employed. The best of these techniques, which were discovered to be x-ray and ultrasonic, were then employed throughout the remainder of Phase I.

X-ray is most sensitive to defects parallel to the beam but if an X-ray attenuator, such as carbon tetrachloride, is introduced into defects that are perpendicular to the beam, they are readily detected. This is clearly seen on Figure 6-1 which shows the difference in bare RPP before and after immersion in carbon tetrachloride. Ultrasonic C-SCAN techniques also reveal the delaminations of the same specimen as can be seen by the comparison with X-ray detection on Figure 6-2.

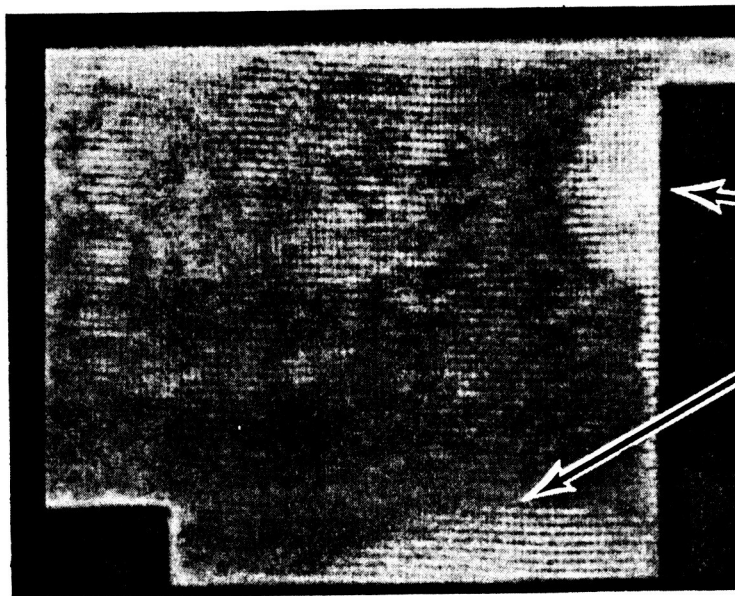
Using another specimen, a comparison between ultrasonic and IR techniques was made. Again bare RPP was used. The excellent correlation can be observed on Figure 6-3 (note that the images are reversed). Edge effects are somewhat obliterated by these methods because of the detector size. The use of X-ray and carbon-tetrachloride overcomes this deficiency. It is of interest, however, that all three techniques do correlate, at least for macrodefects such as those in the test samples.

Another test using X-ray and coated specimens is recorded in Figure 6-4. Here, the variegated texture of the moly/silicon and the tantalum/silicon coating is evident, while the siliconized RPP is uniform by comparison. The significance is that, with coating materials of the type involved in the program, X-ray radiography should be able to detect surface non-uniformity. An ultrasonic C-scan of these same specimens is shown in Figure 6-5. Here, the surface effects do not obliterate subsurface definition. The investigation of the applicability of these two techniques on coated systems was continued.

PRECEDING PAGE BLANK NOT FILMED



BARE RPP – BEFORE IMMERSION



BARE RPP – AFTER IMMERSION
IN CARBON TETRACHLORIDE

DELAMINATIONS

FIGURE 6-1 COMPARISON OF BARE RPP X-RAY PHOTOGRAPHS BEFORE
AND AFTER IMMERSION IN CARBON TETRACHLORIDE

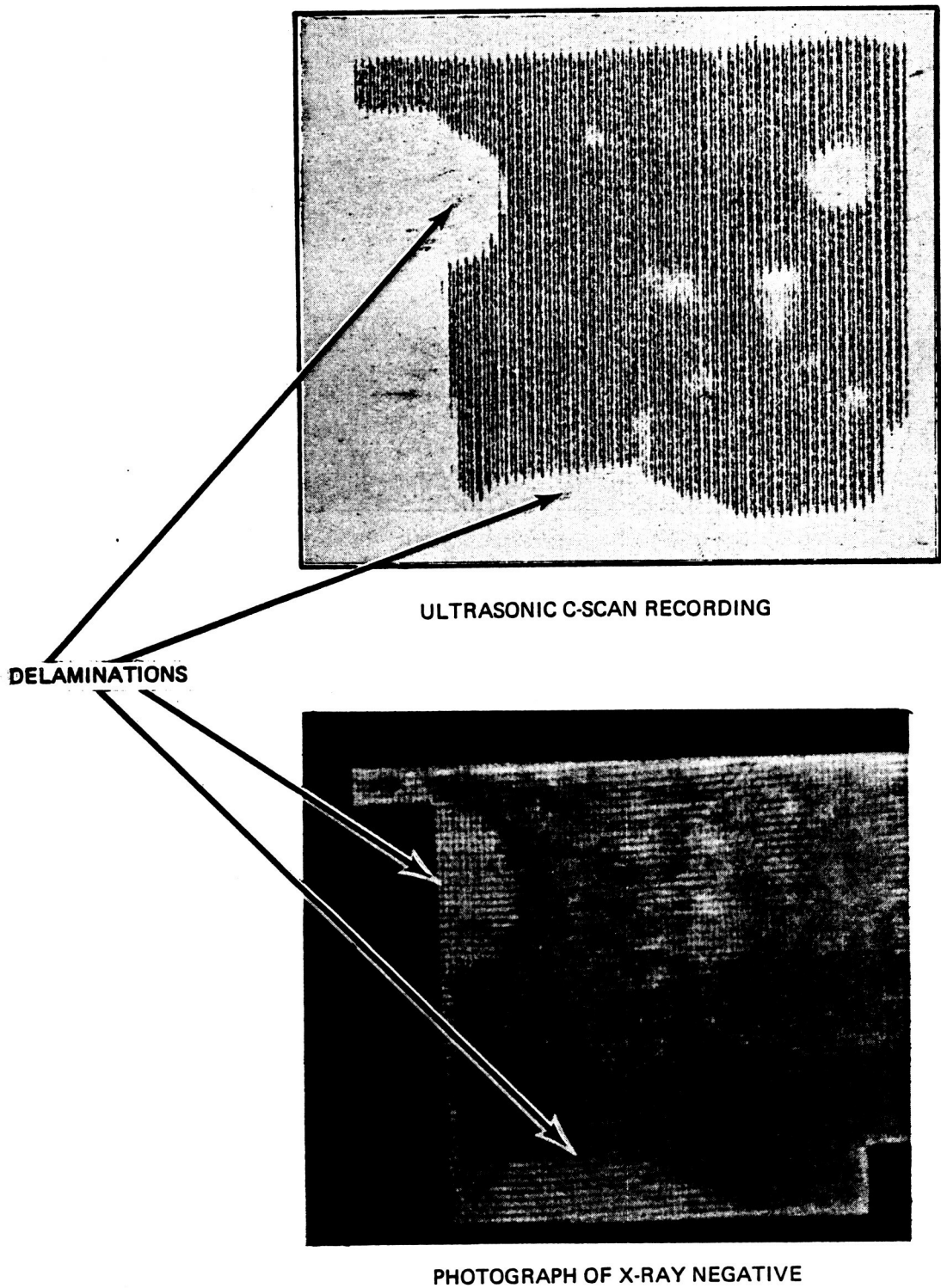
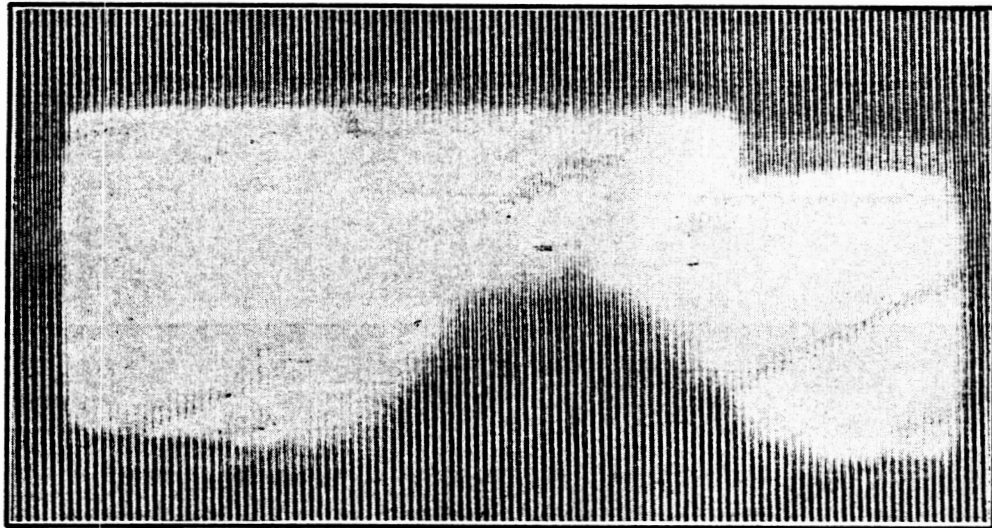
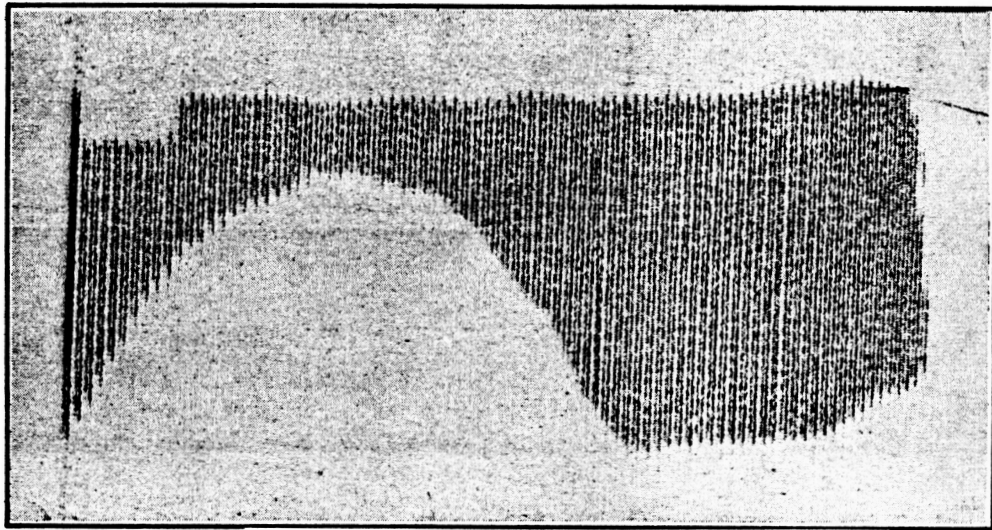


FIGURE 6-2 CORRELATION OF ULTRASONIC C-SCAN RECORDING AND X-RAY OF BARE RPP IMPREGNATED WITH CARBON TETRACHLORIDE, SHOWING DELAMINATIONS AND VOID AREAS

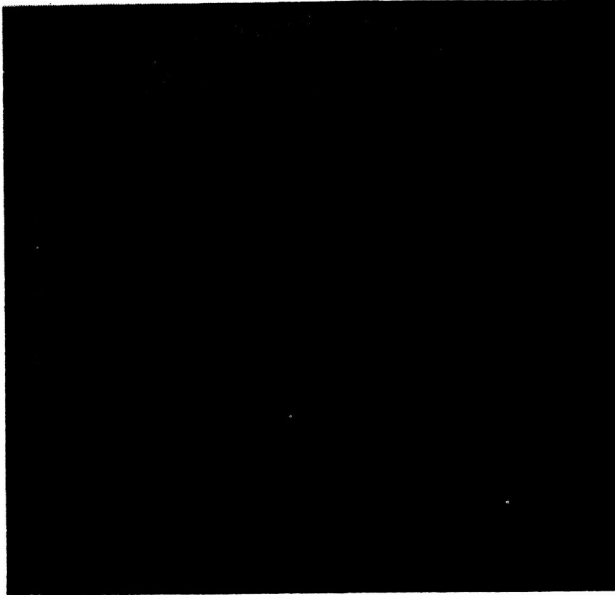


INFRARED THERMOGRAPH

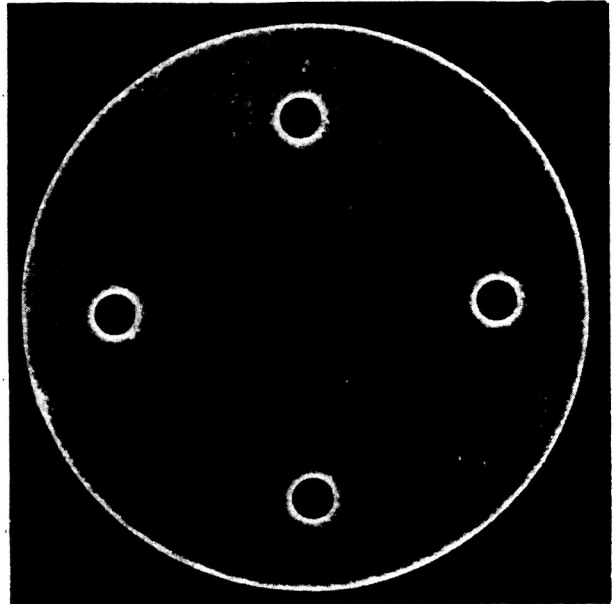


ULTRASONIC C-SCAN RECORDING

FIGURE 6-3 COMPARISON OF INFRARED AND ULTRASONIC INSPECTION TECHNIQUES ON BARE RPP



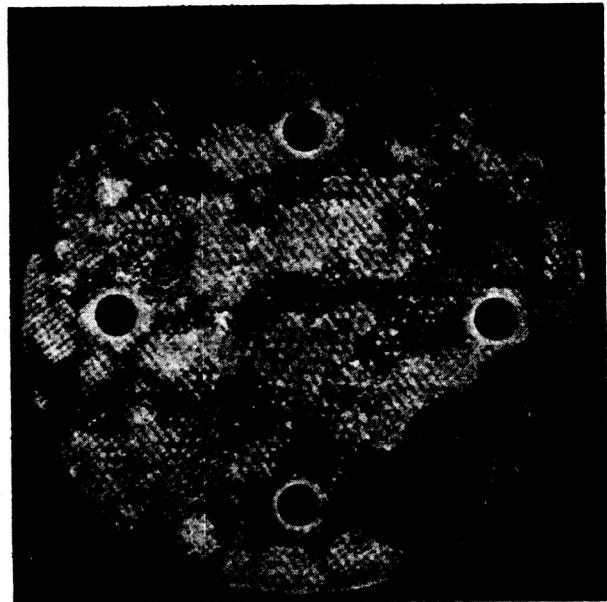
BARE RPP



SILICONIZED RPP

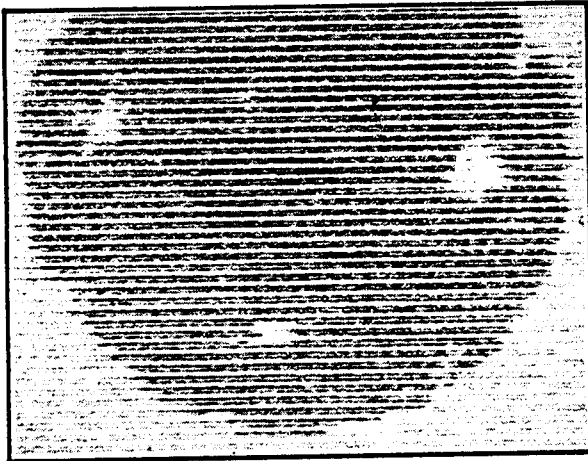


DIFFUSION MOLY/SILICON
COATING ON RPP

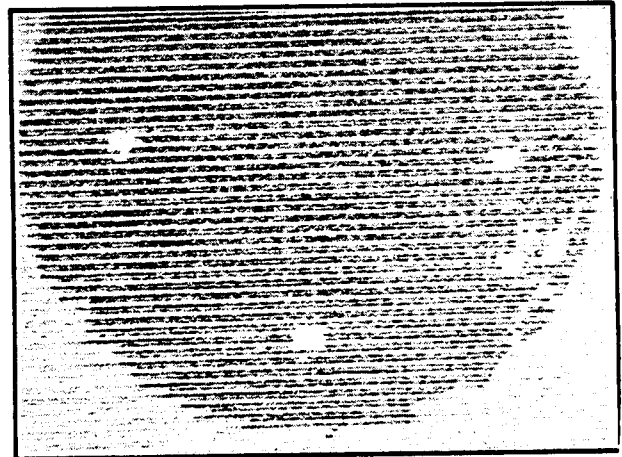


DIFFUSION TANTALUM/SILICON
COATING ON RPP

FIGURE 6-4 PHOTOGRAPHS FROM X-RAY NEGATIVES USING P/N 55 FILM
WITH CONTACT PRINTER



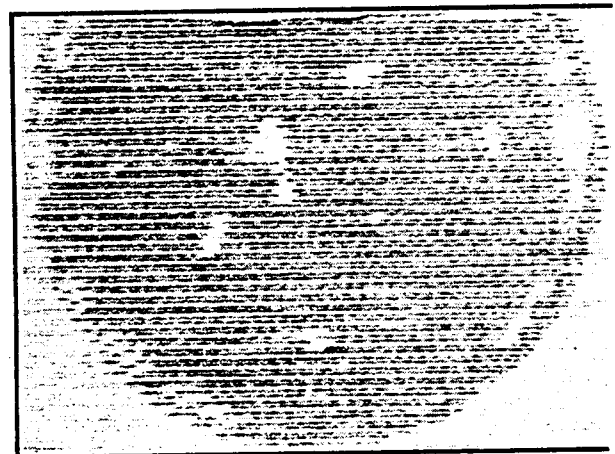
BARE RPP



SILICONIZED RPP



DIFFUSION MOLY/SILICON
COATING ON RPP



DIFFUSION TANTALUM/SILICON
COATING ON RPP

FIGURE 6-5 PHOTOGRAPHS OF ULTRASONIC C-SCAN RECORDINGS FROM BARE AND COATED RPP

Carbon tetrachloride, used as an attenuator for x-ray analysis, and water, used as a couplant in ultrasonic test, were evaluated for potential degradation effects on bare and coated RPP. Test data obtained on flexure bars is included in Table 6-1. A comparison with the controls data indicates there is no clear-cut indication of degradation. Siliconized specimen 1-8, which was subjected to carbon tetrachloride, produced low strength, but specimen 1-9, also infiltrated with carbon tetrachloride, showed strength equal to the control specimen. A similar comparison can be made between specimens 1-10 and 1-9. Evidently the differences obtained are more effected by coating variations than by the introduction of carbon tetrachloride or water. Plasma arc tests were also performed on immersed buttons. These tests confirmed that there is no apparent detrimental effect from immersion in NDT fluids.

TABLE 6-1
Flexure Data After Immersion
in NDT Fluids

Specimen No.	Type	Condition	Failing Stress, psi	Elastic Modulus E x 10 ⁶ psi
1-7	Siliconized	Control	10,200	2.3*
1-8	Siliconized	X-ray (CT) only	7,300	1.8*
1-9	Siliconized	X-ray (CT) and Ultrasonic	10,100	2.0*
1-10	Siliconized	Ultrasonic only	9,200	1.9*
1	Bare	Control	22,600	2.88
2	Bare	Ultrasonic only	21,200	3.18
3	Bare	X-ray (CT) only	21,700	3.21
4	Bare	X-ray (CT) and Ultrasonic	22,400	3.53

*Secant Modulus

Most of the RPP panels fabricated during the modification phase of the program and those fabricated for characterization and NASA specimens were examined radiographically with or without carbon tetrachloride. Panels which showed possible defects were also tested ultrasonically and in selected cases infrared was employed for additional comparison.

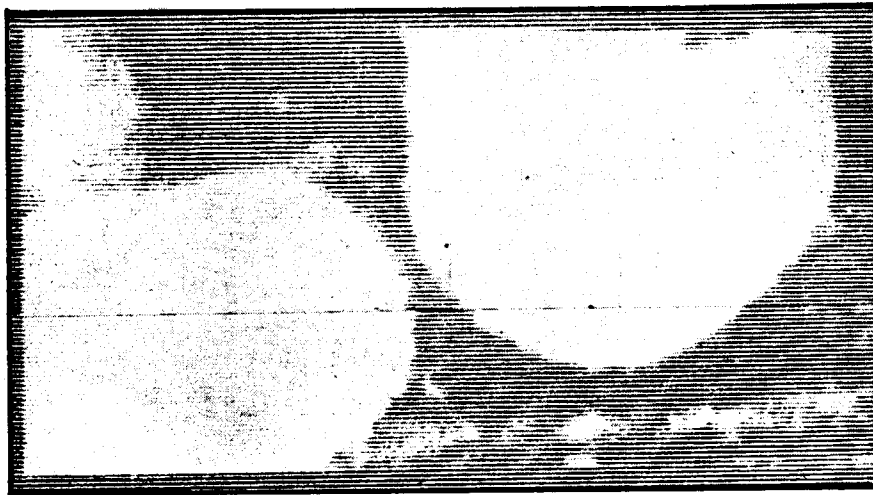
An example of one 6.5 x 12-inch panel tested is given in Figure 6-6. The light areas of the panel indicate a possible delamination. The close correlation between radiographic, ultrasonic, and infrared techniques is apparent. Metallographic examination of a section of this panel from a suspected defect area is shown in Figure 6-7 and confirms the fact that delamination was present.

Additional examples of examination for defects are illustrated by the photomicrographs shown in Figure 6-8. The upper photo shows that what was thought to be a defect when viewed by x-ray was merely the result of adherent pack material. Carbon tetrachloride had penetrated beneath the pack material and gave an indication of a void. Significantly, ultrasonic test correctly did not identify this as a potential defect zone. The lower two photomicrographs show the true conditions that by x-ray and ultrasonic testing indicated identical type defects. In the middle photo the defect was caused by excessive porosity, while in the lower photo delamination was the problem. This illustrates porosity and delamination can produce the same indicator by NDT techniques. However, both conditions can be cause for rejection of the material.

Siliconized specimens M10-5 and M10-6, which are 3 inches in diameter by 0.25 inches thick, are shown in Figures 6-9 and 6-10. Specimen M10-5 was subjected to a heat flux of 100 Btu/ft²-sec and a surface temperature of 3000^oF for 40 minutes without weight loss or surface recession. The x-ray and ultrasonic photos indicate some nature of non-uniformity around the edges, but this specimen has not yet been sectioned to evaluate metallographic the edge areas.

Specimen M10-6 in Figure 6-10 experienced 3220^oF surface temperature until burnthrough of one-third of the coating, whereupon the exposed bare RPP rose to approximately 3520^oF. This high temperature readily conducted across the thickness and is believed responsible for the coating loss on the back side. Cross sectioning showed that the coating remained tightly adherent to the RPP and no obvious subsurface erosion or degradation was incurred outside the burnthrough area.

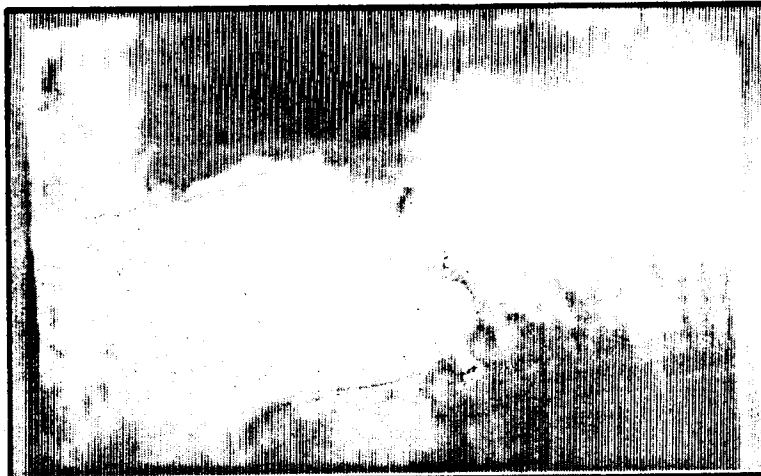
It is concluded from the Phase I NDT work that radiographic and ultrasonic NDT techniques are valuable tools for ascertaining possible laminate defects. More detailed NDT and photomicrograph correlation will be required as the field of inhibited RPP candidates is narrowed and concentration on two systems is initiated. A backlog of data is being compiled for eventual establishment of standards.



ULTRASONIC C-SCAN RECORDING –
THROUGH TRANSMISSION –5.0 Mhz, 100 X 3.0 GAIN

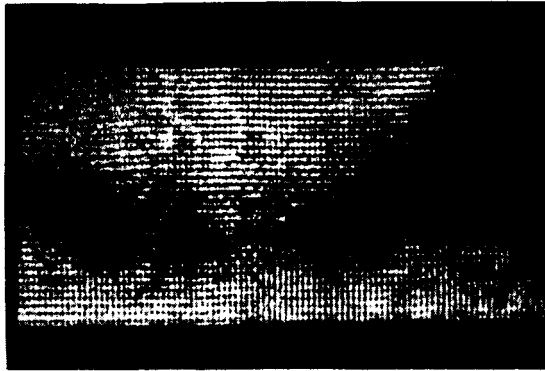


X-RAY PHOTOGRAPH -10 Ma 25 KV, 36" FOCAL – 30 SECONDS

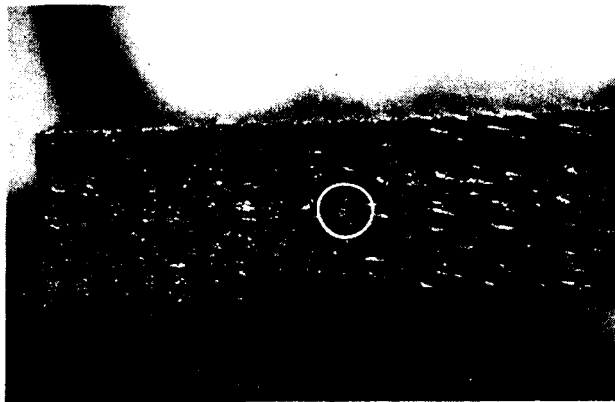


INFRARED RECORDING

FIGURE 6-6 NON-DESTRUCTIVE TESTING OF PANEL 2-1 – CORRELATION OF DEFECT INDICATIONS.

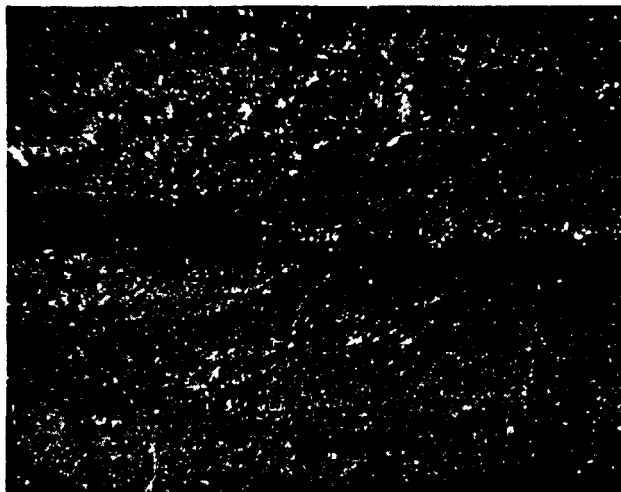


X-RAY PHOTOGRAPH OF SECTION FROM PANEL 2-1



5X

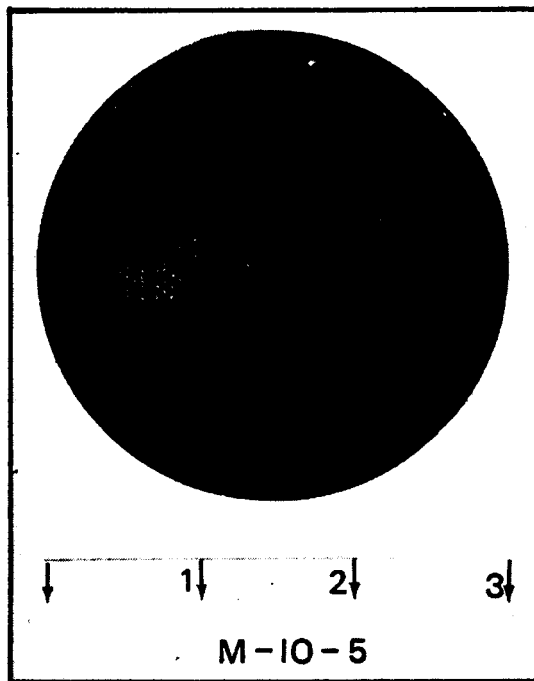
PHOTOGRAPH OF SECTION FROM ABOVE PANEL SHOWING DELAMINATION



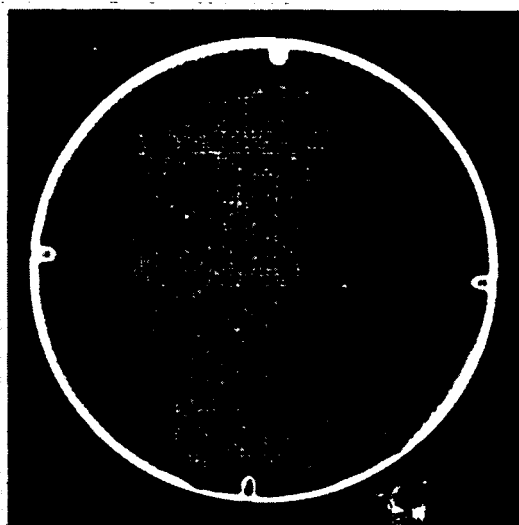
50X

MICROPHOTOGRAPH OF DELAMINATION IN CIRCLES AREA

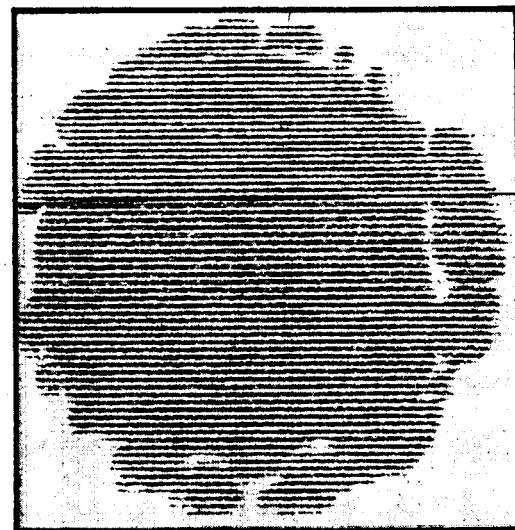
FIGURE 6-7 METALLOGRAPHIC EXAMINATION OF PANEL 2-1 TO CONFIRM NON-DESTRUCTIVE TEST INDICATIONS



MSC
 PLASMA TEST SPECIMEN AFTER EXPOSURE TO 100 BTU/FT² SEC

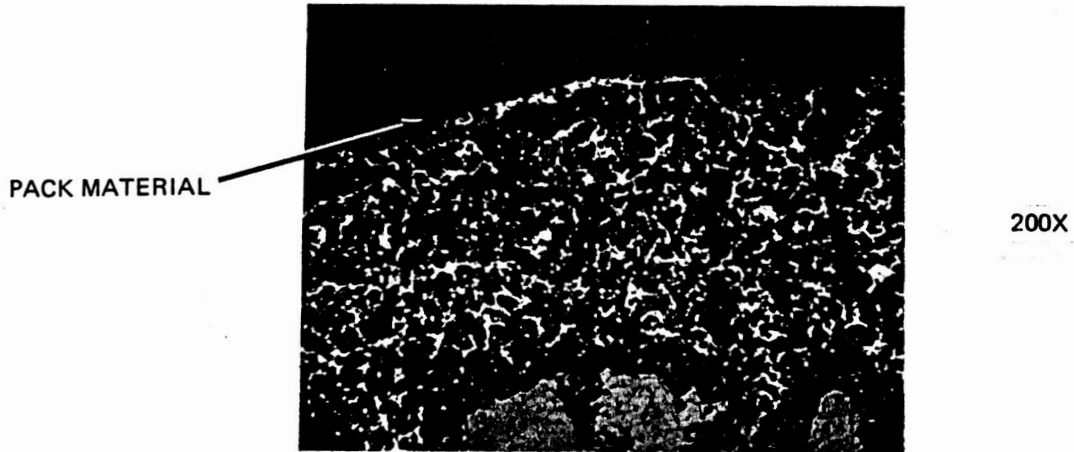


X-RAY PHOTOGRAPH OF MSC PLASMA TEST SPECIMEN M-10-5 10 Ma, 25KV, 36" FOCAL 60 SECONDS

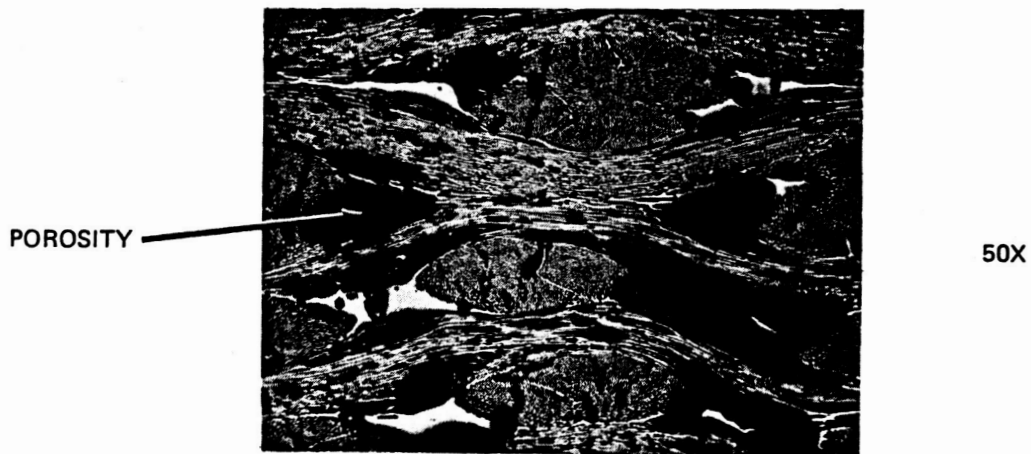


ULTRASONIC C-SCAN OF MSC PLASMA TEST SPECIMEN M-10-5 THROUGH TRANSMISSION 2.25 Mhz 100 X 3.6 GAIN

FIGURE 6-9 EVALUATION OF SILICONIZED SPECIMEN M10-5 TESTED BY NASA-MSC AT HEAT FLUX = 100 BTU/FT²-SEC FOR 40 MINUTES – SURFACE TEMPERATURE = 3000°F



ADHERENT SILICON METAL FROM PACK COATING OBSERVED VISUALLY AND DETECTED BY X-RAY EXAMINATION.



NONUNIFORM IMPREGNATION PRIOR TO PYROLYZATION WHICH WAS DETECTED BY ULTRASONIC EXAMINATION.

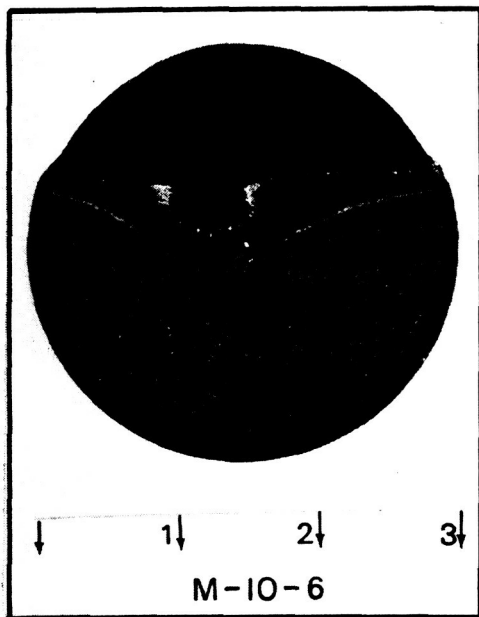


DELAMINATION NOTED BY RADIOGRAPHIC EXAMINATION AFTER IMMERSION IN CARBON TETRACHLORIDE

FIGURE 6-8 METALLOGRAPHIC EXAMINATION OF TYPICAL DEFECTS OBSERVED WITH NON-DESTRUCTIVE TESTING BY RADIOGRAPHIC AND ULTRASONIC INSPECTION TECHNIQUES

REFERENCES

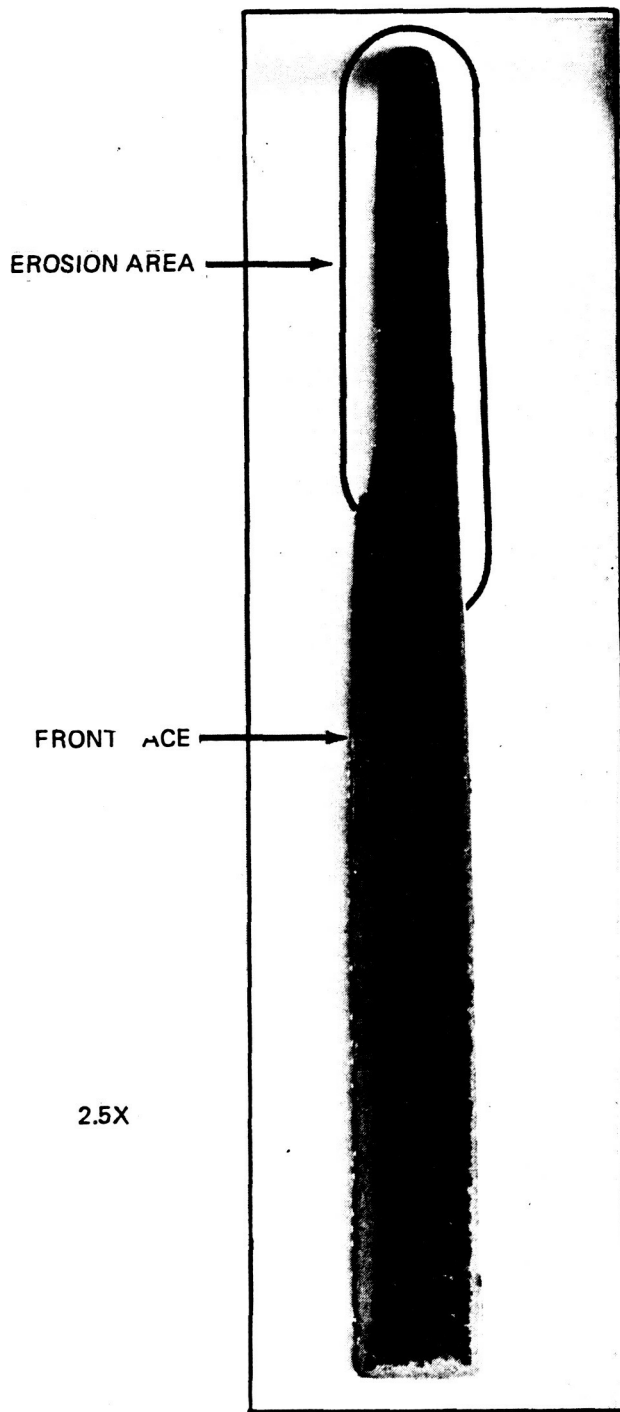
1. Contract for Development of a Thermal Protection System for the Wing of a Space Shuttle Vehicle, Contract No. NAS9-11224 dtd 30 July, 1970.
2. Program Plan for Development of a Thermal Protection System for the Wing of a Space Shuttle Vehicle, MSD Report No. T143-5R-00005, dtd 14 August, 1970.
3. "Space Shuttle Wing Leading Edge Design Criteria", Report No. T143-5R-00011, 23 September 1970.
4. "DC 3 - Space Shuttle Study", April 1970. NASA Manned Spacecraft Ce
5. "Theory of Stagnation Point Heat Transfer in Dissociated Air", Journal the Aeronautical Sciences", February 1958.
6. "Survey of Boundary Layer Heat Transfer at High Velocities and High Temperatures", WADC TR 59-624, April 1960.
7. Space Shuttle Studies Phase B North American Rockwell Data.
8. "Physical and Mechanical Properties of Materials Used for Design of the X-20 Nose Cap" Report No. 3-14000/3R-42, dtd Sept. 1963.
9. "Literature Survey on High Temperature Insulation Materials", Report No. 00.249, 26 June 1963.
10. "Investigation of Insulative Heat Shield Attachment Systems", AFFDL-65-55, April 1965.
11. Engineering Radiation Heat Transfer by J. A. Wiebelt, Holt Rinehart and Winston, Inc., 1965, page 88.
12. High Temperature Materials and Technology - Campbell and Sherwood.
13. "Ternary Phase Equilibria in Transition Metal - Boron - Carbon - Silicon Systems", AFML-TR-65-2, Part II, Volume VII - December 1965, Aerojet-General Corp. E. Rudy, et al
14. B. A. Forcht, et al, "Pyrolyzed Plastic Composites", ML-TDR-64-18 Part II - December, 1963 LTV Astronautics Div.
15. Hansen, Max, "Constitution of Binary Alloys", McGraw-Hill, N. Y., 1958, 2nd Ed.



MSC PLASMA TEST SPECIMEN
AFTER EXPOSURE TO 126 BTU/FT²-SEC



X-RAY PHOTOGRAPH SHOWING
UNDAMAGED AREA OF M-10-6
10 Ma, 50 KV, 36" FOCAL
30 SECONDS



CROSS SECTION THROUGH CENTER
OF SPECIMEN

FIGURE 6-10 METALLOGRAPHIC EXAMINATION OF M-10-6, NASA-MSC PLASMA TEST SPECIMEN – AFTER EXPOSURE TO A HEAT FLUX OF 126 BTU/FT²-SECONDS AND A SURFACE TEMPERATURE OF 3220°F.

16. Forcht, B. A., "Oxidation Inhibited Carbon-Carbon Composites", LTV Report No. 00.1243, 15 Nov. 1969.
17. Process and Design Data on a Boride-Silicon Composition Resistant to Oxidation to 2000°C, ASD-TDR-62-1055.
18. Kaufman, L., et al, "Stability Characterization of Refractory Materials Under High Velocity Flight Conditions", Air Force Report AFML-TR-69-84 (A 9 Volume Series, Dec. 1969 through Feb. 1970).
19. Clougherty, E. V., et al, "Research and Development of Refractory Oxidation Resistant Diborides, Air Force Report AFML-TR-68-190 (An 8 Volume Series, May 1968 through Nov. 1969.).
20. Carlson, R. K., et. al., "Carbonized Plastic Composites for Hyperthermal Environments," ASD-TDR-62-352, June 1962.
21. Forcht, B. A., Haviland, J. K., and McKinney, A. R., "Carbonized Plastics Composites for Hyperthermal Environments, Part II," ASD-TDR-62-352, February 1963.
22. Forcht, B. A., et. al., "Pyrolyzed Plastic Composites," ML-TDR-64-187, Part II, December 1965.
23. Forcht, B. A., et. al., "Pyrolyzed Plastic Composites," ML-TDR-64-187, Part II, December 1965.
24. Haviland, J. K. and Medford, J. E., "The Prediction of Oxidation Rates of Carbonaceous Materials from Plasma Arc Tests," LTV Missiles and Space Division Report No. 00.241, June 1963.
25. Shuford, D. M. and Rogers, D. C., "Oxidation Inhibited Carbon Compsites", LTV Missiles and Space Division Report No. 00.1243 November 1969.
26. Fay, J. A., and Riddell, F. R., "Theory of Stagnation Point Heat Transfer in Dissociated Air", Jour. Aero. Sci., Vol. 25, No. 2, Feb. 1958, pp. 73-85, 121.
27. Lees, Lester, "Convective Heat Transfer with Mass Addition and Chemical Reactions", Third AGARD Combustion and Propulsion Panel Colloquium, Palermo, Sicily, March 17-21, 1958. Pergamon Press, N. Y., pp. 451-498.
28. Lees, Lester, "Laminar Heat Transfer Over Blunt-Nosed Bodies at Hypersonic Flight Speeds", Jet Propulsion, Vol. 26, No. 4, Apr. 1956, pp. 259-269.

29. Kemp, Nelson H., Rose, Peter H., and Detra, Ralph W., "Laminar Heat Transfer Around Blunt Bodies in Dissociated Air", *Jour. Aero/Space Sci.*, Vol. 26, No. 7, July 1959, pp. 421-430.
30. Goodwin, Glen and Chung, Paul M., "Effects of Nonequilibrium Flows on Aerodynamic Heating During Entry into the Earth's Atmosphere from Parabolic Orbits", *Second International Congress for Aeronautical Sciences*, Zurich, Switzerland, September 1960.
31. Goulard, R., "On Catalytic Recombination Rates in Hypersonic Stagnation Heat Transfer", *Jet Propulsion*, November 1958.
32. Vojvodich, N.S., "The Performance of Ablative Materials in a High-Energy, Partially Dissociated Frozen Nitrogen Stream", NASA TN D-1205.
33. Boison, J.C. and Curtiss, H.A., "An Experimental Investigation of Blunt Body Stagnation Point Velocity Gradient", *ARS Journal*, February 1959, pp 130-135.
34. Pope, R.B., "Stagnation-Point Convective Heat Transfer in Frozen Boundary Layers", *AIAA Journal*, April 1968.
35. Development of a Thermal Protection System for the Wing of a Space Shuttle Vehicle, Quarterly Report for Period 1 August 1970 through 31 October 1970, MSD-T Report No. T143-5R-00030.
36. LTV Research Center, Unpublished Work, W. C. Schwemer, T. E. Mackie - 1955-1966
37. Rudy, E., "Ternary Phase Equilibrium in Transition Metal - Boron, Carbon, Silicon Systems" Part II Ternary System, Volume 1 Ta-Hf-C System
38. Curtis, C.E., "Development of Zirconia Resistant to Thermal Shock," *J. Am. Ceram. Soc* 30 (6); 180-196 (1947)
39. Geller, R.F. and Yavorsky, P., "Effects of Some Oxide Additions on the Thermal-Length Changes of Zirconia" *Res. Natl. Bur. Std.* 35 (1), 87-110 (1945)
40. Cambell, I.E., "High Temperature Materials and Technology," John Wiley & Sons, 1967

41. Grier, N. T. and Sands, N., "Regime of Frozen Boundary Layers in Stagnation Region of Blunt Reentry Bodies," NASA TND-865.
42. Wethern, R. J., "Method of Analyzing Laminar Air Arc-Tunnel Heat Transfer Data," AIAA Journal, Vol. 1, No. 7, July 1963, pp. 1665-1666.
43. Rosner, D. E., "Analysis of Air Arc-Tunnel Heat Transfer Data," AIAA Journal, Vol. 2, No. 5, May 1964, pp. 945-948.
44. Chung, P. M., Liu, S. W., and Mirels, H., "Effect of Discontinuity of Surface Catalycity on Boundary Layer Flow of Dissociated Gas," Aerospace Corporation Report TDR-69 (2240-20) TN-1, 7 June 1962.
45. Sheldahl, R. E. and Winkler, E. L., "Effect of Discontinuities in Surface Catalytic Activity on Laminar Heat Transfer in Arc-Heated Nitrogen Streams," NASA TND-3615.

DISTRIBUTION

One (1) copy to:

NASA, Manned Spacecraft Center
Advanced Programs Contract Section
Houston, Texas 77058
Attention: W. M. Chastain/J042

NASA, Manned Spacecraft Center
Advanced Missions Program Office
Houston, Texas 77058
Attention: Wayne Young/HA-JA

Four (4) copies to:

NASA, Manned Spacecraft Center
Technical Information Dissemination Branch
Houston, Texas
Attention: Retha Shirkey/BM6

One (1) copy to:

NASA, Manned Spacecraft Center
Management Services Division
Houston, Texas 77058
Attention: John T. Wheeler/BM7

Three (3) copies to:

NASA, Manned Spacecraft Center
Documentation Management Office
Houston, Texas 77058
Attention: Charles M. Grant/ BM2

Fifteen (15) copies to:

NASA, Manned Spacecraft Center
Project Support Branch
Houston, Texas 77058
Attention: J. E. Pavlosky/ES-4